PALACKÝ UNIVERSITY OLOMOUC

Faculty of Science

Department of Biochemistry

Localization studies of the cytokinin receptor CRE1/AHK4 using fluorescently labelled cytokinin

Ph.D. Thesis

Author:	**Mgr. Karolina Kubiasová**
Study program:	P1406 Biochemistry
Study form:	Full-time
Supervisor:	**RNDr. Ondřej Plíhal, Ph.D.**
Consultants:	**Prof. Eva Benková**
	Juan Carlos Montesinos López, Ph.D.
Submitted:	2020

I hereby declare that this PhD thesis has been written solely by me. All the sources cited in this thesis are listed in the Reference list. All published results included in this work are approved by co-authors.

Olomouc _____   _____

                                                        Karolina Kubiasová

ACKNOWLEDGEMENTS

I wish to express my deep gratitude

to my supervisor RNDr. Ondřej Plíhal, Ph.D. for the opportunity to work on this project focused on localization of cytokinin receptors and for introducing me to Prof. Eva Benková.

to my consultants Prof. Eva Benková and Juan Carlos Montesinos López, Ph.D. for their valuable time, endless support, guidance, fruitful discussions and all the time I could spend at IST Austria.

to current and former members of Benkova and Friml groups for the wonderful time spent with during all my internships, for always finding time to discuss scientific as well as non science-related topics, for the great support and for the inspiring and friendly environment.

to everyone who contributed to both of my first author articles as presented in this thesis and to those who spent time with me discussing the science.

Autor's first name and surname	Mgr. Karolina Kubiasová
Title	Localization studies of the cytokinin receptor CRE1/AHK4 using fluorescently labelled cytokinin
Type of thesis	Ph.D.
Department	Centre of the Region Haná for Biotechnological and Agricultural Research, Faculty of Science, Palacký University Olomouc
Supervisor	RNDr. Ondřej Plíhal, Ph.D.
Consultants	Prof. Eva Benková
	Juan Carlos Montesinos López, Ph.D.
The year of presentation	2020

Abstract

Cytokinins are plant hormones that play an essential role in various aspects of plant growth and development. In *Arabidopsis thaliana* three transmembrane histidine kinases, namely AHK2, AHK3 and CRE1/AHK4, serve as cytokinin receptors. Subcellular localization of the receptors proposed the endoplasmic reticulum (ER) membrane as a principal cytokinin perception site, while the study of cytokinin transport pointed to the plasma membrane (PM)-mediated cytokinin signalling. To gain better insight into the dynamics of cytokinin receptor localization within the cell a series of cytokinin fluorescent probes were developed. The ligand properties of isopentenyladenine (iP)-derived probes were assessed in a bacterial receptor test where the competition of a cytokinin fluoroprobe with radiolabelled *trans*-zeatin was measured. Although the structural changes within the fluorescent probes led mostly to a significant loss of the biological activity, several fluorescent derivatives interacted well. The most promising of them (iP-NBD) was selected as a tool for visualization of the cytokinin receptor pool

inside the cell. By detailed monitoring subcellular localizations of the fluorescently labelled natural cytokinin probe and the receptor ARABIDOPSIS HISTIDINE KINASE 4 (CRE1/AHK4) fused to GFP reporter, it is shown that pools of the ER-located cytokinin receptors can enter the secretory pathway and reach the PM in cells of the root apical meristem, and the cell plate of dividing meristematic cells. A revised view on cytokinin signalling and the possibility of multiple sites of perception at PM and ER is provided.

Jméno a příjmení autora	Mgr. Karolina Kubiasová
Název práce	Studium lokalizace cytokininového receptoru CRE1/AHK4 pomocí fluorescenčně značeného cytokininu
Typ práce	Disertační
Pracoviště	Oddělení molekulární biologie, Centrum regionu Haná pro biotechnologický a zemědělský výzkum, Přírodovědecká fakultra UP v Olomouci
Vedoucí práce	RNDr. Ondřej Plíhal, Ph.D.
Konzultanti	Prof. Eva Benková
	Juan Carlos Montesinos López, Ph.D.
Rok obhajoby práce	2020

Abstrakt

Cytokininy jsou rostlinné hormony, které hrají důležitou roli v mnoha růstových a vývojových procesech rostlin. V *Arabidopsis thaliana* se nachází tři transmembránové histidin kinasy, které fungují jako cytokininové receptory, konkrétně AHK2, AHK3 a CRE1/AHK4. Výsledky subcelulární lokalizace receptorů navrhovaly endoplasmatické retikulum (ER) jakožto hlavní místo cytokininové percepce, zatímco studium cytokininového transportu ukazovalo na plasmatickou membránu (PM) jako místo cytokininové signalizace. Pro lepší pochopení dynamiky lokalizace cytokininových receptorů v buňce byla připravena řada fluorescenčních prób. Vlastnosti prób odvozených od isopentenyladeninu (iP) byly stanoveny v bakteriálním receptorovém testu, kde byla sledována kompetice mezi fluorescenčně značeným cytokininem a radioaktivně značeným *trans*-zeatinem. Přestože strukturní změny fluorescenční proby vedly většinou k výrazným ztrátam biologické aktivity, několik fluorescenčních derivátů

se vázalo dobře. Jeden z nich (iP-NBD) byl vybrán jako nástroj pro vizualizaci cytokininových receptorů v buňce. Pomocí detailní studie subcelulární lokalizace fluorescenčně značeného cytokininu a ARABIDOPSIS HISTIDINE KINASE 4 (CRE1/AHK4) receptoru sfuzovaného s GFP reporterem bylo ukázáno, že ER-lokalizované cytokininové receptory vstupují do sekreční dráhy až k PM v buňkách kořenového apikálního meristému a k buněčné desce dělících se meristematických buněk. Byl tak poskytnut upravený pohled na signalizaci cytokininů a možnost různých míst percepce na PM a ER.

Klíčová slova	cytokininy, cytokininové receptory, CRE1/AHK4, histidin kinasy, fluorescenční značení, konfokální mikroskopie, percepce cytokininů, GFP, NBD, *Arabidopsis thaliana*, endoplasmatické retikulum, plasmatická membrána, brefeldin A
Počet stran	181
Počet příloh	2
Jazyk	Anglický

CONTENTS

AIMS OF THE WORK

o   Literature review on the plant hormones cytokinins, with a focus on cytokinin receptors and their localization.

o   Characterization of a series of fluorescent derivatives of the cytokinin iP as a new tool for cytokinin receptor domain mapping.

o   Detailed biochemical and localization study of fluorescently labelled cytokinin iP-NBD.

o   Preparation and characterization of transgenic *Arabidopsis* lines expressing 35S::CRE1/AHK4-GFP construct.

o   Detailed subcellular localization of the cytokinin receptor CRE1/AHK4 using confocal microscopy.

INTRODUCTION

Karolina Kubiasová

Department of Molecular Biology, Centre of the Region Haná for Biotechnological and Agricultural Research, Šlechtitelů 27, Olomouc 783 71, Czech Republic

Cytokinins

Cytokinins (CKs) represent an important class of plant hormones (phytohormones) which are essential for a wide range of plant growth and developmental processes (Davies, 2010). Their first note falls to the beginning of the 20th century when Austrian plant physiologist Gottlieb Haberlandt found that phloem sap could support cell division in potato parenchyma cells (Haberlandt, 1913). In the 1950s, Carlos Miller and Folke Skoog isolated a compound which was able, in concert with auxin, promote cell division in tobacco cell cultures. This substance (N^6-furfurylaminopurine) was isolated from autoclaved herring sperm DNA and it was given the name kinetin (Kin) for its cytokinesis-stimulating activity (Miller 1955a, 1955b). Since kinetin is formed artificially and does not occur in plant tissues, the first naturally occurring cytokinin identified in plants was *trans*-zeatin (*t*Z), named after the plant species *Zea mays* where it was originally isolated from immature maize endosperm (Miller, 1961; Letham, 1963; Letham and Miller, 1965). Since then, many compounds with cytokinin-like activities have been identified in various plant species and today a wide variety of natural and synthetic cytokinins exist. Cytokinins are also produced by other organisms including mosses (*Physcomitrella patens*), pathogen plant bacteria (*Agrobacterium tumefaciens*, *Pseudomonas savastanoi*) or slime molds (*Dictyostelium discoideum*; Stirk and Staden, 2010).

Molecular structure of cytokinins

Cytokinins exist in numerous molecular forms. From a chemical point of view, naturally occurring cytokinins are derivatives of adenine. Based on the structure of the N^6-side chain attached to the adenine ring, cytokinins can be classified into two groups – isoprenoid and aromatic (Figure 1A, B). The isoprenoid cytokinins have an isopentenyl side chain and include isopentenyladenine (iP) or zeatin. Benzyladenine (BA), topolins or kinetin are representatives of the aromatic cytokinin group (Sakakibara, 2006). The most abundant cytokinins in plants are *trans*-zeatin, isopentenyladenine, *cis*-zeatin (*c*Z) and dihydrozeatin (DHZ; Schmülling, 2004). Generally, the most prevalent derivatives are iP and *t*Z, together with their sugar conjugates (that are much more abundant than

free bases) but their appearance varies depending on the plant species, developmental stage or plant tissue (Novák et al., 2017). Isoprenoid cytokinins are produced mainly by higher plants, for example, iP- and *t*Z-types of cytokinins are the major forms in *Arabidopsis* (Osugi and Sakakibara, 2015). On the other hand, even though *c*Z is generally considered a less active cytokinin form than *t*Z with weaker responses in the receptor activation assays (Spíchal et al., 2004, Yonekura-Sakakibara 2004), it is widely common in some major crops, such as rice or maize (Mok and Mok, 2001). In addition, topolins, the representants of aromatic cytokinins, which are less abundant than isoprenoid cytokinins, were first described in poplar (Strnad, 1997) and later identified also in other species, for example *Arabidopsis* (Tarkowska et al., 2003) and pea (Gaudinová et al., 2005).

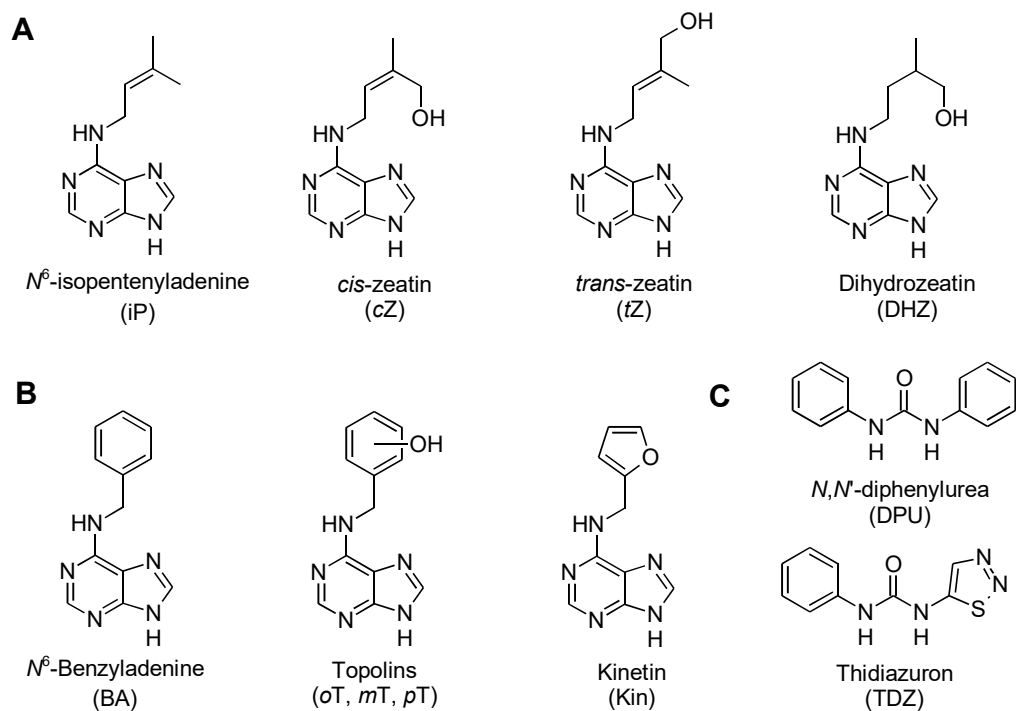**Figure 1:** *Cytokinins and their chemical structures. **A** – isoprenoid, **B** – aromatic, **C** – phenylurea type. Their commonly used abbreviations are in the brackets.*

During the last decades, there have been numerous attempts to prepare synthetic cytokinin derivatives that would preserve a high biological activity, while having no significant negative effects on root or shoot development. Apart from Kin and BA, a

number of other synthetic cytokinins possessing various CK-like activity were developed (for example *N*9-tetrahydropyranyl (THP) or *N*9-tetrahydrofuranyl (THF) derivatives of aromatic cytokinins; Podlešáková et al., 2012). Such cytokinin derivatives are often modified with the aim to find a new, perspective plant growth regulator (Doležal et al., 2007; Mik et al., 2011a; Mik et al., 2011b; Podlešáková et al., 2012; Matušková et al., 2019). Moreover, there are compounds structurally unrelated to natural cytokinins, but keep a high biological activity, such as phenylurea compounds (for example diphenylurea (DPU) or thidiazuron (TDZ); Figure 1C). Their large biological activity is based on their immense stability and capability to strongly inhibit cytokinin oxidase/dehydrogenase (CKX), an enzyme responsible for cytokinin degradation. Yet, no natural phenylurea compounds have been found in plants. (Sakakibara, 2006).

Cytokinin homeostasis – biosynthesis, degradation and modification

To maintain cytokinin homeostasis, a complex regulatory system including biosynthesis, activation, modification, transport and degradation has evolved. Cytokinin free bases possess the highest biological activity. However, the first products of cytokinin biosynthesis are nucleotides which are further dephosphorylated to form ribosides. Subsequently, by eliminating ribose moiety, cytokinin nucleotides are converted to their active forms. Up to now, only the biosynthesis of isoprenoid cytokinins is extensively clarified, while the origin of synthesis of aromatic cytokinins is still shrouded in mystery (Lindner and von Schwartzenberg, 2016). Plant cytokinin biosynthesis consists of two pathways: the *de novo* synthesis pathway by which most of the cytokinins are produced, and the tRNA degradation pathway resulting in the formation of *c*Z (Figure 2; Feng et al., 2017).

The isoprenoid cytokinin biosynthesis is regulated by three key enzymes. Isopentenyl transferase (IPT) is the first crucial enzyme catalyzing the addition of prenyl group from dimethylallyl diphosphate (DMAPP) to the N^6 position of adenosine triphosphate (ATP), adenosine diphosphate (ADP) or adenosine monophosphate (AMP). The *Arabidopsis* genome encodes nine IPT homologs (AtIPT1-AtIPT9) which differ in cellular localization (Kasahara et al., 2004). Seven of these homologs (AtIPT1, AtIPT3-8) are adenylate IPTs that add prenyl moiety to AMP, ADP or ATP whereas rest

two (AtIPT2 and AtIPT9) homologs are tRNA-IPTs transferring prenyl on adenine bound in tRNA (Frébort et al., 2011).
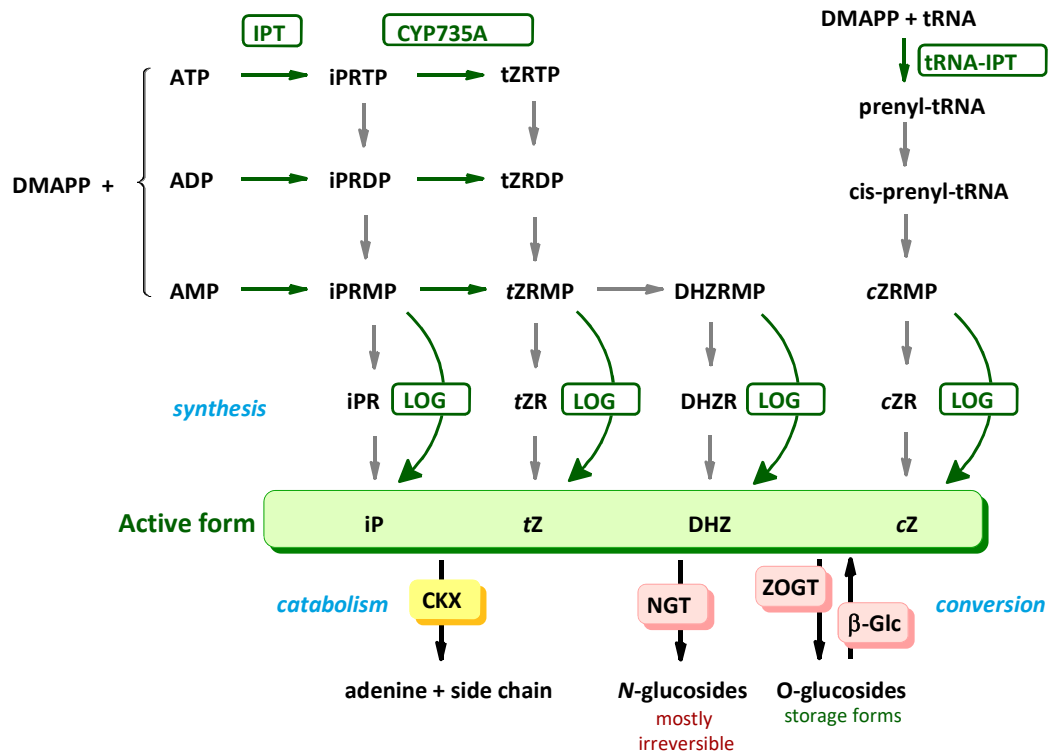
Figure 2: *The key enzymes and metabolites of cytokinin metabolism pathway. AMP - adenosine monophosphate; ADP – adenosine diphosphate; ATP – adenosine triphosphate; DMAPP – dimethylallyl diphosphate; iPRMP – isopentenyl riboside monophosphate; tZRMP – trans-zeatin riboside monophosphate; DHZRMP – dihydrozeatin riboside monophosphate; cZRMP – cis-zeatin riboside monophosphate; iPR – isopentenyl riboside; tZR - trans-zeatin riboside; DHZR – dihydrozeatin riboside; cZR – cis-zeatin riboside; DHZ – dihydrozeatin; cZ – cis-zeatin; CKX – cytokinin oxidase/dehydrogenase; NGT – N-glucosyltransferase; ZOGT – O-glucosyltransferase; β-Glc – β-glucosidase. The active forms of cytokinins (iP, tZ, DHZ and cZ) are in the green box (figure modified from Sakakibara, 2006; Hirose et al., 2008; Li et al., 2018).*

Moreover, IPTs use as their preferred substrate ATP and ADP predominantly in higher plants while AMP serves as a substrate for the first step in cytokinin biosynthesis in *Dictyostelium discoideum*, *Agrobacterium tumefaciens*, and plant tissues transformed with *A. tumefaciens* (Kakimoto, 2001; Miyawaki et al., 2006). IPT action leads to the production of iP ribotides which can be subsequently converted into *t*Z-type ribotides via hydroxylation of the isoprenoid side chain. This reaction is catalysed by cytochrome P450 monooxygenase CYP735A (Takei et al., 2004). The final single-step reaction in

cytokinin biosynthesis results in the formation of active free bases from cytokinin ribotides catalyzed by phosphoribohydrolase LONELY GUY (LOG; Figure 2; Kurakawa et al., 2007).

The level of biologically active cytokinins can be fine-tuned through conversion among cytokinin bases, ribosides, ribotides and conjugation with a sugar moiety or irreversible cytokinin degradation (Figure 2; Schmülling, 2004). The first way how plants control the amount of active forms of cytokinins is their reversible or irreversible deactivation by glycosylation. Glucose moiety can be attached to the *N3-*, *N7-* or *N9-* position of the purine ring. This reaction is catalyzed by *N*-glucosyltransferases (NGT) and leads to the formation of *N*-glucosides (Mok and Mok, 2001). The *N7-* and *N9-* cytokinin conjugates are irreversibly deactivated and almost inactive in cytokinin bioassays (Spíchal et al., 2004). A very recent data show that *t*Z *N7-* and *N9*-glucosides are metabolized *in vivo*, efficiently releasing free cytokinin bases (Hošek et al., 2020; Hoyerová and Hošek, 2020). Authors thus refute the generally accepted hypothesis that *N*-glycosylation irreversibly inactivates cytokinins. Cytokinins bearing hydroxyl group on side chain (*t*Z, *c*Z, DHZ) can undergo *O*-glycosylation catalyzed by *O*-glucosyltransferases (ZOGT). Cytokinin *O*-glycosides serve as inactive storage forms of cytokinins and together with kinetin *N3*-glucoside can be converted back to active free bases by β-glucosidase (Brzobohatý et al., 1993; Kiran et al., 2012). Another way to maintain the cytokinin levels is by irreversible degradation via cytokinin oxidase/dehydrogenase (Galuszka et al., 2008). CKXs mediate the cleavage of unsaturated isoprenoid side chain resulting in the production of adenine and the corresponding N^6 side-chain aldehyde (Galuszka et al., 2000). iP, *t*Z and *c*Z and their corresponding ribosides serve as preferred substrates for CKXs, whereas BA, DHZ, *N7*-glucoside and *O*-glucosides showed resistance to CKX activity (Avalbaev et al., 2012; Zalabák et al., 2014).

Cytokinin transport

Cytokinins are highly mobile signalling molecules, which are synthesised in different cell types in both roots and shoots. They can be transported locally at the place of their synthesis (paracrine signal) or throughout the plant in the vascular system (endocrine

signal; Liu et al., 2019). *t*Z-type cytokinins (mostly *t*Z-ribosides) are synthesised predominantly in the root and are transported acropetally through the xylem to the shoot by transpiration flow. On the other hand iP-forms of cytokinins (iP-ribosides, iP-ribotides) are formed mainly in leaves and transported via symplastic pathways in the phloem to the root (Kudo et al., 2010; Zürcher and Müller, 2016).

The molecular mechanisms of cytokinin transport are not completely elucidated. So far, three kinds of proteins are involved in cytokinin transport: purine permeases (PUPs; Gillisen et al., 2000), equilibrative nucleoside transporters (ENTs; Wormit et al., 2004) and G subfamily ATP-binding cassette transporters (ABCG; Ko et al., 2014).

The PUP family consists of over 20 members in *Arabidopsis*. The ability of AtPUP1 and AtPUP2 to import iP and *t*Z was demonstrated in yeast and *Arabidopsis* cells. Apart from free cytokinin nucleobases, they are also able to transport purines, such as adenine or caffeine. However, further genetic or biochemical studies in plants are still required (Gillissen et al., 2000; Burkle et al., 2003). Recently, a cytokinin uptake transporter AtPUP14 was found to be involved in the early stages of development in *Arabidopsis*. Unlike PUP1 and PUP2 which act as a proton-gradient dependent symporter, activity of PUP14 requires the presence of ATP (Zürcher et al., 2016).

The second family of cytokinin transporters, ENTs, include eight homologous members in *Arabidopsis* (AtENT1-8; Li et al., 2003) and four in rice (OsENT1-4; Hirose et al., 2005). Although some of the *Arabidopsis* ENTs when expressed in yeast showed transport activity for the cytokinin ribosides iPR and *t*ZR, their biological roles as cytokinin transporters *in planta* require further experimental studies (Hirose et al., 2008).

Recently, a member of ATP-binding cassette transporters (ABCG14) was proven to be crucial in the loading of *t*Z-type cytokinins into the xylem in *Arabidopsis*. ABCG14 is highly expressed in the root vasculature, localized in the plasma membrane and its loss of function mutants showed to be defective in xylem loading of *t*Z. The impaired transport resulted in accumulation of *t*Z in the roots causing developmental defects, however, exogenous *t*Z application rescued the retarded shoot phenotype. Together with grafting experiments, ABCG14 is recognized as an essential long-distance cytokinin transporter (Ko et al., 2014; Zhang et al. 2014).

Functions of cytokinins

Cytokinins have caught the scientists' interest since their discovery in the middle of the 20th century. They are implicated in a wide range of growth and developmental processes throughout the plant's life (Mok and Mok, 2001; Schmülling, 2004; Sakakibara, 2006; Kieber and Schaller, 2014). Cytokinins are present in all parts of the plant body, however, they are largely abundant in the dividing tissues like root tip, the shoot apex or immature organs. The endogenous concentration of cytokinins is at the low nanomolar range and it can vary depending on the plant organ, age or environmental conditions (Schmülling, 2004; Osugi and Sakakibara, 2015).

The discovery of cytokinins was originally connected with their ability to promote cell division. The initial experiments by Skoog and Miller demonstrated how the ratio of exogenously applied cytokinins and auxins affect stimulation of cell division and callus growth in the plant tissue culture (Skoog and Miller, 1957; Hurný and Benková, 2017).

Interestingly, the different effect of cytokinins on the shoot and root growth is pointing to the diverse regulation mechanisms of cell division in shoot and root meristems. Generally, cytokinins are considered to be involved in the formation, maintenance and growth of shoot apical meristem whereas in the root, exogenous application of cytokinins negatively affects growth by decreasing the rate of cell divisions at the root tip (Ioio et al., 2008; Schaller et al., 2014; Kieber and Schaller, 2010). Moreover, cytokinins act as negative regulators of lateral root formation in *Arabidopsis* by blocking the first divisions of the pericycle founder cells (Li et al., 2006; Werner and Schmülling, 2009).

Apart from cell growth and differentiation, cytokinins also affect chloroplast development, lateral bud development, delay of leaf senescence (through delayed degradation of chlorophyll), apical dominance or floral development (Mok and Mok, 2001; Schmülling, 2004; Sakakibara, 2006). Furthermore, cytokinins have been also linked with plant defence against biotic and abiotic factors such as cold, salt or drought stresses (Nishiyama et al., 2011; Ha et al., 2012; Kieber and Schaller, 2014; Zwack and Rashotte, 2015).

Cytokinin perception and signal transduction

In order to survive constant surrounding changes, all living organisms have developed different, sophisticated signalling mechanisms that allow them to recognize and respond quickly to environmental cues (Mira-Rodado, 2019). In prokaryotic and eukaryotic cells the perception mechanism involved in intracellular signal transduction is protein phosphorylation (West and Stock, 2001). While eukaryotes mostly rely on kinases that phosphorylate Ser (serine), Thr (threonine) or Tyr (tyrosine) residues, phosphorylation cascade in prokaryotes is mediated by the His-Asp phosphotransfer system (Urao et al., 2001). This signalling pathway referred to as the „two-component system" (TCS; Figure 3A), is typically composed of a sensory histidine kinase (HK) and a response regulator (RR). The HK usually forms a homodimer, that perceives environmental stimuli by autophosphorylation of a conserved His (histidine, H) residue and the response regulator propagates the signal by accepting the phosphate on a conserved Asp (aspartic acid, D) and directly regulates the transcription of target genes (Kieber and Schaller, 2014). In 1993, two independent groups reported the discovery of histidine kinases in eukaryotes for the first time (Schaller et al., 2011). One of them employed the plant system and cloned a gene encoding an *Arabidopsis* two-component histidine kinase ETR1 (Ethylene receptor 1), which functions as an ethylene receptor (Chang et al., 1993). The second group used a fungal system cloning the SLN1 (Osmosensing histidine protein kinase) gene from yeast that plays a crucial role in the osmosensing (Ota and Varshavsky, 1993). A more complex version of TCS, the so-called multistep-phosphorelay (MSP), includes two additional phosphotransfers which occur on the His-Asp-His-Asp residues (Figure 3B). Briefly, MSP employs a sensor hybrid histidine kinase, which after autophosphorylation transfers the phosphate to the Asp residue of its own receiver domain. The phosphate is then passed to a histidine phosphotransfer protein (HPt) and subsequently to a response regulator acting as a transcriptional factor activating target genes and performing the desired response. MSP is a signalling mechanism which is, apart from bacteria and fungi, found in plants, specifically in the cytokinin response pathway (Kieber and Schaller, 2010).
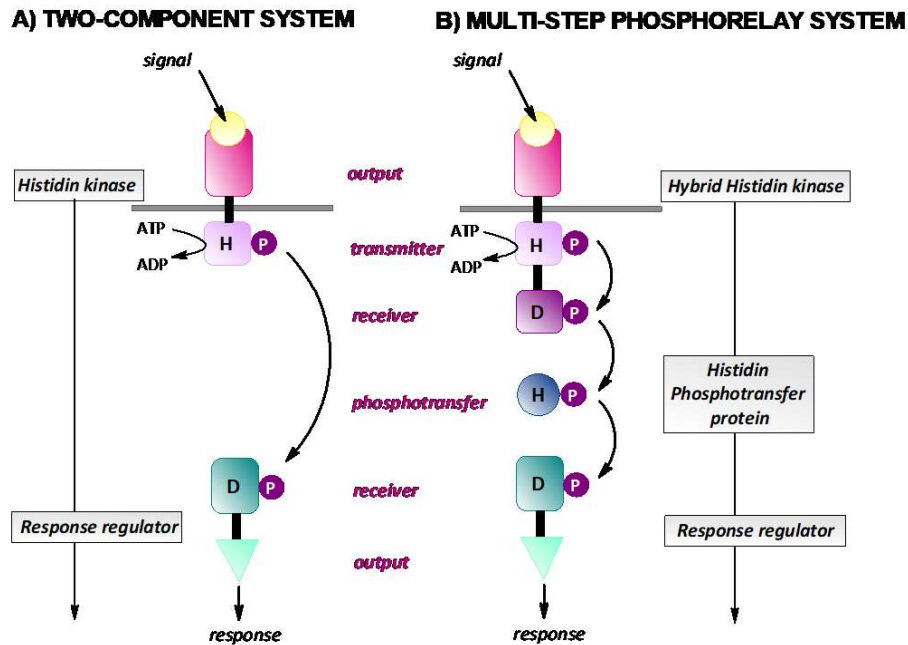
A) TWO-COMPONENT SYSTEM

B) MULTI-STEP PHOSPHORELAY SYSTEM

Figure 3: *Models of a signal transduction in a canonical bacterial two-component system (**A**; TCS) and a multistep-phosphorelay (**B**; MSP) in Arabidopsis. H – His, D – Asp, P – phosphoryl group (figure modified from Sharan et al., 2017).*

Molecular mechanism of cytokinin signalling

In the past decade, enormous progress has been achieved in understanding the mechanisms of cytokinin signalling pathway, numerous receptors and components of the downstream signal cascade were identified and characterized (Lomin et al., 2011). Most of the research on the cytokinin signalling has been done on the plant model *Arabidopsis* which encodes genes for sensor histidine kinases (AHK), histidine phosphotransfer proteins (AHP) and response regulators (ARR) which yielded the current model of cytokinin signalling pathway (Pils and Heyl, 2009; Hurný and Benková, 2017). As previously mentioned, cytokinin signal transduction pathway resembles a modified bacterial TCS system that adapted to sense and respond to environmental stimuli. The first components of the cytokinin signalling pathway are the cytokinin receptors which are localized predominantly in the endoplasmic reticulum (cytokinin receptors and their localization are described in more detail on page 24 and 35,

respectively; Kim et al., 2006, Caesar et al., 2011; Lomin et al., 2011; Wulfetange et al., 2011; Zürcher et al., 2016).

The *Arabidopsis* cytokinin signalling (Figure 4) starts with the histidine kinases serving as cytokinin receptors, concretely AHK2 (ARABIDOPSIS HISTIDINE KINASE 2), AHK3 (ARABIDOPSIS HISTIDINE KINASE 3) and CRE1/AHK4 (CYTOKININ RESPONSE 1/ARABIDOPSIS HISTIDINE KINASE 4). Their structure includes an ~270 amino acid long extracellular so-called CHASE domain (cyclase/histidine-kinase associated sensory extracellular) and a cytoplasmic HK transmitter, a receiver-like domain and a receiver domain (Figure 5; Anantharaman and Aravind, 2001; Schmülling, 2004).
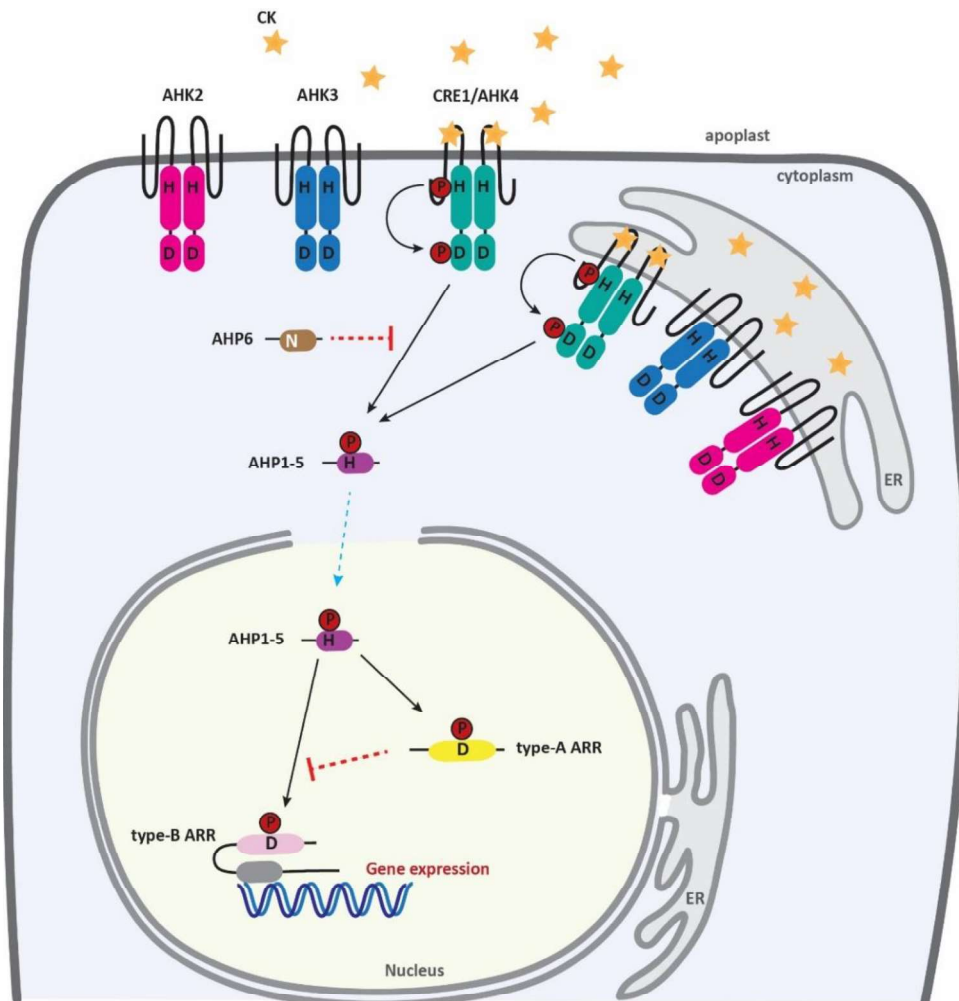

Figure 4: *Model of cytokinin signalling pathway in Arabidopsis thaliana. Cytokinins are perceived by AHK receptors and phosphorelay transmits the phosphate group via AHPs onto the nuclear ARRs (modified from Zürcher and Müller, 2016).*

Cytokinin binding into the CHASE domain leads to a conformational change of the receptor, dimerization, followed by autophosphorylation on the conserved His residue and subsequent transfer of phosphoryl group to a conserved Asp in the receiver domain at the C-terminus of the receptor. Phosphorylated AHKs further transfer this phosphate to a conserved His of the mobile AHP which moves into the nucleus, transferring the phosphate and activating the nuclear localized type-B ARRs. Phosphorylated type-B ARRs serve as transcription factors and regulate the expression of CK-response genes (Inoue et al., 2001; Hwang et al., 2002; Müller and Sheen, 2007).

AHPs (*Arabidopsis* histidine phosphotransfer proteins) serve as signalling intermediates by migrating between the cytosol and the nucleus. The *Arabidopsis* genome encodes six AHPs, each AHP protein consist of about 150 amino acids (Figure 5).
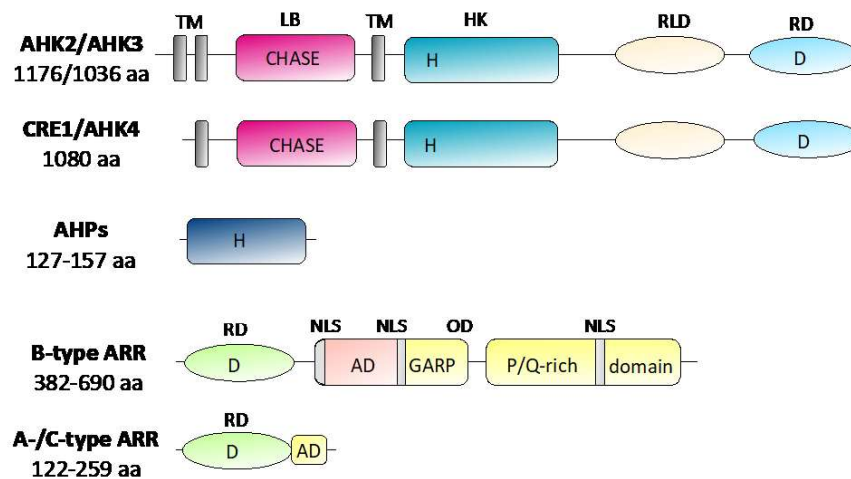
Figure 5*: Structures of the cytokinin receptors and other proteins involved in the cytokinin signalling pathway. aa – amino acids; AD – acidic domain; CHASE – cyclases/histidine kinases associated sensory extracellular; GARP – DNA-binding motif; HK – histidine kinase; LB – ligand binding domain; NLS – nuclear localization signal; OD – output domain; RD – receiver domain; RLD – receiver-like domain; TM – transmembrane domain (figure modified from Heyl and Schmülling, 2003).*

Five of them (AHP1-AHP5) contain the conserved His residue required for activity while, AHP6 is a pseudo AHP, carries Asp and lacks the His phosphorylation site (Tanaka et al., 2004; Hutchison and Kieber, 2007). AHP6 is not able to accept the phosphoryl group and therefore serves as a negative regulator. It counteracts cytokinin

signalling by interacting with the cytokinin receptors and competing with AHP1-AHP5. Furthermore, AHP6 expression is induced by cytokinin, thus providing a negative feedback loop in the signalling pathway (Mähönen et al., 2006a). Interestingly, AHP proteins are actively transported into and out of the nucleus in a CK-independent manner. Therefore, their subcellular cytosolic/nuclear distribution is not dependent on their phosphorylation level (Punwani and Kieber, 2010).

The final components involved in the last step of the cytokinin signalling are the ARRs (*Arabidopsis* Response Regulators). The *Arabidopsis* genome contains 23 ARRs and all of them hold a conserved Asp residue required for their receiver domain phosphorylation (Figure 5). Based on their protein structure and function, ARRs are classified into three subgroups: type-A (ARR3-9, 15-17), type-B (ARR1-2, 10-14, 18-21) and type-C (ARR22 and 24; To and Kieber, 2008; Schaller et al., 2008).

The type-B ARRs are localized in the nucleus and serve as transcription factors (Sakai et al., 2000). Apart from the conserved Asp in their receiver domain they also posses Myb-like DNA binding domain, referred as GARP (glutamic acid/alanine-rich protein) domain at their C-terminus by which they directly bind to target DNA sequences. In addition, the C-terminal region contains nuclear localization signals (NLS) and transactivation, P/Q-rich acidic domains (Imamura et al., 1999; Hosoda et al., 2002). Type-B ARRs function as positive regulators of cytokinin signalling and their expression is not induced by cytokinins. They regulate transcription of immediate-early response genes, including the type-A ARRs genes which are quickly upregulated within minutes after a cytokinin pulse (D'Agostino et al., 2000; Brenner et al., 2005). On the contrary, type-A ARRs serve as negative regulators and attenuate the plant sensitivity to cytokinin. They contain the receiver domain but unlike the type-B ARRs, they lack the DNA-binding and transactivation domains and have only a short acidic C-terminal extension (Mason et al., 2004). Depending on the conditions, type-A ARRs has shown to have different intracellular localization patterns as they can appear in the cytosol, nucleus or both (Imamura et al., 2001; Kiba et al., 2002). The expression of type-A ARRs is induced by phosphorylated type-B ARRs leading in accumulation of type-A ARR proteins. Since both type-A and type-B ARRs interact with AHPs, they may compete for a phosphoryl group of activated AHPs and thus type-A ARRs may suppress the

cytokinin signalling (Dortay et al., 2006). Moreover, type-A ARRs proteins can be stabilised by their phosphorylation as a result of exogenous cytokinin application (To et al., 2007). The third subclass of ARRs is type-C, consisting of only two members. They are structurally similar to type-A ARRs, likewise missing DNA-binding domain and their expression is not activated by cytokinins (Kiba et al., 2004). However, the role of type-C ARRs in cytokinin signalling remains elusive (Kang et al., 2013).

Another set of proteins linked in the cytokinin signalling are cytokinin response factors (CRFs) which interact with the components of MSP and modulate the expression of CK-regulated genes (Cutcliffe et al., 2011). The relationship of CRFs with the rest of the two-component pathway is complex, as some CRFs appear to be targets of type-B ARRs and some appear to interact directly with AHPs (Hallmark and Rashotte, 2019). However, only some CRFs are transcriptionally induced by cytokinin. Interestingly, in the absence of cytokinin, all six CRF-GFP fusion proteins show relatively uniform fluorescence in the cell. After cytokinin application, the signal relocates and accumulates in the nucleus, where it mediates cytokinin-regulated gene expression (Rashotte 2006).

To fine-tune the cytokinin signalling pathway, the activity of cytokinin signalling is tightly controlled and a few inactivation mechanisms are employed. As noted above, the negative feedback loops to reduce sensitivity to cytokinin are through AHP6 (Mähönen et al., 2000a) or type-A ARRs (Dortay et al., 2006). Another feedback loop works through the cytokinin receptor CRE1/AHK4 which holds a dual role; upon cytokinin binding, it acts as a kinase to initiate the MSP resulting in phosphorylation of AHPs. However, in the absence of cytokinin, this receptor acts as a phosphatase and removes phosphate from AHPs to attenuate the cytokinin signalling (Mähönen et al., 2006b). Lastly, upregulation of CKX transcripts by cytokinin might also provide a negative feedback mechanism to control endogenous cytokinin level and the signalling (Werner et al., 2003; Werner et al., 2006).

Characterization of histidine kinases in Arabidopsis thaliana

Analysis of the *Arabidopsis* genome revealed the existence of six histidine kinases which are not ethylene or phytochrome receptors, namely CKI1, CKI2/AHK5, plant

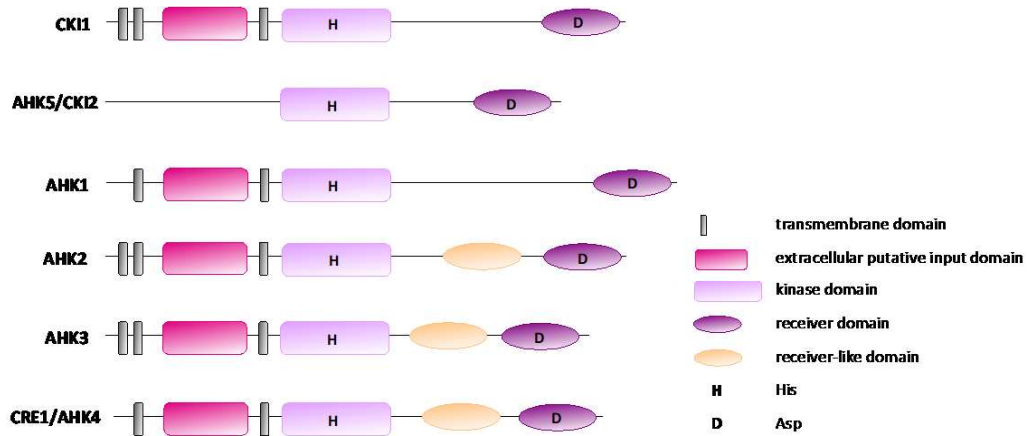osmosensor AHK1, and three cytokinin receptors AHK2, AHK3 and CRE1/AHK4/WOL (Figure 6; Kakimoto 2003).

Figure 6: *Schematic representation of protein domain structures of the AHK family (figure modified from Ueguchi et al., 2001b; Hwang et al., 2002; Grefen and Harter, 2004).*

The first clue regarding the identity of the genuine cytokinin receptor was in 1996 when CKI1 (CYTOKININ INDEPENDENT1) was identified as a protein homologous to the HKs in the bacterial TCS pathway. When CKI1 was overexpressed in callus cultures, it resulted in a typical cytokinin response (rapid cell division, greening and shoot formation) even in the absence of exogenous cytokinin (Kakimoto 1996). CKI1 is expressed in vascular tissues of inflorescence stems and floral organs, especially in procambium cells and localizes to the plasma membrane in tobacco leaf cells (Hejátko et al., 2009). CKI1 is also critical in female gametophyte development and interacts with AHP2, AHP3 and AHKP5 (Hejátko et al., 2003; Liu et al., 2017). However, CKI1 lacks the CHASE domain essential for cytokinin binding and does not bind cytokinins *in vitro.* Moreover, its activity did not fluctuate at all in response to the exogenous cytokinins in *E. coli* assay system (Yamada et al., 2001). Thus, the CK-related phenotype resulting from CKI1 overexpression may arise due to non-physiological crosstalk triggering the cytokinin signalling pathway (Schaller et al., 2008).

The callus formation is also stimulated when CKI2/AHK5 is overexpressed, however, CKI2 is neither thought to be directly involved in cytokinin signalling (Kakimoto, 2003). CKI2 is predominantly expressed in roots and weakly in flowers

(Iwama et al., 2007) and it localizes to both, cytoplasm and plasma membrane (Desikan et al., 2008). AHP1, AHP2 and AHP5, as well as the response regulators ARR4 and ARR7, were identified acting downstream of CKI2 (Mira-Rodado et al., 2012). CKI2 is the only plant HK, which is missing the extracellular domain and N-terminal transmembrane domains but instead contains two coiled domains, which are presumably needed for interaction with other proteins in the cytoplasm (Hwang et al., 2002). The role of CKI2 is in response to biotic and abiotic stresses. It acts to maintain the H_2O_2/redox homeostasis in stomatal guard cells in response to the environmental stimuli (Desikan et al., 2008). Furthermore, CKI2 functions as a negative regulator in the signalling pathway where ethylene and abscisic acid inhibit the root elongation through ethylene receptors in *A. thaliana* (Iwama et al., 2007).

Another HK that is structurally similar to the other AHKs is AHK1. It was initially implicated in osmosensing because its expression complemented a yeast double mutant lacking its two osmosensors and allowed the mutant to grow in high-salt media. The AKH1 transcript is most abundant in roots and its expression is regulated by external osmolarity changes (Urao et al., 1999). Tran et al. (2007) also showed that AHK1 plays role in osmotic stress signalling, germination, and plant growth as a positive regulator in plants. *AHK1* expression was increased under dehydration stress and consequently enhanced drought tolerance of transgenic plants.

With the advent of advanced genetic, biochemical and molecular methods, the first authentic cytokinin receptor, CRE1 (CYTOKININ RESPONSE1) was discovered and independently reported by different research groups at the beginning of the 21st century (Inoue et al., 2001; Suzuki et al., 2001; Ueguchi et al., 2001a; Yamada et al., 2001).

Inoue et al. identified a cytokinin receptor by screening of *Arabidopsis* mutants which exhibited reduced responses to cytokinin. They showed that the mutated gene *CRE1* encodes a histidine kinase. Subsequent analysis showed that root growth in the *cre1* mutant also displayed increased resistance to inhibition by cytokinin. Moreover, expression of CRE1 successfully rescued the growth defect of a yeast strain lacking the SLN1 in a CK-dependent manner. These results provided convincing evidence that CRE1 is, indeed, a cytokinin receptor (Inoue et al., 2001). Moreover, CRE1 was shown

to be capable to serve as a cytokinin sensor in fission yeast and *E. coli* (Suzuki et al., 2001). Complementation analysis and sequencing revealed that *CRE1* was identical to the previously described *AHK4* (ARABIDOPSIS HISTIDINE KINASE4) and *WOL* (WOODEN LEG) genes. The *wol* mutant phenotype was published earlier showing defects in the root vasculature including a reduction in the total number of cells and lack of phloem (Scheres et al., 1995). This disruption was caused by a single amino acid Thr278Ile substitution in the putative receptor domain, therefore it was proposed that the WOL protein is a receptor required for vascular morphogenesis (Mähönen et al. 2000). In addition to the *CRE1/AHK4/WOL* gene, sequence comparison and functional studies revealed two other cytokinin receptors encoded in the *Arabidopsis* genome, namely AHK2 and AHK3 (Ueguchi et al., 2001a; Yamada et al., 2001). Cytokinin receptors have been extensively studied in the model organism *Arabidopsis thaliana*. A wide range of species, including plants and prokaryotes, showed to possess cytokinin receptor genes such as maize (Yonekura-Sakakibara 2004; Lomin et al., 2011), tomato (Shi et al., 2013), rice (Ito and Kurata, 2006), poplar tree (Jaworek et al., 2020), potato (Lomin et al. 2018a), apple tree (Daudu et al., 2017), mosses (Gruhn et al., 2014), cyanobacteria (Frébortová et al., 2017; Kabbara et al., 2018) and many others.

All three cytokinin receptors are transmembrane proteins sharing a similar structural organization. They are composed of an extracytosolic region for signal input, a transmembrane region and a cytosolic region for signal output (Figure 6). Their protein structure consists of either two (CRE1/AHK4) or three (AHK2, AHK3) transmembrane segments on the N-terminal part enclosing a CHASE domain, followed by a cytosolic region containing a histidine kinase domain, a non-active receiver-like domain and a receiver domain at the C-terminus (Ueguchi et al., 2001a; Grefen and Harter, 2004; Heyl et al., 2011). The CHASE domain is responsible for ligand binding and is an exclusive element of the cytokinin receptors (Anantharaman and Aravind, 2001). Based on proteomics approach and binding assay, four amino acids were identified to be crucial for cytokinin sensing. Point mutations within the CHASE domain were found to cause loss of function or decrease of cytokinin binding to the AHK4 CHASE domain (Heyl et al., 2007).

In 2011, the crystal structures of CRE1/AHK4 sensor domain in complex with various cytokinin ligands (including iP, *t*Z, BA, DHZ, Kin and TDZ) was described (Figure 7; Hothorn et al., 2011). The AHK4 ligand-binding pocket is occupied by both, the adenine portion of iP and its isopentenyl tail, which is found deeply inserted into the cavity. Hydrogen bonds are established between Asp262 and atoms in the N^6 and the *N7* positions of the adenine ring and these interactions seem to be critical for receptor function. Additionally, polar interactions are mediated by water molecules, which in turn contact the *N1* and *N3* atoms of the cytokinin iP. The structure with bound *t*Z reveals that its hydroxylated isopentenyl side chain establishes an additional hydrogen bond with Thr294 (Hothorn et al., 2011; Steklov et al., 2013).
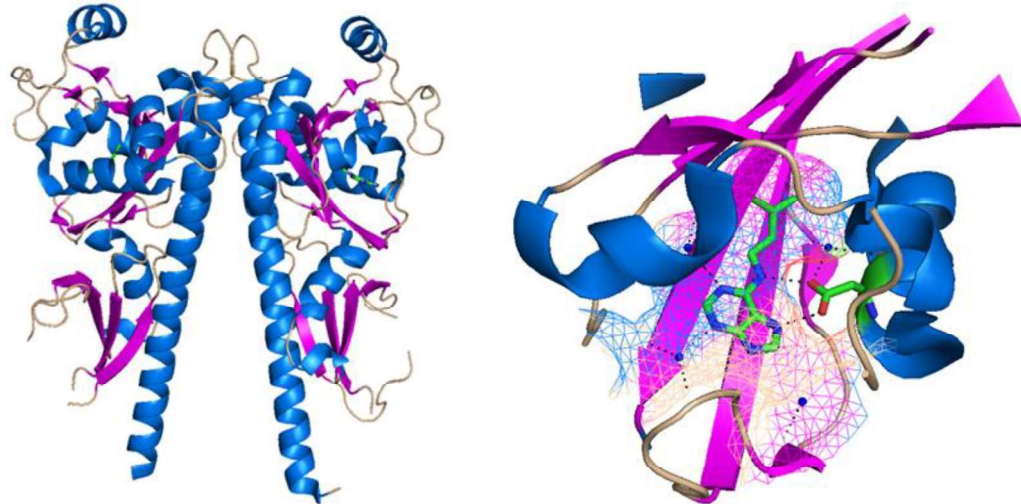
Figure 7: *CRE1/AHK4 sensor domain in complex with iP. **Left** – ribbon structure of the sensor domain homodimer. **Right** – detail of the cytokinin binding pocket complexed with iP (blue-green). N^6 and N7 atoms of the ligand form hydrogen bonds (black dashed lines) with Asp262 (red stick), water molecules (blue balls; pdb 3T4J; figure modified from Hothorn et al., 2011).*

The fact that the AHK4 fragment co-crystalled with cytokinins helped to understand the different affinities for various ligands. In general, all three receptors are sensitive to free bases but differ in their recognition of cytokinin metabolites (Spíchal, 2012). A detailed comparison of the ligand preference of AHK3 and CRE1/AHK4 receptors revealed that *t*Z, iP and TDZ belong to the most potent cytokinins in *Arabidopsis*. Moreover, the specific binding of *t*Z to both receptors is pH

dependent. Specifically, AHK3 receptor is more sensitive to pH change than CRE1/AHK4 (Romanov et al., 2006). On the other hand, the products of cytokinin metabolism show less affinity to the cytokinin receptors. Furthermore, the *cZ* presents a significant reduction in activity compared to the *tZ* in *Arabidopsis*. Kin and BA, that belong to the group of aromatic cytokinins widely used in tissue cultures, showed moderate activity in the bacterial binding assay. More concretely, the sequences of the different cytokinin compounds affinity for the cytokinin receptors were established as follows: for AHK4, iP ≥ *t*Z > TDZ > *t*ZR > iPR > BA > DHZ > *c*Z >> Ade ~ *t*ZOG; for AHK3, *t*Z > TDZ > *t*ZR > DHZ > iP > *c*Z > BA > iPR >> Ade ~ *t*ZOG, and for AHK2, iP >TDZ > *t*Z > iPR > *t*ZR > BA > *c*Z > DHZ >> Ade ~ *t*ZOG (Spíchal et al., 2004; Romanov et al., 2006; Stolz et al., 2011; Lomin et al., 2012). However, Lomin et al. (2015) showed that cytokinin ribosides displayed a strong affinity reduction to AHK receptors in the plant assay system indicating that these derivatives have non- or very weak cytokinin activity. This suggested that the free bases are the main biologically active cytokinin forms. It was suggested that in the previous experiments made in *E. coli*, the cells quickly convert ribosides into the corresponding bases which in turn activated the receptors. The crystallographic structure supported the absence of hormonal activity of *t*Z ribosylated at the *N*9 position. The riboside moiety does not fit into the binding pocket when the *N3*, *N7* and *N9* positions of the adenine ring are buried inside (Hothorn et al., 2011).

Cytokinin receptors are involved in the regulation of various developmental aspects. All three cytokinin receptors show a high level of redundancy in plant growth and development, their functions partially overlap and each receptor contributes to a different extent to cytokinin responses (Ueguchi et al., 2001a; Nishimura et al., 2004; Higuchi et al., 2004; Riefler et al., 2006). The study of individual, double or triple loss-of-function cytokinin receptor mutants has been a common tool to determine the biological functions of individual receptors. Each of the cytokinin receptors has been shown to have different expression pattern *in planta*. While AHK2 and AHK3 are primarily expressed in aerial tissues (AHK2 in leave veins, petioles, inflorescence stems, flowers and siliques, moderately in the roots; AHK3 ubiquitously expressed in root and shoot tissues including leaves, inflorescence stems and flowers), CRE1/AHK4 shows a

high level of expression predominantly in the root, concretely in the vascular cylinder and pericycle (Ueguchi et al., 2001b; Mähönen et al., 2006b, Higuchi et al., 2004). In general, knock-outs of a single receptor result in minor or any defective phenotype (only a slight reduction of rosette size in *ahk3* mutant plants; Figure 8A). Additionally, different double loss-of-function mutant combinations show some phenotypes (Higuchi et al., 2004; Riefler et al., 2006).

Plants lacking all three cytokinin receptors exhibit severe phenotypes, including dwarfism, retarded root growth, larger seed size due to increased size of the embryos or altered time of germination (Figure 8A, B). An interesting phenotype can be observed in the roots - at 14 DAG (days after germination), the *cre1* mutant and the *ahk2ahk3* double mutant show longer primary root when compared to WT (wild type; Figure 8C). Surprisingly, in all double mutants, the root branching is enhanced, but *ahk2ahk3* mutants have more than twice the number of lateral roots in comparison with WT, as a result of disrupted cytokinin signalling. Furthermore, all double mutant plants, especially *ahk2ahk3*, form secondary lateral branches which are completely absent in WT (Riefler et al., 2006).

The cytokinin sensitivity of roots of all single mutants and mutant combinations has been described (Figure 8D). When cytokinin applied, *cre1* mutant exhibit CK-insensitive root growth. However, the root growth of *ahk2* and *ahk3* single mutants and the *ahk2ahk3* double mutant is sensitive to cytokinin in a similar manner to WT plants, indicating that the roots of *ahk2* and *ahk3* single mutants respond normally to cytokinin. This result confirms a major role of CRE1/AHK4 in sensing of exogenous cytokinin in the primary root. At last, the triple ahk mutant seems insensitive to cytokinin suggesting a lack of a mechanism for cytokinin perception in absence of the three cytokinin receptors (Ueguchi et al., 2001a; Higuchi et al., 2004; Nishimura et al., 2004; Riefler et al., 2006).
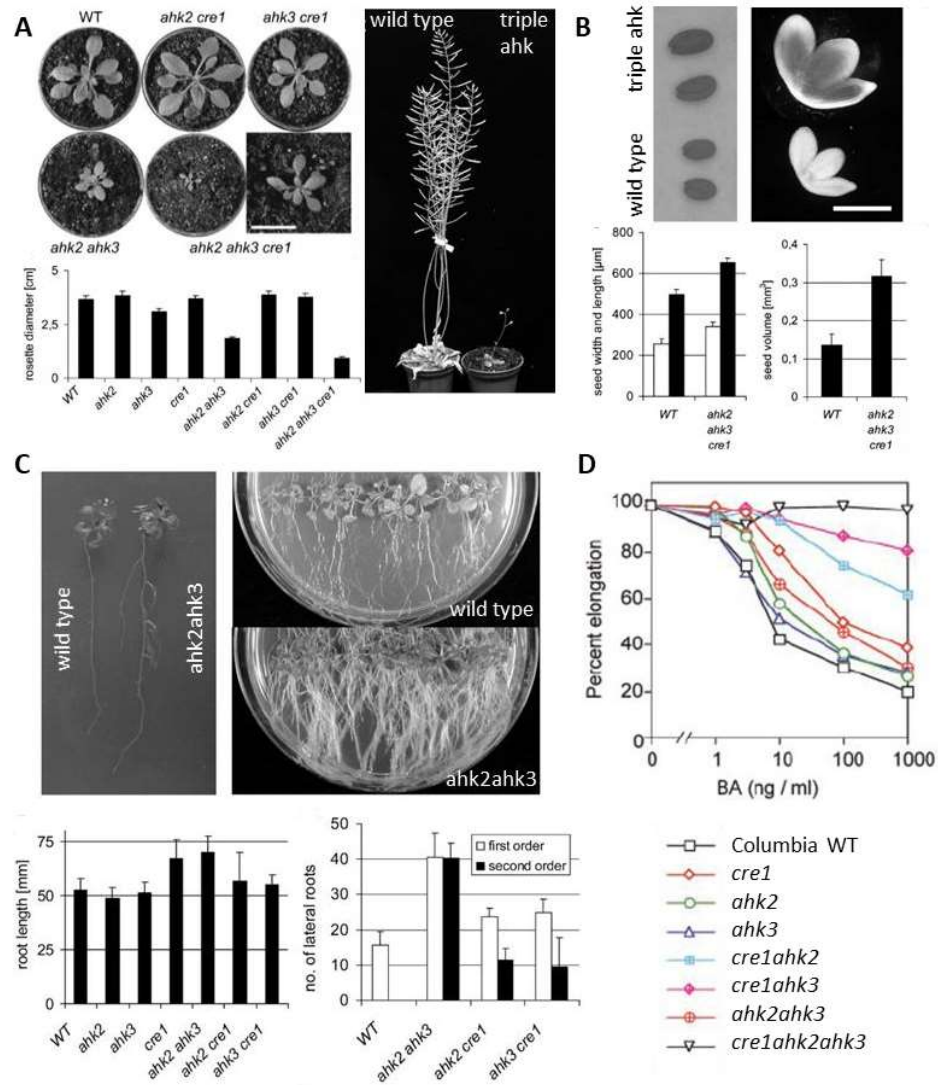
Figure 8: *Phenotypes of cytokinin receptor mutant plants. A – rosettes of WT and ahk mutant plants grown on soil at 25 DAG (left top); rosette size at 25 DAG (left bottom); triple ahk mutant plant at 70 DAG compared to WT plant (right); B – seeds (left) and embryos (right) of the triple ahk mutant compared to the WT and their measured width, length and volume (bottom); C – root system of WT and ahk2ahk3 mutant plants, 14 DAG (left top) and 28 DAG (right top); elongation of primary roots 14 DAG (left bottom) and number of lateral roots 14 DAG (right bottom); D – Elongation of root of ahk mutants in the presence of increasing concentration of BA, root length of each genotype without cytokinin is set as 100 % (figures modified from Riefler et al., 2006; Higuchi et al., 2004).*

Molecular tools for analysis of cytokinin signalling activity and cytokinin bioassays to study receptor affinity and activation

To study cytokinin signalling, various molecular methods have been developed such as ARR5::GUS, TCS::LUC, TCS::GFP, qRT-PCR or cytokinin bioassays (D'Agostino et al., 2000; Suzuki et al., 2001; Spíchal et al., 2004; To et al., 2007; Müller and Sheen, 2008; Zürcher et al., 2013). Generally, these systems are based on a rate of expression of particular genes involved in the cytokinin signalling. In *Arabidopsis*, one of the most common reporter gene used is *ARR5*, and more specifically, the ARR5::GUS gene expression reporter. This assay is based on the ability of cytokinin to induce gene expression of type-A ARR, concretely *ARR5*, which shows the greatest induction in response to cytokinin (D'Agostino et al., 2000). ARR5::GUS bioassay employs the *GUS* (β-glucoronidase) reporter gene under the control of the CK-dependent promoter of the *ARR5* gene. The assay is specific for cytokinins, sensitive, rapid (a rise in the *ARR5* transcript occurs within 10 min) and is also widely used to monitor the distribution of cytokinin activity in different tissues (D'Agostino et al., 2000). Additional methods to study genes expression regulated by cytokinin signalling is the qRT-PCR that allows a quantitative analysis of various ARR genes expression, especially types-A which are induced by type-B ARRs serving as positive regulators of cytokinin signalling (To et al., 2007).

Another system to monitor transcriptional activation in response to a cytokinin stimulus is a synthetic promoter, a two-component output sensor (TCS). The reporter system harbours concatemeric 5′-(A/G)GAT(T/C)-3′ type-B ARR binding motifs (Hosoda et al., 2002). TCS-based reporters allow specific and sensitive detection of activated type-B ARR and thus can be used as a proxy to monitor the cytokinin-initiated signalling. This method is widely used *in planta* to visualise the cytokinin response in different developmental contexts (Liu and Müller, 2017). One of the TCS reporter systems is TCS::LUC; when transiently transfected into *Arabidopsis* mesophyll protoplasts serve as a cellular model for CK-responsive cells. Therefore, this system is ideal for screening various candidate genes potentially functioning in cytokinin signalling under diverse treatments (Müller and Sheen, 2008). Afterwards, an alternative TCS reporter was introduced, the TCS::GFP. The TCS::GFP system is

commonly used as an instrument to uncover roles of cytokinin and to report the transcriptional output profile of phosphorelay signalling networks in *Arabidopsis*. Initially, the TCS-induced expression system had few limitations: weak expression in certain developmental contexts (in the embryo sac, in the vasculature and in the shoot) or progressively reduced GFP expression with subsequent generations. Later, an improved version with an increased number of binding elements TCSn::GFP was published (Zürcher et al., 2013). The corrected version TCSn, compared to TCS, shows much brighter GFP signal, stable GFP expression during propagation and higher sensitivity to phosphorelay signalling in *Arabidopsis* assays (Zürcher et al., 2013).

Shortly after the discovery of cytokinin receptors in 2001, two significant bacterial cytokinin tests for detecting the ability of cytokinin receptors of *Arabidopsis thaliana* and *Zea mays* to perceive cytokinins *in vitro* were introduced (Figure 9; Suzuki et al., 2001; Spíchal et al., 2004).
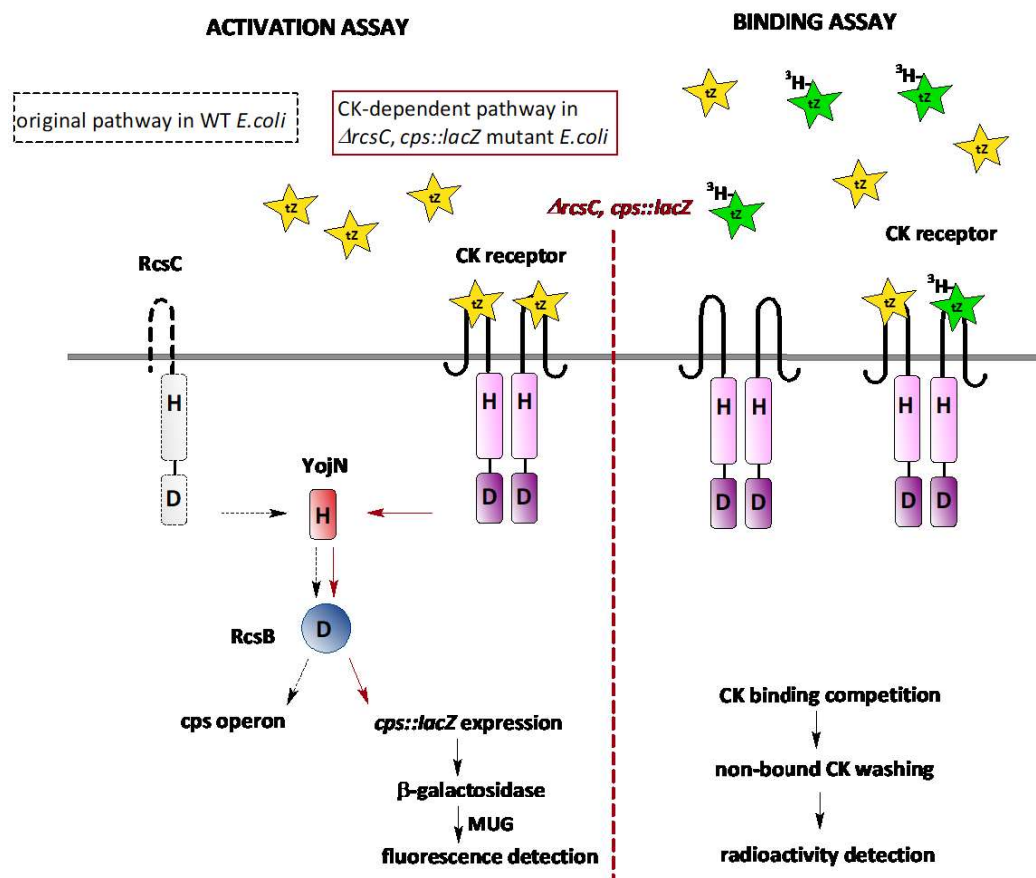

Figure 9: *Two bacterial assays based on the expression of AHK in E. coli mutant strain to measure activity and affinity of cytokinin receptors. D – receiver domain, H – histidine*

kinase/histidine phosphotransfer protein (red), MUG – 4-methyl umbelliferyl galactoside; yellow stars – non-labelled CK, green star – radioactively labelled cytokinin (figure modified from Suzuki et al., 2001; Spíchal, 2011).

Generally, *E. coli* bacteria posses Rcs-phosphorelay system resembling the *A. thaliana* cytokinin signalling pathway. (Suzuki et al., 2001). AHK histidine kinases share some structural features with the bacterial RcsC receptor: the part of the two-component signalling pathway that leads to activation of the cps (capsular polysaccharide synthesis) operon through phosphorylation of the Hpt element YojN, and the response regulator RscB (Takeda et al., 2001; Spíchal, 2011). In this assay, AHK3 or CRE1/AHK4 receptors are cloned into the *ΔrcsC*, *cps::lacZ* mutant strain (Suzuki et al., 2001). These bacteria are able to detect cytokinin activity because the receptor couples to an *E.coli* HPt which in turn activates a *cps::lacZ* reporter gene. Produced β-galactosidase can be determined quantitatively with MUG (4-methyl umbelliferyl galactoside) serving as a fluorogenic substrate (Romanov et al., 2006; Spíchal, 2011).

To study the ligand affinity of cytokinin receptors, the same *E. coli* mutant strain expressing AHK receptor is used. The assay is based on competition of not radioactively labelled cytokinin and radioactive ^{3}H-labelled cytokinin ([^{3}H]*t*Z); the unbound compounds are washed out and radioactivity is measured. The affinity constant values (K_D) show the concentration of ligand displacing 50 % of the bound [^{3}H]*t*Z and can be used to compare different ligand affinities (Romanov et al., 2005; Romanov and Lomin, 2009).

Localization of cytokinin receptors

Signal transduction pathways can be regulated by changing subcellular localization of the participating proteins, thus influencing their functioning mode in the cell (Dortay et al., 2008). Plant receptor kinases located on the cell surface mediate plenty of responses according to developmental and environmental inputs. During their lifespan, receptors undergo a complex set of subcellular trafficking events. The endoplasmic reticulum is a place of protein synthesis and maturation, while delivery to the plasma membrane involves passage through the Golgi apparatus. Receptors are eventually inserted into the plasma membrane to perform their function as sensors. Retrieval from the PM comprises of the endocytic pathway and subsequent sorting, either for targeting to late endosomes and eventual degradation in the vacuole or for recycling back to the PM (Geldner and Robatzek, 2008).

Perception of plant hormones occur at different sites of the cell: ethylene receptors are localized in the ER (Chen et al., 2002), brassinosteroid receptors are at the PM (Friedrichsen et al., 2000; Irani et al., 2012) and other hormones like auxins, ABA (abscisic acid) or GAs (gibberellins) possess soluble receptor proteins in the cytosol and/or nucleus (Shan et al., 2012; Larrieu and Vernoux, 2015). The subcellular localization of cytokinin receptors and the initiation of signalling are particularly relevant to understand the cellular architecture of the cytokinin system. However, the sites of cytokinin perception and signal transduction are still under extensive study since the discovery of cytokinin receptors in 2001 (Romanov et al., 2018). The first model of *Arabidopsis* cytokinin signalling presumed the receptor localization at the plasma membrane. This suggestion was based on the prediction of a bioinformatic approach using the PSORT program (Nakai and Horton, 1999). However, the certainty of the prediction for localization in the plasma membrane was 0.6 in all cases, which is far from the maximum of 1 (Ueguchi et al., 2001b). Also, cytokinin receptors were considered to be localized at the PM because of the structural similarity with the sensor His kinase localization in bacteria and yeast (Inoue et al., 2001; Ueguchi et al., 2001a). Moreover, His kinase ethylene receptors were presumed to reside at the PM too (Hirayama and Alonso, 2000). The very first experimental evidence of cytokinin

receptor localization came in 2006 when Kim et al. showed transient expression of an AHK3-GFP fusion at the PM in *Arabidopsis* protoplasts (Figure 10A). However, the authors provided only low-resolution supplementary data in a semi-artificial system. Any use of PM/ER markers supporting AHK plasma membrane localization was missing (Kim et al., 2006).

A few years later, three articles focused on subcellular localization of cytokinin receptors were published (Caesar et al, 2011; Lomin et al., 2011; Wulfetange et al., 2011). Fluorescent cytokinin receptor fusion proteins AHK3-GFP and CRE1/AHK4-GFP expressed under the control of 35S constitutive promoter in the epidermal cells of tobacco leaves pointed to the majority of overexpressed cytokinin receptors to be localized inside the cell within the ER membranes (Figure 10B). In the case of AHK2, neither N- nor C-terminal fusion with GFP led to a detectable signal *in planta*. Until now, any attempts to generate transgenic *Arabidopsis* lines stably expressing the receptor-GFP fusion under the control of the 35S promoter have not been successful, most likely due to cellular toxicity of the gene products (Wulfetange et al., 2011).
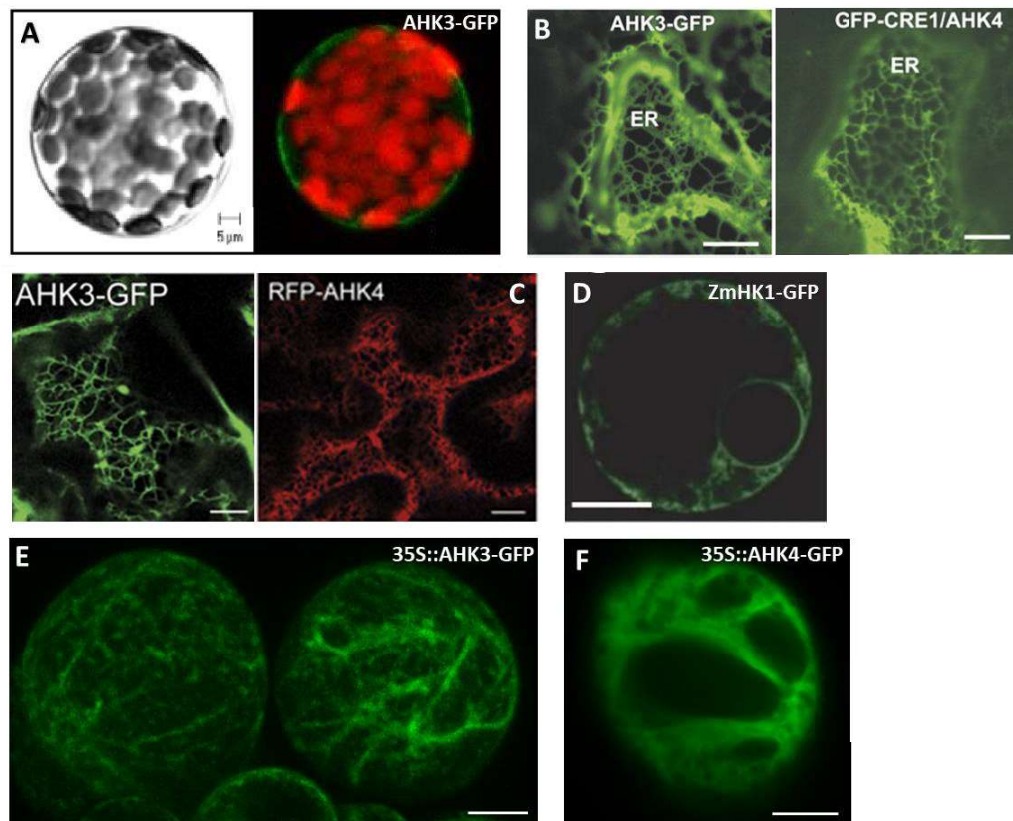
Figure 10: *Localization of cytokinin receptors.* ***A*** *− transient expression of AHK3-GFP in the Arabidopsis protoplasts (Kim et al., 2006);* ***B*** *− transient expression of AHK3-GFP and CRE1/AHK4-GFP in the epidermal cells of tobacco leaves (Wulfetange et al., 2011);* ***C*** *− transient expression of AHK3-GFP and CRE1/AHK4-RFP of tobacco leaf cells (Caesar et al., 2011);* ***D*** *− transient expression of ZmHK1-GFP in maize protoplasts (Lomin et al., 2011);* ***E, F*** *− stable 35::AHK3-GFP expression (**E**) and transient 35::CRE1/AHK4-GFP expression (**F**) in the Arabidopsis Ler suspension culture (Kubiasová, 2014).*

The localization of *Arabidopsis* receptor-fluorescent protein fusions in the ER was further supported with experiments of transiently transformed tobacco leaf epidermal and *Arabidopsis* cotyledon cells (Figure 10C; Caesar et al., 2011) and of the maize receptor ZmHK1 expressed in the protoplasts derived from maize leaves (Figure 10D; Lomin et al., 2011). Similar results corresponding to the ER network were obtained also with *Arabidopsis* L*er* cell suspension culture stably expressing fluorescently labelled AHK3 (Figure 10E) or transiently expressing CRE1/AHK4 receptor under the control of constitutive promoter (Figure 10F; Kubiasová, 2014).

Also, other biological and biochemical methods were used to investigate the location of cytokinin receptors. Isolated membranes (PM fraction and endomembrane fraction) separated by the two-phase partitioning method showed that [^{3}H]*t*Z binds with high affinity in the fraction containing endomembranes, both in *Arabidopsis* (Wulfetange et al., 2011) and maize (Lomin et al., 2011). Moreover, fractionation of cell membranes by sucrose gradient centrifugation of AHK-Myc fusion proteins under the control of their own promoters showed, that AHK2-Myc and AHK3-Myc fusion proteins were also detected in the endomembrane fraction. Altogether these data suggest that the endomembrane system is the main compartment for localization of cytokinin receptors (Wulfetange et al., 2011). In addition, AHK3 protein was shown to be susceptible to EndoH treatment (Caesar et al., 2011). Endoglycosidase H cleaves the asparagin-linked high-mannose type and hybrid oligosaccharides that are typical for ER glycoproteins but is not specific for highly processed complex-type oligosaccharides that are associated with the post-Golgi secretory pathway. This observation was used as an argument for ER localization of the AHK3 receptor (Caesar et al., 2011). However, these data have to be carefully considered since other proteins localized on PM (e.g. brassinosteroid receptor BRI1) are also sensitive to endoglycosidase H (Jin et al., 2007; Hong et al., 2008).

As Romanov and colleagues already demonstrated in the bacterial assay, the binding of cytokinin to the receptor is pH-dependent. The maximal hormone-binding activity is close to a neutral or weak alkaline pH, and the ability to bind the cytokinin decreases with decreasing pH. An acidic pH is characteristic for the apoplast whereas neutral or weak alkaline pH is typical for the cytoplasm and the endoplasmic reticulum. These findings lead to a suggestion, that cytokinin receptors may function inside of the cell (Romanov et al., 2006). The authors carried out an analysis of the pH dependence of numerous plant proteins with their known subcellular localization. The analysis showed that the pH optimum of the protein activity strongly corresponds to the compartment where this protein is operating. Therefore, proteins functioning in the ER should have an optimum close to pH 7-8, whereas proteins operating in the apoplast should possess their optimum mainly in the range of pH 4.5-6 (Romanov et al., 2018). This rule helps to predict the localization of active proteins residing in compartments with contrasting pH. The *Arabidopsis* cytokinin receptors AHK2 and AHK3 show a drastic decrease in hormone-binding activity at pH 5. (Romanov et al., 2006; Lomin et al., 2015). Also, after 1h incubation at pH 5, the ligand-binding capacity of AHK3 is not restored upon transfer to the optimal pH conditions. This indicates an irreversible rearrangement in the ligand-binding domain of AHK3 caused by incubation at pH 5. Results from analysis and the cytokinin binding assays performed in various pH corroborate, that cytokinin receptors not only reside but also operate in the ER (Lomin et al., 2015; Romanov et al., 2018). On the other hand, it would be premature to exclude the presence of functioning receptors within the PM since at pH 5 the CRE1/AHK4 receptors, and its maize ortholog ZmHK1, retain a noticeable ligand-binding ability corresponding to 23.4% and 37.2% of the binding at pH 7, respectively (Lomin et al., 2015). Also, the *ahk2ahk3* mutant plants expressing only CRE1/AHK4 receptor showed higher specific binding in the PM fraction than in the endomembranes fraction (Wulfetange et al., 2011). Moreover, in their recently published work, Jaworek and colleagues (Jaworek et al., 2020) show the influence of pH on the binding strength of cytokinins to the receptors from poplar. Authors showed that binding of cytokinin to PcHK3 (AHK3 ortholog) increases towards alkaline pH values, whereas binding of PcHK4 (CRE1/AHK4 ortholog) displays the strongest ligand

binding ability at pH 5.5. These findings support the idea that CRE1/AHK4 can effectively sense cytokinins from the apoplast.

The first step of cytokinin signal transduction includes a transfer of a phosphate group from the activated receptor to a phosphotransfer protein. Lomin et al. (2018b) recently investigated the interaction of a cytokinin receptor with different AHPs in the epidermal tobacco cells. To study the subcellular localization of receptor-AHP interaction, bimolecular fluorescence complementation (BiFC) experiments were performed. Receptor-AHP pairs interacted in every possible combination in a pattern reflecting the ER localization. Moreover, receptor dimers, considered as an active form of the receptors, were also detected in the ER. Based on the BiFC and protease protection assay, the catalytic part of the receptor is exposed to the cytoplasm whereas the hormone-binding module is oriented with its N-terminal portion facing the ER lumen. This topology is favourable for receptor signalling from the ER membrane. Additionally, *in vitro* kinase assay for visualising the phosphorylation of AHPs was tested using the different membrane fractions. The detected cytokinin-dependent phosphotransfer activity was much higher in the ER-enriched fraction. However, the existence of a small pool of active receptors in the PM was not totally excluded (Wulfetange et al., 2011; Lomin et al., 2018b).

One of the features of how cytokinin homeostasis is maintained is by cytokinin-degrading enzymes CKXs. In *Arabidopsis*, the cytokinin breakdown is controlled by seven CKX proteins (encoded by *AtCKX1-AtCKX7*). They differ in the subcellular localization which displays the importance of compartmentalization of cytokinin metabolism for cytokinin action and plant development (Frébort et al., 2011). Moreover, all of the AtCKX isomers have pH optimum in the neutral and weakly basic pH pointing to their intracellular place of activity (Galuszka et al., 2007). The importance of CKX-mediated degradation at different sites of the plant cell and its effect on plant growth was described (Werner et al., 2003; Niemann et al., 2018). Analysis of the subcellular localization of CKX1- and CKX3-GFP fusion proteins pointed to the ER and occasionally vacuole as a place of their activity. When overexpressed, the mutant plants showed retarded shoot development. These results propose ER as a relevant site of cytokinin degradation with an apparent impact on cytokinin signalling

(Werner et al., 2003; Niemann et al., 2018). On the other hand, CKX2 resides in the ER and the apoplast. Its overexpression shows milder shoot phenotype compared to CKX1 and CKX3 overexpressors. This result suggests, that the cytokinin pool affected by CKX2 has less impact on the signalling in the shoot. These phenotypic consequences support the ER as a main cellular platform for active cytokinin receptors at least in some tissues (Romanov et al., 2018). However, the localization of individual *Arabidopsis* CKX proteins is still under study (Werner et al., 2003; Frébort et al., 2011; Hoyerová and Hošek, 2020).

The advantages of ER localization as a place of cytokinin perception and transduction are already widely discussed (Wulfetange et al., 2011; Lomin et al., 2018b; Romanov et al., 2018). The velocity and reliability of the cytokinin signalling could be increased due to the better interaction with AHPs. AHPs are distributed withing the whole intracellular space therefore it would shorten the distance for reaching the nucleus to trigger the cytokinin response genes. Moreover, such localization could be from an energetic point of view more efficient and alleviate the disadvantages caused by the long distance export to the PM through the secretory system. Finally, ER-localized receptors would also facilitate intracellular hormonal cross-talk as some other plant receptors are also localized inside the cell (Chen et al., 2002). Nevertheless, the hormone-binding CHASE domain part of the cytokinin receptor would be faced to the lumen of ER but at the moment it stays unclear how cytokinins penetrate the ER lumen and reach the receptor sensor module located inside the ER (Romanov et al., 2018).

Even though most of the results published on the subcellular localization of the cytokinin receptors primarily rely on gene expression studies, using transient systems and constitutive promoters, there is nevertheless strong experimental evidence that a bulk of cytokinin receptor intracellular pool is present within the ER (Caesar et al, 2011; Lomin et al., 2011; Wulfetange et al., 2011). However, there is also a possibility that some part of the receptors reaches the PM - this should also be considered even though direct evidence of cytokinin receptor localization at the PM has not been demonstrated yet. In that case, cytokinins from apoplast would directly interact with the PM-localized binding domain and trigger the signalling at the surface of the cell

(Romanov et al. 2018). As previously published, localization studies of the cytokinin receptors were performed only using protoplasts (transient expression assays); the localization of fusion cytokinin receptors AHK3-GFP and AHK2-GFP were observed in the above-group parts of the plant using transiently transformed *Arabidopsis* cotyledon cells (Caesar et al., 2011) and transiently transformed tobacco epidermal leaf cells (Wulfetange et al., 2011), all in the differentiated stages. Any clear evidence of localization of stable expression of CRE1/AHK4 cytokinin receptor in various cell types is missing (Romanov et al., 2018). The signalling of the receptors starting at the plasma membrane is supported by the observation, that the CRE1/AHK4 receptor interacts in the yeast-two hybrid system with proteins (adaptin, ADL1A, GNOM) involved in vesicular trafficking. The identification of these interactors could show that the cytokinin receptors are not only located at the PM but also in other cellular compartments supporting an intracellular transport of cytokinin receptors between PM and endosomes (Dortay et al., 2008; Wulfetange et al., 2011). A recent publication by Zürcher et al. (2016) shed light on the activity of cytokinin receptors at the PM. As a model, they used *Arabidopsis* heart-stage embryos of synthetic cytokinin reporter TCSn::GFP. Authors reported that a member of the transporter PUP family (PUP14) is involved in the modulation of the cellular cytokinin signalling. Interestingly, a PM-localized PUP14 imports bioactive cytokinins inside the cell in order to suppress the response to cytokinin. Moreover, PUP14 was expressed only in the cells that failed to respond to cytokinins. Also, silencing of *PUP14* produced ectopic cytokinin responses causing morphological defects. In the scenario proposed by Zürcher and colleagues, apoplastic cytokinins are important to initiate the PM-related signalling response, whereas the cytoplasm represents a sink for non-functional bioactive ligands. To test this hypothesis, authors performed experiments comparing the effect of PUP14 uptake with the effects of CKXs differentially targeted (apoplast/cytoplasm) on the cytokinin signalling response. *Arabidopsis* protoplasts transiently transfected with CKX2 (secreted to apoplast) were able to attenuate the cytokinin response triggered by *t*Z but not by the degradation-resistant BA. In contrast, CKX2 lacking the N-terminal signal sequence peptide, thus localized to the cytoplasm, did not affect the cytokinin response. Similar results were obtained with the cytosolic localized CKX7. These results

suggest that apoplastic, but not cytoplasmic cytokinins, initiate the signalling (Zürcher et al.; 2016). Nevertheless, the affinity of the PUP transporters and the cytokinin receptors to the ligands would need further investigation to fully support the Zürcher et al. conclusions (Durán-Medina et al., 2017; Kang et al., 2017; Romanov et al., 2018).

Currently, it is clear, that the subcellular localization of cytokinin receptors is only partially resolved. Based on the published results, the AHK receptors are localized predominantly in the membranes of ER (Caesar et al, 2011; Lomin et al., 2011; Wulfetange et al., 2011). However, recent results pointed to the possibility of different subcellular localizations including the PM (Zürcher et al.; 2016). Romanov et al. proposed multiple signalling pathways that may include different localization of the cytokinin receptors, including the PM. Thus, it could be speculated that the different localization of cytokinin receptors and perception of active cytokinin may respond to a different organ or tissue and/or developmental stage, e.g. meristematic activity, differentiation, etc. Also, individual cytokinin receptors might differ in localization within the cell dependent on the cell/tissue type. Therefore, to define the different subcellular origin of cytokinin signalling of all AHK receptors remains elusive and needs to be investigated (Romanov et al., 2018).

Design, synthesis and perception of fluorescently labelled isoprenoid cytokinins

Karolina Kubiasová[3#], Václav Mik[2#], Jaroslav Nisler[1,2], Martin Hönig[1,2], Alexandra Husičková[4], Lukáš Spíchal[2], Zuzana Pěkná[2], Olga Šamajová[5], Karel Doležal[1,2], Ondřej Plíhal[3], Eva Benková[6], Miroslav Strnad[1] and Lucie Plíhalová[1,2,*]

[1]*Laboratory of Growth Regulators, Centre of the Region Haná for Biotechnological and Agricultural Research, Faculty of Science, Palacký University & Institute of Experimental Botany AS CR, Šlechtitelů 27, Olomouc 783 71, Czech Republic*
[2]*Department of Chemical Biology and Genetics, Centre of the Region Haná for Biotechnological and Agricultural Research, Faculty of Science, Palacký University, Olomouc 783 71, Czech Republic*
[3]*Department of Molecular Biology, Centre of the Region Haná for Biotechnological and Agricultural Research, Šlechtitelů 27, Olomouc 783 71, Czech Republic*
[4]*Department of Biophysics, Centre of the Region Haná for Biotechnological and Agricultural Research, Faculty of Science, Palacký University, Šlechtitelů 27, Olomouc 783 71, Czech Republic*
[5]*Department of Cell Biology, Centre of the Region Haná for Biotechnological and Agricultural Research, Šlechtitelů 27, Olomouc 783 71, Czech Republic*
[6]*Institute of Science and Technology (IST), 3400 Klosterneuburg, Austria*

[#]authors contributed equally

Abstract

Isoprenoid cytokinins play a number of crucial roles in the regulation of plant growth and development. To study cytokinin receptor properties in plants, fluorescent derivatives of iP with several fluorescent labels attached to the C2 or *N9* atom of the purine moiety via a 2- or 6-carbon linker were designed and prepared. The fluorescent labels included dansyl (DS), fluorescein (FC), 7-nitrobenzofurazan (NBD), Rhodamine B (RhoB), coumarin (Cou), 7-(diethylamino)coumarin (DEAC) and cyanine 5 dye (Cy5). All prepared compounds were screened for affinity for the *Arabidopsis thaliana* cytokinin receptor (CRE1/AHK4). Although the attachment of the fluorescent labels to iP via the linkers mostly disrupted binding to the receptor, several fluorescent derivatives interacted well. For this reason, three derivatives, two RhoB and one NBD-Cl labelled iP were tested for their interaction with CRE1/AHK4 and *Zea mays* cytokinin receptors in detail. It was further shown that the three derivatives were able to activate transcription of cytokinin response regulator ARR5 in *Arabidopsis* seedlings. The activity of fluorescently labelled cytokinins was compared with the corresponding dimethyladenine (diMeAde) fluorescently labelled negative controls. Selected RhoB C2-labelled compounds **17**, **18** and NBD *N*9-labelled compound **28** and their respective negative controls (**19**, **20** and **29**, respectively) were used for *in planta* staining experiments in *Arabidopsis thaliana* seedlings and L*er* cell suspension culture using live cell confocal microscopy.

Introduction

Naturally occurring isoprenoid cytokinins, such as iP, *t*Z and *c*Z, are plant signalling molecules. For this reason, they have attracted the attention of biologists owing to their importance in numerous aspects of plant growth and development, cell division, seed germination, the formation and activity of shoot and root meristems, apical dominance, auxiliary bud release, nutrition mobilization, leaf senescence and responses to pathogens (Davies, 2007). Fluorescently labelled isoprenoid cytokinins may be a useful alternative tool for research into cytokinin perception and signalling in plants. Although several cytokinin receptors have been already described, e.g., in

species such as *Arabidopsis* (Inoue et al., 2001; Suzuki et al., 2001), maize (Yonekura-Sakakibara et al., 2004), legumes *Medicago truncatula* (Gonzalez-Rizzo et al., 2006), *Lotus japonicus* (Murray et al., 2007; Tirichine et al., 2007) and rice (Du et al., 2007), there remains the need for mapping the receptor domain in order to understand the relation between the chemical structure and activity of cytokinin derivatives. This approach is indispensable developing new strategies in plant biotechnology, such as plant tissue culture, modern agriculture and plant protection against stress (Plíhalová et al., 2016).

Fluorescent labelling is an important tool in cell biology research, e.g., staining and immunostaining techniques (Mason, 1999; Doskočilová et al., 2013; Ovečka et al., 2014; Šamajová et al., 2014), and for visualizing of small bioactive molecules. It offers several advantages over traditional radio-ligand binding techniques; fluorescence labels are relatively safe and inexpensive compared to tritiated or iodinated compounds and a wide range of fluorophores are available to suit different experimental setups (McGrath et al., 1996; Daly and McGrath, 2003). Fluorescent ligands are continually being developed to meet the demands of the pharmacological community and are being used to study pharmacological receptor systems (Daly and McGrath, 2003). Hiratsuka and Kato used a fluorescent analogue of colcemid with NBD (NBD-colcemid) to visualize tubulin (Hiratsuka and Kato, 1987). Fluorescent labelling of small active molecules has been shown to be effective for visualizing plant hormones, such as auxins, abscisic acid, jasmonates, gibberellins, brassinosteroids and even strigolactones. In one such study, abscisic acid was coupled with fluorescein isothiocyanate (FITC) and used to study direct interaction of ABA with the plasma membrane as although ABA receptors were unknown at the time, they were predicted to lie in the membrane (Asami et al., 1997). Fluorescent brassinosteroid was prepared by labelling castasterone with Alexa Fluor 647 (AFCS) and the endocytosis of BRI1-AFCS complexes in living cells was visualized (Irani et al., 2012). Fluorescent labelling at the cellular level has also been done using gibberellins labelled with FITC (Pulici et al., 1996). 1,4-Dithiobutylene and 1,3-dithiopropylene spacers were employed between the fluorescent label and GA. It was shown that derivatives with longer spacers between gibberellin and FITC were more active in the ability to induce α-amylase

activity in the embryoless half grain, a process known to be specifically induced by active gibberellins synthesized by the embryo. However, an approximately 10-fold higher concentration of the fluorescent probe than GA_3 was needed to obtain a comparable biological effect (Pulici et al., 1996; Lace and Prandi, 2016). Synthesis of fluorescently labelled strigolactone analogs (DS, FC, BODIPY) has been used to search for possible strigolactone receptors *in vivo* (Prandi et al., 2013). Rhodamine and fluorescein auxin derivatives have been synthesized by direct conjugation of FITC and RhoB to the NH group of IAA (Sokolowska et al., 2014). Both fluoroprobes were shown to retain auxin activity in three different bioassays (Sokolowska et al., 2014). Tsuda and Hayashi introduced an NBD label into 5-hydroxy-IAA and 7-hydroxy-NAA but the prepared auxin analogs were found to be inactive toward auxin receptors (Tsuda et al., 2011; Hayashi et al., 2014; Lace and Prandi, 2016). Recently, Bieleszová et al. prepared four fluorescently labelled derivatives of IAA in the form of a conjugate with NBD. These compounds did not possess auxin activity but rather inhibited auxin-induced effects. Moreover, the authors demonstrated the importance of the length of the linker, proper fluorophore and optimal choice of the labelling site in the preparation of fluorescently labelled auxins as important variables influencing their biological activity and fluorescent properties (Bieleszová et al., 2019). Fluorescently labelled jasmonate has been synthesized by bonding jasmonoyl-L-isoleucine to coumarin 343 via the carboxyl group of isoleucine (Liu et al., 2012). The fluorescent probe was examined in cabbage using a root growth inhibition bioassay and the effect of the fluorescently labelled probe on the root growth of cabbage seedlings was similar to that of the methyl jasmonate, the standard bioactive jasmonate.

Like approaches to other plant growth regulators, in preparing a fluorescent probe for visualizing a cytokinin receptor, the compound has to possess high affinity for the receptor while nonspecific binding to other cellular structures needs to be minimized. When the first attempts to prepare a cytokinin fluorescent probe failed in the 1970s, a different strategy based on the construction of mimetic adenine-like molecules was developed (Skoog et al., 1975; Specker et al., 1976). Modifications of cytokinins, particularly in the purine moiety, has led to the preparation of fluorescent imidazo[4,5-g]- and imidazo[4,5-f]-quinazolines, 4-substituted 2-methylthiopyrido[2,3-

d]pyrimidines and 7-phenylethynylimidazo[4,5-b]pyridines and their ribosides, which were shown to have only weak or negligible cytokinin activity in a tobacco callus bioassay (Specker et al.,1976; Hamaguchi et al.,1985; Nishikawa et al., 2000). Zawadski's group prepared synthetic cytokinin N-phenyl-N0-(4-pyridyl) urea labelled with NBD-Cl and RhoB fluorescent labels and detected binding of the cytokinin-specific protein VrCSBP by fluorescence correlation spectroscopy (Zawadski et al., 2010). It has been suggested that the loss of biological activity could be prevented by separation of the pharmacophore from the fluorescent moiety through the introduction of a spacer or linker (Leopoldo et al., 2009). However, so far, only a few studies have systematically evaluated spacer length for fluorescent probes and none have directly evaluated purine based cytokinins. Spacer length and position of the spacer (label) in the purine moiety can both have a large impact on the biological activity of such cytokinin derivatives. Appropriate positional attachment of fluorophores to small molecule ligands is critical for retaining both receptor binding affinity and efficacy (Leopoldo et al., 2009). In addition to standard fluorophores such as fluorescein and Rhodamine, an attempt to find new efficient fluorolabels with fewer limitations for use in biological systems and during confocal microscopy imaging was made. For example, fluorescein is known to self-quench after bioconjugation (Lace and Prandi, 2016; Sjöback et al., 1995) as the emission properties of fluorescein greatly depend on environmental pH (Lavis et al., 2007) and it often exists as an equilibrium between lactone and quinoid forms (Lace and Prandi, 2016). Although Rhodamine dyes are less sensitive to pH than fluorescein, they are poorly soluble in water (Lace and Prandi, 2016). Despite these limitations, both are widely used for labelling bioactive molecules. A small heterocyclic molecule NBD-Cl has also been used, which is a benzoxadiazole compound with low molecular weight. Derivatives of NBD-Cl have been used for the preparation of novel kinase substrates, lipid probes and fluorescent analogues of native lipids and the study of a variety of processes (Chattopadhyay, 1990; Lavis and Raines, 2008; Lace and Prandi, 2016).

In this work, fluorescently labelled iP derivatives were prepared because iP is known to bind to the *Arabidopsis thaliana* CRE1/AHK4, *Zea mays* ZmHK1 and other cytokinin receptors. Dimethyladenine analogues with no cytokinin activity were also

prepared to obtain fluorescent negative controls for receptor bioassays. The prepared compounds contained a 2- or 6- carbon linker between the iP or diMeAde molecule and the fluorescent labels. The fluorescent labels used included dansyl, fluorescein, 7-nitrobenzofurazan, Rhodamine B, coumarin, 7-(diethylamino)coumarin and cyanine 5 dye. The C2 or *N9* atom of the purine moiety was selected for linker attachment to prepare 2,6- and 6,9-disubstituted purine derivatives. The ability of all prepared compounds to bind the cytokinin receptor CRE1/AHK4 was tested. The three most successful derivatives were also tested for interaction with the CRE1/AHK4 and ZmHK1 in detail as well as for their ability to activate the expression of the *ARR5* gene, which is the primary cytokinin response regulator in *Arabidopsis* (D'Agostino et al., 2000). Two active C2-fluorescent probes labelled with RhoB and one active *N*9-fluorescent probe labelled with NBD together with their fluorescent controls were used for staining of *Arabidopsis thaliana* seedlings and L*er* cell suspension culture using confocal microscopy.

Material and Methods

Chemicals and general procedures used in this part of the thesis are given in Supplementary information I.

Syntheses

A detailed description of the synthesis of necessary intermediates required for fluorescent marker attachment, C2 fluorescently labelled derivatives and *N9* fluorescently labelled derivatives are given in Supplementary information I including their yields, m.p. HPLC purity, ESI+ MS m/z and ^{1}H and ^{13}C NMR data.

Live cell hormone binding assays

Receptor direct binding assays were conducted using the *E. coli* strain KMI001 harboring the plasmid pIN-III containing a coding sequence for the cytokinin receptor CRE1/AHK4 (Yonekura-Sakakibara et al., 2004) or ZmHK1 (Podlešáková et al., 2012) or the plasmid pSTV28 containing a coding sequence for AHK3 (Suzuki et al., 2001; Yamada et al., 2001). Bacterial strains were kindly provided by Dr. T. Mizuno (Nagoya,

Japan). The assays were performed according to a published procedure (Nisler et al., 2010). The competition reaction of the tested compounds was allowed to proceed with 2 nM 2-[³H]*t*Z. Labelled *t*Z was provided by the Isotope Laboratory, Academy of Sciences, Czech Republic.

ZmHK1 receptor activation assay

The assay was performed with *E. coli* strain KMI001 harboring the plasmid pIN-III containing a coding sequence for the cytokinin receptor ZmHK1 according to a previously published protocol (Spíchal et al., 2009, Podlešáková et al., 2012).

ARR5::GUS reporter gene assay

The assay was performed according to a published protocol (Romanov et al., 2005).

Growth conditions and confocal laser scanning microscopy

Surface-sterilized seeds of *Arabidopsis* ecotype Columbia (Col-0) were plated on half-strength (0.5x) Murashige and Skoog (MS) medium (Duchefa) with 1% (w/v) sucrose and 1 % (w/v) agar (pH 5.7). The seeds were stratified for 2-3 days at 4 °C in darkness. Seedlings were grown on vertically oriented plates in growth chambers at 21 °C under long day conditions (16 h light and 8 h darkness) using white light (W), which was provided by blue and red LEDs (70-100 µmol $m^{-2}s^{-1}$ of photosynthetically active radiation). 4-day-old seedlings were transferred onto liquid 0.5x MS medium with the indicated chemicals and imaging was carried out within 20 min time frame with LSM 800 inverted confocal scanning microscope Zeiss, with a 40× Plan-Apochromat water immersion objective. Cell suspension culture of *Arabidopsis thaliana* ecotype Landsberg erecta (L*er*) was cultivated under continuous darkness at 23 °C on a rotary shaker with subculture intervals of 3 days in 1 x MS medium (Duchefa) containing 3% (w/v) sucrose. Fluorescent probes at a concentration of 5 µM were used for *in situ* staining procedure – stained cells in MS medium were immediately mounted onto microscope slides and observed with a Zeiss 710 CLSM platform (Carl Zeiss, Jena, Germany) equipped with Plan-Apochromat 40x/1.4 Oil (Carl Zeiss, Germany) objective using excitation laser 458nm and 514 nm and emission filters 501-573 nm and 531-

703nm for NBD-based and RhoB-based fluoroprobes, respectively. The post-processing of images was done using ZEN 2010 software, Photoshop 6.0/CS, and Microsoft PowerPoint.

Results and discussion

A part of the fluorescently labelled compounds was synthesized as a part of a bachelor thesis (Synthesis and characterization of fluorescently labelled cytokinin derivatives; Kubiasová, 2012) and a Ph.D. thesis (Synthesis and characterization of novel compounds interacting with metabolic pathways of plant hormones cytokinins. Structure-activity relationship; Mik, 2012).

Synthesis

Thirty new 2,6- or 6,9-disubstituted adenine derivatives with the linker attached to an appropriate fluorescent label either at the C2- or *N9*-atom of the purine moiety were prepared (Figure 11).
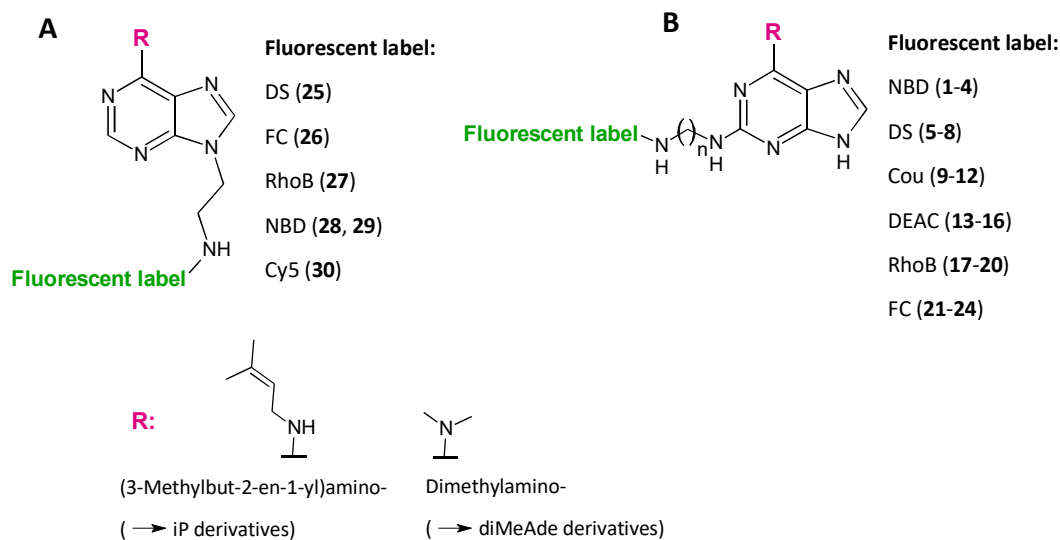

Figure 11: *Preparation of the fluorescently labelled N9- (A) and C2- (B) substituted derivatives.*

Elemental analyses, a fluorescent label, length of the linker, ESI-MS and spectral data are shown in Table 1. In addition to the fluorescently labelled iP derivatives,

diMeAde analogues labelled with the same fluorescent labels as the iP derivatives for use as negative controls in future experiments were also prepared. The syntheses of fluorescently labelled iP and diMeAde derivatives consisted of several steps, as described in the Supplementary information I.

In the first step, an appropriate intermediate substituted with a linker terminating in an amino group was prepared (Supplementary information I, Schemes 1 and 2). This derivative was labelled with an appropriate fluorescent label (Supplementary information I, Schemes 3 and 4). For substitutions at the C2 atom of the purine moiety, only fluorescent labels that could be attached to an amino group were used, e.g., NBD-Cl, NHS activated coumarin-3-carboxylic acid, DS-Cl, NHS activated DEAC, FITC and NHS activated RhoB. For the *N*9 position of the purine atom moiety, an appropriate linker terminating in an amino group was used and NBD-Cl, Cy5-NHS, RhoB-NHS and FITC as fluorescent labels. Since the two carbon linker has proved to be more efficient in the case of C2 derivatives, this design strategy was adopted for *N*9 fluorescent probes (**25**, **26**, **27**, **28** and **30**). Compound **29**, diMeAde-*N*9-NBD, was also prepared as the only negative control (specifically for comparison with the only active compound **28**).

Table 1: *Table of prepared fluorescently labelled purine derivatives. C. – compound; 2AmEtAm – 2-aminoethylamino-; 6AmHexAm – 6-aminohexylamino-; NBD – 7-nitrobenzofurazan; Cou – coumarin; DEAC – 7-(Diethylamino)coumarin; DS – dansyl, RhoB – Rhodamine B; FC – fluorescein; v.w.f.: very weak fluorescence.*

C.	C6	C2	*N*9	Fluorescent label	HPLC purity [%]	ESI-MS [M+H]$^+$	Spectral properties λex_{max} [nm]	λem_{max} [nm]
1	(3-Methylbut-2-en-1-yl)amino-	2AmEtAm	H	NBD	98.2	425	460	525
2	(3-Methylbut-2-en-1-yl)amino-	6AmHexAm	H	NBD	99.2	481	465	525
3	Dimethylamino-	2AmEtAm	H	NBD	98.4	385	v.w.f.	v.w.f.
4	Dimethylamino-	6AmHexAm	H	NBD	99.9	441	464	526
5	(3-Methylbut-2-en-1-yl)amino-	2AmEtAm	H	DS	99.9	495	257	507
6	(3-Methylbut-2-en-1-yl)amino-	6AmHexAm	H	DS	99.9	551	256	507
7	Dimethylamino-	2AmEtAm	H	DS	99.8	455	254	508
8	Dimethylamino-	6AmHexAm	H	DS	99.6	511	255	505

9	(3-Methylbut-2-en-1-yl)amino-	2AmEtAm	H	Cou	99.9	434	v.w.f.	v.w.f.
10	(3-Methylbut-2-en-1-yl)amino-	6AmHexAm	H	Cou	99.4	490	290	406
11	Dimethylamino-	2AmEtAm	H	Cou	99.9	394	v.w.f.	v.w.f.
12	Dimethylamino-	6AmHexAm	H	Cou	98.9	450	290	407
13	(3-Methylbut-2-en-1-yl)amino-	2AmEtAm	H	DEAC	99.9	505	416	464
14	(3-Methylbut-2-en-1-yl)amino-	6AmHexAm	H	DEAC	98.2	561	416	464
15	Dimethylamino-	2AmEtAm	H	DEAC	99.9	465	416	464
16	Dimethylamino-	6AmHexAm	H	DEAC	99.9	521	416	464
17	(3-Methylbut-2-en-1-yl)amino-	2AmEtAm	H	RhoB	98.0	686	544	566
18	(3-Methylbut-2-en-1-yl)amino-	6AmHexAm	H	RhoB	98.1	742	546	546
19	Dimethylamino-	2AmEtAm	H	RhoB	95.0	646	546	568
20	Dimethylamino-	6AmHexAm	H	RhoB	98.0	702	544	566
21	(3-Methylbut-2-en-1-yl)amino-	2AmEtAm	H	FC	92.4	651	544	566
22	(3-Methylbut-2-en-1-yl)amino-	6AmHexAm	H	FC	97.7	707	497	518
23	Dimethylamino-	2AmEtAm	H	FC	91.4	612.1	498	518
24	Dimethylamino-	6AmHexAm	H	FC	92.0	668.3	497	518
25	(3-Methylbut-2-en-1-yl)amino-	H	2AmEtAm	DS	98.3	481	342	500
26	(3-Methylbut-2-en-1-yl)amino-	H	2AmEtAm	FC	97.0	636	v.w.f.	v.w.f.
27	(3-Methylbut-2-en-1-yl)amino-	H	2AmEtAm	RhoB	96.5	672	554	588
28	(3-Methylbut-2-en-1-yl)amino-	H	2AmEtAm	NBD	96.8	410	475	552
29	Dimethylamino-	H	2AmEtAm	NBD	98.0	370	v.w.f.	v.w.f.
30	(3-Methylbut-2-en-1-yl)amino-	H	2AmEtAm	Cy5	97.7	713	270	641

Live cell hormone binding assays

Cytokinin receptor interaction is a crucial step in the initiation of cytokinin signalling in plant cells (Romanov et al., 2005). The functionality and ability of the intended fluorescent probe to enter the cells can be verified by activation of the appropriate receptors. Therefore, the prepared compounds were tested in a direct binding assay with *E. coli* expressing functional CRE1/AHK4 or AHK3 receptors from *A. thaliana* to

test their ability to compete with the radiolabelled natural ligand *tZ* (2-[^{3}H]*tZ*). Unlabelled *tZ*, iP, adenine and DMSO were used as positive and negative controls, respectively (Figure 12; Spíchal et al., 2009). The activity of fluorescently labelled diMeAde derivatives **3**, **4**, **7**, **8**, **11**, **12**, **15**, **16**, **19**, **20**, **23**, **24** and **29** prepared as the negative controls was compared with iP fluorescently labelled probes at CRE1/AHK4 receptor. DiMeAde, as well as iP derivatives, were fluorescently labelled via a two or six carbon linker attached to the C2 or *N9* atom of the purine moiety. DiMeAde control derivatives were chosen given that the isopentenyl substituent is considered to be responsible for the cytokinin receptor binding properties (Hothorn et al., 2011).
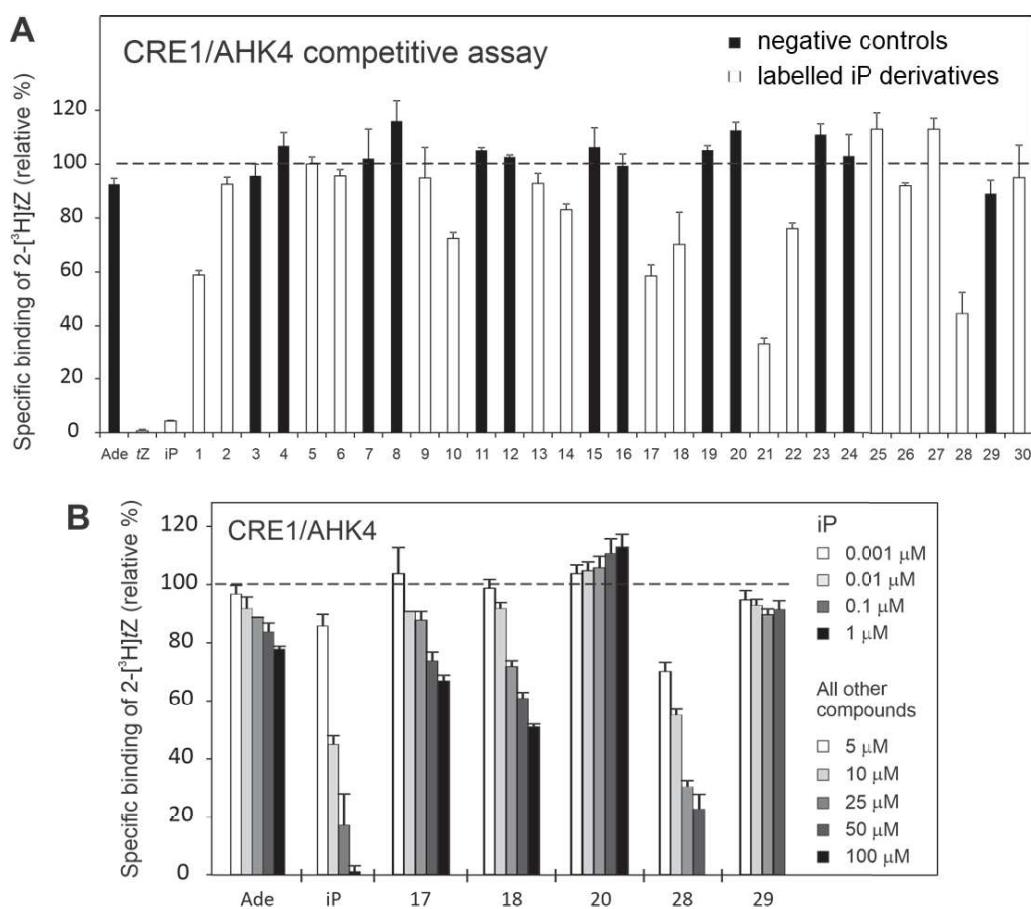

Figure 12: *The ability of the compounds to bind to the cytokinin receptor CRE1/AHK4 in live cell hormone binding assay. **A** – Fluorescently labelled diMeAde and iP derivatives (both 20 μM) competed with 2 nM 2-[^{3}H]tZ. **B** – Selected compounds in more detail. Negative control (**19**) for compound **17** is not shown but exhibited the same affinity pattern as negative control **20**. Adenine (Ade) and DMSO were used as negative controls. The value obtained with DMSO was set as 100% (dashed line). The value obtained with 10 μM iP was set as 0% and was used to*

discriminate the non-specific binding of 2-[³H]tZ on the bacteria. Error bars show s.d. values for three replicates.

As predicted, all control derivatives (black columns in Figure 12A) were inactive. Some of the desired fluorescently labelled derivatives of iP, namely **2**, **5**, **6**, **9**, **13**, **14**, were also found to be unable to compete with 2-[³H]*t*Z at the CRE1/AHK4 receptor (Figure 12A). Whereas DS and DEAC fluorescent labels deactivated iP probes regardless of the linker length, iP derivatives of NBD (**1**, **28**), Cou (**10**), RhoB (**17**, **18**) and FC (**21** and **22**) showed at least partial affinity to the cytokinin receptor CRE1/AHK4. Although the RhoB labelled C2-derivatives **17** and **18** were active in competing with 2-[³H]*t*Z at the receptor binding site, the iP RhoB labelled *N*9-derivative **27** was inactive. The FC labelled derivatives behaved similarly. Whereas the activity of both RhoB labelled derivatives **17** and **18** was comparable, the FC labelled derivative **21** with a shorter two-carbon linker exhibited a higher affinity than the derivative **22** with a six-carbon linker. A similar trend was observed for the NBD labelled iP fluorescent probes: the two-carbon linker of **1** was found to be more efficient than the six-carbon linker of **2**, which was inactive. C2-labelled iP derivative **21** exhibited the highest affinity for the receptor, displacing more than 65% of 2-[³H]*t*Z from the receptor at a 20 µM concentration. The compound **21** thus appeared to be a promising candidate for fluorescent staining until it was found that the substance was chemically unstable and spontaneously decomposed during storage. Another promising active compound was *N*9-labelled **28**. This compound (bearing the NBD label) was the only *N*9 derivative to exhibit affinity for the CRE1/AHK4 receptor, displacing approximately 57% of 2-[³H]*t*Z from receptor binding site at 20 µM concentration. As shown in Figure 12A, except for compound **28**, the other prepared *N*9-substituted compounds, i.e., **25**-**27** and **30**, appeared to be non-active in displacing 2-[³H]*t*Z in the competition assay. In contrast to **28**, compound **29** (negative control) was found to be inactive.

Finally, two RhoB labelled C2-derivatives **17** and **18** and one NBD labelled *N*9-derivative **28** were selected to test their interaction with CRE1/AHK4 within a wider concentration range (Figure 12B). The compounds' affinity for the receptor was compared to the affinity of adenine (negative control) and iP (positive control). The affinity of compounds **17** and **18** for CRE1/AHK4 was relatively weak compared to the

control, better results were achieved with compound **28**, whose affinity was approximately ten times higher than compound **18**. Compound **28** decreased the binding of 2-[^{3}H]tZ to the receptor to 55% at 10 µM concentration. Cytokinin iP decreased the binding of 2-[^{3}H]tZ to the receptor to 45% at 10nM concentration. Compound **28** showed approximately 1000 times lower affinity to the CRE1/AHK4 receptor than iP and although the affinity of **28** appeared to be low, it was shown that it was sufficient for *in planta* staining studies. Although the effective concentrations of the active fluorescent probes were high in relation to the positive standard iP, the selected micromolar concentration was necessary for effective visualization of target cellular structures during confocal or fluorescent microscopy staining. Similar approaches have been reported for other phytohormone-based fluorescent probes (Irani et al., 2012). This aside, the results of the competition assay corresponded to the published structure of the CRE1/AHK4 sensor domain (Hothorn et al., 2011). The crystal structure of the CRE1/AHK4 sensor domain in complex with iP showed four hydrogen bonds formed between the receptor cavity and the adenine moiety and these interactions appeared to be critical for receptor function. Both N6H and N7H hydrogen bonds are linked to Asp262 while N1H atom and N3H hydrogen bonds are linked to water molecules. While C2 and *N*9 point out of the receptor cavity, they might be accessible for linkers bearing spherically advantageous fluorescent labels in molecules **17**, **18** and **28**. The C2-substituted derivatives were also tested with *Arabidopsis* cytokinin receptor AHK3, however, none showed any affinity toward this receptor (data not shown).

Compounds **17**, **18** and **28** were further tested as to whether they interact with the cytokinin receptor ZmHK1, a maize orthologue of CRE1/AHK4 receptor to extend the potential use of the prepared fluorescent cytokinins to other plant species (Yonekura-Sakakibara et al., 2004). In the assay, ZmHK1 was functionally expressed in *E. coli* strain KMI001 (Podlešáková et al., 2012). Unfortunately, in the bacterial receptor competitive assay, compound **17** showed no affinity to the receptor (data not shown) while compound **18** exhibited an affinity for the ZmHK1 receptor comparable to adenine (Figure 13A).
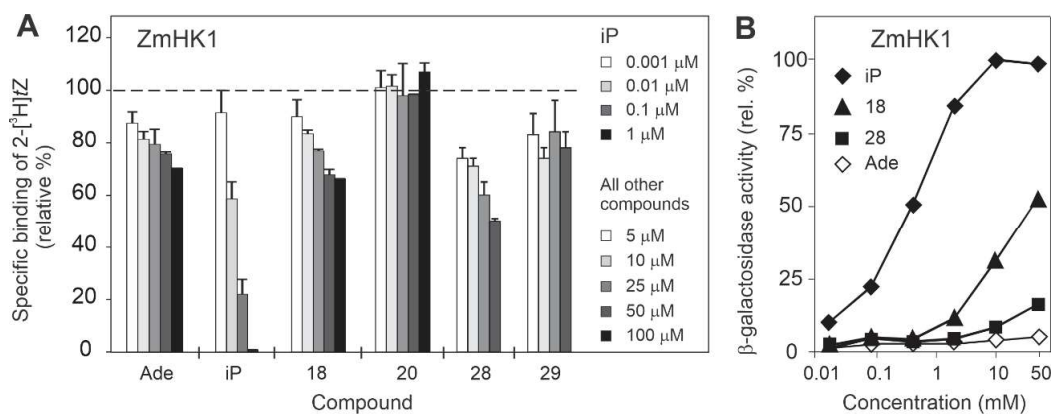
Figure 13: *Interaction of the selected compounds with the cytokinin receptor ZmHK1. Adenine (Ade) and DMSO were used as negative controls. **A** – The ability of the compounds to bind to the receptor in live cell hormone binding assay. The value obtained with DMSO was set as 100% (dashed line). The value obtained with 10 μM iP was set as 0% and was used to discriminate the non-specific binding of 2-[³H]tZ on the bacteria. Error bars show s.d. values for three replicates. **B** – The ability of the compounds to activate the receptor. The value obtained with DMSO was set as 0% activation. The value obtained with 10 μM iP was set as 100% activation. Compound **17** activated the receptor similarly to compound **28** and for clarity is not shown. s.d. values did not exceed 15%.*

This result contrasted with the results from the CRE1/AHK4 competition assay, where both compounds showed higher affinity than adenine. However, derivative **28** decreased binding of 2-[³H]tZ to the receptor by approximately 70% at 10 μM concentration, while adenine had the same effect at 100 μM concentration. In the higher concentration ranges, **28** was also more effective than adenine, decreasing binding of 2-[³H]tZ to the receptor by approximately 50% at 50 μM concentration (Figure 13A). The effect of **28** (and its negative control, **29**) at 100 μM concentration was not evaluated as the compounds were not completely soluble in the tested system at such high concentrations. In the ZmHK1 receptor activation assay, several unexpected observations were made. First, compound **18** was able to activate the receptor (Figure 13B), even though the ligand-receptor interaction did not seem to be specific; compound **18** was a 100 times weaker activator of ZmHK1 than iP. In contrast, compound **28** was unable to activate this receptor, although it exhibited a significant affinity for this receptor. Therefore, the compound bound to the cytokinin receptor without triggering its activation in a manner, which was described and characterized as anti-cytokinin behaviour (Nisler et al., 2010). This may be advantageous for

56

fluorescently labelled cytokinin probes because it allows for specific interaction with the cytokinin receptor and at the same time limits potential constraints linked to high intracellular cytokinin concentrations.

Activation of the cytokinin primary response gene ARR5

Transgenic *Arabidopsis* plants harboring the *ARR5::GUS* reporter gene were employed (D'Agostino et al., 2000) to gain more information as to whether compounds **17**, **18** and **28** are able to trigger the cytokinin signalling pathway *in planta*. ARR5 is a primary response gene with a cytokinin-dependent promoter, activation of which integrates the responses of several putative cytokinin signalling pathways. As shown in Figure 14, compounds **17**, **18** and **28** were able to activate transcription of the *ARR5::GUS* gene in *Arabidopsis* in a concentration dependent manner, demonstrating their ability to trigger the cytokinin response in *Arabidopsis*. Negative controls for the compounds were inactive in this assay. BA and iP showed maximal activity at 1 µM concentration. None of the tested compounds was able to attain this activity even in 100 µM concentration. However, the selected compounds exhibited activity (20-30%) starting from a concentration of 10 µM. The compounds were approximately 1000 times weaker than iP, which showed activity from 10 nM concentration (Figure 14) in this assay. The biologically insignificant activity of the compound **28** (compared to **17** and **18**) is not surprising, and it is consistent with the negative results of the ZmHK1 receptor activation assay.
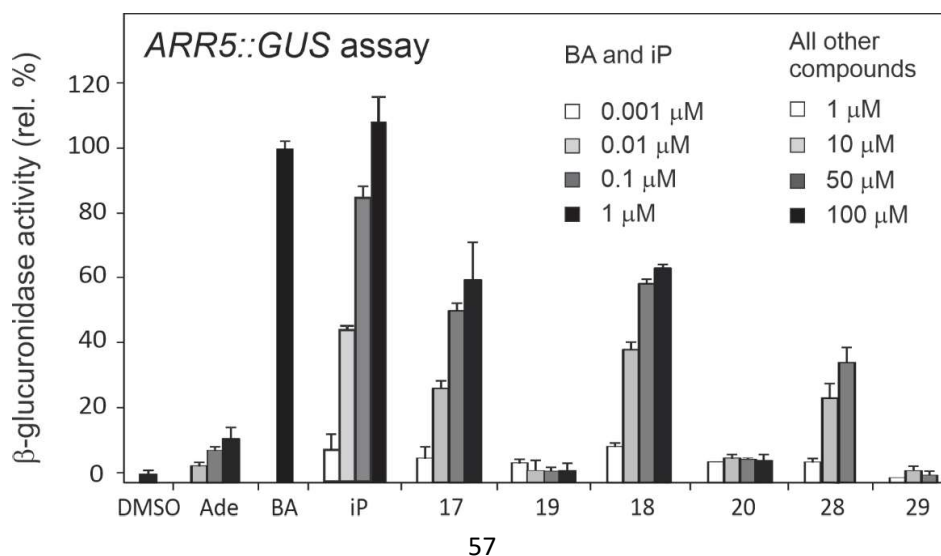
Figure 14: *The ability of the compounds to activate transcription of the cytokinin primary response gene ARR5 in Arabidopsis seedlings three days after germination. The value obtained with DMSO was set as 0% activation. The value obtained with 1 µM BA was set as 100%. Adenine (Ade) and iP were used as negative and positive controls, respectively. Error bars show s.d. values for three replicates.*

Visualization of cellular structures by fluorescent cytokinin derivatives

Arabidopsis suspension cell culture was used and allowed for fast and homogenous staining of individual cells, gave insight into the distribution of the fluorescent signal at the subcellular level and adopted a simple staining procedure for visualizing the subcellular structures with selected fluorescent probes. For staining experiments, first compounds **17** and **18** and their corresponding diMeAde fluorescent derivatives **19** and **20**, respectively that were used as negative controls to filter out nonspecific background signals, were observed.

   Arabidopsis cells were treated with 5 µM solution of a fluorescent probe or negative control, immediately applied on slides and observed under the confocal microscope. The internalization of RhoB-based compounds was relatively fast, reaching apparently constant pattern after approximately 15-20 min of treatment. The fluorescent signal was rather weak in all staining experiments and increased concentration of the fluorescent probe (up to 20 µM) did not significantly change the signal distribution. The signal recorded for the fluorescent probes, compounds **17** and **18**, and their respective negative controls, derivatives **19** and **20**, appeared to be similar in all cases and cytoplasmic distribution of the signal combined with a characteristic patchy-pattern was observed (Figure 15). Similar results were obtained also when RhoB-based compounds were applied to *Arabidopsis* seedlings (Figure 15).

   It can be hypothesized that RhoB derivatives may not represent a good candidate for synthesis of cytokinin-based fluorescent probes due to possible nonspecific interactions with cell components that prohibit efficient and specific binding to cytokinin-binding sites. For this reason, derivative **28** was introduced, an NBD-based green fluorescent cytokinin probe, for *in planta* screening. Based on the results from the cytokinin CRE1/AHK4 competitive bioassay (Figure 12A) only compound **28** proved to be significantly active in displacing radiolabelled *t*Z out of all synthesized C2- and

*N*9-based NBD fluorescent probes and concurrently stable. Compound **29**, showed negligible binding to the cytokinin receptor and for this reason, it was used as a negative control.
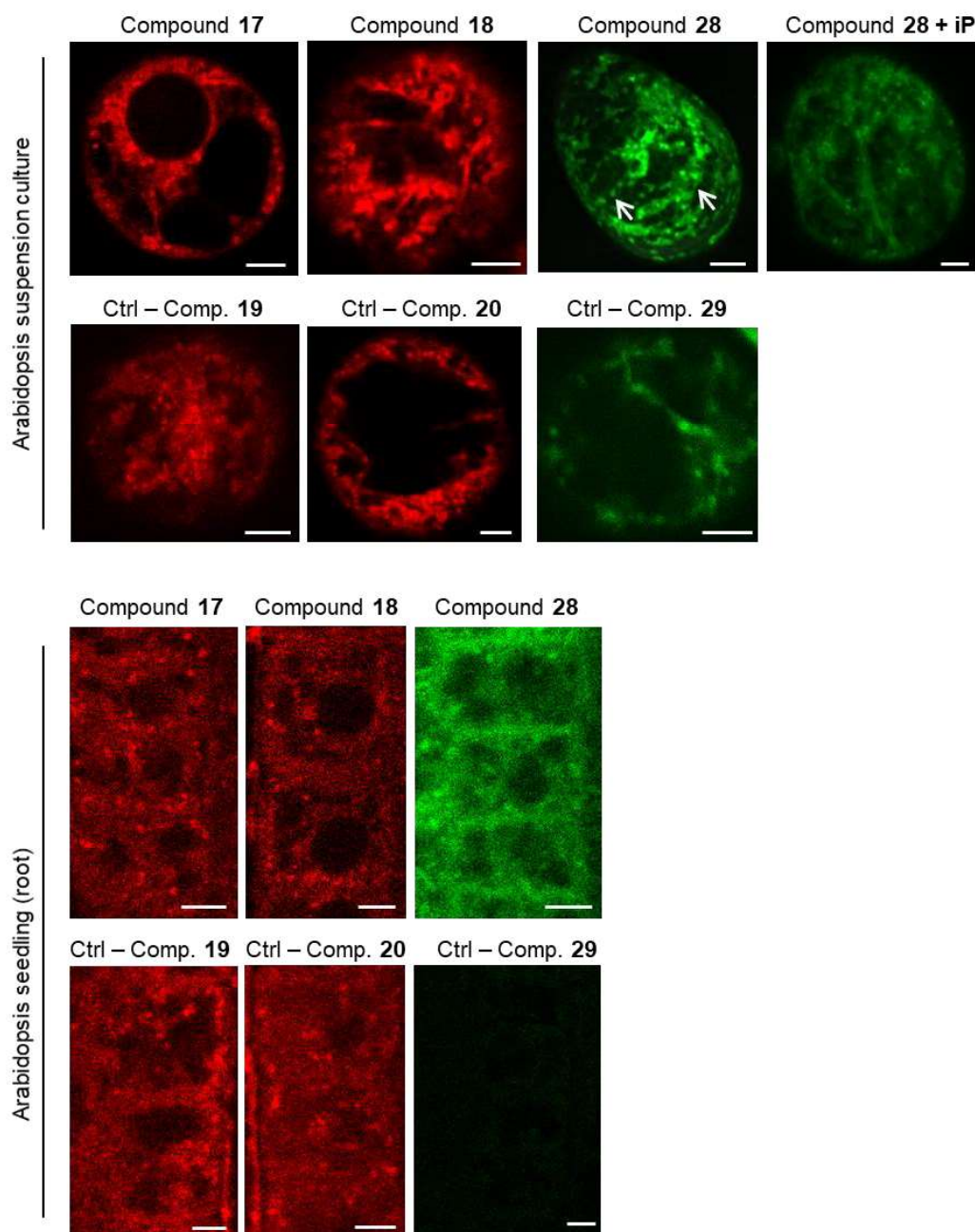

Figure 15: *Confocal fluorescence images of the Arabidopsis suspension culture cells and the root epidermal cells treated with different fluorescent probes (Compound **17**, **18** and **28**) and their controls (Ctrl - Compound **19**, **20** and **29**), all in 5 µM concentrations and observed after 15-20 min. RhoB-based compounds are shown in red, NBD-based compounds are shown in green. A mesh-like localization pattern (marked by arrows) characteristic for ER was visible in the cell cortex of Arabidopsis cell after treatment with compound **28**, but it was lost when*

*compound **28** was co-administered together with an equimolar concentration of iP. Scale bars, 5 μm.*

The results from live cell imaging of NBD-based probes are shown in Figure 15. Similar to RhoB-based probes, staining of *Arabidopsis* cells with the NBD fluorescent probe was fast, reaching a plateau of the intracellular signal intensity after approximately 10 min of continuous treatment with 5 μM of compound **28** (Figure 15).

In the both *Arabidopsis* cell types, the negative control showed significantly weaker fluorescent signal compared to the compound **28**. In the publication Bieleszova et al. (2019), authors showed clear evidence that the fluorescence intensity of NBD fluorophores depends on the polarity of the solvent. Binding of the cytokinin to the AHK receptor is based on a simple size-selectivity filter and most interactions between receptor and ligand are mediated by small hydrophobic residues. There are two main polar interactions Asp262 and Thr294 discriminating binding of correct stereoisomers and forming a non-polar binding cavity (Hothorn et al., 2011). Based on this information it can be assumed that non-bound NBD labelled cytokinin freely distributed in the cell shows a weaker signal intensity due to the polar environment. While the negative control showed only weak cytoplasmic fluorescent signal, the NBD-based fluorescent probe at the same concentration showed a clear signal distribution represented by typical mesh-like structures at the suspension cell cortex suggestive of ER structures (Figure 15 arrows). This is in accordance with the reported localization pattern of the three known cytokinin HK receptors in *Arabidopsis* (Wulfetange et al., 2011; Caesar et al., 2011). Further, co-administration of compound **28** together with natural cytokinin iP led to a moderate decrease of the fluorescent signal and the signal seemed to be less focused (Figure 15). This suggests that compound **28** is transported to the cell even in the presence of the endogenous iP, but the competition with intracellular iP leads to the unspecific staining pattern. Therefore, it seems that some NBD-based cytokinin probes can be used for the visualization of the cytokinin HK receptors, but further experiments will be needed to confirm the specificity of the ligand-receptor interaction. *N*9-based cytokinin fluorescent probes may be particularly suitable for the live cell imaging as the introduction of fluorescent label into *N*9

position should prevent the metabolic conversion of the cytokinin analogue through *N*-glycosylation that prevents entry into the receptor domain cavity.

Conclusion

Thirty new 2,6- and 6,9-disubstituted fluorescently labelled purines bearing fluorescent labels, such as DS, FC, NBD, RhoB, Cou, and Cy5 were synthesized. These fluorescent derivatives and their negative controls prepared by labelling of diMeAde were synthesized with the aim to design probes with ligand affinity to the histidine kinase receptor domain. Several derivatives that were able to bind in the active sites of two different cytokinin receptors - CRE1/AHK4 from *Arabidopsis thaliana* and ZmHK1 from *Zea mays*, and to trigger cytokinin response *in planta* were prepared. Promising derivatives, two 2,6-iP derivatives **17**, **18** and one 6,9-iP derivative **28** underwent more precise binding study in three cytokinin receptors and were found to be active, although at higher concentration ranges than the positive iP control. Overall, the results showed that it is possible to prepare biologically active fluorescent cytokinins by the attachment of a fluorescent label to their purine moiety via an appropriate linker without causing extensive structural change. The activity of the prepared probes depended on the position and type of attached label on the adenine moiety. Therefore, the choice of label is also very important for maintaining the cytokinin receptor affinity. Compounds **17**, **18** and **28** and their controls for *in planta* staining were used but only compound **28** was an effective competitor as confirmed by radiolabelled *t*Z receptor binding experiments. Staining of *Arabidopsis* suspension cells with compound **28** was fast, showed clear intracellular signal distribution represented by typical mesh-like structures at the cell cortex suggestive of ER after approximately 10 min of a continuous treatment with 5 µM fluorescent probe while negative fluorescent control **29** at the same concentration levels showed only a weak cytoplasmic fluorescent signal. This is in agreement with reported localization pattern of the three known cytokinin HK receptors in *Arabidopsis* but further data are needed to confirm the ER localization of receptor-ligand complexes. Therefore compound **28** (further referred as iP-NBD) was selected to study in more detail.

Cytokinin fluoroprobe reveals multiple sites of cytokinin perception at plasma membrane and endoplasmic reticulum

Karolina Kubiasová[1,#], Juan Carlos Montesinos[2,#], Olga Šamajová[3], Jaroslav Nisler[4,5], Václav Mik[4], Hana Semerádová[2], Lucie Plíhalová[4,5], Ondřej Novák[5], Peter Marhavý[2,6], Nicola Cavallari[2], David Zalabák[1], Karel Berka[7], Karel Doležal[4,5], Petr Galuszka[†], Jozef Šamaj[3], Miroslav Strnad[5], Eva Benková[2], Ondřej Plíhal[1,4,5] and Lukáš Spíchal[4]

[1]*Department of Molecular Biology, Centre of the Region Haná for Biotechnological and Agricultural Research, Faculty of Science, Palacký University, Šlechtitelů 27, 783 71 Olomouc, Czech Republic*

[2]*Institute of Science and Technology (IST), 3400 Klosterneuburg, Austria*

[3]*Department of Cell Biology, Centre of the Region Haná for Biotechnological and Agricultural Research, Faculty of Science, Palacký University, Šlechtitelů 27, 783 71 Olomouc, Czech Republic*

[4]*Department of Chemical Biology and Genetics, Centre of the Region Haná for Biotechnological and Agricultural Research, Faculty of Science, Palacký University, Šlechtitelů 27, 783 71 Olomouc, Czech Republic*

[5]*Laboratory of Growth Regulators, Institute of Experimental Botany of the Czech Academy of Sciences and Faculty of Science of Palacký University, Šlechtitelů 27, 783 71 Olomouc, Czech Republic*

[6]*Umeå Plant Science Centre, Department of Forest Genetics and Plant Physiology, Swedish University of Agricultural Sciences, 90183 Umeå, Sweden*

[7]*Department of Physical Chemistry, Regional Centre of Advanced Technologies and Materials, Faculty of Science, Palacký University, 17. listopadu 1192/12, 771 46 Olomouc, Czech Republic*

[#] authors contributed equally

[†] deceased

Abstract

Plant hormone cytokinins are perceived by a subfamily of sensor histidine kinases, which via a two-component phosphorelay cascade activate transcriptional responses in the nucleus. Subcellular localization of the receptors proposed the ER membrane as a principal cytokinin perception site, while study of cytokinin transport pointed to the PM-mediated cytokinin signalling. Here, by detailed monitoring of the subcellular localizations of the fluorescently labelled natural cytokinin probe and the receptor CRE1/AHK4 fused to GFP reporter, it is shown that pools of the ER-located cytokinin receptors can enter the secretory pathway and reach the PM in cells of the root apical meristem, and the cell plate of dividing meristematic cells. Brefeldin A (BFA) experiments revealed vesicular recycling of the receptor and its accumulation in the BFA compartments. A revised view on cytokinin signalling and the possibility of multiple sites of perception at PM and ER is provided.

Introduction

The plant hormone cytokinin regulates various cell and developmental processes, including cell division and differentiation, embryogenesis, activity of shoot and root apical meristems, formation of the shoot and root lateral organs and others (Kieber and Schaller, 2018). Cytokinins are perceived by a subfamily of sensor histidine kinases, which via a two-component phosphorelay cascade activate transcriptional responses in the nucleus. Based on the subcellular localization of cytokinin receptors in various transient expression systems, such as leaf epidermal cells of tobacco (*Nicotiana benthamiana*), and membrane fractionation experiments of *Arabidopsis* and maize, the ER membrane has been proposed as a principal hormone perception site (Caesar et al., 2011; Lomin et al., 2011; Wulfetange et al., 2011). Intriguingly, a recent study of the cytokinin transporter PUP14 has pointed out that the PM-mediated signalling might play an important role in the establishment of cytokinin response gradients in various plant organs (Zürcher et al., 2016). However, localization of the cytokinin HK receptors to the PM, although initially suggested (Kim et al., 2006), remains ambiguous. Here, by monitoring subcellular localizations of the fluorescently labelled

63

cytokinin probe iP-NBD (Kubiasová et al., 2018), derived from the natural bioactive cytokinin iP, and the cytokinin receptor CRE1/AHK4 fused to GFP reporter, it is shown that pools of the ER-located cytokinin fluoroprobes and receptors can enter the secretory pathway and reach the PM. It is demonstrated that in cells of the root apical meristem, CRE1/AHK4 localizes to the PM and the cell plate of dividing meristematic cells. The BFA experiments revealed vesicular recycling of the receptor and its accumulation in the BFA compartments. Our results provide a revised view on cytokinin signalling and the possibility of multiple sites of perception at both PM and ER, which may determine specific outputs of cytokinin signalling.

Material and Methods

Additional material and methods are given in Supplementary information II.

Plant material

Arabidopsis thaliana (L.) Heynh (*Arabidopsis*) plants were used. The transgenic lines have been described elsewhere: *cre1-2* (Inoue et al., 2001), triple mutant *cre1-12, ahk2-2, ahk3-3* (Juan Carlos Montesinos), *TCSn::ntdT:tNOS-pDR5v2::n3GFP* (Smet et al., 2019), *pup14* (Zürcher et al., 2016), p24δ5-RFP (Montesinos et al., 2012), HDEL-RFP (Nelson et al., 2007), Wave lines 2R/RabF2b (LE/PVC), 9R/VAMP711 (Vacuole), 13R/VTI12 (TGN/EE), 18R/Got1p (Golgi), 22R/SYP32 (Golgi), 34R/RabA1e (Endosomal/Recycling endosomal), 131R/NPSN12 (PM) and 138R/PIP1;4 (PM; Geldner et al. 2009), *ARR5::GUS* (D'Agostino et al., 2000), *35S::GFP* line was kindly provided by Shutang Tan (IST Austria, Austria). *35S::CRE1/AHK4-GFP* plants were generated as described below.

Growth conditions

Surface-sterilized seeds of *Arabidopsis* ecotype Columbia (Col-0) and the other transgenic lines were plated on half-strength (0.5x) Murashige and Skoog (MS) medium (Duchefa) with 1% (w/v) sucrose and 1 % (w/v) agar (pH 5.7). The seeds were stratified for 2-3 days at 4 °C in darkness. Seedlings were grown on vertically oriented plates in growth chambers at 21 °C under long day conditions (16 h light and 8 h

darkness) using white light (W), which was provided by blue and red LEDs (70-100 µmol m^{-2}s^{-1} of photosynthetically active radiation), if not stated otherwise.

Pharmacological treatments for bio-imaging

Seedlings 4 to 5-day-old were transferred onto solid 0.5x MS medium with or without the indicated chemicals. The drugs and hormones used were: BA in different concentrations (0.1 µM, 0.5 µM, 1 µM and 2 µM), *t*Z (0.1 and 1 µM), iP (5 µM). Mock treatments were performed with equal amounts of solvent (DMSO). Treatments with 5 µM iP-NBD and 5 µM Ade-NBD were performed in liquid 0.5x MS medium and imaging was carried out within 30 min time frame. For co-localization of the cytokinin fluoroprobe with PM marker, seedlings were pre-treated with 2 µM FM4-64 for 5 min and transferred into 5 µM iP-NBD supplemented 0.5x MS medium, followed by imaging within 30 minutes time frame. To explore affinity of iP-NBD to the BFA endosomal compartments, seedlings were incubated in 50 µM BFA for 1 h and afterwards transferred into iP-NBD supplemented medium and imaged. Localization of the CRE1/AHK4-GFP in the BFA endosomal compartments was examined in 4 to 5- day-old seedlings incubated in 50 µM BFA for 1 h. For BFA washout experiments, seedlings were placed in a fresh BFA-free 0.5x MS medium, which was replaced every 10 min for at least 1 h.

Recombinant DNA Techniques

The coding region of the cytokinin receptor CRE1/AHK4 (*At2g01830*) was amplified without the stop codon by PCR using a gDNA from *Arabidopsis thaliana* Col-0 as a template and cloned into the Gateway vector *pENTR_2B* dual selection (primers: AHK4_Fw_SalI_KOZAK *CGCGTCGACccaccATGAGAAGAGATTTTGTGTATAATAATAATGC* and AHK4_R_NotI *TTTTCCTTTTGCGGCCGCgaCGACGAAGGTGAGATAGGATTAGG*). To construct C-terminal fusion of *CRE1/AHK4* with *GFP*, *CRE1/AHK4* was shuttled into the destination vector *pGWB5* (Nakagawa et al., 2007) containing *35S* promoter to create *35S::CRE1/AHK4-GFP* construct. For the transient Luciferase assay in *Arabidopsis* protoplasts, *CRE1/AHK4-GFP* fusion construct was re-cloned into *p2GW7,0* vector. *CRE1/AHK4-GFP* region was amplified by PCR using *pGWB5_CRE1/AHK4-GFP* as a

template (primers: *35S_FW CCACTATCCTTCGCAAGAC*CCTTC and AHK4_5A_NheI_RE *TATTCCAATgctagcTTACTTGTACAGCTCGTCCATGC*) and ligated into the Gateway *pENTR_2B* dual selection entry vector. *CRE1/AHK4-GFP* was shuttled into the destination vector *p2GW7,0*.

Plant transformation

Transgenic *Arabidopsis* plants were generated by the floral dip method using *Agrobacterium tumefaciens* strain GV3101 (Clough et al., 1998). Transformed seedlings were selected on medium supplemented with 30 µg mL^{-1} hygromycin.

Competitive binding assay in E. coli strains

Receptor direct binding assays were conducted using the *E. coli* strain KMI001 harbouring either the plasmid *pIN-III-AHK4* or *pSTV28-AHK3*, which express the *Arabidopsis* histidine kinases CRE1/AHK4 or AHK3 (Suzuki et al., 2001; Yamada et al., 2001). Bacterial strains were kindly provided by Dr. T. Mizuno (Nagoya, Japan). The competitive binding assays (Romanov et al., 2005; Nisler et al., 2010) were performed with homogenous bacterial suspension with an OD$_{600}$ of 0.8 and 1.2 for the CRE1/AHK4 and the AHK3 expressing strains, respectively. The competition reaction was allowed to proceed with 3 nM [2-^{3}H]*t*Z and 6-18 nM [2-^{3}H]iP, and various concentrations of iP and iP-NBD, 0.1% (v/v) DMSO was added as a solvent control. After 30 min incubation at 4 °C, the sample was centrifuged (6000 g, 6 min, 4 °C), the supernatant was carefully removed, and the bacterial pellet was resuspended in 1 mL of a scintillation cocktail (Beckman, Ramsey, MN, USA) in an ultrasonic bath. Radioactivity was measured by scintillation counting by a Hidex 300 SL scintillation counter (Hidex, Finland). To discriminate between specific and nonspecific binding, a high excess of unlabelled natural ligand *t*Z, or iP (at least 3000-fold) was used for competition. The functional inhibition curves were used to estimate the IC$_{50}$ values. The K$_i$ values were calculated using equation K$_i$ = IC$_{50}$/(1+ [radioligand]/K$_D$) according to Cheng and Prusoff (Cheng and Prusoff, 1973). [2-^{3}H]*t*Z and [2-^{3}H]iP were provided by Dr. Zahajská from the Isotope Laboratory, Institute of Experimental Botany, Czech Academy of Sciences.

Quantitative RT–PCR

RNA was extracted with Monarch® Total RNA Miniprep Kit (NEB) from roots of 5-day-old plants that were sprayed with mock (DMSO) or 0.01μM iP, 0.1μM iP, 1μM iP, 10μM iP-NBD, 100μM iP-NBD or co-treatment of 0.1μM iP + 10μM iP-NBD, 0.1μM iP + 100μM iP-NBD for 15 min (Figure 18B); mock (DMSO) or 5 μM iP (Figure 28E); for 15 min. Poly(dT) cDNA was prepared from 1 μg of total RNA with the iScript cDNA Synthesis Kit (Biorad) and analyzed on a LightCycler 480 (Roche Diagnostics) with the Luna® Universal qPCR Master Mix (NEB) according to the manufacturer's instructions. The expression of *CRE1/AHK4* of the two independent lines was quantified either with a specific primer pair (AHK4-GFP_FW: *TATCTCACCTTCGTCGTCGC* and *AHK4-GFP*_RE: *CCTTGCTCACCATGGATCCTC*) and their relative expressions were compared to the house-keeping gene *PP2A* (PP2A_FW: *TAACGTGGCCAAAATGATGC* and PP2A_RE: *GTTCTCCACAACCGCTTGGT*) or with AHK4_FW: *GAACTGGGCACTCAACAATCA* and AHK4_RE: *ACGAATTCAGAGCACCACCA* pair of primers and their relative expression refer to the Col-0 mock treatment. All qRT-PCR quantifications were done using PP2A as a reference gene (Figure 18B, Figure 28A, E) For the *ARR* expressions (ARR5_FW: *TGCCTGGGATGACTGGATATG,* ARR5_RE: *CTCCTTCTTCAAGACATCTATCG,* ARR7_FW: TACTCAATGCCAGGACTTTCAGG, ARR7_RE: TCTTTGAGACATTCTTGTATACGAGG, ARR16_FW: *CGTAAACTCGTTGAGAGGTTGCTC* and ARR16_RE: *GCATTCTCTGCTGTTGTCACTTTG*), the fold change refer to the Col-0 mock treatment. The experiment was performed in 3 technical and 3 biological replicates.

Measurements of iP-NBD cell transport kinetics

Seedlings of 4-day-old *Arabidopsis* Col-0 were pre-treated for 20 min with 5 μM iP or DMSO and transferred into MS media containing 5 μM iP-NBD and 5 μM iP/DMSO and instantly imaged. To examine PUP14 dependent iP-NBD transport kinetics, 4-day-old seedlings of *pup14* and Col-0 were treated with 5 μM iP-NBD and immediately imaged. For both experiments imaging was performed in the same area of the root for 12 min every 2, 7 and 12 min to minimize photobleaching. iP-NBD fluorescence was measured with ImageJ in the LRC cells (iP pre-treatment experiment) and in the root epidermal cells (*pup14* experiment) from 4-7 cells originating from 4-5 roots.

Imaging

For confocal microscopy imaging, a vertical-stage laser scanning confocal Zeiss 700 (LSM 700) and Zeiss 800 (LSM 800), described in von Wangenheim et al., 2011, with a 20×/0.8 Plan-Apochromat M27 objective, a LSM 800 inverted confocal scanning microscope Zeiss, with a 40× Plan-Apochromat water immersion objective and a Zeiss LSM 880 inverted fast Airyscan microscope with a Plan-Apochromat 63x NA 1.4 oil immersion objective were used. Samples were imaged with excitation lasers 488 nm for GFP (emission spectrum 490-560 nm) and NBD (emission spectrum 529-570 nm) and 555/561 nm (inverted/vertical) for RFP (emission spectrum 583-700 nm), FM4-64 (emission spectrum 650-730 nm), mCherry (emission spectrum 570-700 nm) and tdTomato (emission 560-700 nm).

For super-resolution SIM microscopy, an Axioimager Z.1 with Elyra PS.1 system coupled with a PCO.Edge 5.5 sCMOS camera was used. Samples were excited with the 488nm and 561nm laser lines. Oil immersion objective (63x/1.40) and standard settings (the grating pattern with 5 rotations and 5 standard phase shifts per angular position) were used for image acquisition. Image reconstruction was done in Zeiss Zen software (black version with structured illumination module) using manual mode with adjusting the noise filter and super-resolution frequency weighting sliders as described in (Komis et al., 2015a). For image post-processing, profile measurements and co-localization analysis, the Zeiss Zen 2011, ImageJ (National Institute of Health, http://rsb.info.nih.gov/ij), Photoshop 6.0/CS, GraphPad Prism 8 and Microsoft PowerPoint programs were used. For the SIM co-localization experiments 30 PM regions originating from the root cells of 5 seedling plants were used.

Receptor activation assay

The receptor activation assays were conducted using the *E. coli* strain KMI001 harbouring either the plasmid *pIN-III-AHK4* or *pSTV28-AHK3*, which express the *Arabidopsis* histidine kinases CRE1/AHK4 or AHK3 (Suzuki et al., 2001; Yamada et al., 2001). Bacterial strains were kindly provided by Dr. T. Mizuno (Nagoya, Japan). The assays were performed in liquid M9 media enriched with 0.1% casamino acids (casein hydrolysate, acid hydrolyzed; Merck, Germany) and antibiotics (ampicilin/carbenicilin,

and chloramphenicol for culturing of CRE1/AHK4- and AHK3-expressing bacteria, respectively) using 96-well plate format (Spíchal, 2011). First, the *E. coli* strains were grown overnight in M9 medium (containing 0.1% casamino acids and antibiotics) to OD_{600} ~ 1. These precultures were diluted 1:600 in M9 medium (containing 0.1% casamino acids and antibiotics) and a 96-well plate was filled up with 200 µL of the diluted culture per well. 1 µL stock solution of either the tested compound or solvent control was added to reach desired final concentrations and the cultures were further grown while shaking for 17 h at 25 °C. 50 µL aliquots of the culture were transferred to wells of a 96-well plate containing 2 µL of 25 mM 4-methyl umbelliferyl galactoside (MUG, Sigma)/well. The plate was subsequently incubated for 30 min at 37 °C and the reaction was stopped by adding 100 µL glycine carbonate stop buffer (133 mM glycine, 83 mM Na_2CO_3, pH 10.7). OD_{600} of remaining culture was determined using a spectrophotometer. Fluorescence was measured using Synergy H4 Multi-Mode Microplate Reader (BioTek, USA) at the excitation and emission wavelengths of 365 and 460 nm, respectively. β-galactosidase activity was calculated as nmol 4-methylumbelliferone OD_{600}^{-1} h^{-1}.

ARR5::GUS reporter gene assay

Arabidopsis ARR5::GUS transgenic seeds were surface-sterilized and plated on 0.5x MS medium with 0.1% (w/v) sucrose and 0.05% (w/v) MES–KOH (pH 5.7) in 24-well plates, 20 seeds per well. The plates were stratified for 3 days at 4 °C in darkness and then grown under long-day conditions (16 h light/8 h dark) at 22 °C in a growth chamber. To the wells containing 3-day-old seedlings, BA and/or tested compound or DMSO (solvent control, final concentration 0.1%) was added and the seedlings were grown for an additional 16 h. After that, the seedlings were flash frozen in liquid nitrogen. Quantitative determination of GUS activity in seedlings extracts was performed using 4-methylumbelliferyl glucuronide as a substrate (Nisler et al., 2010) and the fluorescence was measured using Synergy H4 Multi-Mode Microplate Reader (BioTek, USA) at excitation and emission wavelengths of 365 and 450 nm, respectively. The GUS activity was expressed in relative fluorescence units (RFU) of MU per seedling.

Western blot analysis of AHK4-GFP protein levels

 To evaluate levels of the CRE1/AHK4-GFP protein expression, total protein extract was obtained from 5-day-old seedlings extracted with 1x Laemmli buffer (2-Mercaptoethanol, 0.1% Bromophenol blue, 0.0005% Glycerol, 10% SDS (electrophoresis-grade), 2% Tris-HCl, 63 mM pH 6.8). Protein extracts were used for SDS–PAGE using gels acrylamide 10%, and blotted to PVDF transfer membrane (Millipore). Two hours incubation with monoclonal mouse anti-GFP (JL-8, Clontech) 1:5000; or 1 hour incubation with monoclonal mouse anti-Actin (10-B3, Sigma) 1:5000 for protein loading control; as primary antibodies were used. As a secondary antibody, 1 hour incubation sheep anti-mouse IgG Horseradish Peroxidase - Linked F(ab')2 Fragment (NA9310, GE Healthcare) 1:15000 was used. SuperSignal™ West Femto Maximum Sensitivity Substrate Thermo Fisher (4 minutes incubation) was used for detection of the signal.

TCS reporter expression in planta

5-day-old seedlings expressing the cytokinin signalling reporter *TCSn::ntdT:tNOS* (line *TCSn::ntdT:tNOS-pDR5v2::n3GFP*) were transferred on non- or with cytokinin (1 µM iP, 1µM iP-NBD or iP 1 µM + 1 µM iP-NBD) supplemented Murashige and Skoog media for 6 or 15 h. The *TCS:ntdT* expression (red, LUT inferno) in root tip was monitored using a confocal microscope. Fluorescence intensity (arbitrary numbers) of TCS:ntdT signal was measured in cells of provasculature at the root tip meristematic zone (n > 8 roots per treatment).

Luciferase transient expression assay

The Luciferase transient expression assays were performed on the protoplasts isolated from 4-days-old *Arabidopsis* root suspension culture. The protoplasts were isolated in an enzyme solution (1% cellulose; Serva, 0.2% Macerozyme; Yakult in B5-0.34M glucose-mannitol solution; 2.2 g MS with vitamins, 15.25 g glucose, 15.25 g mannitol, H_2O to 500 mL pH to 5.5 with KOH) with slight shaking for 3-4 h and centrifuged at 800 g for 5 min. The pellet was washed with B5-0.34M glucose-mannitol solution and resuspended in B5-0.34M glucose-mannitol solution to a final concentration of $2x10^5$

protoplasts per 50 μl. The protoplasts were co-transfected with 3 μg of a reporter plasmid expressing *Firefly* Luciferase (*f*LUC), 2 μg of a normalization plasmid containing the *Renilla* Luciferase (*r*LUC) and 10 μg of the p2GW7,0 plasmid carrying either the cytokinin receptor (*35S::AHK4-GFP*) or reporter only (*35S::GUS* or *35S::GFP*) constructs. DNAs were gently mixed with 50 μl of protoplast suspension and 60 μl of PEG solution (0.1M $Ca(NO_3)_2$, 0.45M mannitol, 25% PEG 6000) and incubated in the dark for 30min. Then 140 μl of 0.275M $Ca(NO_3)_2$ solution was added to wash off PEG, wait for sedimentation of the protoplasts and remove 240 μl of the supernatant. The protoplast pellet was resuspended in 200 μl of B5-0.34M glucose-mannitol solution and incubated for 16 h with either 0.5 μM BA or in mock solution in the dark at room temperature. After transfection, the protoplasts were centrifuged at 1200g for 5 min and lyzed; *f*LUC and *r*LUC activities were determined with the Dual-Luciferase reporter assay system (Promega). Variations in transfection efficiency and technical errors were corrected by normalization of *f*LUC by the *r*LUC activities. The mean value was calculated from four measurements and experiment was repeated three times.

Root growth analysis

Root growth and lateral root density were measured on seedlings grown vertically on Murashige and Skoog medium. Images were taken with a vertically positioned scanner, EPSON perfection v800 Photo. The root growth rate was evaluated using 5-day-old seedlings (n ≥ 16). Lateral root density quantification was performed using 9-day-old seedlings (n ≥ 16). Relative root growth inhibition by cytokinin was measured per day (24h) and was calculated as a ratio of 1 μM BA to DMSO treated *Arabidopsis* seedlings in the corresponding days after germination. The statistical significance was evaluated with the Student's t-test and two-way ANOVA.

Statistics

The statistical significance was evaluated with the Student's t-test and two-way ANOVA.

Results and discussion

Cytokinin fluoroprobe iP-NBD exhibits affinity to the cytokinin receptors

Fluorescently labelled analogues of phytohormones including auxin, gibberellin, brassinosteroid and strigolactone have been successfully used to map the intracellular fate of their receptors *in planta* (Lace and Prandi, 2016). To adopt this tool for mapping subcellular localization of cytokinin receptors, using docking experiments and cytokinin activity screening bioassays, a fluorescently labelled bioactive compound that interacts with the binding site of a cytokinin receptor was selected.

Cytokinin groups a collection of N^6-substituted adenine derivatives, including *t*Z and iP. They show different localization pattern and distinct partially overlapping functions *in planta*. *t*Z-type cytokinins play a role of acropetal messengers, whereas iP-type cytokinins operate as systemic or basipetal messengers (Kudo et al., 2010). The isoprenoid cytokinins (*t*Z- or iP-types) showed similar distribution patterns in different cell type populations within the root apex (Antoniadi et al., 2015). While *t*Z-type cytokinins were detected at much lower levels than other isoprenoid cytokinins, when concerns free cytokinin bases, the *t*Z content was found to be the highest among the free bases, followed by free iP that showed relatively enhanced content also in the stele (Antoniadi et al., 2015). Hence, iP seems to be a good candidate for a cytokinin fluoroprobe design. Moreover, iP is a natural cytokinin that cannot be transformed through *O*-glycosylation at the cytokinin side chain and thus the possibility of metabolic conversions of the cytokinin fluoroprobe by cytokinin deactivation enzymes *in planta* is minimized. Furthermore, a covalent attachment of NBD, a small fluorophore, to the *N*9 position of iP eliminates the risk of metabolic conversion of the final cytokinin fluorescent probe iP-NBD (Figure 16A) through *N*-glycosylation, or formation of cytokinin nucleotides.

The stable attachment of the *N*9-substituent also prevents modifications at the *N*7 position by making this cytokinin derivative completely inaccessible for *N*-glucosyltransferases (Hou et al., 2004). Docking simulations using the CRE1/AHK4-iP crystal structure (Hothorn et al., 2011) and corresponding homology models suggested

that iP-NBD may be fully embedded into the active sites of all AHK receptors (Figure 16B) with micromolar range affinity.
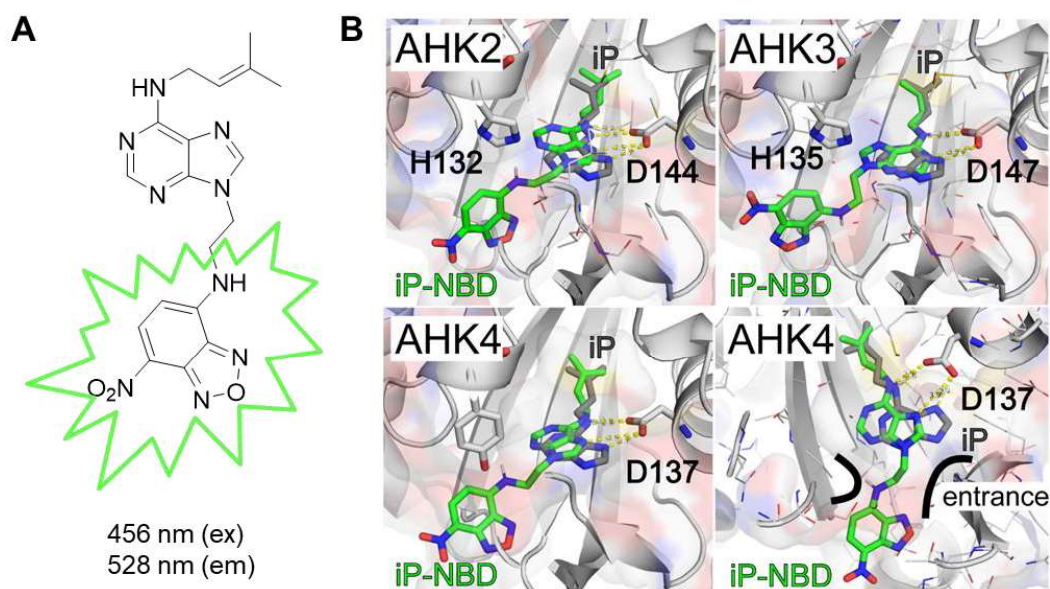

Figure 16: *Structure and docking simulations of iP-NBD. **A** – Chemical structure of iP-NBD with excitation and emission wavelengths. **B** – Superposition of docking simulation of iP-NBD (in green) and natural ligand iP (in grey) in AHK2, AHK3 (upper row) and CRE1/AHK4 (left panel of lower row) receptor cavity showing the embedded position of the ligands. CRE1/AHK4 (right panel of lower row) with visualized entrance channel and the fluorophore fitting into an antechamber through the ethylene linker.*

The affinity of iP-NBD to the cytokinin receptors was measured using bacterially expressed recombinant AHK3 and CRE1/AHK4 (Spíchal et al., 2004). Both receptors share ligand preference for *t*Z, but AHK3 has about 10-fold lower affinity towards iP compared to CRE1/AHK4 (Spíchal et al., 2004; Romanov et al., 2006). Competitive binding assays with *E. coli* expressing either AHK3 or CRE1/AHK4 (Romanov et al., 2005) showed that iP-NBD competes for receptor binding with radiolabelled natural cytokinins iP and *t*Z in different ranges of ligand concentrations (Figure 17A, B), corresponding with the receptor ligand preferences. As predicted, iP-NBD had a lower affinity to the AHK3 (with $K_i \sim$ 37 μM and > 100 μM against radiolabelled *t*Z and iP, respectively) than to the CRE1/AHK4 (with $K_i \sim$ 1.4 μM and$\sim$ 31 μM against radiolabelled *t*Z and iP, respectively), indicating that this fluoroprobe is more specific to CRE1/AHK4 (Figure 17A, B).

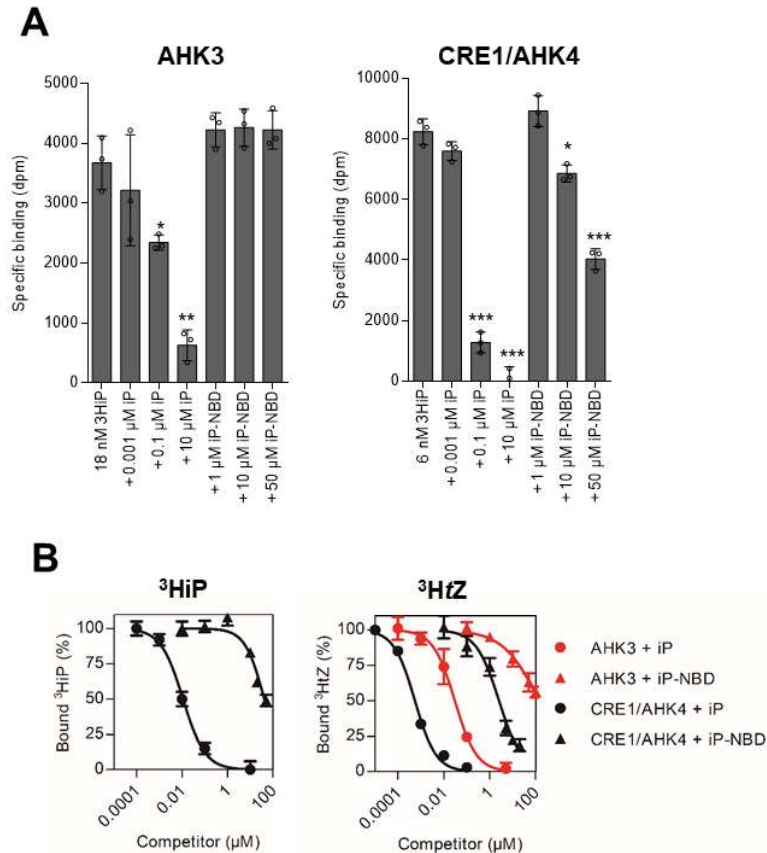**Figure 17:** *iP-NBD interacts with cytokinin perception. **A** – Competitive binding assay with E. coli expressing AHK3 and CRE1/AHK4. Binding of [2-³H]iP (18 nM and 6 nM in the case of AHK3 and CRE1/AHK4, respectively) was assayed together with increasing concentrations of unlabelled iP and iP-NBD. The bars represent mean ± s.d., *** = p < 0.001, ** = p < 0.01, * = p < 0.05; n = 3 (Student's t-test). **B** – Competitive binding assay with E. coli expressing AHK3 and CRE1/AHK4. Binding of 6 nM [2-³H]iP and 3 nM [2-³H]tZ was assayed together with increasing concentrations of of iP-NBD (triangles) and unlabelled iP (circles). The functional inhibition curves for AHK3 and CRE1/AHK4 are presented in red and black, respectively.*

Docking into the CRE1/AHK4-iP crystal structure (Hothorn et al., 2011) showed that iP-NBD binds into the receptor cavity in a similar manner to iP, but the lack of interaction via *N*9 (which links the fluorescent probe) causes the purine ring shift leading to the larger distance and thus weaker interaction between *N*7 and Asp137 (Figure 16B). Despite iP-NBD being accommodated into the cytokinin-binding pockets of the receptors, it showed limited ability to trigger cytokinin response in *E. coli* (*ΔrcsC, cps::lacZ*) receptor activation assay (Spíchal et al., 2004; Figure 18A). In *Arabidopsis* seedlings, iP-NBD in a concentration dependent manner significantly increased

expression of the early cytokinin response gene *ARABIDOPSIS RESPONSE REGULATOR5* (*ARR5*) already 15 minutes after its application, suggesting that the synthetic cytokinin fluoroprobe can activate cytokinin signalling pathway *in planta* (Figure 18B, C).
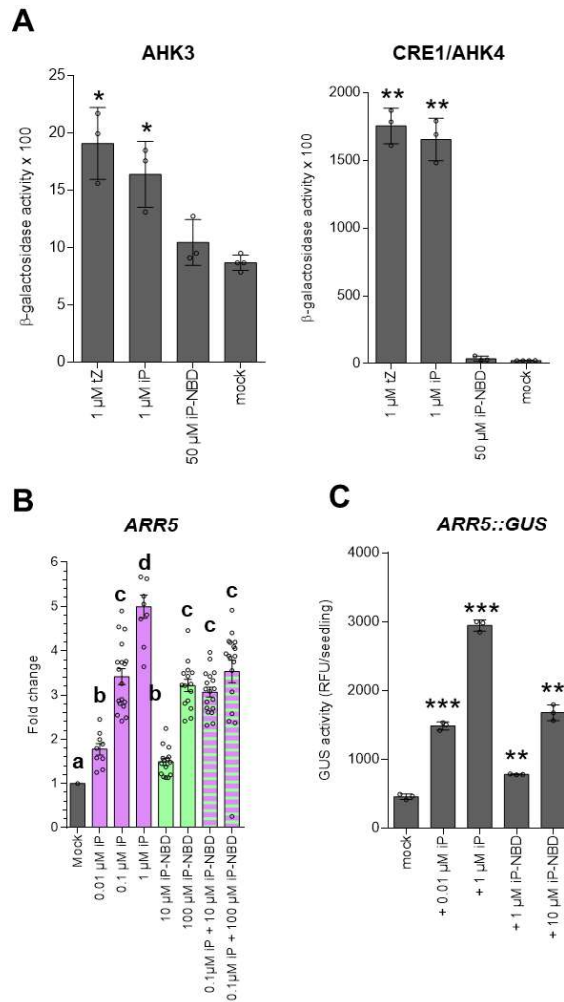

Figure 18: *A – Comparison of the cytokinin response in E. coli (ΔrcsC, cps::lacZ) receptor activation assay with recombinant AHK3 and CRE1/AHK4 receptors, triggered by 1 µM tZ and 1 µM iP (positive controls) and 50 µM iP-NBD. Mock treatment represents solvent control DMSO (0.1%). The bars represent mean ± s.d., ** = p < 0.01, * = p < 0.05; by Student's t-test, n = 3. **B** – Expression of the early cytokinin response gene ARR5 in 5-day-old seedlings of Col-0 treated with 0.01 µM iP, 0.1 µM iP, 1 µM iP, 10 µM iP-NBD, 100 µM iP-NBD or co-treatments of 0.1 µM iP + 10 µM iP-NBD, 0.1 µM iP + 100 µM iP-NBD or DMSO for 15 min. (mean ± s.d., p < 0.05 by two-way ANOVA. n = 9-18; 3 technical replicates from 3 biological replicates per condition). **C** - Quantitative evaluation of β-glucuronidase activity in Col-0 seedlings harbouring ARR5::GUS after incubation with 0.01 µM and 1 µM cytokinin iP, and 1 µM and 10 µM fluoroprobe iP-NBD. Mock treatment represents solvent control DMSO (0.1%). The bars represent mean ± s.d., *** = p < 0.001, ** = p < 0.01; n = 3 (Student's t-test).*

In comparison to iP, a natural cytokinin, iP-NBD triggered cytokinin response with significantly lower efficacy and when applied together with iP no additive effect on the *ARR5* expression could be detected (Figure 18B). In the *pTCSn::ntdTomato:TNOS* cytokinin reporter assay (Smet et al., 2019), iP-NBD did not increase expression of the reporter 6 hours after treatment, but when applied simultaneously with iP, iP-NBD partially attenuated iP-mediated enhancement of the TCS reporter expression (Figure 19).
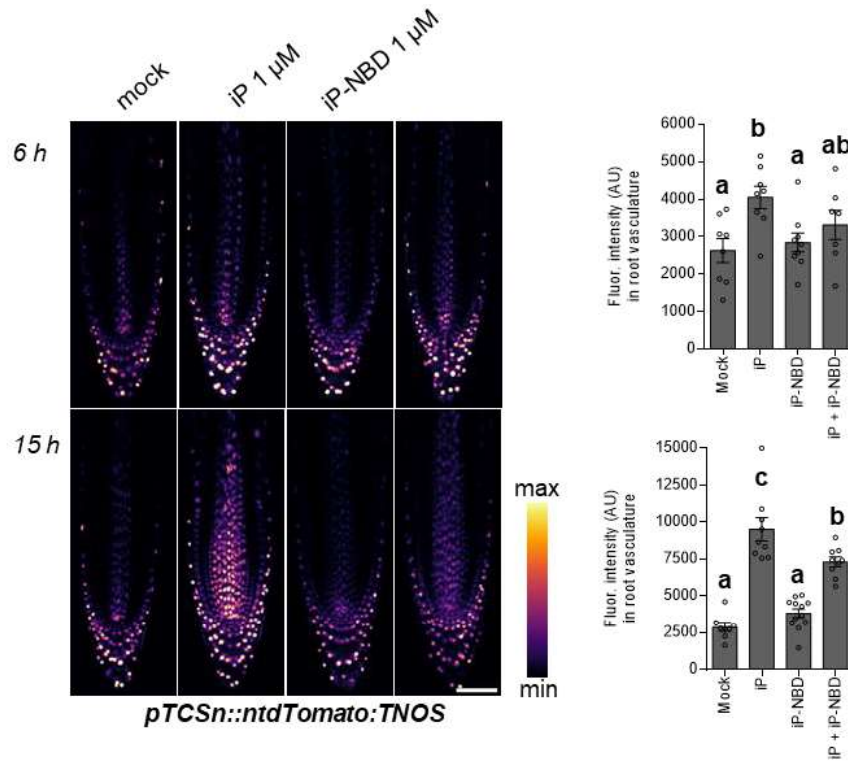
Figure 19: *Expression of the cytokinin sensitive reporter pTCSn::ntdTomato:TNOS in Arabidopsis roots treated with 1 µM iP (positive control) and 1 µM iP-NBD for 6 and 15 h. Fluorescence intensity measured in the root vasculature (mean ± s.d., p < 0.05 by two-way ANOVA, n > 8 root tips per condition). Scale bar = 50 µm.*

Altogether, these analyses suggest a partial agonistic mode of action of iP-NBD that binds to a cytokinin receptor and activates it with only minimal efficacy compared to a natural cytokinin ligand. At excess concentrations, iP-NBD is then acting as a competitive antagonist, competing with the full agonist (a natural cytokinin) for receptor occupancy. Altogether, the above experiments show that iP-NBD binds to

cytokinin receptors and has potential for specifically tracking their subcellular localization *in planta*.

Biological characteristics of iP-NBD

To reliably monitor iP-NBD distribution *in planta*, its biological stability, fluorescence characteristics and saturation kinetics was evaluated as first. iP-NBD stability across the different pH conditions that appear in apoplast, cytosol and different cell organelles, was tested *in vitro* in the pH ranging from 4 to 8 by quantitative liquid chromatography-tandem mass spectrometry (LC-MS/MS). No significant changes of iP-NBD concentration were found in the buffered solutions under both 6 and 16 hours of incubation pointing to a broad pH stability of iP-NBD (Figure 20A).

Figure 20: *Evaluation of iP-NBD biological stability. **A** – In vitro pH stability of iP-NBD. Stability of iP-NBD was followed by LC-MS/MS analysis in water solution after 0.5 h and 6 h of incubation in the McIlvaine buffer (pH range 4-8; left panel) and after 16 hours of incubation in the McIlvaine buffer (pH 4 and pH 6; right panel). Bars represent relative peak areas of iP-NBD, which was incubated for given time periods in the respective buffer solution as compared to the iP-NBD control (0 h) at the same concentration (mean ± s.d., n≥3). **B** – In vivo iP-NBD stability. iP-NBD was applied to Arabidopsis (Ler) cells suspension and in the timeframe of 0.5-5 h its intracellular processing was followed by quantitative LC-MS/MS analysis using iP-NBD and Ade-*

Taking into account the chemical structure of iP-NBD that prevents *O-* and/or *N*-glycosylation, the presumed *in planta* catabolic pathway of this molecule might be N^6 side-chain cleavage by endogenous CKX activity. Hence, the *in vivo* stability of the fluoroprobe was tested. iP-NBD was applied to *Arabidopsis* cells, and its intracellular processing was followed over a period of 0.5 - 5 h by LC-MS/MS analysis. Thus, iP-NBD and *N*9-NBD-labelled adenine (Ade-NBD), the expected product of iP-NBD deprenylation by CKXs, were used as molecular standards. Under these conditions, iP-NBD showed high stability within the first 30 minutes ($\geq$ 90% recovery of intact molecule), dropping drastically after 5 hours. The concentration of Ade-NBD steadily increased, reaching the maximal concentration after 4 hours (Figure 20B). The fact that iP-NBD can be recognized by CKXs as a substrate was confirmed by *in vitro* enzymatic reaction with AtCKX2, one of the most active CKX isoforms with an apoplastic localization (Werner et al., 2003). AtCKX2 converted iP-NBD to the product with approx. 6-times lower turnover rate k_{cat} compared to the parental iP molecule, but only with 33% lower catalytic efficiency V_{max}/K_m (Figure 20C).

Cellular internalization of iP-NBD follows rapid saturation kinetics

In terms of fluorescent characteristics, the emission maximum of the cytokinin fluoroprobe was in the yellow-green part of the spectrum at 528 nm suitable for co-localization with fluorescent markers emitting at red wavelengths (Figure 21A, B).
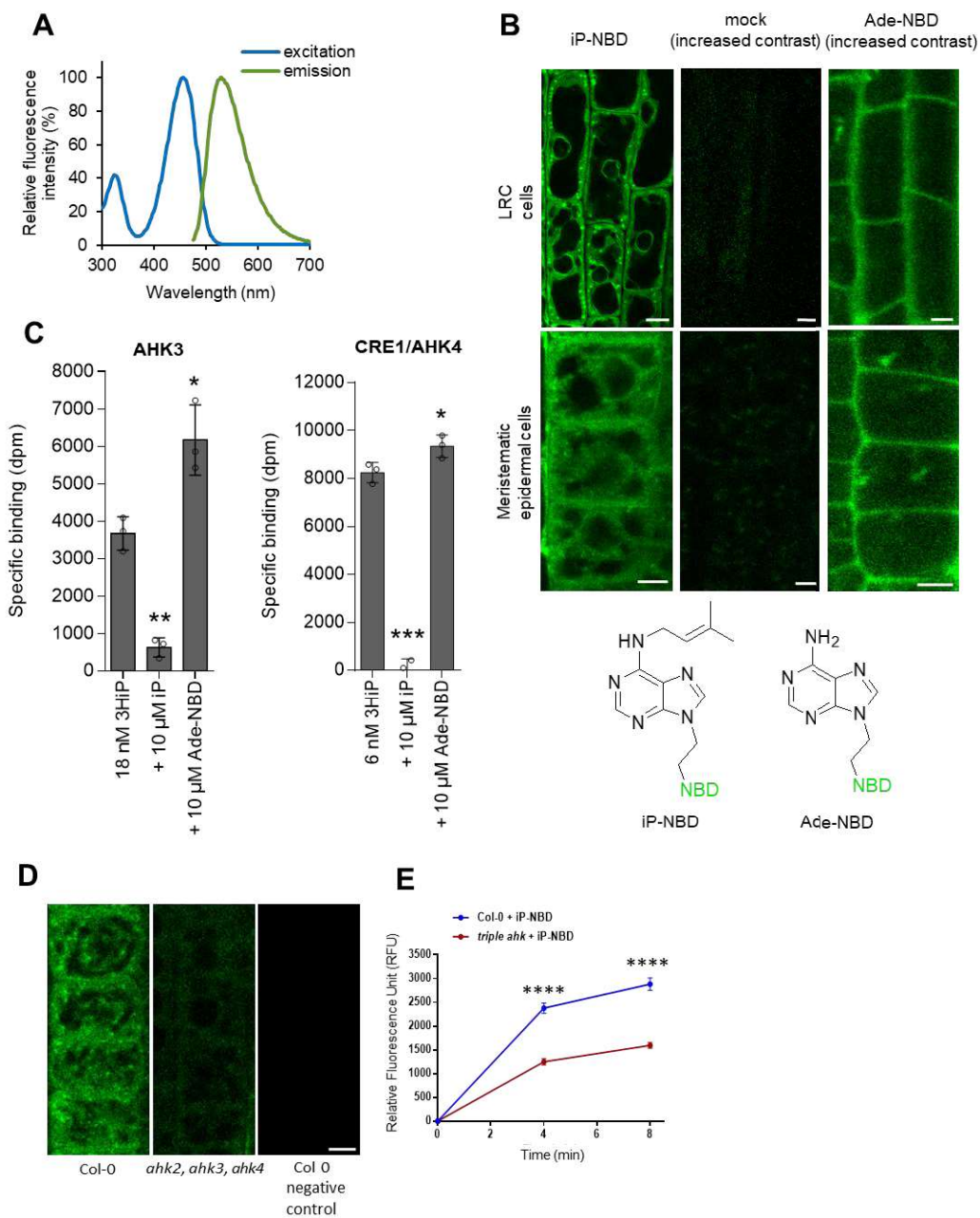
Figure 21: *Evaluation of iP-NBD fluorescence characteristics. **A** – Fluoroprobe absorption-emission spectral diagram measured with 100 µM iP-NBD dissolved in 100% ethanol. Absorption (excitation) and emission spectra are reaching their maximal fluorescence intensities in 456 nm (ex) and 528 nm (em). **B** – Chemical structures and differential localization of iP-NBD and Ade-NBD in Arabidopsis LRC and epidermal cells. Roots were treated for 10 min with iP-NBD or Ade-NBD (5 µM). Roots without any treatment (mock) were used as a control. **C** – Competitive binding assay with E. coli expressing AHK3 and CRE1/AHK4 with Ade-NBD. Binding of [2-^{3}H]iP (18 nM and 6 nM in the case of AHK3 and CRE1/AHK4, respectively) was assayed together with high excess concentration of Ade-NBD (10 µM), and unlabelled iP (10 µM) as a positive control (mean ± s.d., **** = p < 0.0001, *** = p < 0.001, ** = p < 0.01, * = p <*

0.05; by Student's t-test, n = 3). **D, E** *– Localization of iP-NBD (5 µM) in the Arabidopsis epidermal cells stained for 8 min in wild type (Col-0) and triple ahk mutant. All pictures were taken with the same settings. Col-0 without any treatment was used as a control (**D**). Graph shows kinetics of 5 uM iP-NBD uptake in the root epidermal cells of wild type and triple ahk mutant. Fluorescence was measured in 3 time points (0, 4, 8 min). The bars represent average ± s.e., **** = p < 0.0001; n ≥ 30 (Student's t-test). Scale bar = 5 µm.*

The quantitative fluorescence microscopy of the wild type plants (Col-0) showed that the cellular internalization of iP-NBD followed rapid saturation kinetics, reaching a plateau after approximately 12 min (Figure 22A). Pre-treatment with non-labelled iP and subsequent application of iP-NBD resulted in a significant reduction of intracellular iP-NBD fluorescence (Figure 22A). This suggested that transport and/or intracellular binding competition between iP-NBD and the natural cytokinin competitor was taking place, further pointing to the cytokinin-like properties of the iP-NBD molecule. Significantly slower progression of iP-NBD accumulation in cells of a *pup14* mutant (lacking the functional cytokinin transporter PUP14) confirmed that specific cytokinin transport partially accounts for the amount of iP-NBD detected intracellularly (Figure 22B).
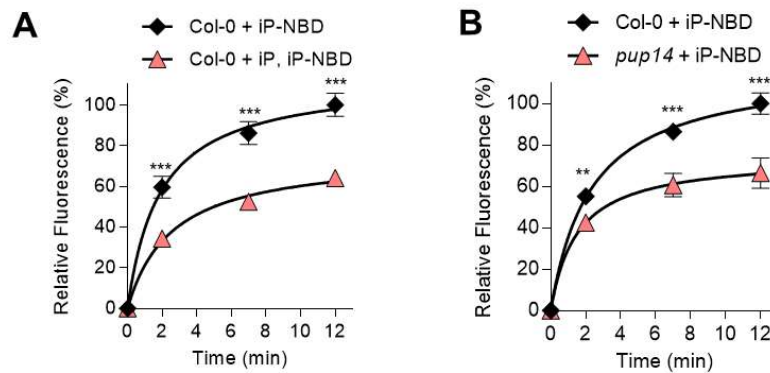

Figure 22: *iP-NBD interacts with cytokinin transport.* **A** *– Kinetics of 5 µM iP-NBD uptake in Arabidopsis LRC cells of wild type (Col-0) pre-treated with 5 µM iP.* **B** *– Kinetics of 5 µM iP-NBD uptake in root meristem epidermal cells of wild type (Col-0) and pup14. iP-NBD fluorescence was measured in four time points (0, 2, 7 and 12 min). The bars represent mean ± s.d., *** = p < 0.001, ** = p < 0.01; n ≥ 20 (Student's t-test; A, B).*

Unlike iP-NBD, Ade-NBD, which lacks the cytokinin-specific side chain, has no affinity to the cytokinin receptors (Figure 21C) and exhibited a weak diffused apoplastic and patchy intracellular signal in the epidermal cells (Figure 21B). The

results from analyses of the *ahk2*, *ahk3*, *ahk4* triple mutant show a reduced accumulation of iP-NBD in the root epidermal cells when compared to the WT (Figure 21D, E). However, the mutant lacking all three receptors exhibits severe developmental defects, seedlings are small with short roots. Thus, the reduced iP-NBD signal in cells might be a result of less efficient transport or overall affected fitness of these seedlings.

iP-NBD co-localizes with ER, TGN and early endosomal markers

The affinity of iP-NBD to the cytokinin receptors, in particular to the CRE1/AHK4, motivated us to monitor subcellular localization of this cytokinin fluoroprobe, aiming to trace potential sites of interaction with the receptor. Two cell types, namely differentiated lateral root cap (LRC) cells and epidermal cells at the root meristematic zone of *Arabidopsis* root, were selected for in depth analyses. In a line with reported ER-localization of the AHK cytokinin receptors (Caesar et al., 2011; Wulfetange et al., 2011), iP-NBD co-localized with p24δ5-RFP, an ER-specific marker, in both cell types (Figure 23A, B; red arrowheads; Table 2).
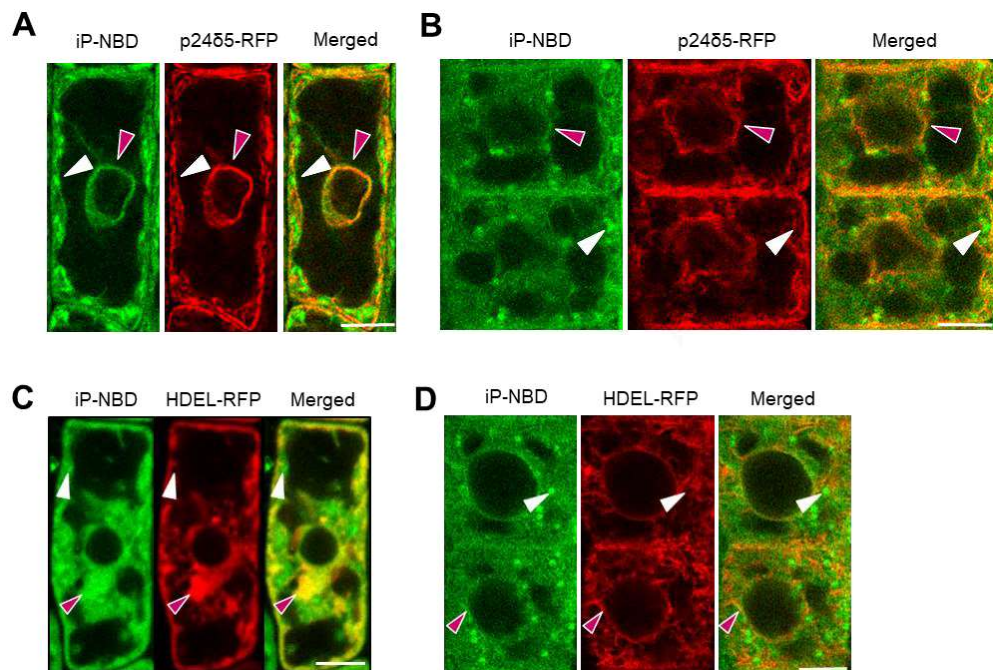

Figure 23: *Monitoring of the fluorescently labelled cytokinin iP-NBD in cells of Arabidopsis root. A, B – Monitoring of the fluorescently labelled cytokinin iP-NBD (green) and ER marker p24δ5-RFP (red) in LRC cells (A) and root meristematic epidermal cells (B). iP-NBD detected partially*

81

*co-localizing with p24δ5-RFP in the ER (red arrowheads) and in non-ER cellular structures (white arrowheads). **C, D** – Monitoring of iP-NBD (green) and ER marker HDEL-RFP (red) in LRC cells (**C**) and epidermal cells (**D**). iP-NBD detected partially co-localizing with HDEL-RFP in ER (red arrowheads) and in non-ER cellular structures (white arrowheads). Scale bars = 5 µm.*

Notably, also a strong iP-NBD fluorescence signal was detected in distinct spot-like structures, which did not overlap with the ER reporter (Figure 23A, B; white arrowheads). Likewise, co-visualization with HDEL-RFP, an ER-specific marker, corroborated dual ER and spot-like localization of iP-NBD in both LRC and epidermal cells (Figure 23C, D).

Table 2: *Pearson's correlation coefficients of iP-NBD co-localization with marker lines. Quantification of co-localization of iP-NBD staining with various markers for different subcellular compartments (ER – endoplasmic reticulum, GA – Golgi apparatus, RE – recycling endosomes, TGN/EE – trans-Golgi network, early endosomes, LE/PVC – late endosomes/pre-vacuolar compartments). Average ± s.e., n = 8-25.*

iP-NBD colocalization with marker lines			Pearson's correlation coefficient	
line	compartment	fusion protein	LRC cells	Meristematic epidermal cells
p24δ5-RFP	*ER*	p24δ5-RFP	0.61 ± 0.02	0.50 ± 0.02
W18	*GA*	Got1p-mCherry	0.67 ± 0.02	0.56 ± 0.03
W22	*GA*	SYP32-mCherry	0.69 ± 0.02	0.53 ± 0.03
W34	*endosomes, RE*	RabA1e-mCherry	0.39 ± 0.06	0.43 ± 0.04
W13	*TGNIEE*	VTI12-mCherry	0.28 ± 0.04	0.32 ± 0.04
W2	*LE/PVC*	RabF2b-mCherry	-0.15 ± 0.03	-0.18 ± 0.05
W9	*vacuoles*	VAMP711-mCherry	-0.12 ± 0.04	0.00 ± 0.00

To further explore the nature of the peripheral and spot-like subcellular structures showing affinity to the iP-NBD, co-staining with FM4-64, the membrane selective dye labelling PM and endosomal/recycling vesicles in plant cells was performed (Jelínková et al., 2010). In both epidermal and LRC cells, iP-NBD signal was detected intracellularly and partially co-localized with the FM4-64 stained vesicles corresponding to the internalized and recycling endosomes (Figure 24A, C and Figure 25A). Interestingly, detailed profiles of fluorescence intensity distributions of iP-NBD and FM4-64 revealed their partial co-localization at the PM of the epidermal cells, which was not the case for

LRC (Figure 24B compared to 24D). These observations suggested that apart from ER, iP-NBD might accumulate in subcellular vesicles and at the PM.
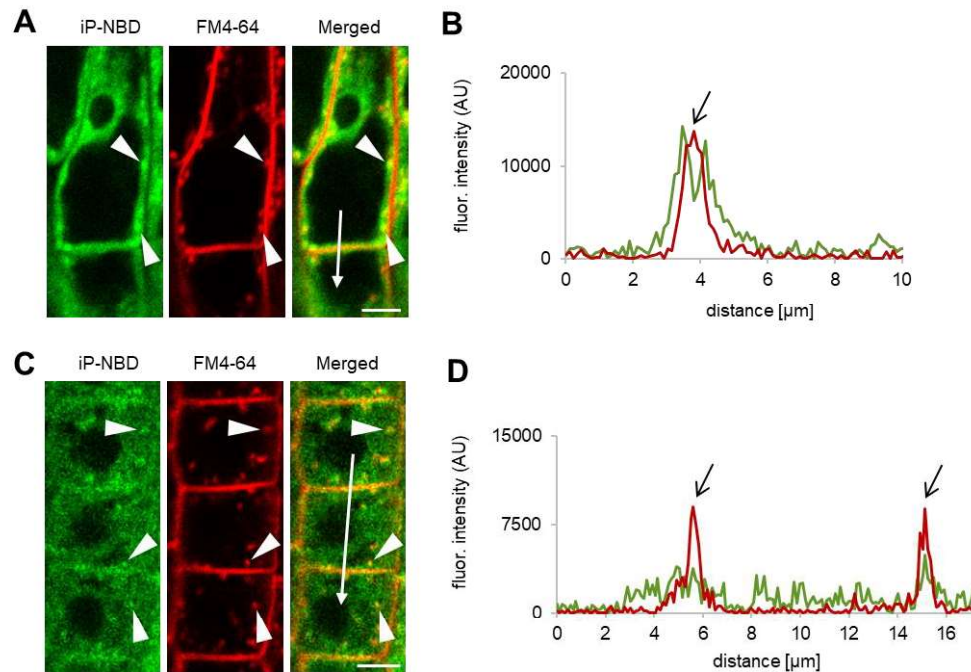

Figure 24: *Monitoring of iP-NBD (green) and FM4-64 (red, membrane selective dye) in LRC (**A,** **B**) and root meristematic epidermal cells (**C, D**). White arrowheads (**A, C**) indicate co-localization of iP-NBD and FM4-64 in vesicles. Profiles of the fluorescence intensity distribution of both FM4-64 (red line) and iP-NBD (green line) in LRC (**B**) and epidermal (**D**) cells were measured along the white lines (**A, B**) starting from the upper end (0 µm) towards the arrowhead. Peaks of FM4-64 fluorescence maxima (black arrows) correlate with the PM staining. iP-NBD fluorescence maximum does not overlap with FM4-64 fluorescence peak at the PM in LRC cell (**B**). Peaks of iP-NBD signal partially overlap with FM4-64 maxima and indicate the presence of cytokinin fluoroprobe at the PM of epidermal cells (**D**). Scale bars = 5 µm.*

To gain further insights into the iP-NBD subcellular localization and to test its affinity to endomembrane structures the impact of brefeldin A (BFA) was analysed. BFA is a fungal toxin, inhibiting ER-Golgi and post-Golgi trafficking to the PM and to vacuoles, thus causing the formation of endosomal clusters, so-called BFA compartments (Orci et al., 1993). Strikingly, in the root epidermal cells accumulation of iP-NBD signal in clusters corresponding to the BFA compartments stained with FM4-64 was observed (Figure 25B, blue arrowheads).
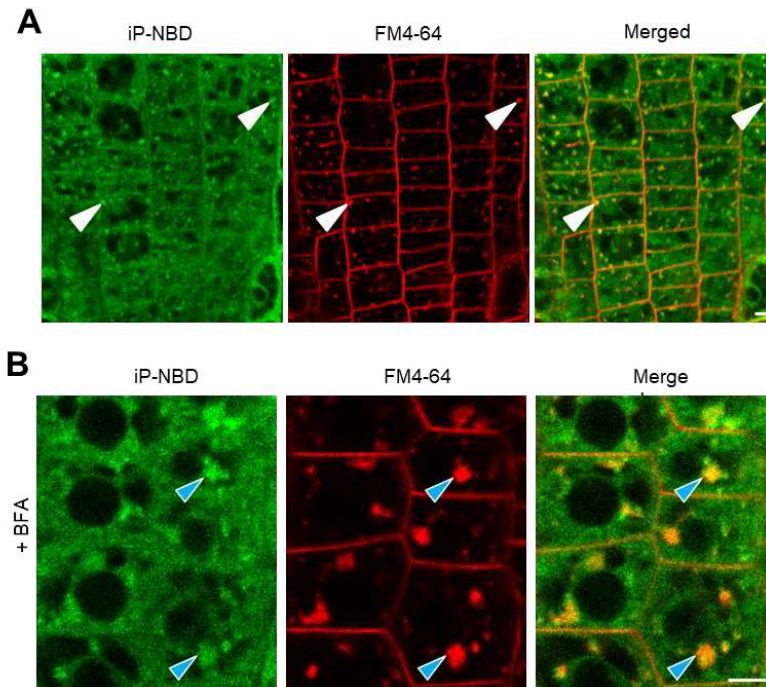
Figure 25: *Monitoring of iP-NBD subcellular localization in Arabidopsis root cells. **A** – Co-staining of root epidermal cells with iP-NBD (green) and FM4-64 (red) monitored 15 minutes after co-treatment. White arrowheads indicate co-localization of iP-NBD and FM4-64 in vesicles. **B** – Co-localization of iP-NBD and FM4-64 in endosomal compartments (blue arrowheads) formed in root meristematic epidermal cells treated with 50 μM in BFA for 1 h. Scale bars = 5 μm.*

Co-localization with RabA1e-mCherry, a BFA-sensitive endosome/recycling endosome marker, provided additional supporting evidence that in the root epidermal cells iP-NBD exhibits affinity to the vesicular endomembrane system where subpopulations of cytokinin receptors may be localized (Figure 26A; Table 2). Next, the localization of the cytokinin fluoroprobe using a set of Wave marker lines specific for various subcellular organelles was traced (Geldner et al., 2009). Notably, in the root epidermal cells, a partial co-localization of iP-NBD with a *cis*-Golgi (GA) marker, SYP32-mCherry (Figure 26B; Table 2), an integral GA membrane protein, Got1p homolog-mCherry (Figure 26C; Table 2), and with TGN/early endosome marker, VTI12-mCherry (Figure 26D; Table 2) was observed. Interestingly, iP-NBD did not co-localize with a late endosome marker, RabF2b/W2R-mCherry (Figure 26E; Table 2) nor with a vacuolar marker, VAMP711-mCherry (Figure 2F; Table 2).
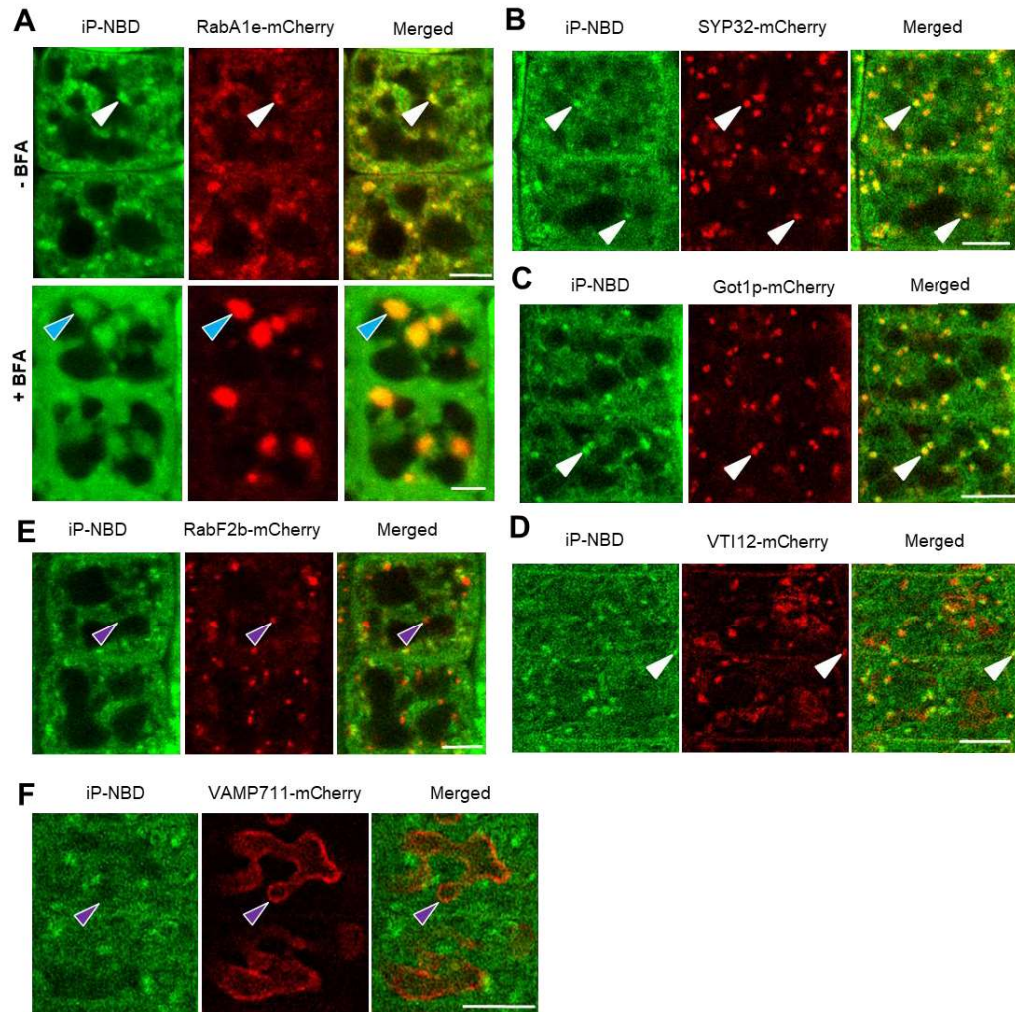
Figure 26: *Monitoring of iP-NBD subcellular localization in Arabidopsis root epidermal cells. **A** – Co-localization of iP-NBD (green) and RabA1e-mCherry (red) endosome/recycling endosome marker. Upper panel: co-localization of iP-NBD with RabA1e in vesicles (white arrowheads) before BFA treatment. Lower panel: accumulation of iP-NBD and RabA1e in endosomal compartments (blue arrowheads) formed in root epidermal cells treated with 50 µM BFA for 1 h. **B** – Partial co-localization of iP-NBD (green) with a cis-GA marker SYP32-mCherry in root epidermal cells. White arrowheads indicate overlapping signals. **C, D** – Partial co-localization of iP-NBD (green) with an integral GA membrane protein Got1p-mCherry (**C**) and TGN/early endosome marker VTI12-mCherry (**D**) in root epidermal cells. White arrowheads indicate overlapping signals. **E, F** – Non-overlapping signals of iP-NBD (green) and late endosome marker RabF2b-mCherry (red, **E**) or vacuolar marker VAMP711-mCherry (red, **F**) in root epidermal cells. Purple arrowheads indicate RabF2-mCherry stained endosomes (**E**) and VAMP711-mCherry vacuolar compartments (**F**). Scale bars = 5 µm.*

In cells of LRC, a partial co-localization with the GA markers, SYP32-mCherry (Figure 27A; Table 2) and Got1p homolog-mCherry (Figure 27B; Table 2), an

endosome/recycling endosome marker RabA1e-mCherry (Figure 27C; Table 2) and with the TGN/early endosomal marker VTI12 (Figure 27D; Table 2) was observed. However, no co-localization was detected with late endosomal RabF2b-mCherry (Figure 27E; Table 2) or vacuolar VAMP711-mCherry markers (Figure 27F; Table 2).
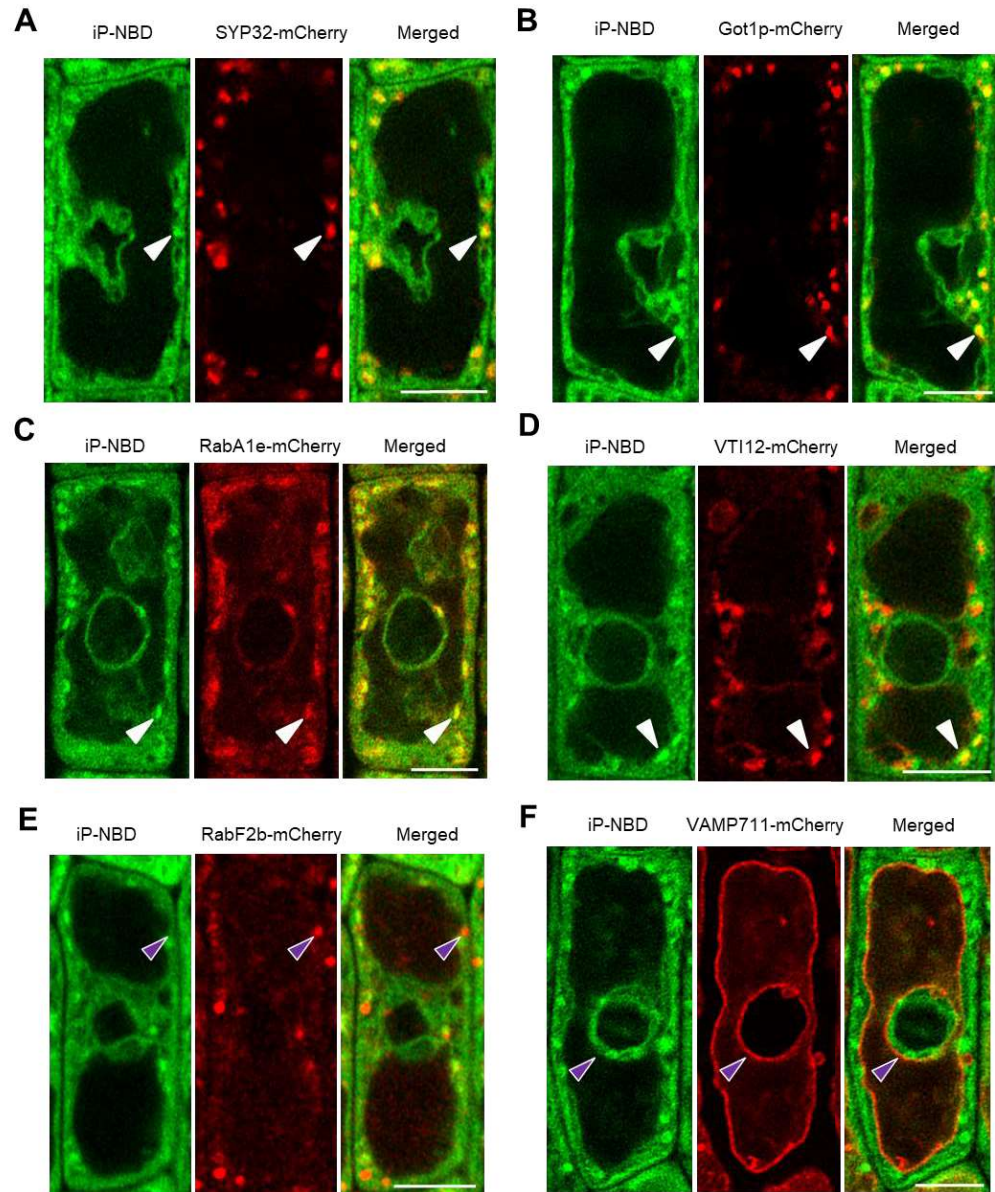

Figure 27: *Monitoring of iP-NBD subcellular localization in Arabidopsis lateral root cap cells. A-D – Co-localization of iP-NBD (green) with a cis-GA marker SYP32-mCherry (red, A), an integral GA membrane protein Got1p-mCherry (red, B), endosome/recycling endosome marker RabA1e-mCherry (red, C) and TGN/early endosome marker VTI12-mCherry (D) in the LRC cells. White arrowheads indicate overlapping signals. E, F – Non-overlapping signals of iP-NBD (green) and late endosome marker RabF2b-mCherry (E) or vacuolar marker VAMP711-mCherry (F, red) in*

the LRC cells. Purple arrowheads indicate subcellular compartments visualised by specific markers. Scale bars = 5 μm.

Overall, monitoring of iP-NBD in the LRC and epidermal cells corroborate the ER as an organelle with affinity to cytokinin. However, co-localization of iP-NBD with TGN and early endosomal markers as well as its accumulation in the BFA compartments indicate that proteins with the affinity to iP-NBD, such as cytokinin receptors, do not reside exclusively at ER, but may enter the endomembrane trafficking system and possibly localize also to the PM.

Generation and isolation of the CRE1/AHK4-GFP transgenic lines

Previously, ER-localization of *Arabidopsis* cytokinin receptors has been demonstrated using transiently transformed *Nicotiana benthamiana* (Caesar et al., 2011; Wulfetange et al., 2011) and *Arabidopsis* (Caesar et al., 2011), and by employing cytokinin-binding assays with fractionated *Arabidopsis* cells expressing Myc-tagged receptors (Wulfetange et al., 2011). However, so far no experimental support has been provided for their possible entry into the subcellular vesicular trafficking and PM localization. Yet, the possibility of cytokinin HKs localization to the PM has been hypothesised within the context of an integrative model for cytokinin perception and signalling (Romanov et al., 2018). The potential sites of CKs perception had been questioned in relation to the pH dependence of the binding by HKs. It was shown that the cytokinin binding to AHK3 is pH dependent with an optimum at basic pH and a dramatic decrease at acidic pH (Romanov et al., 2006). This finding fits with the ER-localization of cytokinin receptors and has also been used to cast doubt on PM-function of the receptors due to the acidic pH of apoplast acting as a constraint on efficient cytokinin binding. However, in contrary to the AHK3, CRE1/AHK4 affinity was shown not to be dramatically altered at acidic pH (Romanov et al., 2006). Importantly, a recent work by Jaworek et al. (Jaworek et al., 2020) shows a detailed analysis of pH influence on binding strength of CKs to the receptors from poplar (*Populus × canadensis* cv. *Robusta*). They showed that cytokinin binding to PcHK3 (ortholog of AHK3) steadily increases towards higher pH values, whereas binding to PcHK4 (ortholog of

CRE1/AHK4) linearly decreased from an optimum for ligand binding at pH 5.5. These findings support the idea that CRE1/AHK4 can effectively sense CKs from the apoplast.

The only cytokinin receptor studied for its localization using stably-transformed *Arabidopsis* plants was AHK3 (Caesar et al., 2011). Unlike this receptor, subcellular localization of CRE1/AHK4 has not been addressed in much detail. Taking into account a higher affinity of iP-NBD to this receptor, this study focused on monitoring its subcellular localization using *Arabidopsis* stable transgenic lines carrying *CRE1/AHK4-GFP* construct driven by a constitutive *35S* promoter. Two independent lines displaying significantly increased transcription of *CRE1/AHK4-GFP* when compared to the wild type were selected for detailed observations (Figure 28A). Western blot analyses confirmed the accumulation of the CRE1/AHK4-GFP product of proper ~150 kDa size in both lines, although lower levels of the fusion protein were detected in the *35S::CRE1/AHK4-GFP* line (1) when compared to the line (2) (Figure 28B, C). To test the functionality of the CRE1/AHK4-GFP fusion protein, transient expression assays in the *Arabidopsis* protoplasts were performed. Co-expression of *35S::CRE1/AHK4-GFP* with a cytokinin sensitive reporter *TCS::LUCIFERASE* (*TCS::LUC*) resulted in 85 $\pm$ 6.9 fold upregulation of the reporter activity by cytokinin when compared to protoplasts co-transformed with controls (plasmids carrying either *GFP* or *GUS* reporter only resulting in 28 $\pm$ 2.4 and 32 $\pm$ 1.5 fold increase of Luciferase activity, respectively; Figure 28D). *In planta,* the functionality of the CRE1/AHK4-GFP was tested by expression analyses of the type-A early cytokinin response genes in the *35S::CRE1/AHK4-GFP* transgenic lines. Application of cytokinin resulted in a strong upregulation of *ARR5* and *ARR7* in a wild type and both transgenic lines expressing CRE1/AHK4-GFP (Figure 28E). However, a significantly enhanced transcription of *ARR5* and *ARR7* in response to cytokinin compared to wild type was detected only in the *35S::CRE1/AHK4-GFP* line (2)*,* which displayed a higher accumulation of CRE1/AHK4-GFP. *ARR5* and *ARR7* have been reported as being among the most sensitive type-A early cytokinin response genes, reaching expression maxima within 10-15 minutes following cytokinin application (D'Agostino et al., 2000). It can be argued that high responsiveness of these genes to cytokinin might hinder the detection of more subtle changes in cytokinin sensitivity in the line with lower expression of the CRE1/AHK4-GFP.
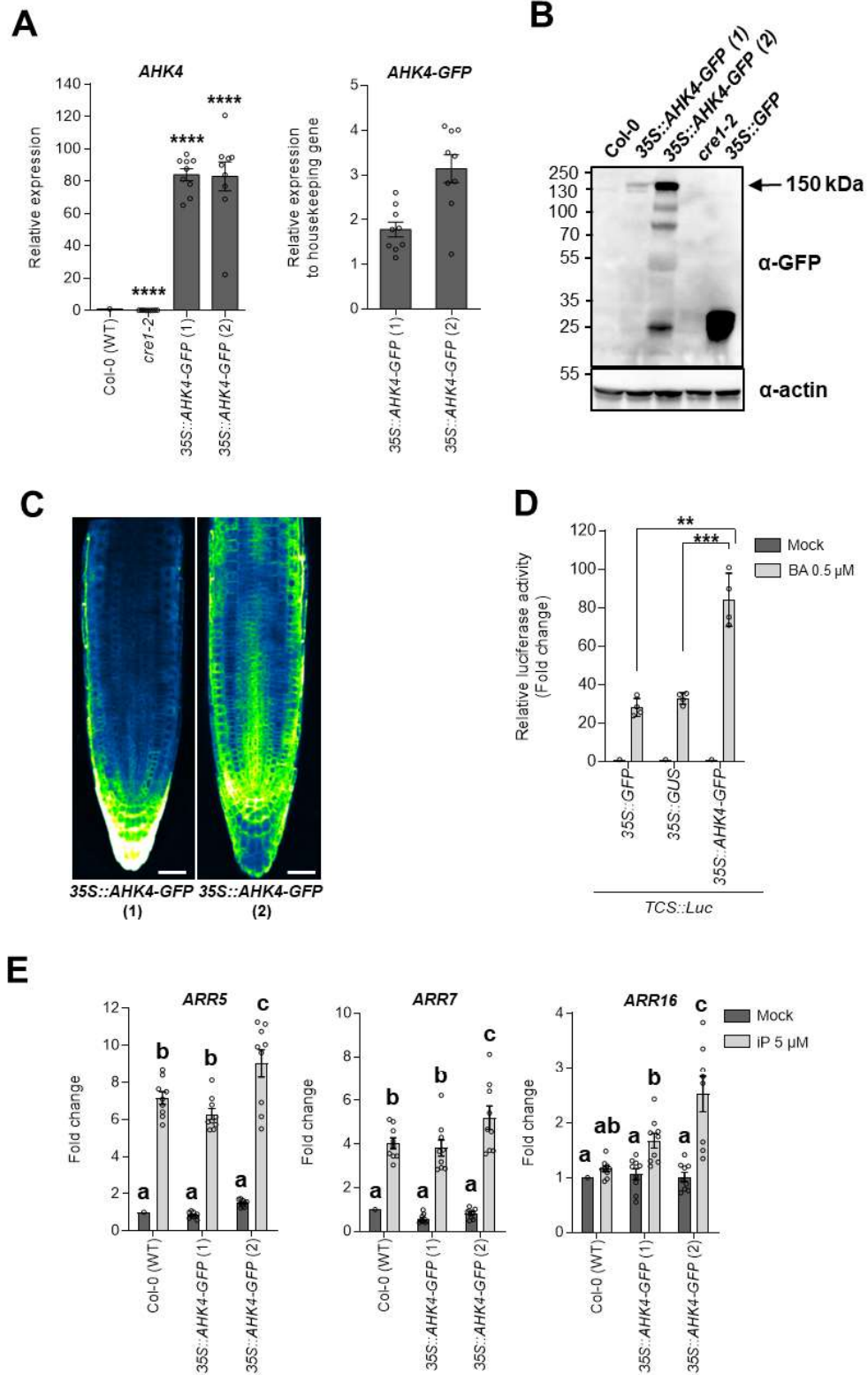
Figure 28: *Analysis of CRE1/AHK4-GFP functionality in vivo.* ***A*** *– Expression analysis of AHK4 and AHK4-GFP in 5-day-old seedlings using quantitative RT-PCR. Relative expression of*

*cytokinin reporter in two 35S::AHK4-GFP independent lines was evaluated when compared to Col-0 (WT; left panel), or housekeeping gene (right panel). Mean ± s.d., p < 0.05 by two-way ANOVA. n = 9 (3 technical replicates from 3 biological replicates) per condition. Specific primer pairs for CRE1/AHK4 (left graph) and CRE1/AHK4-GFP (right graph) were used. **B** – Western blot analysis of AHK4-GFP in total protein extracts from the two independent 35S::AHK4-GFP lines. Col-0, cre1-2, 35S::GFP used as controls. Membranes were incubated with anti-GFP and anti-actin antibodies. The arrow marks the expected molecular weight of AHK4-GFP (150 kDa). **C** – Monitoring of CRE1/AHK4-GFP signal in the meristematic zone of the Arabidopsis root in two independent 35S::AHK4-GFP lines. **D** – TCS::LUCIFERASE cytokinin reporter activity in Arabidopsis protoplasts co-transformed with the CRE1/AHK4-GFP reporter is significantly upregulated in response to cytokinin (0.5 µM BA) when compared to protoplasts co-transformed with either GFP or GUS reporter only (mean ± s.d; *** p < 0.001 Student's t-test indicates significant difference when compared to protoplasts transformed with 35S::GUS, n = 4). **E** – Expression of early cytokinin response genes ARR5, ARR7 and ARR16 in 5-day-old seedlings of Col-0 and the two independent 35S::AHK4-GFP lines treated with 5µM iP or DMSO for 15 min. (mean ± s.d., p < 0.05 by two-way ANOVA. n = 9; 3 technical replicates from 3 biological replicates per condition). Scale bar = 10 µm (**C**).*

When compared to *ARR5* and *ARR7*, *ARR16* showed maximum transcription within 40-60 min following cytokinin application (D'Agostino et al., 2000). A significantly higher expression of *ARR16* after cytokinin application for 15 minutes was detected in both CRE1/AHK4-GFP overexpressing lines when compared to the wild type. These results suggest that proportionally with levels of CRE1/AHK4-GFP expression, the sensitivity of both lines to cytokinin stimulus is enhanced (Figure 28E), indicating that CRE1/AHK4-GFP maintains its biological activity.

The transgenic *Arabidopsis* lines expressing CRE1/AHK4-GFP exhibited phenotypes typical of plants with enhanced activity of cytokinin such as a shorter primary root, slower root growth rate and decreased lateral root density (Figure 29A-D). Both transgenic lines expressing CRE1/AHK4-GFP displayed hypersensitive-like responses to exogenous cytokinin treatment on the primary root growth compared to the wild type control, and in contrast to the cytokinin insensitive *ahk4/cre1-2* loss of function mutant (Figure 29E).
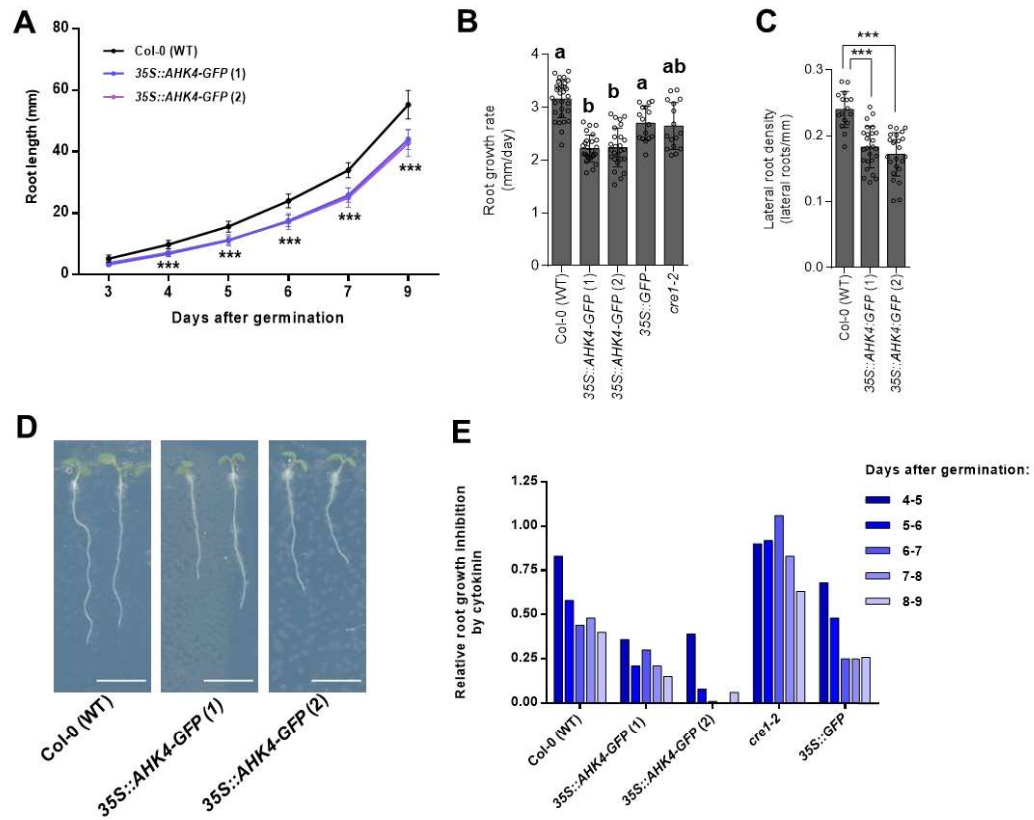
Figure 29: *Analysis of CRE1/AHK4-GFP functionality in vivo.* ***A*** *– Root length of 3- to 9-day-old seedlings of control Col-0 (black) and two independent 35S::AHK4-GFP lines (mean ± s.d., *** = p < 0.001 by Student's t-test, n ≥15).* ***B*** *– Average root growth rate (mm/day) of control Col-0, two independent 35S::AHK4-GFP lines, 35S::GFP and cre1-2 seedlings during 5 days (mean ± s.d.; p < 0.01 by ANOVA test, n ≥ 15).* ***C*** *– Lateral root density (number of lateral roots/root length) was evaluated in 9-day-old seedlings of control Col-0 and two independent 35S::AHK4-GFP lines (mean ± s.d.; *** = p < 0.001 by Student's t-test, n ≥15).* ***D*** *– Representative images of 5-day-old seedlings of control Col-0 and two independent 35S::AHK4-GFP lines.* ***E*** *– Relative inhibition of root growth by cytokinin in control Col-0, two independent 35S::AHK4-GFP lines, 35S::GFP and cre1-2 seedlings. Root growth on medium with and without cytokinin (BA 1 µM) monitored during 5 days (day 4 to 9 after germination) and relative root growth inhibition per day calculated (n = 10-15 roots). Scale bar = 5 mm (**D**).*

CRE1/AHK4-GFP co-localizes with the ER and the PM markers

As previously reported and in line with iP-NBD subcellular localization, CRE1/AHK4-GFP in the LRC and epidermal cells of root apical meristem co-localized with the ER marker p24δ5-RFP (Figure 30A-C; red arrowheads). Intriguingly, in the epidermal cells of root meristematic zone, CRE1/AHK4-GFP signal at the PM area, not co-localizing with the ER reporter, could also be detected (Figure 30D, E).
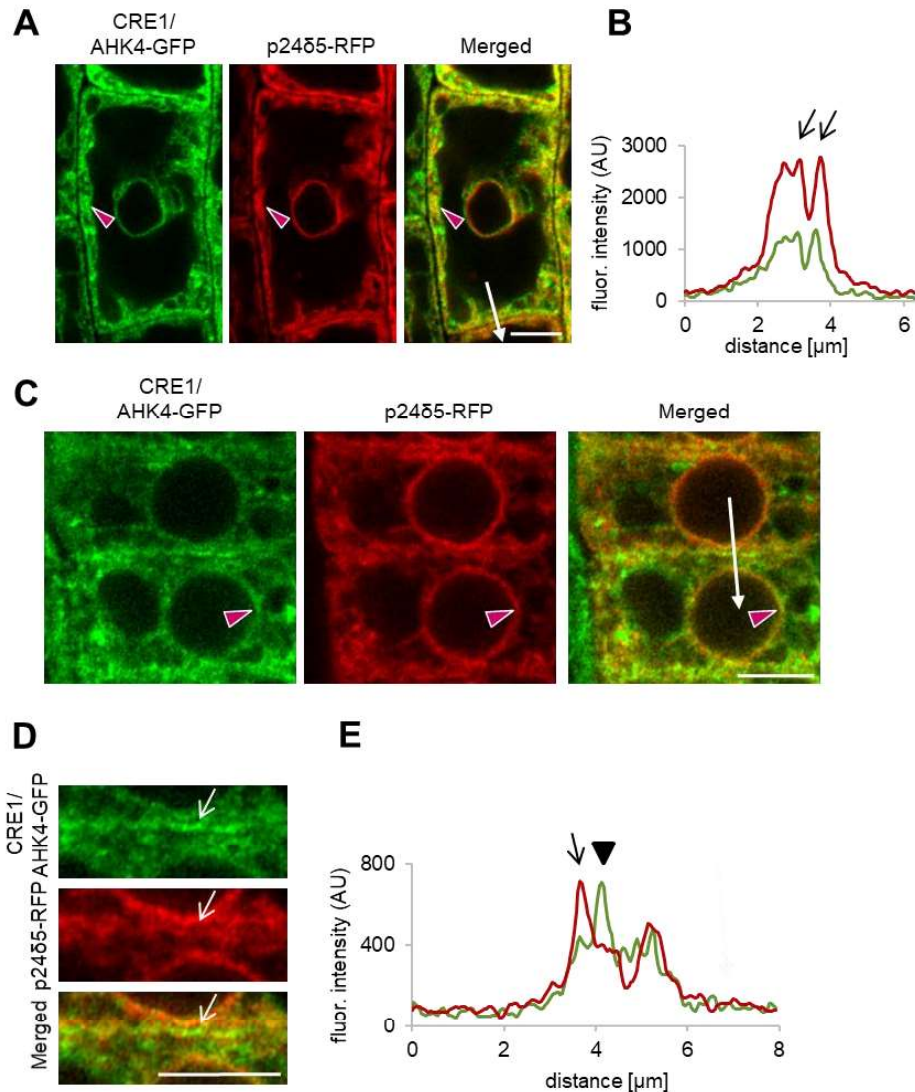
Figure 30: *CRE1/AHK4-GFP subcellular localization in cells of Arabidopsis root. **A-E** – Monitoring of the CRE1/AHK4-GFP cytokinin receptor (green) and ER marker p24δ5-RFP (red) in LRC cells (**A, B**) and root meristematic epidermal cells (**C-E**). Red arrowheads mark areas of co-localization. Fluorescence intensity profiles of the ER marker (red line) and CRE1/AHK4-GFP (green line; **B, E**) were measured along the white lines (**A, C**) starting from the upper end (0 µm) towards the arrowhead. Peaks of p24δ5-RFP fluorescence maxima at the ER overlap with CRE1/AHK4-GFP signal maxima in LRC cells and root meristematic epidermal cells (black arrows; **B, E**). Peak of CRE1/AHK4-GFP non-overlapping with peaks of p24δ5-RFP in root meristematic epidermal cells indicates localization at the PM (black arrowhead; **E**). Detailed view (**D**; white arrows point to CRE1/AHK4-GFP signal at the area of the PM). Scale bars = 5 µm.*

The subsequent analysis revealed a strong overlap of the CRE1/AHK4-GFP with the PM reporter PIP1;4-mCherry and NPSN12-mCherry (Figure 31A-D), thus hinting at localization of the cytokinin receptor at the PM. Moreover, in the dividing meristematic cells CRE1/AHK4-GFP could also be detected at the expanding cell plate (Figure 31C-F; asterisks) while it co-localized there with the established cell plate vesicular marker FM4-64 (Figure 31E, F).
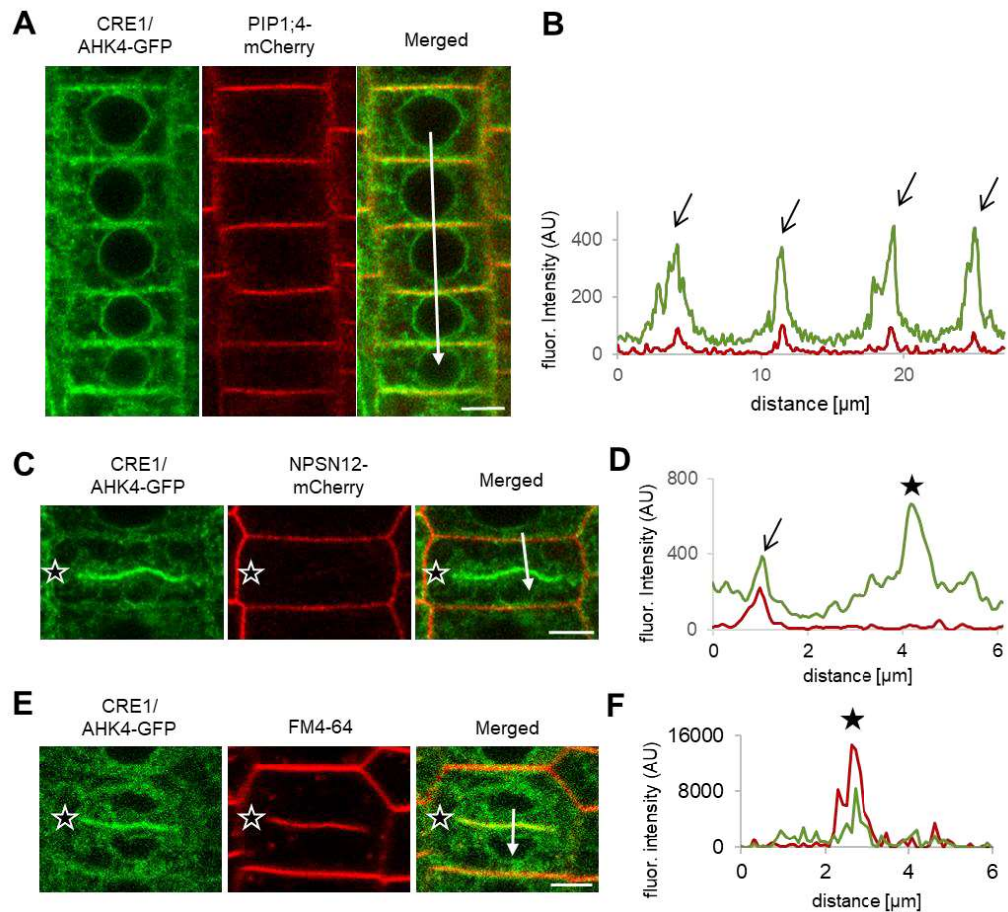

Figure 31: *CRE1/AHK4-GFP co-localization with the PM markers in Arabidopsis root cells. A-F – Co-localization of CRE1/AHK4-GFP with the PM markers PIP1;4-mCherry (A, B), NPSN12-mCherry (C, D) and FM4-64 (E, F) in root meristematic epidermal cells. Profiles of fluorescence intensity of the PM marker (red line) and CRE1/AHK4-GFP (green line; B, D, F) were measured along the white lines (A, C, E) starting from the upper end (0 µm) towards the arrowhead. Peaks of PIP1;4-mCherry and NPSN12-mCherry fluorescence maxima correlate with the PM staining and overlap with CRE1/AHK4-GFP signal maxima (black arrows; A-D). CRE1/AHK4-GFP signal detected at the cell plate of dividing cell (black stars on C, E) co-localizes with the FM4-64 marker (E, F; black stars) but not with the PM marker NPSN12-mCherry (C, D; black stars). Scale bars = 5 µm (A, C, E).*

Importantly, it has been shown that during cytokinesis the cell plate might receive material both from post-Golgi compartments as well as from the PM through sorting and recycling endosomes (Dhonukshe et al., 2006). Hence, detection of CRE1/AHK4-GFP at the cell plate provides further supporting evidence that the cytokinin receptor might reside outside of ER, namely on cytokinetic vesicles forming a cell plate (Smertenko et al., 2017).

Further evidence confirming localization of the CRE1/AHK4-GFP to the PM resulted from the subcellular study using super-resolution structural illumination microscopy (SIM; Komis et al., 2015b). This SIM analysis revealed co-localization of the CRE1/AHK4-GFP with FM4-64 labelled PM with average Pearson's coefficient 0.345 ± 0.113 (n = 30; Figure 32A). Unlike epidermal cells of the root meristematic zone, in LRC cells, the CRE1/AHK4-GFP signal resided in the ER and no co-localization with a PM reporter (NPSN12-mCherry) could be detected (Figure 32B, C). Inhibition of endocytic trafficking and vesicular recycling in meristematic cells by BFA resulted in co-accumulation of the CRE1/AHK4-GFP and FM4-64 in the BFA compartments in line with the presence of the receptor in the endomembrane system (Figure 32D). Wash-out of BFA allowed re-localization of the cytokinin receptor back to the PM indicating that it might cycle between PM and TGN (Figure 32F). Although occasionally in some cells of LRC co-staining with FM4-64 revealed CRE1/AHK4-GFP in the BFA compartments, they were relatively rare and randomly scattered in some LRC cells indicating that CRE1/AHK4-GFP trafficking in differentiated cells of LRC might differ from that observed in the epidermal cells of root apical meristem (Figure 32G). Importantly, no accumulation of the ER marker p24δ5-RFP in the BFA compartments in either epidermal cells of the meristem (Figure 32E) or the LRC cells (Figure 32H) could be detected, suggesting that the CRE1/AHK4-GFP signal is specifically enriched in the BFA bodies and not related to structural changes of ER in the BFA-treated cells.

Altogether, these results indicate that in the LRC cells CRE1/AHK4 may reside preferentially at the ER, whereas in the epidermal cells of root apical meristem the cytokinin receptor can enter the endomembrane system and localizes both at the ER and the PM.
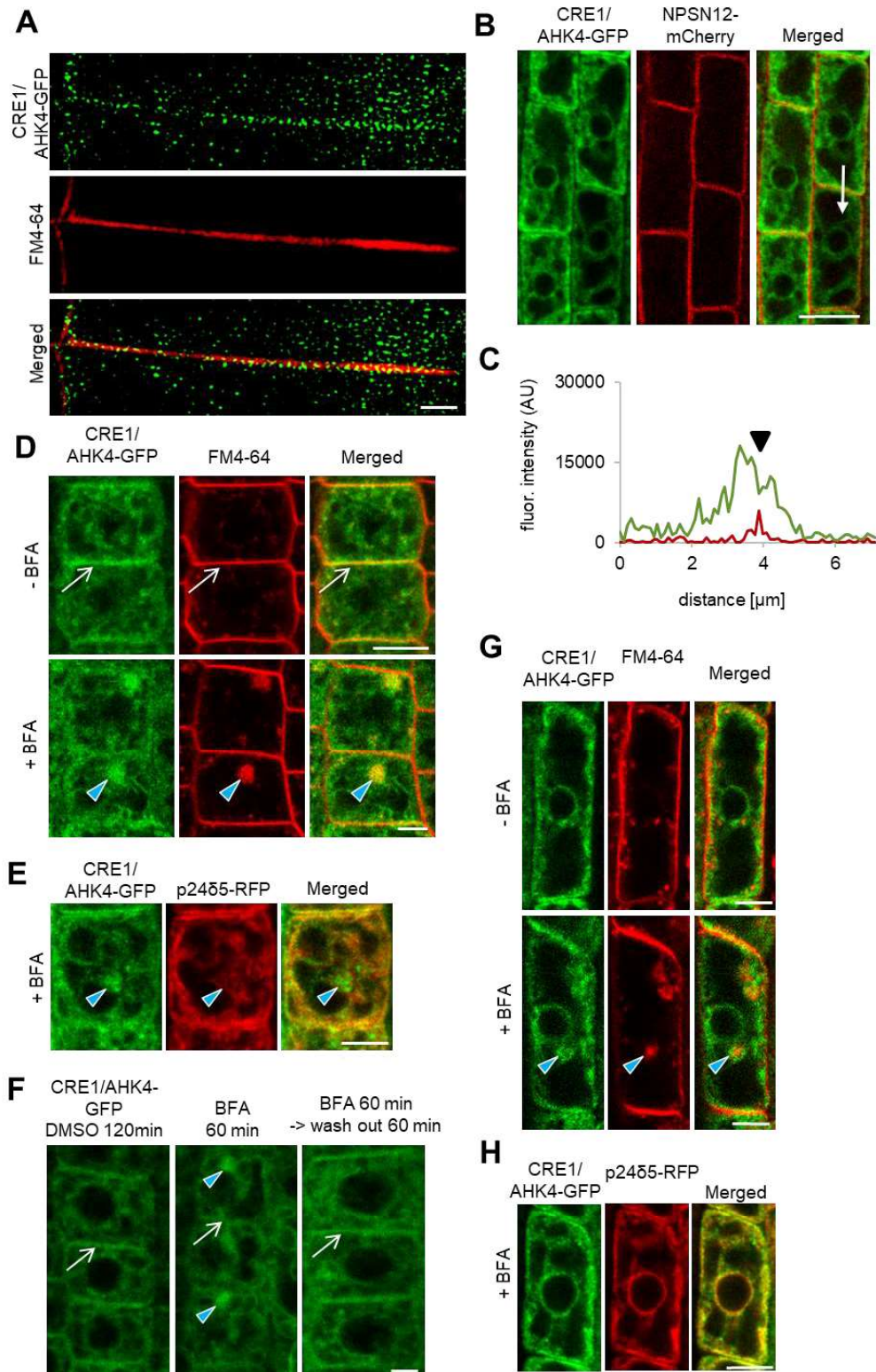
Figure 32: *CRE1/AHK4-GFP localization in Arabidopsis root cells. **A** – Super-resolution imaging (SIM) of CRE1/AHK4-GFP subcellular co-localization with the FM4-64 labelled PM. **B, C** – Monitoring of the CRE1/AHK4-GFP cytokinin receptor (green) and the NPSN12-mCherry PM*

reporter (red) in the LRC cells (**B**). Profiles of fluorescence intensity of the PM marker (red line) and CRE1/AHK4-GFP (green line) were measured along the white line (**B**) starting from the upper end (0 μm) towards the arrowhead. Peak of NPSN12-mCherry fluorescence maxima at the PM does not overlap with CRE1/AHK4-GFP fluorescence maximum (black arrowhead, **C**). **D**, **E** – Co-localization of CRE1/AHK4-GFP and FM4-64 (**D**), but not p24δ5-RFP (**E**) in the endosomal compartments (blue arrowheads) formed in the root meristematic epidermal cells treated with 50 μM in BFA for 1 h. Note CRE1/AHK4-GFP localization at the PM (white arrows) prior BFA treatment. **F** – Re-location of the CRE1/AHK4-GFP cytokinin receptor from the endosomal compartments to the PM after BFA wash-out in the root epidermal cells. Blue arrowheads indicate CRE1/AHK4 in the BFA-bodies. Note the attenuated AHK4-GFP signal at the PM and its re-localization back after 60 min wash-out of BFA (white arrows). **G**, **H** – Monitoring of the CRE1/AHK4-GFP (green), FM4-64 (red; **G**) and p24δ5-RFP (red; **H**) in the LRC cells treated for 1 h with 50 μM BFA. FM4-64, but not p24δ5-RFP detected in the BFA endosomal compartments (blue arrowheads). In some cells of LRC, CRE1/AHK4-GFP signal scattered around BFA bodies detected (**G**). Scale bars = 5 μm (**B**, **D**, **E**, **F**, **G**, **H**) and 2 μm (**A**).

To further explore whether the cytokinin receptor might occupy a different subcellular location in cells at a distinct stage of differentiation, CRE1/AHK4-GFP in different cell types was monitored. Similarly to the epidermis, in the provasculature cells in the root meristematic zone, the CRE1/AHK4-GFP seems to localize at the ER, the PM and at the cell plate of dividing stele cells (Figure 33A). To strengthen the conclusion that in the meristematically active cells cytokinin receptor might enter the secretory pathway and reach the PM, real time monitoring of the CRE1/AHK4-GFP in the developing lateral root primordia (LRP) was performed. Although expression of CRE1/AHK4-GFP driven by *35S* promoter in the LRP was relatively weak, similarly to cells in the root meristem, the CRE1/AHK4-GFP tends to localize at the ER and the PM (Figure 33B). Furthermore, in actively dividing cells a weak CRE1/AHK4-GFP signal could be detected during the cell plate formation (Supplementary movie).

Unlike cells located at the root apical meristem, in the differentiated cells of the LRC the CRE1/AHK4-GFP was detected in the ER, but not at the PM. To support further our conclusion about dominant localization of the cytokinin receptor at the ER in differentiated cells, detailed observations of the CRE1/AHK4-GFP in the differentiated root epidermal cells above the meristematic zone were performed. In these cells, the CRE1/AHK4-GFP was located at the ER (Figure 33C, D), but no co-localization with the PM reporter NPSN12 could be detected (Figure 33E, F).
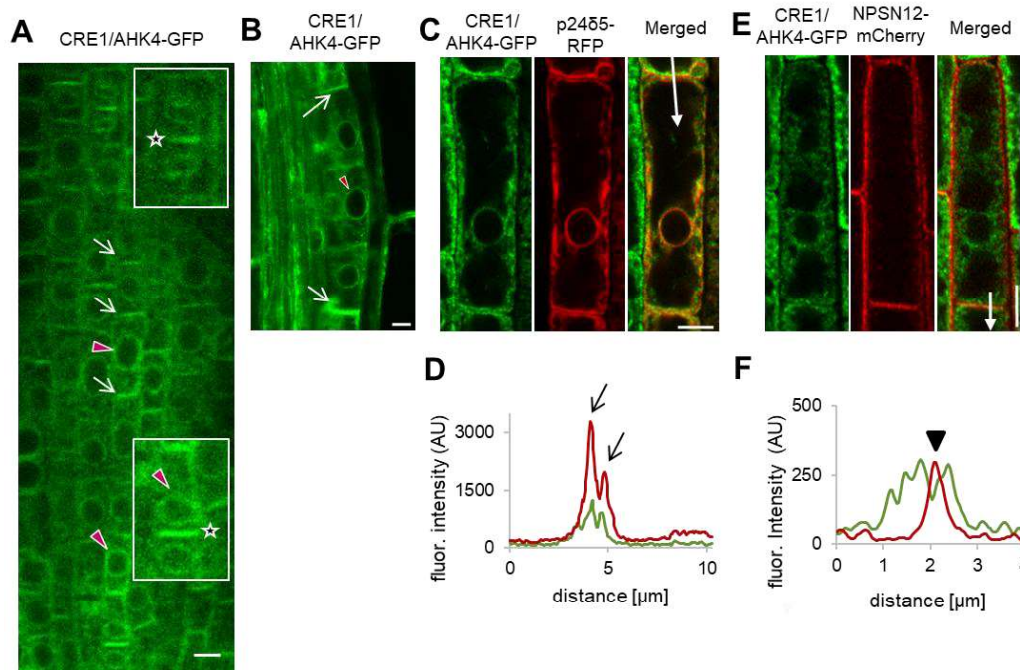
Figure 33: *CRE1/AHK4-GFP localization in Arabidopsis root cells. **A, B** – Monitoring of the CRE1/AHK4-GFP signal in the cells of provasculature at the root meristematic zone (**A**) and the developing lateral root primordia (**B**). Black stars mark AHK4-GFP signal at the cell plate of diving cells, white arrows and red arrowheads point to the PM and ER structures, respectively. **C-F** – Monitoring of the CRE1/AHK4-GFP cytokinin receptor (green), ER marker p24δ5-RFP (red; **C, D**) and the PM marker NPSN12-mCherry (red; **E, F**) in the differentiated epidermal cells at the root elongation zone. Profile of fluorescence intensity of p24δ5-RFP ER marker (red line) and CRE1/AHK4-GFP (green line; **D**) was measured along the white line (**C**) starting from the upper end (0 μm) towards the arrowhead. Peaks of p24δ5-RFP fluorescence maxima correlate with ER signal and overlap with CRE1/AHK4-GFP signal maxima (black arrows; **D**). Profile of fluorescence intensity of the NPSN12-mCherry PM marker (red line) and CRE1/AHK4-GFP (green line; **F**) was measured along the white line (**E**) starting from the upper end (0 μm) towards the arrowhead. Peak of NPSN12-mCherry fluorescence maxima at the PM signal does not overlap with CRE1/AHK4-GFP signal maxima in epidermal cells (black arrowhead; **F**). Scale bars = 5 μm (**A-C, E**).*

Based on these observations it can be hypothesised that the CRE1/AHK4-GFP located either at the ER or at the PM might activate distinct branches of downstream signalling to control specific process in the differentiated versus meristematically active cells. Internalization and re-cycling of the receptor between PM and endosomal compartments in the meristematic cells may represent another level in controlling signalling receptor function. Whether similarly to the CRE1/AHK4-GFP, also AHK2 and

AHK3 might enter secretory pathway and reach the PM in the meristematically active cells remains to be addressed. In previously reported studies localizations of the AHK3-GFP and AHK2-GFP have been observed in above-ground plant parts using transiently transformed *Nicotiana benthamiana* epidermal leaf cells (Wulfetange et al., 2011) and transiently transformed *Arabidopsis* cotyledon cells (Caesar et al., 2011), all in the differentiated stages. Hence, whether in specific cell types AHK2 and AHK3 might localize to the PM needs to be examined.

It is necessary to mention, that presented findings of PM localization of the cytokinin receptor CRE1/AHK4 are supported by a recently published article by Antoniadi et al. (2020). Both independent back-to-back articles (Kubiasova et al., 2020 and Antoniadi et al., 2020) were accepted in Nature Communications and the research groups were separately studying cellular sites of cytokinin signalling, especially the localization of receptors on different plant membranes. Each paper has used almost completely non-overlapping approaches and yet both came to the same conclusion (that cytokinin receptors not only exist at the ER but also on the PM).

Both works are set in the context of the long-standing debate on the localization of cytokinin receptors, with substantial evidence in recent years supporting predominant location on the ER. The presence of PM receptors was also proposed by Zürcher et al., 2016 as the logical implication of their cytokinin transporter and metabolism data. Moreover, three recent reviews have highlighted the ER versus PM debate and have pointed to the lack of convincing direct data (Kieber and Schaller, 2018; Romanov et al., 2018; Durán-Medina et al., 2017). Therefore multiple strands of evidence that individually and collectively support the hypothesis that some of the cytokinin perception occurs at the cell surface rather than intracellularly were provided.

Antoniadi and colleagues provided functional evidence that extracellular cytokinin ligands acting through the cell surface receptors are effective at initiating cytokinin signalling. Authors used cytokinins covalently linked to Sepharose beads that could not enter the cell and yet are able to increase the expression of both *TCSn::GFP* and *CRFs*. Lastly, super-resolution microscopy of GFP-labelled receptors and diminished

TCSn::GFP response to immobilised cytokinins in cytokinin receptor mutants, further indicate that receptors can function at the cell surface. Dual location of receptors may potentially provide plants with additional flexibility in cytokinin responses. It remains to be discovered whether different biological functions are associated with each location (Antoniadi et al., 2020).

Conclusion

Taken together, monitoring of intracellular localization of the fluorescent cytokinin probe iP-NBD with higher affinity to the CRE1/AHK4 cytokinin receptor, as well as direct visualization of the CRE1/AHK4-GFP leads to the conclusion that besides ER, cytokinin signal might also be perceived at other cellular compartments including the PM. As suggested by different localization of the CRE1/AHK4 receptor in the differentiated cells of LRC when compared to the epidermal cells of root apical meristem, perception of cytokinin at either ER or PM might be cell- and developmental- context dependent. In particular, the strong expression of the cytokinin sensitive reporter TCS::GFP detected in the columella and LRC cells (Bielach et al., 2012) suggests that the ER-located cytokinin receptors activate cytokinin signalling cascade in these particular cell types. On the other hand, it remains to be resolved whether there is a specific branch of cytokinin signalling activated by receptors located at the PM of meristematic cells.

GENERAL CONCLUSIONS

o Thirty fluorescent derivatives of the cytokinin iP were characterized and the most potent one (iP-NBD) was selected as a possible new tool for cytokinin receptor domain mapping, and for detailed biochemical and localization studies.

o Transgenic *Arabidopsis* lines expressing 35S::AHK4-GFP construct were prepared. They were characterized by qRT-PCR, Western blot and through phenotype analysis methods such as root growth inhibition assays.

o CRE1/AHK4-GFP was found to co-localize with both the ER markers (p24δ5-RFP and HDEL-RFP) and the PM markers (FM4-64 and PIP1;4-mCherry). Importantly, the cytokinin receptor localizes predominantly at the ER in the differentiated cells of the lateral root cap, whereas a significant proportion of the receptor is detected at the PM in cells of the root apical meristem.

o CRE1/AHK4-GFP is sensitive to an inhibitor of vesicular trafficking and accumulates in the BFA bodies. The rapid recovery of the CRE1/AHK4-GFP at the PM after washout of BFA inhibitor hints at dynamic cycling of the cytokinin receptor between PM and the endomembrane system.

o The co-localization of CRE1/AHK4-GFP with the PM and ER reporters in different cell types (including lateral root cap cells, epidermal cells in meristematic and differentiation zone, provascular cells and lateral root primordium) was analysed.

o Co-localization analysis of iP-NBD with marker lines for diverse compartments was evaluated and presented as the Pearson coefficients.

ABBREVIATIONS

2-AmEtAm	2-aminoethylamino-
6-AmHexAm	6-aminohexylamino-
ABA	Abscisic acid
ABCG14	ATP-binding cassette transporter subfamily G14
AD	Acidic domain
Ade	Adenine
ADP	Adenosine 5'-diphosphate
AFCS	Alexa Fluor 647 labelled castasterone
AHK	*Arabidopsis* histidine kinase
AHP	*Arabidopsis* histidine phosphotransfer protein
AMP	Adenosine 5'-monophosphate
ARR	*Arabidopsis* response regulator
ARR5::GUS	*Arabidopsis* response regulator 5: β-glucuronidase
AtCKX	*Arabidopsis thaliana* oxidase/dehydrogenase
AtIPT	*Arabidopsis thaliana* isopentenyl transferase
ATP	Adenosine 5'-triphosphate
β-Glc	β-glucosidase
BA	6-benzylaminopurine
BFA	Brefeldin A
BiFC	Bimolecular fluorescence complementation
BRI1	Brassinosteroid insensitive 1
CHASE	Cyclases/Histidine kinase associated sensory extracellular
CK	Cytokinin
CKI	Cytokinin Independent
CKX	Cytokinin oxidase/dehydrogenase
Cou	Coumarin
CRE1/AHK4	Cytokinin Response 1/*Arabidopsis* histidine kinase 4
CRF	Cytokinin response factor
CYP735A	Cytochrome P450 monooxygenase

Cy5	Cyanine 5 dye
cZ	*cis*-zeatin
cZR	*cis*-zeatin riboside
cZRMP	*cis*-zeatin riboside monophosphate
D, Asp	Aspartate
DAG	Days after germination
DEAC	7-(diethylamino)coumarin
DHZ	Dihydrozeatin
DHZR	Dihydrozeatin riboside
DHZRMP	Dihydrozeatin riboside monophosphate
DiMeAde	Dimetyladenine
DMAPP	Dimethylallyl diphosphate
DMSO	Dimethylsulfoxide
DPU	Diphenylurea
DS	Dansyl
EE	Early endosomes
ENT	Transporter for cytokinin nucleosides
ER	Endoplasmatic reticulum
FC	Fluorescein
FITC	Fluorescein isothiocyanate
GA	Gibberellin
GARP	Myb-like DNA binding domain
GFP	Green fluorescent protein
H, His	Histidine
HK	Histidine kinase
HPLC	High-performance liquid chromatography
HPt	Histidine phosphotransfer
IAA	Indole-3-acetic acid
iP	N^6-isopentenyladenine
iPRMP	Isopentenyl riboside monophosphate
iPR	N^6-isopentenyladenine riboside

IPT	Isopentenyl transferase
K_D	Dissociation constant
Kin	Kinetin
LB	Ligand binding domain
LC-MS/MS	Liquid chromatography–mass spectrometry
LE	Late endosomes
L*er*	Landsberg erecta *Arabidopsis* ecotype
LOG	LONELY GUY
LRC	Lateral root cap
LRP	Lateral root primordia
LUC	Luciferase
M9	Minimal medium
MS	Murashige skoog
MSP	Multistep-phosphorelay
MUG	4-methyl umbelliferyl galactoside
NAA	Naphthalene acetic acid
NBD	7-nitrobenzofurazan
NGT	*N*-glucosyltransferase
NHS	*N*-Hydroxysuccinimide
NMR	Nuclear magnetic resonance
NLS	Nuclear localization signal
OD	Output domain
OD_{600}	Optical density
P	Phosphoryl group
PM	Plasma membrane
PUP	Purine permease
PVC	Pre-vacuolar compartments
qRT-PCR	Real-time quantitative PCR
RD	Receiver domain
RE	Recycling endosomes
RhoB	Rhodamine B

RLD	Receiver-like domain
RR	Response regulator
s.d.	Standard deviation
s.e.	Standard error
Ser	Serin
SIM	Super-resolution structural illumination microscopy
SLN1	Osmosensing histidine protein kinase
TCS	Two-component output sensor
TDZ	Thidiazuron
TGN	*trans*-Golgi network
Thr	Threonin
TM	Transmembrane domain
Tyr	Tyrosin
*t*Z	*trans*-zeatin
*t*ZR	*trans*-zeatin riboside
*t*ZRMP	*trans*-zeatin riboside monophosphate
*t*ZOG	*trans*-zeatin-O-glucoside
VrCSBP	Cytokinin-specific binding protein from mung bean (*Vigna radiata*)
WOL	Wooden leg
WT	Wild-type
ZmHK	*Zea mays* histidine kinase
ZOGT	*O*-glucosyltransferase

REFERENCES

Anantharaman V., Aravind L. (2001): The CHASE domain: a predicted ligand-binding module in plant cytokinin receptors and other eukaryotic and bacterial receptors. *Trends Biochem. Sci.*, **26**, 579–582.

Antoniadi I., Plačková L., Simonovik B., Doležal K., Turnbull C., Ljung K., Novák O. (2015): Cell-type-specific cytokinin distribution within the *Arabidopsis* primary root apex. *Plant Cell* **27**, 1955–1967.

Antoniadi I., Novák O., Gelová Z., Johnson A., Plíhal O., Simerský R., Mik V., Vain T., Mateo-Bonmatí E., Karady M., Pernisová M., Plačková L., Opassathian K., Hejátko J., Robert S., Friml J., Doležal K., Ljung K., Turnbull C. (2020): Cell-surface receptors enable perception of extracellular cytokinins. *Nat Commun.* **11**, 4284.

Asami T., Tao L., Yamamoto S., Robertson M., Min Y.K., Murofushi N., Yoshida S. (1997): Fluorescence-labeled abscisic acid possessing abscisic acid-like activity in barley aleurone protoplasts. *Biosci. Biotechnol. Biochem* **61**, 1198–1199.

Avalbaev A.M., Somov K.A., Yuldashev R.A., Shakirova F.M. (2012): Cytokinin oxidase is key enzyme of cytokinin degradation. *Biochemistry (Moscow)* **77**, 1354–1361.

Bartzatt R. (2001): Dansylation of hydroxyl and carboxylic acid functional groups. *J. Pharmacol. Toxicol.* **45**, 247–253.

Bem M., Badea F., Draghici C., Caprolu M.T., Vasilescu M., Voicescu M., Beteringhe A., Caragheorgheopol A., Maganu M., Constantinescu T., Balaban A.T. (2007): Synthesis and fluorescent properties of new derivatives of 4-amino-7-nitrobenzofurazan. *Arkivoc* **8**, 87–104.

Bielach A., Podlešáková K., Marhavý P, Duclercq J., Cuesta C., Müller B., Grunewald W., Tarkowski P., Benková E. (2012): Spatiotemporal regulation of lateral root organogenesis in *Arabidopsis* by cytokinin. *Plant Cell* **24**, 3967–3981.

Bieleszová K., Pařízková B., Kubeš M., Husičková A., Kubala M., Ma Q., Sedlářová M., Robert S., Doležal K., Strnad M., Novák O., Žukauskaitė A. (2019): New fluorescently labeled auxins exhibit promising anti-auxin activity. *New Biotechnol.* **48**, 44–52.

Bilyeu K. D., Cole J. L., Laskey J. G., Riekhof W. R., Esparza T. J., Kramer M. D., Morris R. O. (2001): Molecular and biochemical characterization of a cytokinin oxidase from maize. *Plant Physiol.* **125**, 378–386.

Brenner W.G., Romanov G.A., Köllmer I., Bürkle L., Schmülling T. (2005): Immediate-early and delayed cytokinin response genes of *Arabidopsis thaliana* identified by genome-wide expression profiling reveal novel cytokinin-sensitive processes and suggest cytokinin action through transcriptional cascades. *Plant J.* **44**, 314-333.

Brzobohatý B., Moore I., Kristoffersen P., Bako L., Campos N., Schell J., Palme K. (1993): Release of active cytokinin by a beta-glucosidase localized to the maize root meristem. *Science* **262**, 1051–1054.

Burkle L., Cedzich A., Dopke C., Stransky H., Okumoto S., Gillissen B., Kuhn C., Frommer WB. (2003): Transport of cytokinins mediated by purine transporters of the PUP family expressed in phloem, hydathodes, and pollen of *Arabidopsis*. *Plant J.* **34**: 13–26.

Caesar K., Thamm A. M. K., Witthöft J., Elgass K., Huppenberger P., Grefen C., et al. (2011): Evidence for the localization of the *Arabidopsis* cytokinin receptors AHK3 and AHK4 in the endoplasmic reticulum. *J. Exp. Bot.* **62**, 5571–5580.

Chang, C., Kwok, S.F., Bleecker, A.B., and Meyerowitz, E.M. (1993): *Arabidopsis* ethylene-response gene ETR1: Similarity of product to two-component regulators. *Science* **262**, 539–544.

Chattopadhyay A. (1990): Chemistry and biology of N-(7-nibrobenz-2-oxa-1,3-diazol-4-yl)-labeled lipids: fluorescent probes of biological and model membranes. *Physiol. Rev.* **90**, 1103–1163.

Chen Y.F., Randlett M.D., Findell J.L., Schaller G.E. (2002): Localization of the ethylene receptor ETR1 to the endoplasmic reticulum of *Arabidopsis*. *J Biol Chem.* **277**, 19861–19866.

Cheng Y., Prusoff W. H. (1973): Relationship between the inhibition constant (KI) and the concentration of inhibitor which causes 50 per cent inhibition (I50) of an enzymatic reaction. *Biochem. Pharmacol.* **22**, 3099–3108.

Clough S. J., Bent A. F. (1998): Floral dip: a simplified method for Agrobacterium-mediated transformation of *Arabidopsis thaliana. Plant J.* **16**, 735–743.

Cutcliffe J. W., Hellmann E., Heyl, A., and Rashotte A. M. (2011): CRFs form protein–protein interactions with each other and with members of the cytokinin signalling pathway in *Arabidopsis* via the CRF domain. *J. Exp. Bot.* **62**, 4995–5002.

D'Agostino I. B., Deruere J., Kieber J. J. (2000): Characterization of the response of the *Arabidopsis* response regulator gene family to cytokinin. *Plant Physiol.* **124**, 1706–532.

Daly C. J., McGrath J. C. (2003): Fluorescent ligands, antibodies, and proteins for the study of receptors. *Pharmacol. Ther.* **100**, 101–118.

Daudu D., Allion E., Liesecke F., Papon N., Courdavault V., Dugé de Bernonville T., Mélin C., Oudin A., Clastre M., Lanoue A., Courtois M., Pichon O., Giron D., Carpin S., Giglioli-Guivarch N., Crèche J., Besseau S., Glévarec G. (2017): CHASE-Containing Histidine Kinase Receptors in Apple Tree: From a Common Receptor Structure to Divergent Cytokinin Binding Properties and Specific Functions. *Front. Plant Sci.* **8**, 1614.

Davies P. J. (2007): The nature, occurrence and effects of plant hormones cytokinins (CKs). In: Davies, P.J. (Ed.), Plant Hormones, Biosynthesis, Signal Transduction, Action!, vol. 3. Kluwer Academic Publisher, Dordrecht, 7–8.

Davies P. J. (2010) Plant Hormones: Biosynthesis, Signal Transduction, Action! 3rd Edition: The Plant Hormones: Their Nature, Occurrence, and Functions. Kluwer Academic Publishers, Dordrecht, Netherlands, 5–15.

Desikan R., Horák J., Chaban C., Mira-Rodado V., Witthöft J., Elgass K., Grefen C., Cheung M.K., Meixner A.J., Hooley R., Neill S.J., Hancock J.T., Harter K. (2008): The histidine kinase AHK5 integrates endogenous and environmental signals in *Arabidopsis* guard cells. *PloS One* **3**, 2491.

Dhonukshe P., Baluška F., Schlicht M., Hlavacka A., Šamaj J., Friml J., T. W. J. Gadella Jr. (2006): Endocytosis of cell surface material mediates cell plate formation during plant cytokinesis. *Dev. Cell* **10**, 137–150.

Dobrev P. I., Kamínek M. (2002): Fast and efficient separation of cytokinins from auxin and abscisic acid and their purification using mixed-mode solid-phase extraction. *J. Chromatogr. A.* **950**, 21–29.

Doležal K., Popa I., Hauserová E., Spíchal L., Chakrabarty K., Novák O., Krystof V., Voller J., Holub J., Strnad M. (2007): Preparation, biological activity and endogenous occurrence of N^6-benzyladenosines. *Bioorg. Med. Chem.* **15**, 3737–3747.

Doskočilová A., Kohoutová L., Volc J., Kourová H., Benada O., Chumová J., Plíhal O., Petrovská B., Halada P., Bogre L., Binarová P. (2013): NITRILASE1 regulates the exit from proliferation, genome stability and plant development. *New Phytol.* **198**, 685–698.

Dortay H., Mehnert N., Burkle L., Schmülling T., and Heyl A. (2006): Analysis of protein interactions within the cytokinin-signalling pathway of *Arabidopsis thaliana*. *FEBS J.* **273**, 4631–4644.

Dortay H., Gruhn N. , Pfeifer A., Schwerdtner M., Schmülling T., Heyl A. (2008): Toward an Interaction Map of the Two-Component Signaling Pathway of *Arabidopsis thaliana*. *J. Proteome Res* **7**, 3649–3660.

Du L., Jiao F., Chu J., Jin G., Chen M., Wu P. (2007): The two-component signal system in rice (*Oryza sativa L.*): a genome-wide study of cytokinin signal perception and transduction. *Genomics* **89**, 697–707.

Durán-Medina Y., Díaz-Ramírez D., Masch-Martíınez N. (2017): Cytokinins on the move. *Front. Plant Sci*. **8**, 146.

Feng J., Shi Y., Yang S., Zuo J. (2017): Cytokinins. 10.1016/B978-0-12-811562-6.00003-7.

Frébort I., Kowalska M., Hluska T., Frébortová J., Galuszka P. (2011): Evolution of cytokinin biosynthesis and degradation. *J. Exp. Bot*. **62**, 2431–52.

Frébortová J., Plihal O., Florová V., Kokáš F., Kubiasová K., Šimura J., Novak O., Frébort I. (2017): Light influences cytokinin biosynthesis and sensing in Nostoc (cyanobacteria). *J. Phycol.* **53**, 703–714.

Freeze H. H., Kranz C. (2010): Endoglycosidase and glycoamidase release of N-linked glycans. *Curr Protoc Bioinformatics*, Chapter 17, 10.

Friedrichsen D.M., Joazeiro C.A., Li J., Hunter T., Chory J. (2000): Brassinosteroid-insensitive-1 is a ubiquitously expressed leucine-rich repeat receptor serine/threonine kinase. *Plant Physiol.* **123**, 1247–1256.

Galuszka P., Frébort I., Šebela M., Peč P. (2000): Degradation of cytokinins by cytokinin oxidases in plants. *Plant Growth Regul.* **32**, 315–327.

Galuszka, P., Popelková, H., Werner, T., Frébortová J., Pospíšilová H., Mik V., Schwarz I., Schmülling T., Frébort I. (2007): Biochemical Characterization of Cytokinin Oxidases/Dehydrogenases from *Arabidopsis thaliana* Expressed in *Nicotiana tabacum L.*. J. Plant Growth Regul. **26**, 255–267.

Galuszka P., Spíchal L., Kopečný D., Tarkowski P., Frébortová J., Šebela M., Frébort I. (2008): Metabolism of plant hormones cytokinins and their function in signaling, cell differentiation and plant development. In '*Studies in natural products chemistry* **34**, 203–264.

Gaudinová A., Dobrev P.I., Šolcová B., Novák O., Strnad M., Friedecký D., Motyka V. (2005): The involvement of cytokinin oxidase/dehydrogenase and zeatin reductase in regulation of cytokinin levels in pea (*Pisum sativum L.*) leaves. *J. Plant Growth Regul.* 24, 188–200.

Geldner N., Robatzek S. (2008): Plant Receptors Go Endosomal: A Moving View on Signal Transduction. *Plant Phys.* **147**, 1565–1574.

Geldner N., Dénervaud-Tendon V., Hyman D. L., Mayer U., Stierhof Y.-D., Chory J. (2009): Rapid, combinatorial analysis of membrane compartments in intact plants with a multicolor marker set. *Plant J.* **59**, 169–178.

Gillissen B., Bürkle L., André B., Kühn C., Rentsch D., Brandl B., Frommer W.B. (2000): A new family of high-affinity transporters for adenine, cytosine, and purine derivatives in *Arabidopsis*. *Plant Cell*, **12**, 291–300.

Gonzalez-Rizzo S., Crespi M., Frugier F. (2006): The Medicago truncatula CRE1 cytokinin receptor regulates lateral root development and early symbiotic interaction with Sinorhizobium meliloti. *Plant Cell* **18**, 2680–2683.

Grefen, C., Harter, K. (2004): Plant two-component systems: principles, functions, complexity and cross talk. *Planta* **219**, 733–742.

Gruhn N., Halawa M., Snel B., Seidl M. F., Heyl, A. (2014): A subfamily of putative cytokinin receptors is revealed by an analysis of the evolution of the two-component signalling system of plants. *Plant Physiol.* **165**, 227–237.

Ha S., Vankova R., Yamaguchi-Shinozaki K., Shinozaki K., Tran L.S. (2012): Cytokinins: metabolism and function in plant adaptation to environmental stresses. *Trends Plant Sci* **17**, 172–9.

Haberlandt G. (1913): Zur physiologie der zellteilung. Sitzungsber Akad Wiss Berlin Phys Math Cl: 318–345.

Hallmark H., Rashotte A. (2019): Review – Cytokinin Response Factors: Responding to More than Cytokinin. *Plant Sci* **289**, 110251.

Hamaguchi N., Iwamura H., Fujita T. (1985): Fluorescent anticytokinins as a probe for binding. *Eur. J. Biochem.* **153**, 565–572.

Hayashi K., Shouichi N., Shiho F., Takeshi N., Jenness M. K., Murphy A. S., Motose H., Nozaki H., Furutani M., Aoyama T. (2014): Auxin transport sites are visualized *in planta* using fluorescent auxin analogs. *Proc. Natl. Acad. Sci. U. S. A.* **111**, 11557–11562.

Hejátko J., Pernisová M., Eneva T., Palme K., Brzobohaty B. (2003): The putative sensor histidine kinase CKI1 is involved in female gametophyte development in *Arabidopsis* . *Mol Gen Genomics* **269**, 443–453.

Hejátko J., Ryu H., Kim G. T., Dobesová R., Choi S., Choi S. M., Soucek P., Horák J., Pekárová B., Palme K., Brzobohaty B., Hwang I. (2009): The histidine kinases CYTOKININ-INDEPENDENT1 and ARABIDOPSIS HISTIDINE KINASE2 and 3 regulate vascular tissue development in *Arabidopsis* shoots. *Plant cell*, **21**, 2008–2021.

Heyl A., Schmülling T. (2003): Cytokinin signal perception and transduction. *Curr, Opin. Plant Biol.* **6**, 480–488.

Heyl A., Wulfetange K., Pils B., Nielsen N., Romanov G.A., Schmülling T. (2007): Evolutionary proteomics identifies amino acids essential for ligand-binding of the cytokinin receptor CHASE domain. *BMC Evol. Biol.* **7**, 62.

Heyl A., Riefler M., Romanov G.A., Schmülling T. (2011): Properties, functions and evolution of cytokinin receptors. *Eur. J. Cell Biol.* **91**, 246–56.

Higuchi M., Pischke M. S., Mähönen A. P., Miyawaki K., Hashimoto Y., Seki M., Kobayashi M., Shinozaki K., Kato T., Tabata, S., Helariutta Y., Sussman M.R., Kakimoto T. (2004): *In planta* functions of the *Arabidopsis* cytokinin receptor family. *Proc. Natl. Acad. Sci. U.S.A* **101**, 8821–8826.

Hiratsuka T., Kato T. (1987): A fluorescent analog of colcemid, N-(7-nitrobenz-2-oxa-1,3-diazol-4-yl)-colcemid, as a probe for the colcemid binding sites of tubulin and microtubules. *J. Biol. Chem.* **13**, 6318–6322.

Hirose N., Makita N., Yamaya T., Sakakibara H. (2005): Functional characterization and expression analysis of a gene, OsENT2, encoding an equilibrative nucleoside transporter in rice suggest a function in cytokinin transport. *Plant Phys.***138**, 196–206.

Hirose N., Takei K., Kuroda T., Kamada-Nobusada T., Hayashi H., Sakakibara H. (2008): Regulation of cytokinin biosynthesis, compartmentalization and translocation. *J. Exp. Bot.* **59**, 75–83.

Hong Z., Jin H., Tzfira,T., Li J. (2008): Multiple mechanism-mediated retention of a defective brassinosteroid receptor in the endoplasmic reticulum of *Arabidopsis*. *Plant Cell* **20**, 3418–3429.

Hošek P., Hoyerová K., Kiran N. S., Dobrev P. I., Zahajská L., Filepová R., , Filepova R., Motyka V., Muller K., Kaminek M. (2020): Distinct metabolism of N-glucosides of isopentenyladenine and trans-zeatin determines cytokinin metabolic spectrum in *Arabidopsis*. *New Phytol.* **225**, 2423–2438.

Hosoda K., Imamura A., Katoh E., Hatta T., Tachiki M., Yamada H., Mizuno T., Yamazaki T. (2002): Molecular structure of the GARP family of plant Myb-related DNA binding motifs of the *Arabidopsis* response regulators. *Plant Cell* **14**, 2015–2029.

Hothorn M., Dabi T., Chory J. (2011): Structural basis for cytokinin recognition by *Arabidopsis thaliana* histidine kinase 4. *Nat. Chem. Biol.* **7,** 766–768.

Hou B., Lim E.-K., Higgins G. S., Bowles D. J. (2004): N-glucosylation of cytokinins by glycosyltransferases of *Arabidopsis thaliana*. *J. Biol. Chem.* **279**, 47822–47832.

Hoyerová K., Gaudinová A, Malbeck J., Dobrev P., Kocábek T., Šolcová B., Trávníčková A., Kamínek M. (2006): Efficiency of different methods of extraction and purification of cytokinins. *Phytochemistry* **67**, 1151–1159.

Hoyerová K., Hošek P. (2020): New Insights Into the Metabolism and Role of Cytokinin N-Glucosides in Plants. *Front. Plant Sci.* **11,** 741.

Hurný A., Benková E. (2017): Methodological advances in auxin and cytokinin biology. Auxins and Cytokinins in Plant Biology **1569**, 1–29.

Hutchison C., Kieber J. (2007): Signalling via Histidine-Containing Phosphotransfer Proteins in *Arabidopsis*. *Plant Signal Behav* **2**. 287–9.

Hwang I., Chen H., Sheen J. (2002): Two-Component Signal Transduction Pathways in *Arabidopsis*. *Plant Physiol.* **129**, 500–515.

Hirayama T., Alonso J. M. (2000): Ethylene captures a metal! Metal ions are involved in ethylene perception and signal transduction. *Plant Cell Physiol.* **41**, 548–555.

Imamura A., Hanaki N., Nakamura A., Suzuki T., Taniguchi M.,Kiba T., Ueguchi C., Sugiyama T., Mizuno T. (1999): Compilation and characterization of *Arabidopsis thaliana* response regulators implicated in His-Asp phosphorelay signal transduction. *Plant Cell Physiol.* **40**: 733–742.

Imamura A., Yoshino Y., Mizuno T. (2001): Cellular localization of the signalling components of *Arabidopsis* His-to-Asp phosphorelay. *Biosci Biotechnol Biochem* **65**, 2113–2117.

Inoue T., Higuchi M., Hashimoto Y., Seki M., Kobayashi M., Kato T., Tabata S., Shinozaki K., Kakimoto T. (2001): Identifcation of CRE1 as a cytokinin receptor from *Arabidopsis*. *Nature* **409**, 1060–1063.

Ioio D.R., Nakamura K., Moubayidin L., Perilli S., Taniguchi M., Morita M.T., Aoyama T., Costantino P., Sabatini S. (2008): A genetic framework for the control of cell division and differentiation in the root meristem. *Science* **322**, 1380–1384.

Irani N. G., Di Rubbo S., Myllel E., Van den Begin J., Schneider-Pizoń J., Hnilíková J., Šíša M., Buyst D., Vilarrasa-Blasi J., Szatmári A.-M., Van Damme D., Mishev K., Codreanu M.-C., Kohout L., Strnad M., Caño-Delgado A. I, Friml J., Medder A., Russinova E. (2012): Fluorescent castasterone reveals BRI1 signalling from the plasma membrane. *Nat. Chem. Biol.* **8**, 583–589.

Ito Y., Kurata N. (2006): Identification and characterization of cytokinin-signalling gene families in rice. *Gene* **382**, 57–65.

Iwama A., Yamashino T., Tanaka Y., Sakakibara H., Kakimoto T., Sato S., Kato T., Tabata S., Nagatani A., Mizuno T. (2007): AHK5 histidine kinase regulates root elongation through an ETR1-dependent abscisic acid and ethylene signalling pathway in *Arabidopsis thaliana*. *Plant Cell Physiol.* **48**, 375–380.

Jaworek P., Tarkowski P., Hluska T., Kouřil Š., Vrobel O., Nisler J., Kopečný D. (2020): Characterization of five CHASE-containing histidine kinase receptors from *Populus × canadensis cv. Robusta* sensing isoprenoid and aromatic cytokinins. *Planta* **251**.

Jelínková A., Malínská K., Simon S., Kleine-Vehn J., Parezová M., Pejchar P, Kubes M., Martinec J., Friml J., Zazímalová E., Petrásek J. (2010): Probing plant membranes with FM dyes: tracking, dragging or blocking? *Plant J.* **61**, 883–892.

Jin H., Yan Z., Nam K.H., Li J. (2007): Allele-specific suppression of a defective brassinosteroid receptor reveals a physiological role of UGGT in ER quality control. *Mol. Cell* **26**, 821–830.

Kabbara S., Schmülling T., Papon N. (2018): CHASEing Cytokinin Receptors in Plants, Bacteria, Fungi, and Beyond. *Trends Plant Sci.* **23**, 179–181.

Kakimoto T. (1996): CKI1, a histidine kinase homolog implicated in cytokinin signal transduction. *Science* **274**, 982–985.

Kakimoto, T. (2001): Identification of plant cytokinin biosynthetic enzymes as dimethylallyl diphosphate:ATP/ADP isopentenyltransferases. *Plant Cell Physiol.* **42**, 677–685.

Kakimoto T. (2003): Perception and Signal Transduction of Cytokinins. *Annu. Rev. Plant Physiol.* **54**, 605–627.

Kang N. Y., Cho C., Kim J. (2013): Inducible Expression of *Arabidopsis* Response Regulator 22 (ARR22), a Type-C ARR, in Transgenic *Arabidopsis* Enhances Drought and Freezing Tolerance. *PloS One* **8**, 79248.

Kang J., Lee Y., Sakakibara H., Martinoia E. (2017): Cytokinin transporters: GO and STOP in signaling. *Trends Plant Sci*. **6**, 455–461.

Kasahara H., Takei K., Ueda N., Hishiyama S., Yamaya T., Kamiya Y., Yamaguchi S., Sakakibara H. (2004): Distinct isoprenoid origins of *cis-* and *trans-*zeatin biosyntheses in *Arabidopsis*. *J. Biol. Chem.* **279**, 14049–14054.

Kiba T., Yamada H. and Mizuno T. (2002): Characterization of the ARR15 and ARR16 response regulators with special reference to the cytokinin signalling pathway mediated by the AHK4 histidine kinase in roots of *Arabidopsis thaliana*. *Plant Cell Physiol*. **43**, 1059–1066.

Kiba T., Aoki K., Sakakibara H., and Mizuno T. (2004): *Arabidopsis* response regulator, ARR22, ectopic expression of which results in phenotypes similar to the wol cytokinin-receptor mutant. *Plant Cell Physiol.* **45**, 1063–1077.

Kieber J.J., Schaller G.E. (2010): The perception of cytokinin: a story 50 years in the making. *Plant Physiol.* **154**, 487–492.

Kieber J. J., Schaller G. E. (2014): Cytokinins. *Arab. Book*

Kieber J. J., Schaller G. E. (2018): Cytokinin signaling in plant development. *Development* **145**, 1–7.

Kim H. J., Ryu H., Hong S. H., Woo H. R., Lim P. O., Lee I. Ch., Sheen J., Nam H. G., Hwan I. (2006): Cytokinin-mediated control of leaf longevity by AHK3 through phosphorylation of ARR2 in *Arabidopsis*. *Proc. Natl. Acad. Sci. U.S.A* **103**, 814–819.

Kiran N.S., Benkova E., Rekova A., Dubova J., Malbeck J., Palme K., Brzobohaty B. (2012): Retargeting a maize beta-glucosidase to the vacuole – Evidence from intact plants that zeatin-O-glucoside is stored in the vacuole. *Phytochemistry* **79**, 67–77.

Ko D., Kang J., Kiba T., Park J., Kojima M., Do J., Kim K. Y., Kwon M., Endler A., Song W. Y., Martinoia E., Sakakibara H., Lee Y. (2014): *Arabidopsis* ABCG14 is essential for the root-toshoot translocation of cytokinin. *Proc. Natl. Acad. Sci. U.S.A* **111**, 7150–7155.

Komis G., Mistrik M., Šamajová O., Ovečka M., Bartek J., Šamaj J. (2015a): Superresolution live imaging of plant cells using structured illumination microscopy. *Nat. Protoc.* **10**, 1248–1263.

Komis G., Šamajová O., Ovečka M., Šamaj, J. (2015b): Super-resolution microscopy in plant cell imaging. *Trends Plant Sci.* **20**, 834–843.

Kowalska M., Galuszka P., Frébortova J., Šebela M., Béres T., Hluska T., Šmehilová M., Bilyeu K. D., Frébort I. (2010): Vacuolar and cytosolic cytokinin dehydrogenases of *Arabidopsis thaliana*: Heterologous expression, purification and properties. *Phytochemistry* **71**, 1970–1978.

Kubiasová K. (2012): Synthesis and characterization of fluorescently labelled cytokinin derivatives. Bachelor thesis. Palacký University Olomouc, Czech Republic.

Kubiasová K. (2014): Localization of cytokinin receptors in *Arabidopsis thaliana* using fluorescent labeling. Diploma thesis. Palacký University Olomouc, Czech Republic.

Kubiasová K., Mik V., Nisler J., Honig M., Husičková A., Spíchal L., Pěkná Z., Šamajová O., Doležal K., Plíhal O., Benková E., Strnad M., Plíhalová L. (2018): Design, synthesis and perception of fluorescently labeled isoprenoid cytokinins. *Phytochemistry* **150**, 1–11.

Kudo, T., Kiba T., Sakakibara H. (2010): Metabolism and long-distance translocation of cytokinins. *J. Integr. Plant Biol.* **52**, 53–60.

Kurakawa T, Ueda N, Maekawa M, Kobayashi K, Kojima M, Nagato Y, Sakakibara H, Kyozuka J. (2007): Direct control of shoot meristem activity by a cytokinin-activating enzyme. *Nature* **445**, 652–655.

Lace B., Prandi K. (2016): Shaping small bioactive molecules to untangle their biological function: a focus on fluorescent plant hormones. *Mol. Plant* **9**, 1099–1118.

Larrieu A., Vernoux T. (2015): Comparison of plant hormone signalling systems. *Essays Biochem.* **58**, 165–181.

Lavis L. D., Rutkoski T. J., Raines R. T. (2007): Tuning the pKa of fluorescein to optimize binding assays*. Anal. Chem.* **79**, 6775–6782.

Lavis L. D., Raines R. T. (2008): Bright ideas for chemical biology. *ACS Chem. Biol.* **3**, 142–155.

Letham D. S. (1963): Zeatin, a factor inducing cell division isolated from *Zea mays*. *Life Sci*. **2**, 569–573.

Letham D. S., Miller C.O. (1965): Identity of kinetin-like factors from *Zea mays*. *Plant Cell Physiol.* **6**, 355–360.

Leopoldo M., Lacivita E., Berardi F., Perrone R. (2009): Developments in fluorescent probes for receptor research. *Drug Discov. Today* **14**, 706–712.

Li G. Y., Liu K. F., Baldwin S. A., Wang D. W. (2003): Equilibrative nucleoside transporters of *Arabidopsis thaliana* – cDNA cloning, expression pattern, and analysis of transport activities. *J. Biol. Chem.* **278**, 35732–35742.

Li X., Mo X., Shou H., Wu P. (2006): Cytokinin-mediated cell cycling arrest of pericycle founder cells in lateral root initiation of *Arabidopsis*. *Plant Cell Physiol.* **47**, 1112–1123.

Li H., Duff S. M. G., Bedair M., Fernandes M., Dietrich C. R. (2018): Cytokinin levels and expression profiles of cytokinin metabolic genes in late stage maize kernels. *Int. J. Plant Physiol. Biochem*. **10**, 28–75.

Lindner A.-C., von Schwartzenberg K. (2016): Cytokinins. In *eLS, John Wiley & Sons, Ltd (Ed.).*

Liu Y.-S., Zhao C., Bergbreiter D.E., Romo D. (1988): Simultaneous deprotection and purification of BOC-amines based on ionic resin capture. *J. Org. Chem.* **63**, 3471–3473.

Liu S., Wang W. H., Dang Y. L., Fu Y., Sang R. (2012): Rational design and efficient synthesis of a fluorescent-labeled jasmonate. *Tetrahedron Lett.* **53**, 4235–4239.

Liu J., Müller B. (2017): Imaging TCSn::GFP, a Synthetic Cytokinin Reporter, in *Arabidopsis thaliana*. *Methods Mol Biol.* **1497**, 81–90.

Liu Z., Yuan L., Song X., Yu X., Sundaresan V. (2017): AHP2, AHP3, and AHP5 act downstream of CKI1 in *Arabidopsis* female gametophyte development. *J. Exp. Bot.* **68**, 3365–3373.

Liu Ch.-J., Zhao Y., Zhang K. (2019): Cytokinin Transporters: Multisite Players in Cytokinin Homeostasis and Signal Distribution. *Front. Plant Sci.*, **10**, 1–9.

Lomin S. N., Yonekura-Sakakibara K., Romanov G. A., Sakakibara H. (2011): Ligand-binding properties and subcellular localization of maize cytokinin receptors. *J. Exp. Bot.* **62**, 5149–5159.

Lomin S. N., Krivosheev D. M., Steklov M. Y., Osolodkin D. I., Romanov G. A. (2012): Receptor properties and features of cytokinin signalling. *Acta naturae* **4**, 31–45.

Lomin S. N., Krivosheev D. M., Steklov M. Y., Arkhipov D. V., Osolodkin D. I., Schmülling T., Romanov G.A. (2015): Plant membrane assays with cytokinin receptors underpin the unique role of free cytokinin bases as biologically active ligands. *J. Exp. Bot.* **66**, 1851–1863.

Lomin, S. N., Myakushina, Y. A., Kolachevskaya, O. O., Getman, I. A., Arkhipov, D. V., Savelieva, E. M., Osolodkin D.I., Romanov G.A. (2018a): Cytokinin perception in potato: new features of canonical players. *J. Exp. Bot.* **69**, 3839–3853.

Lomin S., Myakushina Y., Arkhipov D., Leonova O., Popenko V., Schmülling T., Romanov G (2018b): Studies of cytokinin receptor-phosphotransmitter interaction provide evidences for the initiation of cytokinin signalling in the endoplasmic reticulum. *Funct. Plant Biol.* **45**, 192–202.

Mähönen A. P., Bishopp A., Higuchi M., Nieminen K. M., Kinoshita K., Törmäkangas K., Ikeda Y., Oka A., Kakimoto T., Helariutta Y. (2006a): Cytokinin signalling and its inhibitor AHP6 regulate cell fate during vascular development. *Science* **311**, 94–98.

Mähönen, A.P., Higuchi, M., Tormakangas, K., Miyawaki, K., Pischke, M.S., Sussman, M.R., Helariutta, Y. and Kakimoto, T. (2006b): Cytokinins regulate a bidirectional phosphorelay network in *Arabidopsis*. *Curr. Biol.* **16**, 1116–1122.

Mason W. T. (1999): Fluorescent and Luminescent Probes for Biological Activity. A Practical Guide to Technology for Quantitative Real-time Analysis, vol. 2. Academic Press.

Mason M. G., Li J., Mathews D. E., Kieber J. J., Schaller G. E. (2004): Type-B response regulators display overlapping expression patterns in *Arabidopsis*. *Plant Physiol.,* **135**, 927–937.

Matušková V., Zatloukal M., Voller J., Grúz J., Pěkná Z., Briestenská K, Mistríková J., Spíchal L., Doležal K., Strnad M. (2019): New aromatic 6-substituted 2-deoxy-9-(β)-d-ribofuranosylpurine derivatives as potential plant growth regulators. *Bioorg. Med. Chem*. **28,** 115230.

McGrath J. C., Arribas S., Daly C. J. (1996): Fluorescent ligands for the study of receptors. *Trends Pharmacol. Sci.* **17**, 393–399.

Meng Q., Yu M., Zhang H. (2007): Synthesis and application of N-hydroxysuccinimidyl Rhodamine B ester as an amine-reactive fluorescent probe. *Dyes Pigm* **73**, 254–260.

Mik V., Szüčová L., Šmehilová M., Zatloukal M., Doležal K., Nisler J., Grúz J., Galuszka P., Strnad M., Spíchal L. (2011a): N9-substituted derivatives of kinetin: Effective anti-senescence agents. *Phytochemistry* **72**, 821–831.

Mik V., Szüčová L., Spíchal L., Plíhal O., Zahajská L., Doležal K., Strnad M. (2011b): *N*9-substituted *N*^{6}-[(3-methylbut-2-en-1-yl)amino]purine derivatives and their biological activity in selected cytokinin bioassays. *Bioorg. Med. Chem.* **19**, 7244–7251.

Mik V. (2012): Synthesis and characterization of novel compounds interacting with metabolic pathways of plant hormones cytokinins. Structure-activity relationship. Ph.D. thesis. Palacký University Olomouc, Czech Republic.

Miller C. O. (1955a): Kinetin, a cell division factor from deoxyribonucleic acid. *J. Am. Chem. Soc.* **77**, 1392.

Miller C. O. (1955b): Structure and synthesis of kinetin. *J. Am. Chem. Soc.* **77**, 2662–2663.

Miller C. O. (1961): A kinetin-like compound in maize. *Proc. Natl. Acad. Sci. USA*. **47**, 170–174.

Mira-Rodado V., Veerabagu M., Witthöft J., Teply J., Harter K., Desikan R. (2012): Identification of two-component system elements downstream of AHK5 in the stomatal closure response of *Arabidopsis thaliana*. *Plant Signal Behav.* **7**, 1467–76.

Mira-Rodado V. (2019): New Insights into Multistep-Phosphorelay (MSP)/Two-Component System (TCS) Regulation: Are Plants and Bacteria That Different?. *Plants* **8**, 590.

Miyawaki K., Tarkowski P., Matsumoto-Kitano M., Kato T., Sato S., Tarkowska D., Tabata S., Sandberg G., Kakimoto T. (2006): Roles of *Arabidopsis* ATP/ADP

isopentenyltransferases and tRNA isopentenyltransferases in cytokinin biosynthesis. *Proc. Natl. Acad. Sci. U.S.A.* **103**, 16598–16603.

Mok D.W.S., Mok M.C. (2001): Cytokinin metabolism and action. *Annu. Rev. Plant Physiol.* **52**, 89–118.

Montesinos J. C., Sturm S., Langhans M., Hillmer S., Marcotel M.-J., Robinson D. G., Aniento F. (2012): Coupled transport of *Arabidopsis* p24 proteins at the ER-Golgi interface. *J. Exp. Bot.* **63**, 4243-4261 (2012).

Müller B., Sheen J. (2007): Advances in Cytokinin Signalling. *Science* **318,** 68–9.

Müller B., and Sheen J. (2008): Cytokinin and auxin interaction in root stem-cell specification during early embryogenesis. *Nature* **453**, 1094–1097.

Murray J. D., Karas B. J., Sato S., Tabata S., Amyot L., Szczyglowski K. (2007): A cytokinin perception mutant colonized by Rhizobium in the absence of nodule organogenesis. *Science* **315**, 101–104.

Nakagawa T., Kurose T., Hino T., Tanaka K., Kawamukai M., Niwa Y., Toyooka K., Matsuoka K., Jinbo T., Kimura T. (2007): Development of series of gateway binary vectors, pGWBs, for realizing efficient construction of fusion genes for plant transformation. *J. Biosci. Bioeng.* **104**, 34–41.

Nakai K., Horton P. (1999): PSORT: a program for detecting sorting signals in proteins and predicting their subcellular localization. *Trends Biochem Sci* **24**, 34–36.

Nelson B. K., Cai X., Nebenführ A. (2007): A multicolored set of *in vivo* organelle markers for co-localization studies in *Arabidopsis* and other plants. *Plant J.* **51**, 1126–1136.

Niemann M., Weber H., Hluska T., Leonte G., Anderson S., Novak O., Senes A., Werner T. (2018): The cytokinin oxidase/dehydrogenase CKX1 is a membrane-bound protein requiring homooligomerization in the endoplasmic reticulum for its cellular activity. *Plant Physiol.* **176**, 2024–2039.

Nishikawa S., Kurono M., Shibayama K., Okuno S., Inagaki M., Kashimura N. (2000): Synthesis and cytokinin activity of fluorescent 7-phenylethynylimidazo[4,5-d]pyridine and its riboside. *J. Agric. Food Chem.* **48**, 2559–2564.

Nishimura C., Ohashi Y., Sato S., Kato T., Tabata S., Ueguchi C. (2004): Histidine kinase homologs that act as cytokinin receptors possess overlapping functions in the regulation of shoot and root growth in *Arabidopsis*. *Plant Cell* **16**, 1365–1377.

Nishiyama R., Watanabe Y., Fujita Y., Le D.T., Kojima M., Werner T., Vanková R., Yamaguchi-Shinozaki K., Shinozaki K., Kakimoto T., Sakakibara H., Schmülling T., Tran L.S.P. (2011): Analysis of cytokinin mutants and regulation of cytokinin metabolic genes reveals important regulatory roles of cytokinins in drought, salt and abscisic acid responses, and abscisic acid biosynthesis. *Plant Cell* **23**, 2169–2183.

Nisler J., Zatloukal M., Popa I., Dolezal K., Strnad M., Spíchal L. (2010): Cytokinin receptor antagonists derived from 6-benzylaminopurine. *Phytochemistry* **71**, 1052–1062.

Novák, O., Napier, R., Ljung, K. (2017): Zooming In on Plant Hormone Analysis: Tissue- and Cell-Specific Approaches. *Annu. Rev. Plant Biol.* **68**, 323–348.

Orci L., Perrelet A., Ravazzola M., Wieland F. T., Schekman R., Rothman J. E. (1993): "BFA bodies": a subcompartment of the endoplasmic reticulum. *Proc. Natl Acad. Sci. U.S.A* **90**, 11089–11093.

Osugi A., Sakakibara H. (2015): Q and A: How Do Plants Respond to Cytokinins and What Is Their Importance?. *BMC Biol.* **13**, 1–10.

Ota I., Varshavsky A. (1993): A yeast protein similar to bacterial two-component regulators. *Science* **262**, 566–569.

Ovečka M., Takáč T., Komis G., Vadovič P., Bekešová S., Doskočilová A., Šamajová V., Luptovčiak I., Samajová O., Schweighofer A., Meskiene I., Jonak C., Křenek P., Lichtscheidl I., Škultéty L., Hirt H., Šamaj J. (2014): Saltinduced subcellular kinase relocation and seedling susceptibility caused by overexpression of Medicago SIMKK in *Arabidopsis. J. Exp. Bot.* **65**, 2335–2350.

Pils B., Heyl A. (2009): Unraveling the evolution of cytokinin signalling. *Plant Physiol* **151**, 782–91.

Plíhalová L., Vylíčilová H., Doležal K., Zahajská L., Zatloukal M., Strnad M. (2016): Synthesis of aromatic cytokinins for plant biotechnology. *New Biotech.* **33** (Part: B), 614–624.

Podlešáková K., Zalabák D., Čudejková M., Plíhal O., Szüčová L., Doležal K., Spíchal L., Strnad M., Galuszka P. (2012): Novel cytokinin derivatives do not show negative effects on root growth and proliferation in submicromolar range. *PLoS One* **7**, e39293.

Prandi C., Rosso H., Lace B., Occhiato E. G., Oppedisano A., Tabasso S., Alberto G., Blangetti M. (2013): Strigolactone analogs as molecular probes in chasing the (SLs) receptor/s: design and synthesis of fluorescent labeled molecules. *Mol. Plant* **6**, 113–127.

Pulici M., Asami T., Robertson M., Seto H., Youshida S. (1996): Amylase induction activity of fluorescein labeled gibberellin in barley aleurone protoplasts. *Bioorg. Med. Chem. Lett.* **6**, 2549–2552.

Punwani J.A., Kieber J.J. (2010): Localization of the *Arabidopsis* histidine phosphotransfer proteins is independent on cytokinin. *Plant Signal. Behav.* **5**, 896–898.

Rashotte, A. M., Mason, M. G., Hutchison, C. E., Ferreira, F. J., Schaller, G. E., and Kieber, J. J. (2006): A subset of *Arabidopsis* AP2 transcription factors mediates cytokinin responses in concert with a two-component pathway. *Proc. Natl. Acad. Sci. U.S.A* **103**, 11081–11085.

Riefler M., Novak O., Strnad M., Schmülling T. (2006): *Arabidopsis* cytokinin receptor mutants reveal functions in shoot growth, leaf senescence, seed size, germination, root development, and cytokinin metabolism. *Plant Cell* **18**, 40–54.

Romanov G. A., Spíchal L., Lomin S. N., Strnad M., Schmülling T. (2005): A live cell hormone-binding assay on transgenic bacteria expressing a eukaryotic receptor protein. *Anal. Biochem*. **347**, 129–134.

Romanov GA, Lomin SN, Schmülling T. (2006): Biochemical characteristics and ligand-binding properties of *Arabidopsis* cytokinin receptor AHK3 compared to CRE1/AHK4 as revealed by a direct binding assay. *J. Exp. Bot.* **57,** 4051–4058.

Romanov G.A., Lomin S.N. (2009): Hormone-binding assay using living bacteria expressing eukaryotic receptors. *Methods Mol. Biol.* **495**, 111–120.

Romanov G. A., Lomin S. N., Schmülling T. (2018): Cytokinin signaling: from the ER or from the PM? That is the question! *New Phytol.* **218**, 41–53.

Sakai H., Aoyama T., Oka A. (2000): *Arabidopsis* ARR1 and ARR2 response regulators operate as transcriptional activators. *Plant J.*, **24**, 703–711.

Sali A., Blundell T. L. (1993): Comparative protein modelling by satisfaction of spatial restraints. *J. Mol. Biol.* **234**, 779–815.

Sakakibara H. (2006): Cytokinins: Activity, Biosynthesis, and Translocation. *Annu. Rev. Plant Physiol* **57**, 431–439.

Sanner M. F. (1999): Python: a programming language for software integration and development. *J. Mol. Graph. Model.* **17**, 57–61.

Šamajová O., Komis G., Šamaj J. (2014): Immunofluorescent localization of MAPKs and colocalization with microtubules in *Arabidopsis* seedling whole-mount probes. *Methods Mol. Biol.* **1171**, 107–115.

Schaller G. E., Kieber J.J., Shiu S.-H. (2008): Two-Component Signalling Elements and Histidyl-Aspartyl Phosphorelays. *The Arabidopsis Book*, 6.

Schaller G. E., Shiu S. H., Armitage J.P. (211): Two-component systems and their co-option for eukaryotic signal transduction. *Curr Biol.* **21**, 320-330.

Schaller G. E., Street I. H., Kieber J. J. (2014): Cytokinin and the cell cycle. Curr. Opin. Plant Biol. **21**, 7–15.

Scheres B., Di Laurenzio L., Willemsen V., Hauser M.T., Janmaat K., Weisbeek P., Benfey P.N. (1995): Mutations affecting the radial organisation of the *Arabidopsis* root display specific defects throughout the embryonic axis. *Development* **121**, 53–62

Schmülling T. (2004): Cytokinin. In *Encyclopedia of Biological Chemistry* (Eds. Lennarz., W., Lane, M. D.), Academic Press/ Elsevier Science, 562-567.

Shan X., Yan J., Xie D. (2012): Comparison of phytohormone signalling mechanisms. *Curr. Opin. Plant Biol.* **15**, 84–91.

Sharan A., Soni P., Nongpiur R.C., Singla-Pareek S.L., Pareek A. (2017): Mapping the 'Two-Component System' Network in Rice. *Sci Rep* **7**, 1–13.

Shi X., Gupta S., Lindquist I. Cameron C.T., Mudge J. Rashotte A. (2013): Transcriptome Analysis of Cytokinin Response in Tomato Leaves. PloS One 8, 55090.

Sjöback R., Nygren J., Kubista M. (1995): Absorption and fluorescence properties of fluorescein. *Spectrochim. Acta A* **51**, 7–21.

Skoog F., Miller C. O. (1957): Chemical regulation of growth and organ formation in plant tissues cultured in vitro. *Symp Soc Exp Biol.* **11**, 118–130.

Skoog F., Schmitz R. Y., Hecht S. M., Frye R. B. (1975): Anticytokinin activity of substituted pyrrolo[2,3-d]pyrimidines. *Proc. Natl. Acad. Sci. U. S. A.* **72**, 3508–3512.

Smertenko A., Assaad F., Baluška F., Bezanilla M., Buschmann H., Drakakaki G., Hauser M.-T., Janson M., Mineyuki Y., Moore I., Müller S., Murata T., Otegi M. S., Panteris E., Rasmussen C., Schmit A.-C., Šamaj J., Samuels L., Staehelin L. A., Van Damme D., Wasteneys G., Žárský V. (2017): Plant cytokinesis: terminology for structures and processes. *Trends Cell Biol.* **27**, 885–894.

Smet W., Sevilem I., de Luis Balaguer M. A., Wybouw B., Mor E., Miyashima S., Blob B., Roszak P., Jacobs T. B., Boekschoten M., Hooiveld G., Sozzani R., Helariutta Y., De Rybel B. (2019): DOF2.1 controls cytokinin-dependent vascular cell proliferation downstream of TMO5/LHW. *Curr. Biol.* **29**, 520–529.

Sokolowska K., Kizinska J., Szewczuk Z., Banasiak A. (2014): Auxin conjugated to fluorescent dyes e a tool for the analysis of auxin. *Plant Biol.* **16**, 866–877.

Specker M. A., Morrice A. G., Gruber B. A., Leonard N. J., Schmitz R. Y., Skoog F. (1976): Fluorescent cytokinins: stretched-out analogues of N^6-benzyladenine and N^6-(Δ^2-isopentenyl)adenine. *Phytochemistry* **15**, 609–613.

Spíchal L., Rakova N. Y., Riefler M., Mizuno T., Romanov G. A., Strnad M., Schmülling T. (2004): Two cytokinin receptors of *Arabidopsis thaliana*, CRE1/AHK4 and AHK3, differ in their ligand specificity in a bacterial assay. *Plant Cell Physiol.* **45**, 1299–1305.

Spíchal L., Werner T., Popa I., Riefler M., Schülling T., Strnad M. (2009): The purine derivative PI-55 blocks cytokinin action via receptor inhibition. *FEBS J.* **276**, 244–253.

Spíchal L. (2011): Bacterial assay to study plant sensor histidine kinases. *Methods Mol. Biol*. **779**, 139–147.

Spíchal L. (2012): Cytokinins - Recent news and views of evolutionally old molecules. Funct Plant Biol. **39**, 267–284.

Stirk W. A., J. van Staden (2010): Flow of Cytokinins through the Environment. *Plant Growth Regul.* **62**, 101–16.

Steklov M. Y., Lomin S. N., Osolodkin D. I., and Romanov G. A. (2013): Structural basis for cytokinin receptor signalling: an evolutionary approach. *Plant Cell Rep.* **32**, 781–793.

Stolz A., Riefler M., Lomin S. N., Achazi K., Romanov G. A., and Schmülling T. (2011): The specificity of cytokinin signalling in *Arabidopsis thaliana* is mediated by differing ligand affinities and expression profiles of the receptors. *Plant J. Cell Mol. Biol.* **67**, 157–168.

Strnad M. (1997): Aromatic cytokinins. *Physiol. Plant.* **101**, 674–688.

Suzuki T., Miwa K., Ishikawa K., Yamada H., Aiba H., Mizuno T. (2001): The *Arabidopsis* sensor His-kinase, AHK4, can respond to cytokinins. *Plant Cell Physiol.* **42**, 107–113.

Svačinová J. Novák O., Plačková L., Lenobel R., Holík J., Strnad M., Doležal K. (2012): A new approach for cytokinin isolation from *Arabidopsis* tissues using miniaturized purification: pipette tip solid-phase extraction. *Plant Methods* **8**, 17.

Takeda S., Fujisawa Y., Matsubara M., Aiba H., Mizuno T. (2001): A novel feature of the multistep phosphorelay in Escherichia coli: a revised model of the RcsC -> YojN -> RcsB signalling pathway implicated in capsular synthesis and swarming behaviour. *Mol. Microbiol.* **40**, 440–450.

Takei K., Yamaya T., Sakakibara H. (2004): *Arabidopsis* CYP735A1 and CYP735A2 encode cytokinin hydroxylases that catalyze the biosynthesis of trans-zeatin. *J Biol Chem* **279**, 41866–41872.

Tanaka Y., Suzuki T., Yamashino T., Mizuno T. (2004): Comparative studies of the AHP histidine-containing phosphotransmitters implicated in His-to-Asp phosphorelay in *Arabidopsis thaliana*. *Biosci. Biotechnol. Biochem.* **68**, 462–465.

Tarkowská D., Doležal K., Tarkowski P., Åstot C., Holub J., Fuksová K., Schmülling T., Sandberg G., Strnad M. (2003): Identification of new aromatic cytokinins in *Arabidopsis thaliana* and *Populus × canadensis* leaves by LC- (+) ESI-MS and capillary liquid chromatography/frit-fast atom bombardment mass spectrometry. *Physiol. Plant.* **117**, 579–590.

Tirichine L., Sandal N., Madsen L.H., Radutoiu S., Albrektsen A.S., Sato S., Adamitu E., Tabata S., Stougaard J. (2007): A gain-of-function in a cytokinin receptor triggers spontaneous root nodule organogenesis. *Science* **315**, 104–107.

To J. P. C., Deruère J., Maxwell B. B., Morris V. F., Hutchison C. E., Ferreira F. J., Schaller G. E., Kieber J. J. (2007): Cytokinin Regulates Type-A *Arabidopsis* Response Regulator Activity and Protein Stability via Two-Component Phosphorelay. *Plant Cell* **19**, 3901–3914.

To J. P. C., Kieber J. J. (2008): Cytokinin signalling: two-components and more. *Trends Plant Sci.* **13**, 85–92.

Tran L.-S. P., Urao T., Qin F., Maruyama K., Kakimoto T., Shinozaki K., Yamaguchi-Shinozaki K. (2007): Functional analysis of AHK1/ATHK1 and cytokinin receptor histidine kinases in response to abscisic acid, drought, and salt stress in *Arabidopsis*. *Proc. Natl. Acad. Sci. U.S.A* **104**, 20623–20628.

Trott O., Olson A. J. (2010): AutoDock Vina: improving the speed and accuracy of docking with a new scoring function, efficient optimization, and multithreading. *J. Comput. Chem.* **31**, 455–461.

Tsuda E., Yang H., Nishimura T., Uehara Y., Sakai T., Furutani M., Koshiba T., Hirose M., Nozaki H., Murphy A. S., Hayashi K. (2011): Alkoxy-auxins are selective inhibitors of auxin transport mediated by PIN, ABCB and AUX1 transporters. *J. Biol. Chem.* **286**, 2354–2364.

Ueguchi C., Sato S., Kato T., Tabata S. (2001a): The AHK4 gene involved in the cytokinin-signalling pathway as a direct receptor molecule in *Arabidopsis thaliana*. *Plant Cell Physiol* **42**, 751–755.

Ueguchi C., Koizumi H., Suzuki T., Mizuno T. (2001b): Novel Family of Sensor Histidine Kinase Genes in *Arabidopsis thaliana*. *Plant Cell Physiol.* **42**, 231–235.

Urao T., Yakubov B., Satoh R., Yamaguchi-Shinozaki K., Seki M., Hirayama T., Shinozaki K. (1999): A transmembrane hybrid-type histidine kinase in *Arabidopsis* functions as an osmosensor. *Plant Cell* **11**, 1743–1754.

Urao T., Yamaguchi-Shinozaki K., Shinozaki K. (2001): Plant Histidine Kinases: An Emerging Picture of Two-Component Signal Transduction in Hormone and Environmental Responses. *Sci.* STKE, RE18.

von Wangenheim D., Hauschild R., Fendrych M., Barone V., Benkova E., Friml J. (2017): Live tracking of moving samples in confocal microscopy for vertically grown roots. *Elife* **6**, e26792.

Werner T., Motyka V., Laucou V., Smets R., van Onckelen H. (2003): Cytokinin-deficient transgenic *Arabidopsis* plants show multiple developmental alterations indicating opposite functions of cytokinins in the regulation of shoot and root meristem activity. *Plant Cell* **15**, 1–20.

Werner T., Köllmer I., Bartrina y Manns I., Holst K., Schmülling T. (2006): New insights into the biology of cytokinin degradation. *Plant Biol.* **8**, 371–381.

Werner T., Schmülling T. (2009): Cytokinin action in plant development. *Curr. Opin. Plant Biol.* **12**, 527–538.

West A.H., Stock A.M. (2001): Histidine kinases and response regulator proteins in two-component signalling systems. *Trends in Biochem Sci* **26**, 369–376.

Williams D. B. W., Lawton M. (2010): Drying of Organic Solvents: Quantitative Evaluation of the Efficiency of Several Desiccants. *J. Org. Chem.* **75**, 8351–8354.

Wormit A., Traub M., Flörchinger M., Neuhaus H.E., Möhlmann T. (2004): Characterization of three novel members of the *Arabidopsis thaliana* equilibrative nucleoside transporter (ENT) family. *Biochem. J.* **383**, 19–26.

Wulfetange K., Lomin S. N., Romanov G. A., Stolz A., Heyl A., Schmülling T. (2011): The cytokinin receptors of *Arabidopsis* are located mainly to the Endoplasmic reticulum. *Plant Physiol.* **156**, 1808–1818.

Yamada H., Suzuki T., Terada K., Takei K., Ishikawa K., Miwa K., Yamashino T., Mizuno T. (2001): The *Arabidopsis* AHK4 histidine kinase is a cytokinin-binding receptor

that transduces cytokinin signals across the membrane. Plant Cell Physiol **42**, 1017–1023.

Yonekura-Sakakibara K., Kojima M., Yamaya T., Sakakibara H. (2004): Molecular characterization of cytokinin-responsive histidine kinases in maize. Differential ligand preferences and response to *cis*-zeatin. *Plant Physiol.* **134**, 1654–1661.

Zalabák D., Galuszka P., Mrízová K., Podlešáková K., Gu R., Frébortová J. (2014): Biochemical characterization of the maize cytokinin dehydrogenase family and cytokinin profiling in developing maize plantlets in relation to the expression of cytokinin dehydrogenase genes. *Plant Physiol Bioch* **74**, 283–293.

Zawadski P., Slosarek G., Boryski J., Wojtaszek P. (2010): A fluorescence correlation spectroscopy study of ligand interaction with cytokinin-specific binding protein from mung bean. *Biol. Chem.* **391**, 43–53.

Zhang K. W., Novák O. R., Wei Z. Y., Gou M. Y., Zhang X. B., Yu Y., Yang H. J., Cai Y. H., Strnad M., Liu C. J. (2014): *Arabidopsis* ABCG14 protein controls the acropetal translocation of root-synthesized cytokinins. *Nat. Commun.* **5**, 3274–3286.

Zürcher E., Tavor-Deslex D., Lituiev D., Enkerli K., Tarr P. T., Müller B. (2013): A robust and sensitive synthetic sensor to monitor the transcriptional output of the cytokinin signalling network *in planta*. *Plant Physiol.* **161**, 1066–1075.

Zürcher E., Liu J., di Donato M., Geisler M., Müller B. (2016): Plant development regulated by cytokinin sinks. *Science* **353**, 1027–1030.

Zürcher E., Müller B. (2016): Cytokinin synthesis, signalling, and function—advances and new insights. *Int. Rev. Cell Mol. Biol.* **324**, 1–38.

Zwack P. J., Rashotte A. M. (2015): Interactions between cytokinin signalling and abiotic stress responses. *J. Exp. Bot.* **66**, 4863–4871.

CURRICULUM VITAE

Karolina Kubiasová

ORCID iD   0000-0001-5630-9419

Nationality: Czech

Contact: KubiasovaK@seznam.cz

Education:

2014-present   PhD programme, Biochemistry, Faculty of Science,

Palacký University in Olomouc, Czech Republic

(topic: Localization studies of the cytokinin receptor CRE1/AHK4 using

fluorescently labelled cytokinin)

2014   Master's degree in Biochemistry, Faculty of Science,

Palacký University in Olomouc, Czech Republic

(topic: Localization of cytokinin receptors in *Arabidopsis*

thaliana using fluorescent labelling)

2012   Bachelor's degree in Biochemistry, Faculty of Science,

Palacký University in Olomouc, Czech Republic

(topic: Synthesis and characterization of fluorescently

labelled cytokinin derivatives)

Work Experience:

2020-present   Laboratory manager for Benkova and Friml groups,

Institute of Science and Technology Austria (IST Austria)

2014-2019   Research assistant, Department of Molecular Biology,

Centre of the Region Hana for Biotechnological and

Agricultural Research, Palacký University in Olomouc,

Czech Republic

Research Internships:

2016 – 2019   Institute of Science and Technology (IST Austria),

                        Klosterneuburg, Austria; Benkova group

                        16 months divided into 7 stays

October 2015 (1 month)   The Interfaculty Institute for Microbiology and Infection

                        Medicine, Eberhard Karls University of Tübingen, Germany

                        Maldener lab

Courses:

April 2015 (1 week)   Institute of Molecular Biology (IMG), Prague, Czech

                        Republic

                        Course "Processing and analysis of microscopical data in

                        Biomedicine"

November 2013 (1 week)   Center of Medical Biotechnology,

                        University of Duisburg-Essen, Germany

                        COST training school: Chemical probes in chemical

                        proteomics and biosynthesis studies

Grants and projects:

2018-2020   GAČR (18-23972Y): Is *Arabidopsis* AHK4/CRE1 decoy receptor?

                 (a member of the research team)

2019   GAČR (17-23702S): Distinct transcription factor families

                 controlling meristem activity and organogenesis

                 in *Arabidopsis* (a member of the research team)

2016-2018   GAČR (16-04184S): Study of the intracellular distribution of

                 cytokinins and their transport to vacuoles (a member of the

                 research team)

2017   Erasmus+

      Detailed study of localization of cytokinin receptors in

      Arabidopsis thaliana

2017   Internal Grant Agency (IGA) of Palacký University

      Studium prostorové a časové lokalizace cytokininových receptorů a

      jejich funkční charakterizace v *Arabidopsis thaliana*

2016   Endowment Fund of Palacký University

      Zkoumání distribuce klíčových komponent cytokininového

      metabolismu v buňce

2014-2016 GAČR (GAP501/12/0161): Cyanobacterium *Nostoc* as a genetic and

      functional model for the plant cytokinin hormone metabolism (a

      member of the research team)

Teaching Experience:

2014-2018 Basic Course in Laboratory Work (KBC/LABT)

2017   Supervising a bachelor student

Conferences:

2015   Kubiasová K., Plíhal O., Mik V., Šamajová O., Galuszka P., Spíchal L.

      Green for good (G4G), Olomouc, Czech Republic

      Localization of cytokinin receptors in *Arabidopsis thaliana* using

      fluorescent labelling; poster presentation

2014   Kubiasová K., Plíhal O., Mik V., Šamajová O., Galuszka P., Spíchal L.

      KEBR 2014 - 12th PhD Student Conference of Plant Experimental

      Biology, Olomouc, Czech Republic

Localization of cytokinin receptors in *Arabidopsis thaliana* using fluorescent labelling; poster presentation

Publications:

Kubiasová K., Montesinos J.C., Šamajová O., Nisler J., Mik V., Semerádová H., Plíhalová L., Novák O., Marhavý P., Cavallari N., Zalabák D., Berka K., Doležal K., Galuszka P., Šamaj J., Strnad M., Benková E., Plíhal O., Spíchal L. (2020): Cytokinin fluoroprobe reveals multiple sites of cytokinin perception at plasma membrane and endoplasmic reticulum. *Nat. Commun*. **11**, 4285. doi: 10.1038/s41467-020-17949-0

Kubiasová K., Mik V., Nisler J., Hönig M., Husičková A., Spíchal L., Pěkná Z., Šamajová O., Doležal K., Plíhal O., Benková E., Strnad M., Plíhalová L. (2018): Design, synthesis and perception of fluorescently labeled isoprenoid cytokinins. *Phytochemistry* **150**, 1-11. doi:10.1016/j.phytochem.2018.02.015

Frébortová J., Plíhal O., Florová V., Kokáš F., Kubiasová K., Greplová M., Šimura J., Novák O., Frébort I. (2017): Light influences cytokinin biosynthesis and sensing in *Nostoc* (cyanobacteria). *J Phycol.* **53(3)**, 703-714. doi:10.1111/jpy.12538

de Montaigu A., Oeljeklaus J., Krahn J.H., Suliman M.N.S, Halder V., de Ansorena E., Nickel S., Schlicht M., Plíhal O., Kubiasová K., Radová L, Kracher B., Tóth R., Kaschani F., Coupland G., Kombrink E., Kaiser M. (2017): The Root Growth-Regulating Brevicompanine Natural Products Modulate the Plant Circadian Clock. *ACS Chem Biol.* **12(6)**, 1466-1471. doi:10.1021/acschembio.6b00978.

Chemicals

6-Chloropurine and 2,6-dichloropurine were obtained from Olchemim. Fluorescent labels fluorescein isothiocyanate (FITC), [9-(2-carboxyphenyl)-6-diethylamino-3-xanthenylidene]-diethylammonium chloride (rhodamine B), 5-dimethylamino-1-naphthalenesulfonyl chloride (dansyl chloride, DS-Cl) and coumarine-3-carboxylic acid (Cou) were obtained from Sigma-Aldrich, whereas NHS-activated cyanine 5 dye (Cy5) was obtained from Lumiprobe. Dimethylamine, tetrabromomethane, 1,2-diaminoethane and 1,6-diaminohexane were obtained from Sigma-Aldrich. Triethylamine, acetone, dichlormethane (DCM), DMSO, ethyl acetate, hexane, methanol, petroleum ether, *n*-propanol, tetrahydrofuran, toluene and other chemicals, e.g., acetic acid, potassium carbonate and sodium hydrogen carbonate, were obtained from VWR or LachNer. 3-Methylbut-2-en-1-amine hydrochloride and 7-DEAC-OH were prepared at the Department of Chemical Biology and Genetics, CRH, UPOL according to published protocols (Yin et al., 2013). Dry solvents, such as methanol and DMSO, were also prepared according to the literature (Williams and Lawton, 2010). The latter solvents were dried over activated 3Å molecular sieve powder (24 h at 300 °C), then in a $CaCl_2$ drying tube for at least for 72 h. Dry DCM and MeCN were prepared by distillation with calcium hydride.

General procedures

Thin layer chromatography (TLC) was carried out using silica gel 60 WF_{254} plates (Merck, Germany). $CHCl_3$-MeOH (9:1, 4:1, v/v), ethyl acetate-toluene (1:1, v/v) or ethyl acetate: hexane (65:35, v/v) were used as the mobile phase. Selected samples were purified by flash chromatography using a VersaFlash purification station (Supelco) coupled to a 2110 fraction collector (Bio-Rad). Compounds were separated on VersaPak cartridges (23 mm x 110 mm, Supelco) containing 23 g of spherical silica and eluted with a mobile phase containing $CHCl_3$/MeOH (90:10, v/v) or using PharmPrep 60 CC (40-63 µm, Merck) as the stationary phase packed in glass columns (15 mm diameter, Kronlab, or 25 mm diameter columns, Pharmacia Fine Chemicals) using a

mobile phase of hexane:ethyl acetate (3:2, v:v) or chloroform: methanol: NH_4OH, 95:5:0.5.

Column chromatography purification was carried out using Davisil silica gel with pore size 40-63 μm (Grace Davision). Melting points (M.p.)s were determined on Stuart SMP 30 M.p. apparatus (Bibby Scientific, Stone, UK) and were uncorrected. HPLC purity samples were dissolved in the HPLC mobile phase (initial conditions), applied to an RP-column (Symmetry C18, 5 μm, 150 mm × 2.1 mm; Waters Inc.), then separated using an Alliance 2695 Separations Module high-performance liquid chromatograph (Waters Inc.) at a flow rate of 0.2 mL min^{-1} with the following binary gradient: 0 min, 10% B; 0-24 min, linear gradient to 90% B, followed by 10 min isocratic elution of 90% B. At the end of the gradient, the column was re-equilibrated to the initial conditions. 15 mM formic acid adjusted to pH 4.0 by ammonium hydroxide was used as solvent A and methanol as the organic modifier (solvent B). Samples were analyzed using a PDA 2996 detector (Waters Inc.) with detection at wavelengths of 210-700 nm. The chromatograph´s effluent was directed into a Q-ToF Micro tandem mass spectrometer (Waters Inc.) equipped with an electrospray source (source temperature 120 °C, desolvation temperature 300 °C, capillary voltage 3 kV). Nitrogen was used as both the cone gas (50 L/h) and desolvation gas (500 L/h). Data were acquired in full scan mode (50-1000 Da) with a scan time of 0.5 s and cone voltage of 20 V. Analyses were performed in positive mode (ESI+). Therefore, data were collected for protonated ions $[M + H]^+$. Nuclear magnetic resonance spectra (^{1}H and ^{13}C) were recorded on a Bruker Avance 300 or JEOL ECA-500 NMR spectrometer and were reported as chemical shifts in ppm units (ppm, δ). Chemical shifts were calibrated to residual and solvent peaks (CDCl$_3$ ^{1}H = 7.26 and ^{13}C = 77.0 ppm; DMSO-d_6 ^{1}H = 2.49 and ^{13}C = 39.5 ppm). Absorption spectra were acquired on an Agilent 8453E UV-visible spectroscopy system (Agilent Technologies Inc., USA). Samples were prepared by first dissolving the compounds in DMSO and then diluting with methanol to a final concentration of 1 mM (containing 1% DMSO). Fluorescence excitation and emission maxima were measured on a Hitachi F-4500 spectrofluorometer. Samples were dissolved in DMSO and then diluted with methanol to a final concentration of 10 μM (containing 1% DMSO).
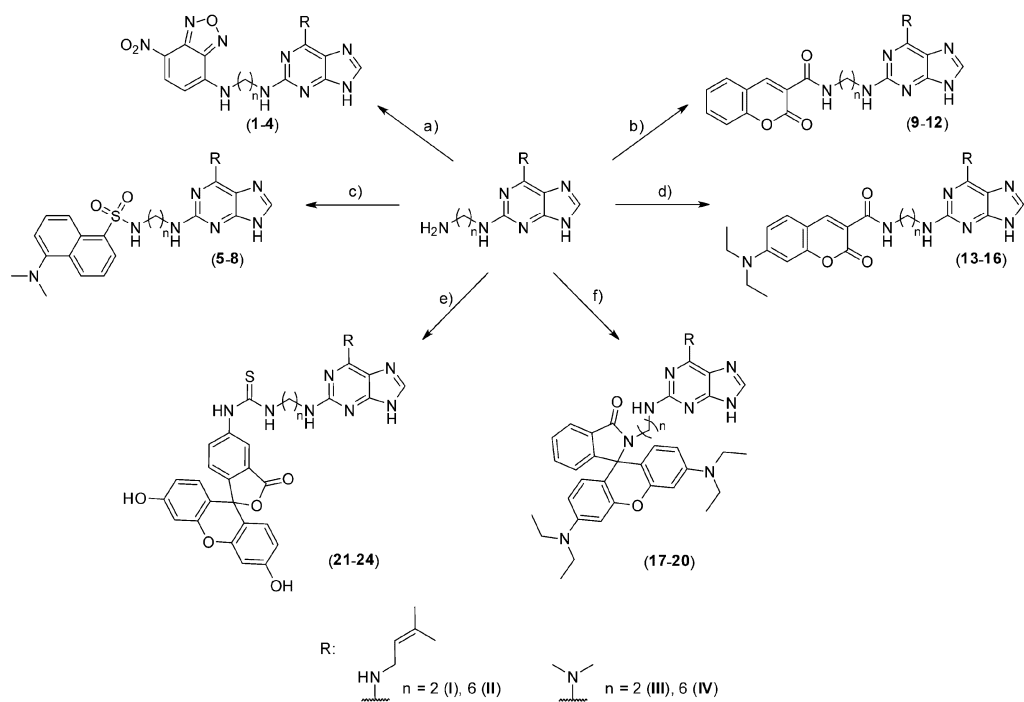
Syntheses
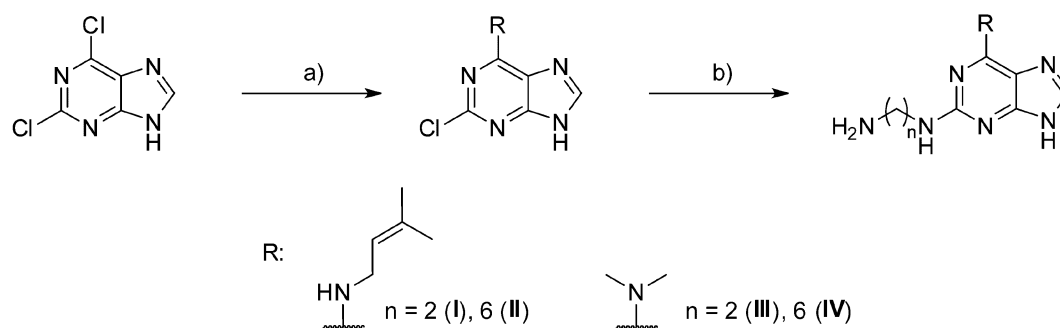
Scheme 1: *Reaction scheme for the synthesis of 2,6-disubstituted purine precursors for fluorescent labelling. a) R-H, Et$_3$N, n-PrOH, 100 °C, 4 h; b) ethane-1,2-diamine, hexane-1,6-diamine, 165 °C, 3 h.*
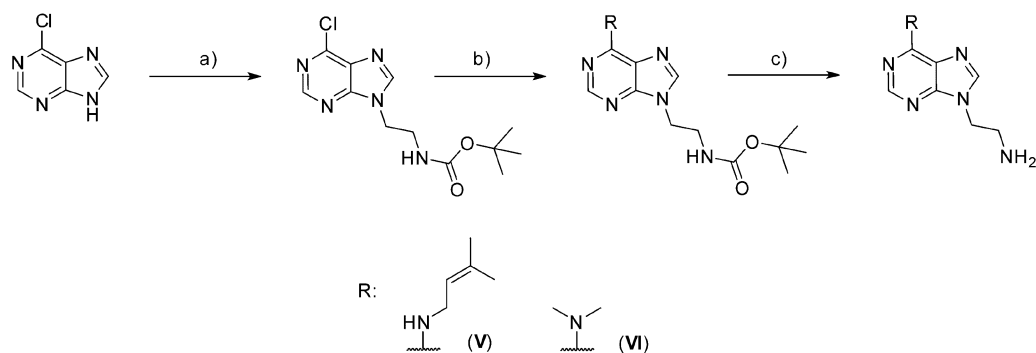
Scheme 2: *Reaction scheme for the synthesis of 6,9-disubstituted purine precursors for fluorescent labelling. a) Boc-2-aminoethanol, PPh$_3$, DIAD, THF, 2 h; b) R-H, Et$_3$N, n-PrOH, 100 °C, 4 h; c) Dowex 50W X8, DCM, reflux followed by 4 M methanolic ammonia, overnight.*

Scheme 3: *Preparation of C2-fluorescently labelled purine derivatives. a) NBD-Cl, NaHCO₃, MeOH, 50 °C, 1 h followed by RT overnight; b) NHS activated coumarin-3-carboxylic acid, DMSO, MeCN, carbonate buffer pH 8.6, overnight; c) dansyl chloride, Et₃N, MeOH, DCM, overnight; d) NHS activated DEAC-OH, DMSO, MeCN, carbonate buffer pH 8.6, overnight; e) FITC, Et3N, MeOH, overnight; f) NHS activated rhodamine B, MeCN, carbonate buffer pH 8.6, overnight.*
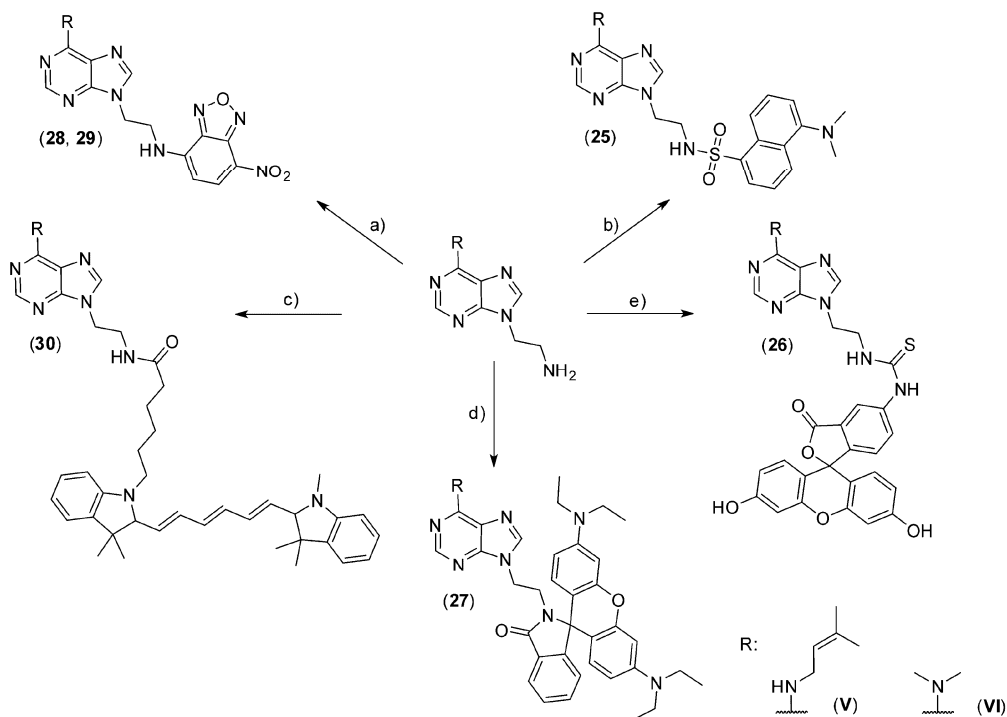
Scheme 4: *Fluorescently labelled N9-substituted derivatives. a) 4-chloro-7-nitrobenzofurazan, NaHCO₃, MeOH, 50 °C, 1 h; b) dansyl chloride, 2M Na₂CO₃, acetone, water, RT, overnight; c) cyanine 5 NHS, 0.1M sodium bicarbonate in water, DMF; d) NHS activated rhodamine B, MeCN, carbonate buffer pH 8.6, overnight; e) FITC, MeOH, NaHCO₃, 50 °C, 1 h. Kation of compound **30** was compensated by [BF4] anion that was which was omitted to simplify the scheme.*

Synthesis of intermediates necessary for the attachement of fluorescent marker

Synthesis of 2-chloro-6-[(3-methylbut-2-en-1-yl)amino]purine *(A)* *and 2-chloro-6-dimethylaminopurine (B) intermediates*

The preparation of both A and B intermediates is given in Scheme 1. **A** was prepared by reaction of 2,6-dichloropurine (1 equiv.) with of 3-methylbut-2-en-1-amine hydrochloride (1.3 equiv.) in the presence of triethylamine (3.5 equiv.). The reaction mixture was refluxed in propanol for 3 h. A white solid was formed after cooling. **A**: white solid; yield 87%; M.p. 236-238 °C. HPLC-UV/VIS retention time, purity (min,%): 23.28, 99.9. ESI⁺-MS *m/z* (rel. int. %): 238.4 (100, [³⁵Cl-M+H]⁺). ¹H NMR (300 MHz, DMSO-*d₆*) δ (ppm): 1.67 (s, 3H), 1.70 (s, 3H), 3.99 (bs, 2H), 5.27 (t, *J* = 6.1 Hz, 1H), 8.09

(bs, 2H,), 13.00 (vbs, 1H). ^{13}C NMR (75 MHz, DMSO-d_6) δ (ppm): 17.8, 25.4, 37.8, 117.8, 121.3, 133.7, 139.2, 150.3, 152.9, 154.5. **B** was prepared by reaction of 2,6-dichloropurine (1 equiv.) and dimethylamine hydrochloride (2 equiv.) in the presence of Et$_3$N (3.5 equiv.). The reaction mixture was refluxed in propanol for 3 h. A white solid was formed after cooling. B: white solid; yield 90%. HPLC-UV/VIS retention time, purity (min, %): 18.18, 99.9. ESI$^+$-MS *m/z* (rel. int. %): 198.3 (100 [^{35}Cl-M+H]$^+$).^{1}H NMR (300 MHz, DMSO-d_6) δ (ppm): 3.20 (bs, 3H), 3.61 (bs, 3H), 8.08 (s, 1H), 13.09 (bs, 1H). ^{13}C NMR (125 MHz, DMSO-d_6) δ (ppm): 37.1, 38.6, 117.9, 138.4, 152.1, 152.3, 154.4.

Synthesis of 2-[(2-aminoethyl)amino]-6-[(3-methylbut-2-en-1-yl)amino]purine **(I),**

2-[(6-aminohexyl)amino]-6-[(3-methylbut-2-en-1-yl)amino]purine **(II),** *2-[(2-aminoethyl)amino]-6-dimethylaminopurine* **(III)** *and 2-[(6-aminohexyl)amino]-6-dimethylaminopurine* **(IV)** *intermediates*

I was prepared by heating 8.4 mmol of **A** with 168.3 mmol of 1,2-diaminoethane in an ACE pressure tube at 165 °C for 3 h. Next, excess 1,2-diaminoethane was distilled off and the residue treated with ice cold water. The pure product was obtained by crystallization from methanol. **I**: pale yellow solid; yield 60%; M.p.: 125-127 °C. HPLC-UV/VIS retention time, purity (min,%): 12.88, 95.9. ESI$^+$-MS *m/z* (rel. int. %): 262.5 (100, [M+H]$^+$).^{1}H NMR (300 MHz, DMSO-d_6) δ (ppm): 1.65 (s, 3H), 1.67 (s, 3H), 2.66 (t, *J* = 6.3 Hz, 2H), 3.21 (dd, *J* = 12.1, 6.3 Hz, 2H), 4.00 (bs, 2H), 5.29 (app. t, 1H), 6.12 (app. t., 1H), 7.09 (bs, 1H), 7.62 (s, 1H). ^{13}C NMR (75 MHz, DMSO-d_6) δ (ppm): 18.2, 25.8, 37.9, 41.8, 45.0, 113.0, 123.2, 132.9, 135.6, 152.5, 154.4, 159.9.

II was prepared by heating 4.2 mmol of A with 84.1 mmol of 1,6-diaminohexane in an ACE pressure tube for 3 h. **II**: pale yellow solid; yield 94%; M.p.: 152-155 °C. HPLC-UV/VIS retention time, purity (min., %): 16.53, 98.2. ESI$^+$-MS *m/z* (rel. int. %): 318.5 (100, [M+H]$^+$). ^{1}H NMR (300 MHz, DMSO-d_6) δ (ppm): 1.28 (bs, 8H), 1.49 (bs, 2H); 1.65 (s, 3H), 1.67 (s, 3H), 3.19 (q, *J* = 6.4 Hz, 2H), 4.00 (bs, 2H), 5.29 (app. t, 1H), 6.10 (app. t, 1H), 7.05 (bs, 1H), 7.60 (s, 1H). ^{13}C NMR (75 MHz, DMSO-d_6) δ (ppm): 17.8, 25.4, 26.3, 26.6, 29.4, 33.5, 37.5, 41.1, 41.6, 112.6, 122.9, 132.4, 135.0, 152.2, 154.0, 159.4.

III was prepared from compound **B** by heating with 1,2-diaminoethane. After reaction, excess 1,2-diaminoethane was distilled off and the pure product was obtained by crystallization from methanol. **III**: pale yellow solid; yield 89%; M.p.: 239-242 °C. HPLC-UV/VIS retention time, purity (min., %): 4.23, 99.3. ESI+ MS m/z (rel. int. %): 222.4 (100, [M+H]+). ^{1}H NMR (300 MHz, DMSO-d_6) δ (ppm): 2.82 (t, J = 6.0 Hz, 2H), 3.32-3.36 (m, 8H), 6.25 (t, J = 5.4 Hz, 1H), 7.66 (s, 1H). ^{13}C NMR (75 MHz, DMSO-d_6) δ (ppm): 2x 37.5, 40.1, 41.9, 113.5, 134.5, 153.2, 154.4, 158.6.

IV was prepared from compound **B** by heating with 1,6-diaminohexane. **IV**: pale yellow solid; yield 98%, M.p.: 151-153 °C. HPLC-UV/VIS retention time, purity (min., %): 10.03, 98.8. ESI+-MS m/z (rel. int. %): 278.4 (100, [M+H]+). ^{1}H NMR (300 MHz, DMSO-d_6) δ (ppm): 1.27 (m, 6H), 1.49 (bs, 2H), 3.19 (bs, 2H), 3.35 (bs, 2H), 4.31 (vbs, 6H), 6.13 (app. t, 1H), 7.61 (s, 1H). ^{13}C NMR (75 MHz, DMSO-d_6) δ (ppm): 26.3, 26.6, 29.4, 33.1, 2x 37.5, 41.0, 41.5, 113.2, 134.2, 153.5, 154.4, 158.7.

Synthesis of *6-[(3-methylbut-2-en-1-yl)amino]-9-(2-aminoethyl)purine (V) and 6-dimethyl-9-(2-aminoethyl)purine (VI)*

6,9-Disubstituted derivatives were synthesized according to Scheme 2. **A** Boc-aminoethyl substituent was introduced in the *N*9-position of 6-chloropurine/iP by the Mitsunobu reaction using *N*-Boc-ethanolamine, PPh$_3$ and DIAD in THF. The resulting 6-chloropurine intermediates were further alkylated at the 6-position by reaction with Et$_3$N in refluxing propanol. Finally, the *N*-Boc protective group was removed by treatment with Dowex WX 8/ 4 M methanolic ammonia according to a slightly modified protocol (Liu et al., 1998). First, 6-chloro-9-{2-[(*tert*-butoxycarbonyl)amino]ethyl}purine was prepared from 6-chloropurine: DIAD (2 equiv.) was dropwise added to the mixture of 6-chloropurine (1 equiv., 12.9 mmol), Ph$_3$P (2 equiv.) and *tert*-butyl (2-hydroxyethyl)carbamate (1.1 equiv.) in THF (75 mL). The mixture was stirred at RT for 2 hs and then concentrated in vacuo. The yellow oily residuum was crystallized from toluene (50 mL) at 4 °C overnight. The product was obtained after purification by silica column chromatography using petroleum

ether/ethyl acetate and later with CHCl$_3$/MeOH. 6-chloro-9-{2-[(*tert*-butoxycarbonyl)amino]ethyl}purine (1 equiv, 1.68 mmol) was refluxed with 3-methylbut-2-en-1-amine hydrochloride (**V**, 1 equiv) or dimethylamine (**VI**, 1.1 equiv) and Et$_3$N (2.5 equiv) in PrOH (15 mL) for 4 hs and then stirred at RT overnight. Simultaneous deprotection and purification of *N*-Boc protected compounds was performed according to a slightly modified protocol (Liu *et al.,* 1998). **V:** white solid, yield 90%, ESI$^+$-MS m/z (rel. int. %): 247.5 (100, [M+H]+).^{1}H NMR (300 MHz, DMSO-d_6) δ (ppm): 1.71 (s, 3H), 3.30 (t, 2H, *J* = 6.0 Hz), 4.06 (bs, 2H), 4.45 (t, 2H, *J* = 6.0 Hz), 5.29 (app. t, 1H), 7.79 (bs, 4H), 8.16 (s, 1H), 8.22 (s, 1H).

VI: white solid: yield 87 %.ESI$^+$-MS m/z (rel. int. %): 207.4 (100, [M+H]$^+$).^{1}H NMR (300 MHz, DMSO-d_6) δ (ppm): 2.90 (t, *J* = 6.3 Hz, 2H), 3.44 (bs, 6H), 4.10 (t, *J* = 6.3 Hz, 2H), 8.11 (s, 1H), 8.19 (s, 1H).

C2 fluorescently labelled derivatives

C2-labelled compounds were prepared according to Scheme 3. An appropriate fluorescent label was reacted with amino groups terminating the above mentioned prepared intermediates. Generally, C2-derivatives marked with NBD were prepared as follows: 0.36 mmol (1 equiv.) of the appropriate intermediate (I, II, III, IV), 1.2 equiv. of NBD-Cl (**1-4**) and 3 equiv. of NaHCO$_3$ were stirred in methanol at 50 °C for 16 h. Afterwards, the solvent was evaporated under reduced pressure and the residue treated with ice cold water (5 mL). The resulting solid material was filtered, washed with ice cold water (4 x 1 mL) and then dried at 50 °C. The crude material was purified by silica column chromatography using CHCl$_3$/MeOH (4:1) as the mobile phase, starting from pure chloroform with a methanol gradient.

1*: N^6-(3-methylbut-2-en-1-yl)-N^2-{2-[(7-nitrobenzo[c][1,2,5]oxadiazol-4-yl)amino]ethyl}-9H-purine-2,6-diamine*: Reddish solid; yield 74%.

2: *N^6-(3-methylbut-2-en-1-yl)-N^2-{6-[(7-nitrobenzo[c][1,2,5]oxadiazol-4-yl)amino]hexyl}-9H-purine-2,6-diamine*: Reddish solid; yield 65%.

3: *N⁶,N⁶-dimethyl-N²-{2-[(7-nitrobenzo[c][1,2,5]oxadiazol-4-yl)amino]ethyl}-9H-purine-2,6-diamine:* Reddish solid; yield 81%.

4: *N⁶,N⁶-dimethyl-N²-{6-[(7-nitrobenzo[c][1,2,5]oxadiazol-4-yl)amino]hexyl}-9H-purine-2,6-diamine (4):* Reddish solid; yield 75%.

C2-derivatives marked with DS-Cl were prepared as follows: 1 equiv., (0.36 mmol) of I, II, III or IV and Et$_3$N (2 equiv.) were dissolved in dry MeOH (0.4 mL) and dry DCM (3 mL) under an argon atmosphere and added to a mixture of DS-Cl (1.5 equiv.) in DCM (2 mL). The reaction mixture was protected against light and stirred at RT for 16 h. Afterwards, the solvents were removed under reduced pressure, the residue was treated with ice cold water (5 mL) and then kept at 4 °C for 2 h. The resulting solid material was filtered, washed with 5% NaHCO$_3$ (3x 1 mL), ice cold water (5 x 1 mL) and dried in a desiccator over 4 Å molecular sieve. The crude material was purified by silica column chromatography using CHCl$_3$ - MeOH as the mobile phase with methanol gradient.

5: *5-(dimethylamino)-N-[2-({6-[(3-methylbut-2-en-1-yl)amino]-9H-purin-2-yl}amino)ethyl] naphthalene-1-sulfonamide:* Pale yellow solid, yield 64%.

6: *5-(dimethylamino)-N-[6-({6-[(3-methylbut-2-en-1-yl)amino]-9H-purin-2-yl}amino)hexyl] naphthalene-1-sulfonamide:* Pale yellow solid, yield 52%.

7: *5-(dimethylamino)-N-(2-{[6-(dimethylamino)-9H-purin-2-yl]amino}ethyl)naphthalene-1*-sulfonamide: Pale yellow solid.

8: *5-(dimethylamino)-N-(6-{[6-(dimethylamino)-9H-purin-2-yl]amino}hexyl)naphthalene-1-sulfonamide:* Pale yellow solid, 63%.

C2- derivatives marked with coumarin-3-carboxylic acid was prepared as follows: 1 equiv., (0.208 mmol) of coumarin-3-carboxylic acid and NHS (1 equiv.) were dissolved under an argon atmosphere in dry MeCN (6 mL) at 45 °C. DCC (1.16 equiv.) was added

and the resulting mixture heated at 45 °C for 1 h, then stirred at RT for 20 h. Next, the solid was filtered off and washed carefully with dry MeCN (3 x 5 mL). 9: white solid, yield 90%.^{1}H NMR (300 MHz, DMSO-d_6) δ (ppm): 2.89 (s, 4H), 7.43-7.50 (m, 2H), 7.83 (t, *J* = 7.2 Hz, 1H), 8.03 (d, *J* = 7.9 Hz, 1H), 9.13 (s, 1H). A solution of *N*-hydroxysuccinimidyl coumarin-3-carboxylic acid ester (1 equiv.) in MeCN (4 mL) was dropwise added to **I, II, III** or **IV** (1 equiv**.**) dissolved in a mixture of carbonate buffer pH 8.6 (2 mL) and DMSO (2 mL). The reaction mixture was protected against light and stirred under an argon atmosphere at RT for 20 h. After dilution with cold water (5 mL) and storing at 4 °C for 2 h, a solid compound was formed. The crude material was purified by silica column chromatography using CHCl$_3$/MeOH as the mobile phase with methanol gradient.

9: *N-[2-({6-[(3-methylbut-2-en-1-yl)amino]-9H-purin-2-yl}amino)ethyl]-2-oxo-2H-chromene-3-carboxamide*: pale yellow solid, yield 92%.

10: *N-[6-({6-[(3-methylbut-2-en-1-yl)amino]-9H-purin-2-yl}amino)hexyl]-2-oxo-2H-chromene-3-carboxamide (10):* Pale yellow solid, yield 64%.

11: *N-(2-{[6-(dimethylamino)-9H-purin-2-yl]amino}ethyl)-2-oxo-2H-chromene-3-carboxamide*: pale yellow solid, yield 69%.

12: *N-(6-{[6-(dimethylamino)-9H-purin-2-yl]amino}hexyl)-2-oxo-2H-chromene-3-carboxamide*: pale yellow solid, yield 63%.

C2 derivatives marked with DEAC were prepared as follows: DEAC-OH (1 equiv., 0.208 mmol) and NHS (1.04 equiv.) were dissolved under an argon atmosphere in dry MeCN (6 mL) at 45 °C. DCC (1.16 equiv.) was added and the resulting mixture was heated at 45 °C for 1 h and then stirred at RT for 20 h. The arising solid was filtered off and filtrate was evaporated under reduced pressure to give NHS ester of DEAC-OH: a yellow solid. A solution of *N*-hydroxysuccinimidyl DEAC-OH ester (1 equiv.) in MeCN (4 mL) was dropwise added to a solution of **I, II, III**, **IV** (1 equiv.) dissolved in a mixture of carbonate buffer pH 8.6 (2 mL) and DMSO (2 mL). The reaction mixture was protected against light and stirred under an argon atmosphere at RT for 20 h. After dilution with cold water (5 mL) and storing at 4 °C for 2 h, a solid was formed. The crude material

was purified by silica column chromatography using CHCl₃/MeOH as the mobile phase with methanol gradient.

13: *7-(diethylamino)-N-[2-({6-[(3-methylbut-2-en-1-yl)amino]-9H-purin-2-yl}amino)ethyl]-2-oxo-2H-chromene-3-carboxamide*: pale yellow solid, yield 61%.

14: *7-(diethylamino)-N-[6-({6-[(3-methylbut-2-en-1-yl)amino]-9H-purin-2-yl}amino)hexyl]-2-oxo-2H-chromene-3-carboxamide*: pale yellow solid, yield 72%.

15: *7-(diethylamino)-N-(2-{[6-(dimethylamino)-9H-purin-2-yl]amino}ethyl)-2-oxo-2H-chromene-3-carboxamide*: pale yellow solid, yield 48%.

16: *7-(diethylamino)-N-(6-{[6-(dimethylamino)-9H-purin-2-yl]amino]hexyl)-2-oxo-2H-chromene-3-carboxamide (16)*: pale yellow solid, yield 52%.

C2- derivatives marked with rhodamine B were prepared as follows: The compound was prepared according to a slightly modified procedure described in the literature (Meng et al., 2007). Briefly, 0.104 mmol of rhodamine B and 0.109 mmol of *N*-hydroxysuccinimide were dissolved in 2 ml of dry acetonitrile at 45 °C. 0.121 mmol of DCC in 1 mL of acetonitrile was added and the reaction mixture heated at 45 °C for one h and then stirred at RT for 20 h. The solid was filtered off and filtrate was evaporated under reduced pressure to give NHS rhodamine B ester: dark green metallic solid. Afterwards, a solution of NHS rhodamine B ester in MeCN (1 mL) was dropwise added to a solution of 0.104 mmol of **I, II, III** or **IV** in 1 mL of carbonate buffer (pH = 8.6). The reaction mixture was stirred at RT for 4 h and then cooled in an ice bath. The obtained solid was filtered off, washed with MeCN, water and dried at 50 °C.

17: *3',6'-bis(diethylamino)-2-{2-[(6-((3-methylbut-2-en-1-yl]amino}-9H-purin-2-yl)amino) ethyl)spiro[isoindoline-1,9'-xanthen]-3-one*: pink solid; yield 99%.

18: *3',6'-bis(diethylamino)-2-{2-[(6-((3-methylbut-2-en-1-yl]amino}-9H-purin-2-yl)amino hexyl)-spiro[isoindoline-1,9'-xanthen]-3-one*: pink solid; yield 99%.

19: *3',6'-bis(diethylamino)-2-(2-{[6-(dimethylamino)-9H-purin-2-yl)amino]ethyl}spiro-[isoindoline-1,9'-xanthen]-3-one*: pink solid, yield 73%.

20:   *3',6'-bis(diethylamino)-2-(2-{[6-(dimethylamino)-9H-purin-2-yl]amino}hexyl)spiro-[isoindoline-1,9'-xanthen]-3-one*: pink solid; yield 86%.

C2 derivatives marked with FITC were prepared as follows: 1 equiv. of FITC was added to a mixture of **I, II, III** or **IV** (1 equiv., 0.136 mmol) and Et₃N (2.76 equiv.) in dry MeOH (2 mL) under an argon atmosphere. The reaction mixture was protected against light and stirred at RT for 20 h. Afterwards, the solvent was evaporated under reduced pressure, the residue was re-suspended in acetate buffer (pH 4.0, 5 mL) and then kept at 4 °C for 1 h. The resulting solid material was filtered, washed with acetate buffer pH 4.0 (5 x 1 mL) followed by water (5 x 2 mL) and dried at 50 °C.

21:   *2-(6-hydroxy-3-oxo-3H-xanthen-9-yl)-5-{3-[2-({6-[(3-methylbut-2-en-1-yl)amino]-9H-purin-2-yl}amino)ethyl]thioureido}benzoic acid*: orange solid; yield 95%.

22:   *2-(6-hydroxy-3-oxo-3H-xanthen-9-yl)-5-{3-[6-({6-[(3-methylbut-2-en-1-yl)amino]-9H-purin-2-yl}amino)hexyl]thioureido}benzoic acid*: orange solid; yield 98%.

23:   *5-[3-(2-{[6-(dimethylamino)-9H-purin-2-yl]amino}ethyl)thioureido]-2-(6-hydroxy-3-oxo-3H-xanthen-9-yl)benzoic acid*: orange solid; yield: 98%.

24:   *5-[3-(6-{[6-(dimethylamino)-9H-purin-2-yl]amino}hexyl)thioureido]-2-(6-hydroxy-3-oxo-3H-xanthen-9-yl)benzoic acid*: orange solid, yield: 98%.

N9 fluorescently labelled derivatives

*N*9 labelled compounds were prepared according to Scheme 4 and given below:

*5-(dimethylamino)-N-{2-[6-((3-methylbut-2-en-1-yl]amino}-9H-purin-9-yl)ethyl)naphthalene-1-sulfonamide (**25**)*

Compound **25** was prepared according to a procedure described in the literature (Bartzatt, 2001). Briefly, a solution of DS-Cl (1.2 equiv.) in acetone (2 mL) was added to a solution of V (1 equiv., 0.406 mmol) dissolved in a mixture of water (5.5 mL) and 2 M Na₂CO₃ (2 mL). The flask was protected from light by wrapping in alufoil and the reaction mixture was stirred at RT overnight. The mixture was then extracted with diethyl ether (3 x 10 mL). The combined organic layers were washed with water (2 x 5

mL) followed by brine (2 x 5 mL), dried over Na_2SO_4 and concentrated *in vacuo*. The product was purified by silica flash column chromatography using $CHCl_3$/MeOH (9:1) as the mobile phase. Pale yellow solid; yield 65%.

2-(6-hydroxy-3-oxo-3H-xanthen-9-yl)-4-[3-(2-{6-[(3-methylbut-2-en-1-yl)amino]-9H-purin-9-yl}ethyl)thioureido]benzoic acid (26)

Compound **V** (1 equiv., 0.406 mmol) was stirred in MeOH (3 mL) with FITC (1.1 equiv.) in the presence of $NaHCO_3$ (3 equiv.) at a temperature of 50 °C for 1 h. The pH of the reaction mixture was adjusted to pH 4 by adding 1 M HCl. The resulting orange solid was filtered and then washed with MeOH. The pure compound was obtained after flash chromatography using $CHCl_3$/MeOH (4:1) as the mobile phase. Orange solid: yield 65%.

3',6'-bis(diethylamino)-2-(2-(6-((3-methylbut-2-en-1-yl)amino)-9H-purin-9-yl)ethyl)spiro[isoindoline-1,9'-xanthen]-3-one (27)

A solution of *NHS* rhodamine B ester (1 equiv.) dissolved in MeCN (1 mL) was dropwise added to a solution of iP (1 equiv., 0.105 mmol) dissolved in carbonate buffer pH 8.6 (1 mL). The resulting mixture was stirred at RT for 4 h and then cooled to form pink solid; yield 25%.

N^6-(3-methylbut-2-en-1-yl)-N^9-{2-[(7-nitro-2,1,3-benzoxadiazol-4-yl)amino]ethyl}-9H-purin-6-amine hydrochloride (28) and N^6-(dimethylamino)-N^9-{2-[(7-nitro-2,1,3-benzoxadiazol-4-yl)amino]ethyl}-9H-purin-6-amine (29)

Compounds **28** and **29** were prepared according to a protocol described in the literature (Bem et al., 2007). Briefly, **V or VI** (1 equiv) was dissolved in MeOH (3 mL) containing 4-chloro-7-nitrobenzofurazan (1.1 equiv.) in the presence of $NaHCO_3$ (2.5 equiv.) at a temperature of 50 °C for 1 h. The reaction mixture was cooled in an ice bath and 1 M HCl was added dropwise up to the formation of orange solid. The resulting solid was filtered, washed with ice cold MeOH (3 x 1 mL) followed by ice cold

water (4 x 1 mL) and dried at 50 °C. **28**: reddish solid; yield 52%, **29**: reddish solid; yield 75%.

*3,3-dimethyl-1-{6-[(2-{6-[(3-methylbut-2-en-1-yl)amino]-9H-purin-9-yl}ethyl)amino]-6-oxohexyl)-2-[(1E,3E)-5-((E)-1,3,3-trimethylindolin-2-ylidene)penta-1,3-dien-1-yl]-3H-indole(**30**)*

Compound **V** (5.84 mg, 16.2 µmol) was dissolved in 0.1 M sodium bicarbonate solution (4.5 mL, pH 8.5) to which was added cyanine 5 NHS (1 equiv., 10 mg, 16.2 µmol) dissolved in amine free DMF (0.5 mL). The reaction mixture was stirred at RT for 4 h and then lyophilized overnight. The resulting residue was dissolved in water (5 mL) and extracted using EtOAc (3 x 5 mL). The product was purified by semi-preparative HPLC. Dark blue solid; yield 50%.

NMR data of prepared fluorescent probes

1: ^{1}H NMR (500 MHz, DMSO-d_6) δ (ppm): 1.64 (s, 3H), 1.66 (s, 3H), 3.54 (bs, 2H), 3.60-3.63 (m,2H), 3.97 (bs, 2H), 5.28 (t, J = 6.0 Hz, 1H), 6.53 (s,1H), 6.63 (bs, 1H), 7.22 (bs, 1H), 7.70 (s, 1H), 8.62 (bs 1H), 9.64 (s,1H), 12.21 (bs, 1H). ^{13}C NMR (125 MHz, DMSO-d_6) δ (ppm): 17.8, 25.4, 37.5, 40.9, 43.5, 99.4, 113.0, 120.7, 122.6, 132.7, 135.4, 138.1, 144.1, 144.4, 145.4, 151.7, 154.5, 159.1.

2: ^{1}H NMR (500 MHz, DMSO-d_6) δ (ppm): 1.32-1.38 (m, 4H), 1.46-1.56 (m, 2H), 1.63-1.70 (m, 8H), 3.20 (q, J = 6.6 Hz, 2H), 3.44 (t, J = 6.7 Hz, 2H), 3.97 (bs, 2H), 5.28 (t, J = 6.7 Hz, 1H), 6.13 (bs, 1H), 6.37 (d, J = 8.9 Hz, 1H), 7.06 (bs, 1H), 7.59 (s, 1H), 8.48 (d, J = 8.9 Hz, 1H), 9.55 (bs, 1H), 12.08 (bs, 1H). ^{13}C NMR (125 MHz, DMSO-d_6) (ppm): 17.8, 25.3, 2x 26.3, 27.6, 29.3, 37.8, 41.0, 43.3, 99.0, 112.7, 120.4, 122.9, 132.3, 134.7, 137.9, 144.1, 144.4, 145.1, 151.7, 154.3, 159.45.

3: ^{1}H NMR (500 MHz, DMSO-d_6) δ (ppm): 3.36 (bs, 6H), 3.54 (bs, 2H), 3.61 (bs, 2H), 6.44-6.60 (m, 2H), 7.70 (s, 1H), 8.61 (bs, 1H), 9.60 (s, 1H), 12.26 (bs, 1H).δ ^{13}C NMR (125 MHz, DMSO-d_6) δ (ppm): 2x 37.6, 40.9, 43.5, 99.4, 113.7, 120.7, 134.5, 138.1, 144.1, 144.4, 145.3, 152.9, 154.4, 158.5.

4: ^{1}H NMR (500 MHz, DMSO-d_6) δ (ppm): 1.32-1.40 (m, 4H), 1.48-1.54 (m, 2H), 1.63-1.69 (m, 2H), 3.20 (q, J = 6.6 Hz, 2H), 3.33 (vbs, 6H), 3.43 (bs, 2H), 6.14 (t, J = 5.8 Hz, 1H), 6.36 (d, J = 8.9 Hz, 1H), 7.61 (s, 1H), 8.47 (d, J = 8.9 Hz, 1H), 9.54 (bs, 1H), 12.15 (bs, 1H). ^{13}C NMR (125 MHz, DMSO-d_6) δ (ppm): 2x 26.3, 27.6, 29.3, 2x 37.5, 41.0, 43.3, 99.0, 113.3, 120.4, 134.2, 137.9, 144.1, 144.4, 145.1, 153.4, 154.3, 158.7.

5: ^{1}H NMR (500 MHz, DMSO-d_6) δ (ppm): 1.62 (s, 3H), 1.63 (s, 3H), 2.79 (s, 6H), 2.93 (q, J = 6.3 Hz, 2H), 3.25 (q, J = 6.4 Hz, 2H), 3.92 (bs, 2H), 5.25 (t, J = 6.0 Hz, 1H), 6.10 (bs, 1H), 7.14 (bs, 1H), 7.20 (d, J = 7.3 Hz, 1H), 7.50 (t, J = 8.1 Hz, 1H), 7.57 (dd, J = 8.3, 7.3 Hz, 1H), 7.62 (s, 1H), 8.01 (t, J = 5.3 Hz, 1H), 8.09 (dd, J = 7.3, 0.9 Hz, 1H), 8.25 (d, J = 8.6 Hz, 1H), 8.42 (d, J = 8.6 Hz, 1H), 12.12 (bs, 1H). ^{13}C NMR (125 MHz, DMSO-d_6) δ (ppm): 17.8, 25.3, 37.3, 40.9, 42.5, 2x 45.0, 113.3, 115.0, 118.9, 122.7, 123.5, 127.7, 128.2, 2x 129.0, 129.3, 132.5, 135.0, 135.8, 151.3, 152.7, 154.2, 159.0.

6*:* ^{1}H NMR (500 MHz, DMSO-d_6) δ (ppm): 1.02-1.11 (m, 4H), 1.21-1.32 (m, 4H), 1.63 (s, 3H), 1.65 (s, 3H), 2.75 (q, J = 6.5 Hz, 2H), 2.79 (s, 6H), 3.08 (q, J = 6.6 Hz, 2H), 3.97 (bs, 2H), 5.28 (t, J = 6.6 Hz, 1H), 6.03 (bs, 1H), 7.06 (bs, 1H), 7.21 (d, J = 7.0 Hz, 1H), 7.55-7.561 (m, 3H), 7.85 (t, J = 5.7 Hz, 1H), 8.08 (dd, J = 7.2, 1.1 Hz, 1H), 8.29 (d, J = 8.6 Hz, 1H), 8.43 (d, J = 8.6 Hz, 1H), 12.09 (bs, 1H).^{13}C NMR (125 MHz, DMSO-d_6) δ (ppm): 17.8, 25.4, 25.8, 26.0, 29.0, 29.2, 37.4, 40.9, 42.3, 2x 45.0, 113.0, 115.0, 119.1, 122.9, 123.5, 127.7, 128.2, 129.0, 129.1, 129.3, 132.3, 134.7, 136.1, 151.3, 151.6, 154.2, 159.4.

7*:* ^{1}H NMR (500 MHz, DMSO-d_6) δ (ppm): 2.79 (s, 6H), 2.93 (q, J = 6.4 Hz, 2H), 3.21-3.36 (m, 8H), 6.10 (t, J = 5.8 Hz, 1H), 7.20 (d, J = 7.6 Hz, 1H), 7.51 (t, J = 8.1 Hz, 1H), 7.57 (t, J = 7.9 Hz, 1H), 7.63 (s, 1H), 8.00 (t, J = 5.5 Hz, 1H), 8.09 (d, J = 7.0 Hz, 1H), 8.25 (d, J = 8.6 Hz, 1H), 8.42 (d, J = 8.6 Hz, 1H), 12.18 (bs, 1H). ^{13}C NMR (125 MHz, DMSO-d_6) δ (ppm): 2x 37.5, 40.9, 42.5, 2x 45.0, 113.5, 115.0, 118.9, 123.5, 127.7, 128.3, 2x 129.0, 129.3, 134.4, 135.7, 151.3, 153.1, 154.3, 158.3.

8*:* ^{1}H NMR (500 MHz, DMSO-d_6) δ (ppm): 1.04-1.09 (m, 4H), 1.21-1.30 (m, 4H), 2.75 (q, J = 6.4 Hz, 2H), 2.79 (s, 6H), 3.08 (q, J = 6.6 Hz, 2H), 3.30-3.39 (m, 6H), 6.04 (t, J = 5.7 Hz, 1H), 7.21 (d, J = 7.3 Hz, 1H), 7.55-7.61 (m, 2H), 7.62 (s, 1H), 7.85 (t, J = 5.7 Hz, 1H), 8.08

(d, *J* = 7.3 Hz, 1H), 8.29 (d, *J* = 8.9 Hz, 1H), 8.43 (d, *J* = 8.6 Hz, 1H), 12.16 (bs, 1H). ^{13}C NMR (125 MHz, DMSO-d_6) δ (ppm): 25.7, 26.0, 29.0, 29.2, 2x 37.5, 40.9, 42.3, 2x 45.0, 113.3, 115.0, 119.1, 123.5, 127.7, 128.2, 129.0, 129.0, 129.2, 134.2, 136.1, 151.3, 153.4, 154.4, 158.7.

9: ^{1}H NMR (500 MHz, DMSO-d_6) δ (ppm): 1.63 (s, 3H), 1.66 (s, 3H), 3.42 (q, *J* = 5.7 Hz, 2H), 3.53 (q, *J* = 5.9 Hz, 2H), 3.99 (bs, 2H), 5.27-5.30 (m, 1H), 6.39 (bs, 1H), 7.14 (bs, 1H), 7.42 (td, *J* = 7.5, 0.9 Hz, 1H), 7.48 (d, *J* = 8.6 Hz, 1H), 7.62 (s, 1H), 7.71-7.74 (m, 1H), 7.96 (dd, *J* = 7.9, 1.5 Hz, 1H), 8.83-8.85 (m, 2H), 12.14 (bs, 1H).^{13}C NMR (125 MHz, DMSO-d_6) δ (ppm): 17.8, 25.4, 37.5, 39.8, 40.9, 113.3, 116.1, 118.4, 118.9, 122.8, 125.1, 130.2, 132.6, 134.0, 135.0, 147.4, 151.5, 153.8, 154.3, 159.4, 160.3, 161.3.

10: ^{1}H NMR (500 MHz, DMSO-d_6) δ (ppm): 1.30-1.33 (m, 4H), 1.43-1.53 (m, 4H), 1.64 (s, 3H), 1.66 (s, 3H), 3.20 (q, *J* = 6.6 Hz, 2H), 3.30 (q, *J* = 6.5 Hz, 2H), 3.98 (bs, 2H), 5.27-5.30 (m, 1H), 6.13 (bs, 1H), 7.05 (bs, 1H), 7.41-7.44 (m, 1H), 7.49 (d, *J* = 8.6 Hz, 1H), 7.59 (bs, 1H), 7.71-7.75 (m, 1H), 7.97 (dd, *J* = 7.8, 1.4 Hz, 1H), 8.68 (t, *J* = 5.7 Hz, 1H), 8.84 (s, 1H), 12.10 (bs, 1H). ^{13}C NMR (125 MHz, DMSO-d_6) δ (ppm): 17.8, 25.4, 2x 26.38, 29.0, 29.3, 37.4, 39.0, 41.1, 112.9, 116.1, 118.5, 119.1, 122.9, 125.1, 130.2, 132.3, 134.0, 134.7, 147.2, 151.7, 153.8, 154.2, 159.4, 160.4, 160.9.

11: ^{1}H NMR (500 MHz, DMSO-d_6) δ (ppm): 3.29-3.43 (m, 8H), 3.52 (q, *J* = 5.7 Hz, 2H), 6.39 (t, *J* = 5.3 Hz, 1H), 7.43 (t, *J* = 7.5 Hz, 1H), 7.48 (d, *J* = 8.3 Hz, 1H), 7.63 (s, 1H), 7.73 (t, *J* = 7.2 Hz, 1H), 7.97 (d, *J* = 7.6 Hz, 1H), 8.82-8.85 (m, 2H), 12.19 (bs, 1H). ^{13}C NMR (125 MHz, DMSO-d_6) δ (ppm): 2x 37.5, 39.7, 40.7, 113.5, 116.1, 118.4, 118.9, 125.1, 130.2, 134.0, 134.4, 147.3, 153.3, 153.8, 154.4, 158.7, 160.2, 161.3.

12: ^{1}H NMR (500 MHz, DMSO-d_6) δ (ppm): 1.31-1.34 (m, 4H), 1.50-1.53 (m, 4H), 3.20 (q, *J* = 6.6 Hz, 2H), 3.29-3.36 (m, 8H), 6.13 (t, *J* = 5.8 Hz, 1H), 7.42 (td, *J* = 7.5, 0.8 Hz, 1H), 7.49 (d, *J* = 8.6 Hz, 1H), 7.61 (s, 1H), 7.71-7.75 (m, 1H), 7.96 (dd, *J* = 7.9, 1.5 Hz, 1H), 8.67 (t, *J* = 5.7 Hz, 1H), 8.83 (s, 1H), 12.17 (bs, 1H).^{13}C NMR (125 MHz, DMSO-d_6) δ (ppm): 2x 26.3, 29.0, 29.3, 2x 37.5, 39.0, 41.0, 113.3, 116.1, 118.4, 119.1, 125.1, 130.2, 133.9, 134.2, 147.2, 153.4, 153.8, 154.4, 158.7, 160.4, 160.9.

13: ^{1}H NMR (500 MHz, DMSO-d_6) δ (ppm): 1.12 (t, J = 7.0 Hz, 6H), 1.64 (s, 3H), 1.67 (s, 3H), 3.36-3.40 (m, 2H), 3.52-3.44 (m, 6H), 3.99 (s, 2H), 5.27-5.30 (m, 1H), 6.37 (s, 1H), 6.59 (d, J = 2.1 Hz, 1H), 6.78 (dd, J = 9.2, 2.4 Hz, 1H), 7.13 (s, 1H), 7.62 (s, 1H), 7.66 (d, J = 9.2 Hz, 1H), 8.65 (s, 1H), 8.78 (t, J = 5.7 Hz, 1H), 12.14 (s, 1H).^{13}C NMR (125 MHz, DMSO-d_6) δ (ppm): 2x 12.3, 17.8, 25.4, 37.5, 39.0, 41.1, 2x 44.3, 95.8, 107.6, 109.4, 110.0, 113.1, 122.9, 131.5, 132.4, 134.9, 147.6, 151.7, 152.3, 154.4, 157.2, 159.3, 161.6, 162.3.

14: ^{1}H NMR (500 MHz, DMSO-d_6) δ (ppm): 1.12 (t, J = 7.0 Hz, 6H), 1.3-1.32 (m, 4H), 1.47-1.52 (m, 4H), 1.64 (s, 3H), 1.66 (s, 3H), 3.19 (q, J = 6.7 Hz, 2H), 3.28 (q, J = 6.6 Hz, 2H), 3.46 (q, J = 7.0 Hz, 4H), 3.98 (bs, 2H), 5.29 (tt, J = 6.7, 1.3 Hz, 1H), 6.12 (bs, 1H), 6.60 (d, J = 2.4 Hz, 1H), 6.78 (dd, J = 9.2, 2.4 Hz, 1H), 7.04 (bs, 1H), 7.59 (bs, 1H), 7.66 (d, J = 9.2 Hz, 1H), 8.61-8.64 (m, 2H), 12.10 (bs, 1H). ^{13}C NMR (125 MHz, DMSO-d_6) δ (ppm): 2x 12.3, 17.8, 25.3, 2x 26.3, 29.2, 29.3, 37.3, 38.8, 41.0, 2x 44.3, 95.8, 107.6, 109.4, 110.0, 113.0, 122.9, 131.5, 132.3, 134.7, 147.6, 151.5, 152.3, 154.4, 157.1, 159.4, 161.8, 162.0.

15: ^{1}H NMR (500 MHz, DMSO-d_6) δ (ppm): 1.12 (t, J = 7.0 Hz, 6H), 3.29-3.52 (m, 14H), 6.37 (t, J = 5.5 Hz, 1H), 6.58 (d, J = 2.4 Hz, 1H), 6.78 (dd, J = 9.0, 2.3 Hz, 1H), 7.64 (s, 1H), 7.66 (d, J = 9.2 Hz, 1H), 8.64 (s, 1H), 8.77 (t, J = 5.7 Hz, 1H), 12.20 (bs, 1H). ^{13}C NMR (125 MHz, DMSO-d_6) δ (ppm): 2x 12.3, 2x 37.5, 39.0, 41.1, 2x 44.3, 95.8, 107.6, 109.4, 110.0, 113.5, 131.5, 134.3, 147.6, 152.3, 153.3, 154.4, 157.1, 158.7, 161.5, 162.4.

16: ^{1}H NMR (500 MHz, DMSO-d_6) δ (ppm): 1.12 (t, J = 7.0 Hz, 6H), 1.29-1.34 (m, 4H), 1.48-1.52 (m, 4H), 3.19 (q, J = 6.7 Hz, 2H), 3.26-3.36 (m, 8H), 3.46 (q, J = 7.1 Hz, 4H), 6.13 (t, J = 5.8 Hz, 1H), 6.59 (d, J = 2.1 Hz, 1H), 6.78 (dd, J = 8.9, 2.4 Hz, 1H), 7.61 (s, 1H), 7.66 (d, J = 9.2 Hz, 1H), 8.61-8.63 (m, 2H), 12.17 (bs, 1H).^{13}C NMR (125 MHz, DMSO-d_6) δ (ppm): 2x 12.3, 2x 26.3, 29.2, 29.3, 2x 37.4, 38.81, 41.05, 2x 44.3, 95.8, 107.6, 109.4, 110.0, 113.3, 131.5, 134.2, 147.6, 152.3, 153.4, 154.4, 157.1, 158.7, 161.8, 162.0.

17: ^{1}H NMR (500 MHz, DMSO-d_6) δ (ppm): 1.05 (t, J = 6.9 Hz, 12H), 1.63 (s, 3H), 1.66 (s, 3H), 2.96 (bs, 2H), 3.21-3.30 (m, 10H), 3.88 (bs, 2H), 5.25 (bs, 1H), 5.94 (bs, 1H), 6.29-6.35 (m, 6H), 6.98-6.99 (m, 2H), 7.47-7.48 (m, 2H), 7.58 (s, 1H), 7.77-7.79 (m, 1H),

12.02 (s, 1H).^{13}C NMR (125 MHz, DMSO-d_6) δ (ppm): 12.3, 17.8, 25.4, 37.2, 43.6, 64.1, 97.2, 104.8, 108.0, 113.2, 122.2, 122.7, 123.5, 128.2, 130.1, 132.6, 134.8, 148.2, 151.4, 152.5, 153.8, 154.0, 158.9, 167.5.

18: ^{1}H NMR (500 MHz, DMSO-d_6) δ (ppm): 0.99 (bs, 6H), 1.04 (t, J = 6.9 Hz, 12H), 1.20-1.24 (m, 2H), 1.62 (s, 3H), 1.63 (s, 3H), 2.93 (s, 2H), 3.04-3.08 (m, 2H), 3.28 (q, J = 6.7 Hz, 8H), 3.96 (bs, 2H), 5.27 (app. t, 1H), 5.96 (bs, 1H), 6.27 (m, 2H), 6.32-6.35 (m, 4H), 7.01-7.03 (m, 2H), 7.47-7.51 (m, 2H), 7.58 (s, 1H), 7.75-7.76 (m, 1H), 12.07 (vbs, 1H). ^{13}C NMR (125 MHz, DMSO-d_6) δ (ppm): 12.3, 17.7, 25.3, 26.1, 26.3, 27.7, 29.0, 37.3, 41.0, 43.6, 63.9, 97.1, 105.2, 108.0, 113.0, 122.1, 122.9, 123.6, 128.2, 128.4, 130.9, 132.2, 132.5, 134.7, 148.3, 151.5, 152.6, 153.0, 154.2, 159.3, 166.6.

19: ^{1}H NMR (500 MHz, DMSO-d_6) δ (ppm): 1.09-1.04 (m, 12H), 2.96-3.01 (m, 2H), 3.23-3.31 (m, 16H), 6.10 (bs, 1H), 6.31-6.37 (m, 6H), 6.95-6.97 (m, 1H), 7.44-7.49 (m, 2H), 7.59 (s, 1H), 7.76-7.78 (m, 1H), 12.07 (bs, 1H). ^{13}C NMR (125 MHz, DMSO-d_6) δ (ppm): 12.3, 37.5, 39.7, 43.6, 64.0, 97.2, 104.8, 107.9, 113.4, 122.3, 123.4, 128.1, 129.9, 132.6, 134.4, 148.2, 152.4, 153.3, 154.0, 154.1, 158.3, 167.5.

20: ^{1}H NMR (500 MHz, DMSO-d_6) δ (ppm): 0.99-1.07 (m, 18H), 1.28-1.31 (m, 2H), 2.93 (bs, 2H), 3.07 (q, J = 6.5 Hz, 2H), 3.26-3.36 (m, 14H), 5.98 (bs, 1H), 6.26-6.36 (m, 6H), 7.01-7.03 (m, 1H), 7.47-7.51 (m, 2H), 7.61 (s, 1H), 7.75-7.77 (m, 1H), 12.15 (bs, 1H). ^{13}C NMR (125 MHz, DMSO-d_6) δ (ppm): 12.3, 26.1, 26.3, 27.7, 29.0, 37.3, 40.9, 43.6, 63.9, 97.1, 105.2, 108.0, 113.3, 122.1, 123.6, 128.2, 128.4, 130.9, 132.5, 134.2, 148.3, 152.6, 153.0, 153.4, 154.3, 158.6, 166.6.

21: ^{1}H NMR (500 MHz, DMSO-d_6) δ (ppm): 1.64 (s, 3H), 1.67 (s, 3H), 3.47-3.49 (m, 2H), 3.72 (bs, 2H), 4.00 (bs, 2H), 5.30 (t, J = 6.4 Hz, 1H), 6.33 (bs, 1H), 6.54-6.60 (m, 4H), 6.66 (d, J = 2.1 Hz, 2H), 7.14-7.19 (m, 2H), 7.63 (s, 1H), 7.73 (d, J = 6.1 Hz, 1H), 8.18 (bs, 1H), 8.25 (s, 1H), 9.99 (bs, 1H), 10.12 (bs, 2H), 12.15 (bs, 1H). ^{13}C NMR (125 MHz, DMSO-d_6) δ (ppm): 17.8, 25.4, 37.5, 40.5, 44.0, 102.2, 109.7, 112.6, 113.3, 122.8, 124.0, 126.5, 129.0, 132.5, 135.0, 141.4, 151.8, 154.3, 159.3, 159.5, 168.5, 180.5.

22: ^{1}H NMR (500 MHz, DMSO-d_6) δ (ppm): 1.34 (s, 4H), 1.53-1.56 (m, 4H), 1.65 (s, 3H), 1.67 (s, 3H), 3.21 (q, J = 6.4 Hz, 2H), 3.49 (bs, 2H), 3.99 (bs, 2H), 5.30 (t, J = 6.4 Hz, 1H),

6.14 (bs, 1H), 6.54-6.60 (m, 4H), 6.66 (d, J = 2.1 Hz, 2H), 7.07 (bs, 1H), 7.16 (d, J = 8.3 Hz, 1H), 7.60 (s, 1H), 7.71 (d, J = 7.0 Hz, 1H), 8.09 (bs, 1H), 8.22 (s, 1H), 9.87 (bs, 1H), 10.14 (bs, 2H), 12.10 (bs, 1H).^{13}C NMR (125 MHz, DMSO-d_6) δ (ppm): 17.8, 25.4, 2x, 26.4, 28.4, 29.4, 37.3, 41.1, 43.8, 102.2, 109.7, 112.6, 113.0, 122.9, 124.1, 126.6, 129.0, 132.4, 134.8, 141.4, 151.9, 154.2, 159.4, 159.5, 168.5, 180.3.

23: ^{1}H NMR (500 MHz, DMSO-d_6) δ (ppm): 3.36 (bs, 6H), 3.46-3.47 (m, 2H), 3.71 (bs, 2H), 6.33 (bs, 1H), 6.54 (dd, J = 8.9, 1.8 Hz, 2H), 6.60 (d, J = 8.9 Hz, 2H), 6.64 (s, 2H), 7.13 (d, J = 8.3 Hz, 1H), 7.65 (s, 1H), 7.72 (d, J = 4.6 Hz, 1H), 8.25 (s, 1H), 8.29 (bs, 1H), 10.11 (bs, 1H), 12.23 (bs, 1H).^{13}C NMR (125 MHz, DMSO-d_6) δ (ppm): 37.5, 40.4, 43.9, 102.2, 109.9, 112.9, 113.5, 124.2, 129.1, 134.4, 141.4, 152.0, 153.3, 154.4, 158.6, 160.1, 168.6, 180.6.

24: ^{1}H NMR (500 MHz, DMSO-d_6) δ (ppm): 1.33 (bs, 4H), 1.52-1.55 (m, 4H), 3.16-3.23 (m, 2H), 3.35 (s, 6H), 3.47 (bs, 2H), 6.15 (t, J = 5.8 Hz, 1H), 6.55 (dd, J = 8.9, 2.4 Hz, 2H), 6.60 (d, J = 8.9 Hz, 2H), 6.65 (d, J = 2.4 Hz, 2H), 7.15 (d, J = 8.3 Hz, 1H), 7.62 (s, 1H), 7.71 (d, J = 7.3 Hz, 1H), 8.17 (bs, 1H), 8.23 (s, 1H), 9.97 (bs, 1H), 12.18 (bs, 1H).^{13}C NMR (125 MHz, DMSO-d_6) δ (ppm): 26.4, 2x, 28.4, 29.4, 37.5, 41.0, 43.8, 102.2, 109.9, 112.9, 113.3, 124.2, 129.1, 134.2, 141.4, 152.0, 153.4, 154.4, 158.8, 160.0, 168.6, 180.2.

25: ^{1}H NMR (300 MHz, DMSO-d_6) δ (ppm): 1.67 (s, 3H), 1.70 (s, 3H), 2.82 (s, 6H), 3.22-3.31 (m, 2H), 4.07 (bs, 2H), 4.15 (t, J = 5.5 Hz, 2H), 5.31 (t, J = 5.9 Hz, 1H), 7.22 (d, J = 7.7 Hz, 1H), 7.54 (dd, J = 18.4 Hz, 7.7 Hz, 2H), 7.68 (bs, 1H), 7.87 (s, 1H), 8.02 (d, J = 7.7 Hz, 1H), 8.08-8.22 (m, 2H), 8.42 (d, J = 7.7 Hz, 1H)

26: ^{1}H NMR (300 MHz, DMSO-d_6) : δ (ppm): 1.65 (s, 3H), 1.69 (s, 3H), 3.89-4.13 (m, 4H), 4.42 (app. t, 2H), 5.29 (app. t., 1H), 6.49-6.63 (m, 4H), 6.67 (bs, 2H,), 7.15 (d, J = 8.0 Hz, 1H), 7.65 (d, J = 8.0 Hz, 1H), 7.78 (bs, 1H), 8.09 (s, 1H), 8.14 (s, 2H), 8.20 (s, 1H), 9.99 (bs, 3H).

27: ^{1}H NMR (300 MHz, DMSO-d_6) δ (ppm): 1.65 (s, 3H), 1.68 (s, 3H), 3.19-3.34 (m, 8H), 3.36 (bs, 2H), 3.40-3.49 (m, 2H), 4.05 (app. t, 2H), 5.30 (t, J = 6.1 Hz, 1H), 6.17 (s, 3H),

6.26-6.43 (m, 3H), 6.97 (dd, J = 5.8 Hz, 2.6 Hz, 1H), 7.34-7.46 (m, 1H), 7.46-7.54 (m, 2H), 7.60 (bs, 1H), 7.70 (s, 1H), 7.78 (dd, J = 5.8 Hz, 2.6 Hz, 1H), 8.03 (bs, 1H).

28: ^{1}H NMR (300 MHz, DMSO-d_6) δ (ppm): 4H$_3$), 1.68 (s, 3H), 3.94 (bs, 2H), 4.04 (bs, 2H), 4.48 (t, J = 5.2 Hz, 2H), 5.27 (t, J = 6.1 Hz, 1H), 6.43 (d, J = 8.7 Hz, 1H), 7.76 (bs, 1H), 8.09 (s, 2H), 8.46 (d, J = 8.7 Hz, 1H), 9.48 (s, 1H).

29: ^{1}H NMR (300 MHz, DMSO-d_6) δ (ppm): 3.40 (bs, 6H), 3.93 (bs, 2H), 4.49 (t, J = 5.5 Hz, 2H), 6.45 (d, J = 8.7 Hz), 8.12 (s, 2H), 8.47 (d, J = 8.7 Hz, 1H), 9.44 (bs, 1H).

30: ^{1}H NMR (500 MHz, DMSO-d_6) δ (ppm): 0.76 – 0.86 (m, 2H), 1.13-1.27 (m, 9H), 1.35-1.47 (m, 2H), 1.53-1.69 (m, 17H), 1.87-1.99 (m, 2H), 3.62 (s, 3H), 3.92-4.03 (m, 2H), 4.06-4.16 (m, 2H), 5.20 (t, J = 6.6 Hz, 1H), 6.16 (d, J = 13.8 Hz, 1H), 6.23 (d, J = 13.8 Hz, 1H), 7.14-7.26 (m, 2H), 7.27-7.39 (m, 3H), 7.55 (d, J = 7.3 Hz, 2H), 7.60-7.69 (m, 1H), 7.88 (t, J = 5.7 Hz, 1H), 7.96 (s, J = 13.8 Hz, 1H), 8.13 (m, J = 15.3 Hz, 1H), 8.24 (td, J = 13.0, 8.3 Hz, 2H).

Supplementary Movie

Real time monitoring of the CRE1/AHK4-GFP localization during lateral root primordia (LRP) development. LRP at stage II was monitored for 6 h. CRE1/AHK4-GFP at the cell plate of dividing cells is indicated by white arrows. The movie is available on CD attached to the Ph.D. thesis.

Homology modelling and molecular docking

CRE/AHK structures were modelled based on CRE1/AHK4-iP crystal structure (PDBID: 3T4L; Hothorn et al., 2012) using Modeller 9.10 (Sali and Blundell, 1993). The geometry of iP-NBD was modelled with Marvin (http://www.chemaxon.com), and then the compounds were prepared for docking in the AutoDockTools program suite (Sanner, 1999). The Autodock Vina program (Trott and Olson, 2010) was used for docking iP-NBD ligand into the set of AHK structures obtained from homology modelling. A 15 Å box centred at the original ligand binding position was used. The exhaustiveness parameter was set to 20.

AtCKX2 activity measurement

The recombinant enzyme AtCKX2 was obtained from cell free medium of *P. pastoris* pGAPZα::AtCKX2 strain (Kowalska et al., 2010). The yeasts were precultivated in YPD medium (1 % yeast extract, 2 % pepton) complemented with 2% glucose and 100 µg mL^{-1} zeocin, at 30 °C for 72 h in dark, while shaking. After that, the preculture was diluted 25-times into fresh YPD medium complemented with 2% glucose and cultivated at the same conditions for another 24 h. Cells were removed by centrifugation at 10.000 rpm and 4 °C for 10 min. pH of the cell free medium containing enzyme was adjusted to pH 8 using 2 M Tris/HCl, pH 8 and then sterilized by passing through 0.2 µm filter. The enzymatic activity determination was done kinetically by the 2,6-dichlorophenolindophenol (DCPIP) method (Bilyeu et al., 2001) adopted for screening in microtitre plates. Each well was filled with 100 µL of reaction mixture containing 100 mM KH_2PO_4 buffer, pH 7.4, 0.2 mM DCPIP (to reach starting

absorbance 1.0 at 590 nM), 2 mM EDTA and 0.2 mg mL^{-1} BSA. iP or iP-NBD were added from 10 mM stock solutions in DMSO to reach the desired final concentration of 1.6 – 200 mM. The same volume of DMSO was used as a blank. The reaction was started by addition of 100 µL enzyme diluted from the source in 0.1 M Tris/HCl, pH 8 to reach activity 50 pkat mL^{-1}. Absorption at 590 nm was recorded in 40 s intervals for 10 min at 37 °C in Synergy H4 Hybrid Multi-Mode Microplate reader (BioTek, USA). Average reaction rates (mOD/min) were determined from linear sections and the reaction rate of the blank was subtracted. The enzymatic kinetic parameters V_{max} and K_m were calculated using GraphPad Prism 5.1.

In vitro pH stability measurement

The pH stability of iP-NBD was analyzed by HPLC-PDA Waters Alliance 2695 Separations Module (Waters, Manchester, UK); analytes were detected at scanning range 210-700 nm using Waters 2996 PDA detector (Waters, Manchester, UK). Solution of iP-NBD (1 mM; DMSO) was prepared and diluted to 10 µM in the McIlvaine buffer (ref) with appropriate pH (4, 5, 6, 7 or 8). The diluted sample was either immediately injected (0 h) onto a reversed phase column (Symmetry C18, 5 µm, 150 mm × 2.1 mm; Waters, Milford, MA, USA), or left incubated at 21 °C for 0.5 h, 6 h or 16 h and then injected on the column. At flow-rate of 0.3 mL min^{-1}, the following binary gradient was used: 0 min, 90 % A; 0–14 min, linear gradient to 10 % A; 14–20 min, isocratic elution of 10 % A; 20–24 min, linear gradient to 90 % A; 24-26 min, isocratic elution of 90 % A, where A was 15 mM formic acid adjusted to pH 4 with ammonium and B was 100 % methanol. Chromatograms were generated under the 270 nm wavelength. Relative peak areas of iP-NBD corresponding to samples incubated for selected time periods in the McIlvaine buffer were calculated as percentages of the corresponding peak areas obtained for the control sample with the same dilution (0h); all peak areas were measured at least in triplicates.

LC-MS/MS method for the detection of iP-NBD biological stability

To study iP-NBD stability *in vivo* 5 µM iP-NBD was applied to *Arabidopsis* (*Ler*) cell suspension and in the timeframe of 0.5 - 5 h samples were taken and deep-frozen for

subsequent quantitative LC-MS/MS analysis of iP-NBD and Ade-NBD (the expected product of side-chain cleavage by endogenous CKXs) contents. The samples (around 50 mg fresh weight) were extracted in 1.0 mL of modified Bieleski buffer (60% MeOH, 10% HCOOH and 30% H_2O; Hoyerová et al., 2006) together with 0.01 pmol of N9-NBD-labelled dimethyladenine (diMeAde-NBD) added as an internal standard to validate LC-MS/MS determination. The extracts were purified using the Oasis MCX column (30 mg/1 mL, Waters) and targeted analytes were eluted using 0.35 M NH_4OH in 60% (v/v) MeOH solution (Dobrev and Kamínek, 2002). The purified samples were eluted using a reversed-phase column (Acquity UPLC® BEH C18, 1.7 µm, 2.1 × 150 mm, Waters) with a 26 min gradient comprised of methanol (A) and 15 mM ammonium formate pH 4.0 (B) at a flow rate of 0.25 mL/min and column temperature of 40 °C (Svačinová et al., 2012). The binary linear gradient of 0-7 min 5:95 A:B, 16 min 20:80 A:B, 23 min 50:50 and 26 min 100:0 was used, after which the column was washed with 100% methanol for 1 min and re-equilibrated to initial conditions for 3 min. The effluent was introduced into the MS system with the following optimal settings: source/desolvation temperature 150/600 °C, cone/desolvation gas flow 150/1000 l h^{-1}, capillary/cone voltage 3500/25 V, collision energy 20 eV and collision gas flow (argon) 0.15 mL min^{-1}. Quantification and confirmation of the NBD-labelled compounds were obtained by the multiple reaction monitoring mode using the following mass transitions: 410>342, 342>136 and 370>164 for iP-NBD, Ade-NBD and diMeAde-NBD, respectively. All chromatograms were analyzed with MassLynx software (version 4.1; Waters Corporation) and the compounds were quantified according to the internal standard added.

Estimation of iP-NBD fluorescence properties

Fluorescence spectrum reaching the maximal fluorescence intensities in 456 nm (ex) and 528 nm (em) was obtained with 100 µM iP-NBD dissolved in 100% ethanol by relative fluorescence intensity scanning in the range of 300-700 nm using Synergy H4 Multi-Mode Microplate Reader (BioTek, USA).

Synthesis of fluorescently-labelled compounds

The fluorescently labelled compounds used in the studies were prepared according to the reaction scheme (Scheme 5). Two carbon linker terminated with an amino group suitable for consecutive NBD fluorophore attachment was coupled to the purine *N*9 position by the reaction of 6-chloropurine with *N*-Boc-ethanolamine under Mitsunobu conditions (Kubiasová et al., 2018). Later, nucleophilic substitution of C6 chlorine with appropriate amines in boiling alcohols followed by Boc protective group cleavage provided purine intermediates for fluorescent labelling. 4-chloro-7-nitro-1,2,3-benzoxadiazol was used as NBD donor and was linked to the purine primary amino group in MeOH under basic conditions. Physico-chemical characterization of the synthesized compounds was done according to Kubiasová et al., 2018.
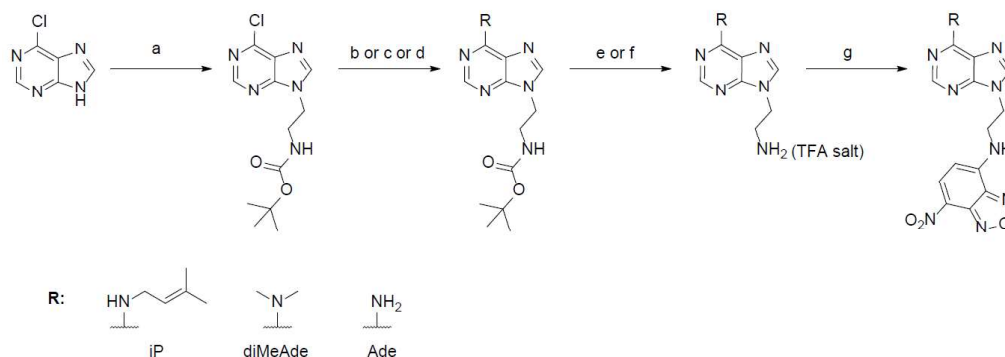
Scheme 5: *Reaction scheme for preparation of fluorescently labelled probes for confocal microscopy studies. a) N-Boc-ethanolamine, PPh₃, DIAD, THF, rt, 2 h, (68%); b) 3-methylbut-2-enylamine.HCl, Et₃N, nPrOH, reflux, 4 h, (93%); c) Me₂NH.HCl, Et₃N, nPrOH, reflux, 4 h, (97%); d) ammonium hydroxide, EtOH, 95 °C, overnight, (76%); e) Dowex 50W X8, DCM, reflux followed by 4 M methanolic ammonia, rt, overnight, (iP - 90%, diMeAde - 87%); f) TFA, DCM, rt, overnight, (Ade.TFA salt - 95%); g) 4-chloro-7-nitro-1,2,3-benzoxadiazole, NaHCO₃, MeOH, 50 °C, 1 h followed by rt overnight (iP - 52%, diMeAde - 75%, Ade - 68%).*

Thin-layer chromatography was carried out on Silica 60 F$_{254}$ plates (Merck) using *n*-PrOH/ammonium hydroxide/water (55:10:35, v/v) or CHCl$_3$/MeOH (9:1, v/v) as developing systems and the spots were detected by UV light (254 nm) and/or by ninhydrin staining (1.5% (w/v) ninhydrin in *n*-butanol containing 3 % of AcOH). The column chromatography purification was performed on silica Davisil 40-63 micron

(Grace Davision). The chromatographic purity and mass of prepared compounds were determined using an Alliance 2695 separation module (Waters) linked simultaneously to a DAD detector PDA 996 (Waters) and a Q-Tof micro (Waters) benchtop quadrupole orthogonal acceleration time-of-flight tandem mass spectrometer. Samples were dissolved in DMSO and diluted to a concentration of 10 μg.mL^{-1} in the initial mobile phase. The samples (10 μL) were injected on a RP-column Symmetry C18 (150 mm × 2.1 mm × 3.5 μm, Waters) and separated at a flow rate of 0.2 mL.min^{-1} with following binary gradient: 0 min, 10% B; 0-24 min, a linear gradient to 90% B, followed by 10 min isocratic elution of 90% B. 15 mM formic acid adjusted to pH 4.0 by ammonium hydroxide was used as a solvent (A) and methanol as the organic modifier - solvent (B). The eluent was introduced into the DAD (scanning range 210-400 nm, with 1.2 nm resolution) and an ESI source (source temperature 110 °C, capillary voltage +3.0 kV, cone voltage +20 V, desolvation temperature 250 °C). Nitrogen was used both as desolvation gas (500 L.h^{-1}) as well as cone gas (50 L.h^{-1}). The data was obtained in positive ionization mode and were acquired in the 50-1000 m/z range. ^{1}H and ^{13}C NMR spectra were recorded on Jeol ECA-500 operating at a frequency of 500 MHz (^{1}H) and 125 MHz (^{13}C), respectively. Samples were prepared by dissolving substances in DMSO-d_6 and the chemical shifts were calibrated to residual solvent peak (2.49 ppm for proton) and DMSO-d_6 (39.5 ppm for carbon). For assignment of ^{1}H and ^{13}C NMR signals 2D NMR spectra such as HMQC, HMBC, and COSY were also measured.

tert-butyl [2-(6-amino-9H-purin-9-yl)ethyl]carbamate

tert-butyl [2-(6-amino-9*H*-purin-9-yl)ethyl]carbamate (0.5 g, 1.68 mmol) was heated in closed vessel with ammonium hydroxide (5 mL) and EtOH (5 mL) at 95 °C overnight. After evaporation of solvents, the residue was purified by silica column chromatography using CHCl$_3$/MeOH (9:1, v/v) as a mobile phase. White solid, yield 76%. HPLC purity 99.9, ESI$^+$-MS 279 (100, [M+H]$^+$), ^{1}H-NMR (500 MHz, DMSO-d_6) δ (ppm): 1.30 (s, 9H, Boc (C$\underline{H}_3$)$_3$), 3.32 (q, *J* = 5.9 Hz, 2H, CH$_2$C$\underline{H}_2$NHBoc), 4.16 (t, *J* = 6.0 Hz, 2H, C$\underline{H}_2$CH$_2$NHBoc), 6.96 (t, *J* = 5.7 Hz, 1H, CH$_2$CH$_2$N$\underline{H}$Boc), 7.15 (s, 2H, Ade NH$_2$), 7.99 (s, 1H, pur H8), 8.11 (s, 1H, pur H2). ^{13}C-NMR (125 MHz, DMSO-d_6) δ (ppm): 28.1 (Boc ($\underline{C}$H$_3$)$_3$C), 39.2 (HMQC based, CH$_2$$\underline{C}H_2$NHBoc), 42.7 ($\underline{C}H_2CH_2$NHBoc), 77.8 (Boc

(CH$_3$)$_3$$\underline{C}$), 118.7 (pur C5), 140.8 (pur C8), 149.6 (pur C4), 152.2 (pur C2), 155.5 (Boc $\underline{C}$O), 155.9 (pur C6).

9-(2-aminoethyl)adenine trifluoroacetate

tert-butyl [2-(6-amino-9*H*-purin-9-yl)ethyl]carbamate (0.35 g, 1.26 mmol) was added to a mixture of DCM (10 mL) and TFA (0.5 mL, 6.54 mmol) and stirred at room temperature overnight. Reaction mixture was evaporated under reduced pressure and the residue was treated with Et$_2$O to obtain white solid. Yield 95%, HPLC purity 99.9, ESI$^+$-MS 179 (100, [M+H]$^+$), ^{1}H-NMR (500 MHz, DMSO-*d$_6$*) δ (ppm): 3.36 (s, 2H, CH$_2$$\underline{CH_2}NH_2$), 4.47 (t, J = 5.7 Hz, 2H, C$\underline{H_2}$CH$_2$NH$_2$), 8.13 (s, 3H, CH$_2$CH$_2$N$\underline{H_3}^+$), 8.34 (s, 1H, pur H8), 8.43 (s, 1H, pur H2), 8.72 (s, 2H, Ade NH$_2$). ^{13}C-NMR (125 MHz, DMSO-*d$_6$*) δ (ppm): 38.3 (CH$_2$$\underline{CH_2}NH_2$), 41.4 ($\underline{CH_2}CH_2NH_2$), 116.5 (q, ^1J_F = 296.3 Hz, $\underline{C}$F$_3$COOH) 118.5 (pur C5), 142.9 (pur C8), 147.5 (pur C2), 149.3 (pur C4), 152.3 (pur C6), 158.8 (q, ^2J_F = 33.5 Hz, CF$_3$$\underline{C}$OOH).

Ade-NBD

Synthesized according to Kubiasová et al., 2018. A suspension of 9-(2-aminoethyl)adenine trifluoroacetate (0.1 g, 0.34 mmol) and NaHCO$_3$ (0.101 g, 1.20 mmol) was stirred in MeOH (3 mL) for 1 h. Then, NBD-chloride (0.084 g, 0.41 mmol) was added and the reaction mixture was heated in the dark at 65 °C for one hour and then stirred at room temperature overnight. Resulting solid was filtered, washed with ice cold MeOH (5 × 1 mL) and water (3 × 1 mL). The product was purified by silica column chromatography using CHCl$_3$/MeOH as a mobile phase with MeOH gradient.

Redish-brown solid, yield 68 %, HPLC purity 99.9, ESI$^+$-MS 342 (100, [M+H]$^+$), ^{1}H-NMR (500 MHz, DMSO-*d$_6$*) δ (ppm): 3.92 (s, 2H, CH$_2$$\underline{CH_2}$NHNBD), 4.46 (s, 2H, C$\underline{H_2}CH_2$NHNBD), 6.44 (d, J = 8.3 Hz, 1H, NBD H6), 7.19 (s, 2H, NH$_2$), 8.04 (s, 1H, pur C2), 8.09 (s, 1H, pur H8), 8.46 (d, J = 8.9 Hz, 1H, NBD H5), 9.48 (s, 1H, CH$_2$CH$_2$N$\underline{H}$NBD). ^{13}C-NMR (125 MHz, DMSO-*d$_6$*) δ (ppm): 41.3 ($\underline{CH_2}$CH$_2$NHNBD), 42.8 (CH$_2$$\underline{CH_2}$NHNBD), 99.3 (NBD C6), 118.7 (pur C5), 121.3 (NBD), 137.7 (NBD C5), 141.0 (pur C8), 144.0 (NBD), 144.4 (NBD), 144.9 (NBD), 149.7 (pur C4), 152.3 (pur C2), 155.9 (pur C6).

Research article

Design, synthesis and perception of fluorescently labeled isoprenoid cytokinins.

Kubiasová K., Mik V., Nisler J., Hönig M., Husičková A., Spíchal L., Pěkná Z., Šamajová O., Doležal K., Plíhal O., Benková E., Strnad M., Plíhalová L.
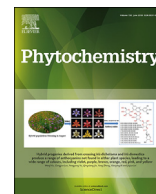
Design, synthesis and perception of fluorescently labeled isoprenoid cytokinins

Karolina Kubiasová [c, 1], Václav Mik [b, 1], Jaroslav Nisler [a, b], Martin Hönig [a, b], Alexandra Husičková [d], Lukáš Spíchal [b], Zuzana Pěkná [b], Olga Šamajová [e], Karel Doležal [a, b], Ondřej Plíhal [c], Eva Benková [f], Miroslav Strnad [a], Lucie Plíhalová [a, b, *]

[a] Laboratory of Growth Regulators, Centre of the Region Haná for Biotechnological and Agricultural Research, Faculty of Science, Palacký University & Institute of Experimental Botany AS CR, Šlechtitelů 27, Olomouc 783 71, Czech Republic
[b] Department of Chemical Biology and Genetics, Centre of the Region Haná for Biotechnological and Agricultural Research, Faculty of Science, Palacký University, Olomouc 783 71, Czech Republic
[c] Department of Molecular Biology, Centre of the Region Haná for Biotechnological and Agricultural Research, Šlechtitelů 27, Olomouc 783 71, Czech Republic
[d] Department of Biophysics, Centre of the Region Haná for Biotechnological and Agricultural Research, Faculty of Science, Palacký University, Šlechtitelů 27, Olomouc 783 71, Czech Republic
[e] Department of Cell Biology, Centre of the Region Haná for Biotechnological and Agricultural Research, Šlechtitelů 27, Olomouc 783 71, Czech Republic
[f] Institute of Science and Technology (IST), 3400 Klosterneuburg, Austria

ARTICLE INFO

ABSTRACT

Isoprenoid cytokinins play a number of crucial roles in the regulation of plant growth and development. To study cytokinin receptor properties in plants, we designed and prepared fluorescent derivatives of 6-[(3-methylbut-2-en-1-yl)amino]purine (N^6-isopentenyladenine, iP) with several fluorescent labels attached to the C2 or N9 atom of the purine moiety via a 2- or 6-carbon linker. The fluorescent labels included dansyl (DS), fluorescein (FC), 7-nitrobenzofurazan (NBD), rhodamine B (RhoB), coumarin (Cou), 7-(diethylamino)coumarin (DEAC) and cyanine 5 dye (Cy5). All prepared compounds were screened for affinity for the *Arabidopsis thaliana* cytokinin receptor (CRE1/AHK4). Although the attachment of the fluorescent labels to iP via the linkers mostly disrupted binding to the receptor, several fluorescent derivatives interacted well. For this reason, three derivatives, two rhodamine B and one 4-chloro-7-nitrobenzofurazan labeled iP were tested for their interaction with CRE1/AHK4 and *Zea mays* cytokinin receptors in detail. We further showed that the three derivatives were able to activate transcription of cytokinin response regulator *ARR5* in Arabidopsis seedlings. The activity of fluorescently labeled cytokinins was compared with corresponding 6-dimethylaminopurine fluorescently labeled negative controls. Selected rhodamine B C2-labeled compounds **17**, **18** and 4-chloro-7-nitrobenzofurazan N9-labeled compound **28** and their respective negative controls (**19**, **20** and **29**, respectively) were used for in planta staining experiments in *Arabidopsis thaliana* cell suspension culture using live cell confocal microscopy.
© 2018 Elsevier Ltd. All rights reserved.

1. Introduction

Naturally occurring isoprenoid cytokinins (ISCK), such as 6-[(3-methylbut-2-en-1-yl)amino]purine (iP), *trans*-zeatin (*t*Z) and *cis*-zeatin, are plant signaling molecules. For this reason, they have attracted the attention of biologists owing to their importance in numerous aspects of plant growth and development, cell division, seed germination, the formation and activity of shoot and root meristems, apical dominance, auxiliary bud release, nutrition mobilization, leaf senescence and responses to pathogens (Davies, 2007). Fluorescently labeled ISCK may be a useful alternative tool for research into cytokinin perception and signaling in plants. Although several cytokinin receptors have been already described, e.g., in species such as Arabidopsis (Inoue et al., 2001; Suzuki et al., 2001), maize (Yonekura-Sakakibara et al., 2004), legumes *Medicago truncatula* (Gonzalez-Rizzo et al., 2006), *Lotus japonicus* (Murray et al., 2007; Tirichine et al., 2007) and rice (Du et al., 2007), there remains the need for mapping the receptor domain in order to understand the relation between the chemical structure and activity of cytokinin derivatives. This approach is indispensable developing new strategies in plant biotechnology, such as plant tissue culture, modern agriculture and plant protection against stress (Plíhalová et al., 2016). Fluorescent labeling is an important tool in cell biology research, e.g., staining and immunostaining techniques (Doskočilová et al., 2013; Mason, 1999; Ovečka et al., 2014; Šamajová et al., 2014), and for visualizing of small bioactive molecules. It offers several advantages over traditional radio-ligand binding techniques, i.e., fluorescence labels are relatively safe and inexpensive compared to tritiated or iodinated compounds and a wide range of fluorophores are available to suit different experimental setups (McGrath et al., 1996; Daly and McGrath, 2003). Fluorescent ligands are continually being developed to meet the demands of the pharmacological community and are being used to study pharmacological receptor systems (Daly and McGrath, 2003). Hiratsuka and Kato used a fluorescent analogue of colcemid with 7-nitrobenzo-furazan (NBD, NBD-colcemid) to visualize tubulin (Hiratsuka and Kato, 1987). Fluorescent labeling of small active molecules has been shown to be effective for visualizing plant hormones, such as auxins, abscisic acid, jasmonates, gibberellins, brassinosteroids and even strigolactones. In one such study, abscisic acid (ABA) was coupled with fluorescein isothiocyanate (FITC) and used to study direct interaction of ABA with the plasma membrane as although ABA receptors were unknown at the time, they were predicted to lie in the membrane (Asami et al., 1997). Fluorescent brassinosteroid was prepared by labeling castasterone with Alexa Fluor 647 (AFCS) and the endocytosis of BRI1-AFCS complexes in living cells was visualized (Irani et al., 2012). Fluorescent labeling at the cellular level has also been done using gibberellins labeled with FITC (Pulici et al., 1996). 1,4-Dithiobutylene and 1,3-dithiopropylene spacers were employed between the fluorescent label and gibberellin, particularly for the compound 17-mercaptobutylthio-3α,10-dihydroxy-20-norgibberella-7,19-dioic acid-19,10-lactone. It was shown that derivatives with longer spacers between gibberellin and FITC were more active in the ability to induce α-amylase activity in the embryoless half grain, a process known to be specifically induced by active Gas synthesized by the embryo. However, an approximately 10-fold higher concentration of the fluorescent probe than GA$_3$ was needed to obtain a comparable biological effect (Pulici et al., 1996; Lace and Prandi, 2016). Synthesis of fluorescently labeled strigolactone analogs (DS, FC, BODIPY) has been used to search for possible strigolactone receptors *in vivo* (Prandi et al., 2013). Rhodamine and fluorescein auxin derivatives have been synthesized by direct conjugation of FITC and rhodamine B to the NH group of IAA (Sokolowska et al., 2014). Both fluoroprobes were shown to retain auxin activity in

three different bioassays (Sokolowska et al., 2014). Tsuda and Hayashi introduced an NBD label into 5-hydroxy-IAA and 7-hydroxy-NAA but the prepared auxin analogs were found to be inactive toward auxin receptors (Tsuda et al., 2011; Hayashi et al., 2014; Lace and Prandi, 2016). Fluorescently labeled jasmonate has been synthesized by bonding jasmonoyl-ʟ-isoleucine to coumarin 343 *via* the carboxyl group of isoleucine (Liu et al., 2012). The fluorescent probe was examined in cabbage using a root growth inhibition bioassay and the effect of fluorescently labeled probe on the root growth of cabbage seedlings was similar to that of the methyl jasmonate, the standard bioactive jasmonate. Like approaches to other plant growth regulators, in preparing a fluorescent probe for visualizing a cytokinin receptor, the compound has to possess cytokinin activity and high affinity for the receptor while nonspecific binding to other cellular structures needs to be minimized. When the first attempts to prepare a cytokinin fluorescent probe failed in the 1970s, a different strategy based on the construction of mimetic adenine-like molecules was developed (Skoog et al., 1975; Specker et al., 1976). Modifications of cytokinins, particularly in the purine moiety, has led to the preparation of fluorescent imidazo[4,5-*g*]- and imidazo[4,5-*f*]-quinazolines, 4-substituted 2-methylthiopyrido[2,3-*d*]pyrimidines and 7-phenylethynylimidazo[4,5-*b*]pyridines and their ribosides, which were shown to have only weak or negligible cytokinin activity in a tobacco callus bioassay (Specker et al., 1976; Hamaguchi et al., 1985; Nishikawa et al., 2000). Zawadski's group prepared synthetic cytokinin *N*-phenyl-*N′*-(4-pyridyl) urea labeled with 4-chloro-7-nitrobenzofurazan and rhodamine B fluorescent labels and detected binding of the cytokinin-specific protein VrCSBP by fluorescence correlation spectroscopy (Zawadski et al., 2010). It has been suggested that the loss of biological activity could be prevented by separation of the pharmacophore from the fluorescent moiety through the introduction of a spacer or linker (Leopoldo et al., 2009). However, so far, only a few studies have systematically evaluated spacer length for fluorescent probes and none have directly evaluated purine based cytokinins. Spacer length and position of the spacer (label) in the purine moiety can both have a large impact on the biological activity of such cytokinin derivatives. Appropriate positional attachment of fluorophores to small molecule ligands is critical for retaining both receptor binding affinity and efficacy (Leopoldo et al., 2009). In addition to standard fluorophores such as fluorescein and rhodamine, we have also endeavoured to find new efficient fluorolabels with fewer limitations for use in biological systems and during confocal microscopy imaging. For example, fluorescein is known to self-quench after bioconjugation (Lace and Prandi, 2016; Sjöback et al., 1995) as the emission properties of fluorescein greatly depend on environmental pH (Lavis et al., 2007) and it often exists as an equilibrium between lactone and quinoid forms (Lace and Prandi, 2016). Although rhodamine dyes are less sensitive to pH than fluorescein, they are poorly soluble in water (Lace and Prandi, 2016). Despite these limitations, both are widely used for labeling bioactive molecules. We have also used the small heterocyclic molecule 4-chloro-7-nitrobenzofurazan (NBD-Cl), which is a benzoxadiazole compound with low molecular weight. Derivatives of NBD-Cl have been used for the preparation of novel kinase substrates, lipid probes and fluorescent analogs of native lipids and the study of a variety of processes (Chattopadhyay, 1990; Lavis and Raines, 2008; Lace and Prandi, 2016).

In this work, we prepared fluorescently labeled iP derivatives because iP is known to bind to *Arabidopsis thaliana* CRE1/AHK4, *Zea mays* ZmHK1 and other cytokinin receptors. 6-Dimethylaminopurine (DAP) analogs with no cytokinin activity were also prepared to obtain fluorescent negative controls for receptor bioassays. The prepared compounds contained a 2- or 6-

carbon linker between the iP or DAP molecule and the fluorescent labels. The fluorescent labels used included dansyl (DS), fluorescein (FC), 7-nitrobenzofurazan (NBD), rhodamine B (RhoB) and coumarin (Cou), 7-(diethylamino)coumarin (DEAC) and cyanine 5 dye (Cy5). We selected the C2 or N9 atom of the purine moiety for linker attachment to prepare 2,6- and 6,9-disubstituted purine derivatives. The ability of all prepared compounds to bind the cytokinin receptor CRE1/AHK4 was tested. The three most successful derivatives were also tested for interaction with CRE1/AHK4 and ZmHK1 in detail as well as for their ability to activate the expression of the *ARR5* gene, which is the primary cytokinin response regulator in Arabidopsis (D'Agostino et al., 2000). Two active C2-fluorescent probes labeled with RhoB and one active N9-fluorescent probe labeled with NBD together with their fluorescent controls were used for staining of *Arabidopsis thaliana* cell suspension culture and live cell imaging using confocal microscopy.

2. Results and discussion

2.1. Synthesis

We prepared thirty new 2,6- or 6,9-disubstituted adenine derivatives with the linker attached to an appropriate fluorescent label either at the C2- or N9-atom of the purine moiety and elemental analyses, fluorescent label, length of the linker, ESI-MS and spectral data are shown in Table 1. In addition to the fluorescently labeled iP derivatives, we also prepared DAP analogs labeled with the same fluorescent labels as the iP derivatives for use as negative controls in future experiments. The syntheses of fluorescently labeled iP and DAP derivatives consisted of several steps, as described in the Experimental section and in the Supplementary data. In the first step, an appropriate intermediate substituted with a linker terminating in an amino group was prepared (Schemes 1 and 2). This derivative was labeled with an appropriate fluorescent label (Schemes 3 and 4). For substitutions at the C2 atom of the purine moiety, only fluorescent labels that could be attached to an amino group were used, e.g., NBD-Cl, NHS activated coumarin-3-carboxylic acid, DS-Cl, NHS activated DEAC, FITC and NHS activated RhoB. For the N9 position of the purine atom moiety, we used an appropriate linker terminating in an amino group and NBD-Cl, Cy5-NHS, RhoB-NHS and FITC as fluorescent labels. Since the two carbon linker has proved to be more efficient in the case of C2 derivatives, we have adopted this design strategy for N9 fluorescent probes (25–28 and 30). Compound 29, i.e., DAP-N9-NBD, was also prepared as the only negative control (specifically for comparison with the only active compound 28).

2.2. Live cell hormone binding assays

Cytokinin–receptor interaction is a crucial step in the initiation of cytokinin signaling in plant cells (Romanov et al., 2005). The functionality and ability of intended fluorescent probe to enter the cells can be verified by activation of the appropriate receptors. Therefore, the prepared compounds were tested in a direct binding assay with *E. coli* expressing functional CRE1/AHK4 or AHK3 receptors from *A. thaliana* to test their ability to compete with the radiolabeled natural ligand *trans*-zeatin (2-[^{3}H]*t*Z). Unlabeled *trans*-zeatin, isopentenyladenine (iP), adenine and DMSO were used as positive and negative controls, respectively (Fig. 1A and B; Spíchal et al., 2009).

We compared the activity of fluorescently labeled DAP derivatives 3, 4, 7, 8, 11, 12, 15, 16, 19, 20 and 29 prepared as the negative controls with iP fluorescently labeled probes at CRE1/AHK4 receptor. DAP as well as iP derivatives were fluorescently labeled *via* a two or six carbon linker attached to the C2 or N9 atom

of the purine moiety. DAP control derivatives were chosen given that the isopentenyl substituent is considered to be responsible for the cytokinin receptor binding properties (Hothorn et al., 2011; PDB:3T4J). As predicted, all control derivatives (black columns in Fig. 1A) were inactive.

Some of the desired fluorescently labeled derivatives of iP, namely 2, 5, 6, 9, 13, 14, were also found to be unable to compete with 2-[^{3}H]*t*Z at the CRE1/AHK4 receptor (Fig. 1A). Whereas DS and DEAC fluorescent labels deactivated iP probes regardless of the linker length, iP derivatives of NBD (1, 28), Cou (10), RhoB (17, 18) and FC (21 and 22) showed at least partial affinity to the cytokinin receptor CRE1/AHK4. Although the RhoB labeled C2-derivatives 17 and 18 were active in competing with 2-[^{3}H]*t*Z at the receptor binding site, the iP RhoB labeled N9-derivative 27 was inactive. The FC labeled derivatives behaved similarly.
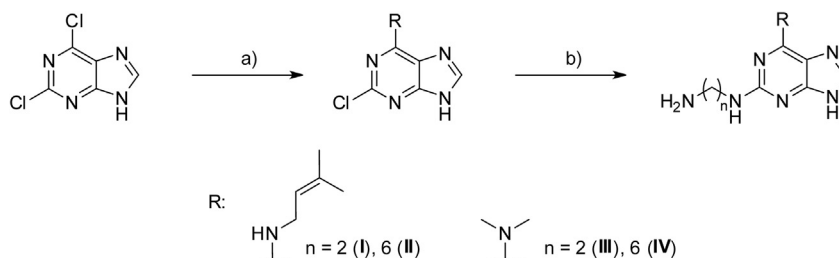
Whereas the activity of both RhoB labeled derivatives 17 and 18 was comparable, the FC labeled derivative 21 with a shorter two-carbon linker exhibited a higher affinity than the derivative 22 with a six-carbon linker. A similar trend was observed for the NBD labeled iP fluorescent probes: the two-carbon linker of 1 was found to be more efficient than the six-carbon linker of 2, which was inactive. C2-labeled iP derivative 21 exhibited highest affinity for the receptor, displacing more than 65% of 2-[^{3}H]*t*Z from the receptor at a 20 μM concentration. The compound 21 thus appeared to be a promising candidate for fluorescent staining until we found that the substance was chemically unstable and spontaneously decomposed during storage. Another promising active compound was N9-labeled 28. This compound (bearing the NBD label) was the only N9 derivative to exhibit affinity for the CRE1/AHK4 receptor, displacing approximately 57% of 2-[^{3}H]*t*Z from receptor binding site at 20 μM concentration. As shown in Fig. 1A, with the exception of compound 28, the other prepared N9-substituted compounds, i.e., 25–27 and 30, appeared to be non-active in displacing 2-[^{3}H]*t*Z in the competition assay. In contrast to 28, compound 29, (negative control), was found to be inactive.

Finally, we selected two RhoB labeled C2-derivatives 17 and 18 and one NBD labeled N9-derivative 28 to test their interaction with CRE1/AHK4 within a wider concentration range (Fig. 1B). The compounds affinity for the receptor was compared to the affinity of adenine (negative control) and iP (positive control). The affinity of compounds 17 and 18 for CRE1/AHK4 was relatively weak compared to the control, better results were achieved with compound 28, whose affinity was approximately ten times higher than compound 18. Compound 28 decreased the binding of 2-[^{3}H]*t*Z to the receptor to 55% at 10 μM concentration. Cytokinin iP decreased the binding of 2-[^{3}H]*t*Z to the receptor to 45% at 10 nM concentration. Compound 28 showed approximately 1000 times lower affinity to the CRE1/AHK4 receptor than iP and although the affinity of 28 appeared to be low, we showed that it was sufficient for *in planta* staining studies. Although the effective concentrations of the active fluorescent probes were high in relation to the positive standard iP, the selected micromolar concentration was necessary for effective visualization of target cellular structures during confocal or fluorescent microscopy staining. Similar approaches have been reported for other phytohormone-based fluorescent probes (Irani et al., 2012).

This aside, the results of the competition assay corresponded to the published structure of the CRE1/AHK4 sensor domain (Hothorn et al., 2011; PDB:3T4J). The crystal structure of the CRE1/AHK4 sensor domain in complex with iP showed four hydrogen bonds formed between the receptor cavity and the adenine moiety and these interactions appeared to be critical for receptor function. Both N6H and N7H hydrogen bonds are linked to Asp262 while N1H atom and N3H hydrogen bonds are linked to water molecules. While C2 and N9 point out of the receptor cavity, they might be

Table 1
Table of prepared fluorescently labeled purine derivatives. 2AmEtAm − 2-aminoethylamino-; 6AmHexAm − 6-aminohexylamino-; NBD − 7-nitrobenzofurazane; Cou − coumarin; DEAC − 7-(Diethylamino)coumarin; DS − dansyl, RhodB − Rhodamine B; FC − fluorescein, v.w.f.: very weak fluorescence.
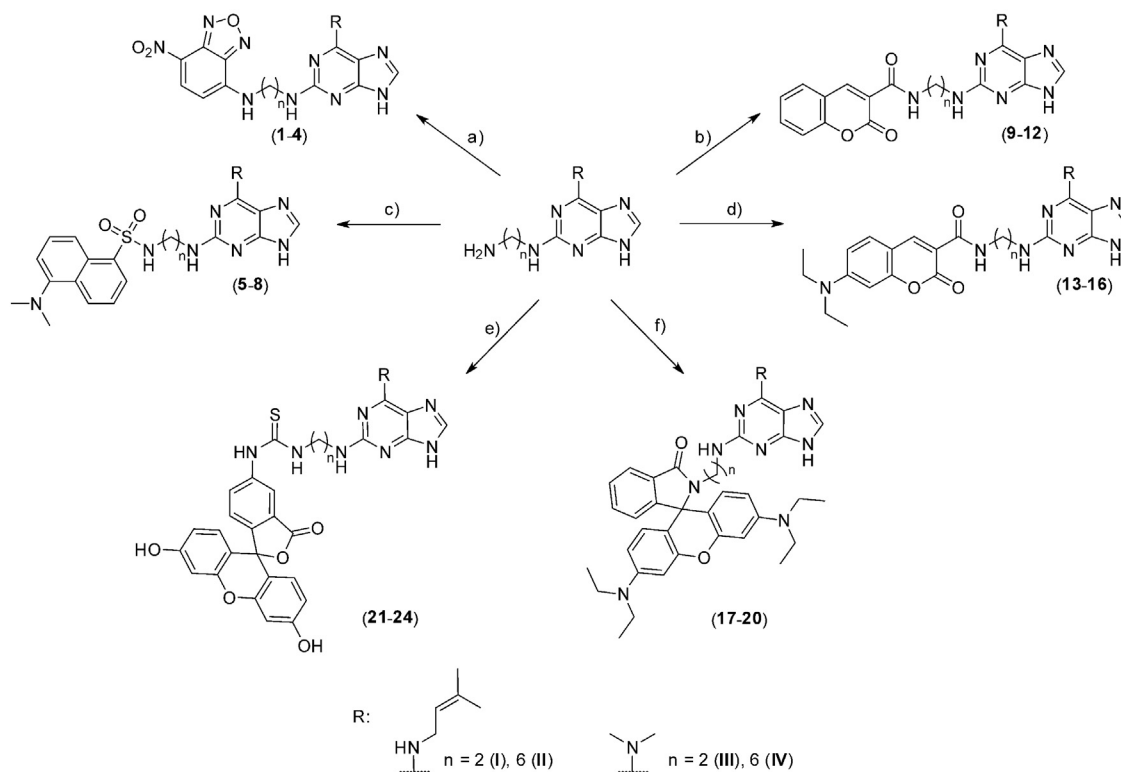
| Comp.	C6	C2	N9	Fluorescent label	HPLC purity [%]	ESI-MS $[M + H]^+$	Spectral properties λex_{max} [nm]	λem_{max} [nm]
1	(3-Methylbut-2-en-1-yl)amino-	2AmEtAm	H	NBD	98.2	425	460	525
2	(3-Methylbut-2-en-1-yl)amino-	6AmHexAm	H	NBD	99.2	481	465	525
3	Dimethylamino-	2AmEtAm	H	NBD	98.4	385	v.w.f.	v.w.f.
4	Dimethylamino-	6AmHexAm	H	NBD	99.9	441	464	526
5	(3-Methylbut-2-en-1-yl)amino-	2AmEtAm	H	DS	99.9	495	257	507
6	(3-Methylbut-2-en-1-yl)amino-	6AmHexAm	H	DS	99.9	551	256	507
7	Dimethylamino-	2AmEtAm	H	DS	99.8	455	254	508
8	Dimethylamino-	6AmHexAm	H	DS	99.6	511	255	505
9	(3-Methylbut-2-en-1-yl)amino-	2AmEtAm	H	Cou	99.9	434	v.w.f.	v.w.f.
10	(3-Methylbut-2-en-1-yl)amino-	6AmHexAm	H	Cou	99.4	490	290	406
11	Dimethylamino-	2AmEtAm	H	Cou	99.9	394	v.w.f.	v.w.f.
12	Dimethylamino-	6AmHexAm	H	Cou	98.9	450	290	407
13	(3-Methylbut-2-en-1-yl)amino-	2AmEtAm	H	DEAC	99.9	505	416	464
14	(3-Methylbut-2-en-1-yl)amino-	6AmHexAm	H	DEAC	98.2	561	416	464
15	Dimethylamino-	2AmEtAm	H	DEAC	99.9	465	416	464
16	Dimethylamino-	6AmHexAm	H	DEAC	99.9	521	416	464
17	(3-Methylbut-2-en-1-yl)amino-	2AmEtAm	H	RhoB	98.0	686	544	566
18	(3-Methylbut-2-en-1-yl)amino-	6AmHexAm	H	RhoB	98.1	742	546	546
19	Dimethylamino-	2AmEtAm	H	RhoB	95.0	646	546	568
20	Dimethylamino-	6AmHexAm	H	RhoB	98.0	702	544	566
21	(3-Methylbut-2-en-1-yl)amino-	2AmEtAm	H	FC	92.4	651	544	566
22	(3-Methylbut-2-en-1-yl)amino-	6AmHexAm	H	FC	97.7	707	497	518
23	Dimethylamino-	2AmEtAm	H	FC	91.4	612.1	498	518
24	Dimethylamino-	6AmHexAm	H	FC	92.0	668.3	497	518
25	(3-Methylbut-2-en-1-yl)amino-	H	2AmEtAm	DS	98.3	481	342	500
26	(3-Methylbut-2-en-1-yl)amino-	H	2AmEtAm	FC	97.0	636	v.w.f.	v.w.f.
27	(3-Methylbut-2-en-1-yl)amino-	H	2AmEtAm	RhoB	96.5	672	554	588
28	(3-Methylbut-2-en-1-yl)amino-	H	2AmEtAm	NBD	96.8	410	475	552
29	Dimethylamino-	H	2AmEtAm	NBD	98.0	370	v.w.f.	v.w.f.
30	(3-Methylbut-2-en-1-yl)amino-	H	2AmEtAm	Cy5	97.7	713	270	641

Scheme 1. Reaction scheme for the synthesis of 2,6-disubstituted purine precursors for fluorescent labeling. a) R-H, Et₃N, n-PrOH, 100 °C, 4 h; b) ethane-1,2-diamine, hexane-1,6-diamine, 165 °C, 3 h.
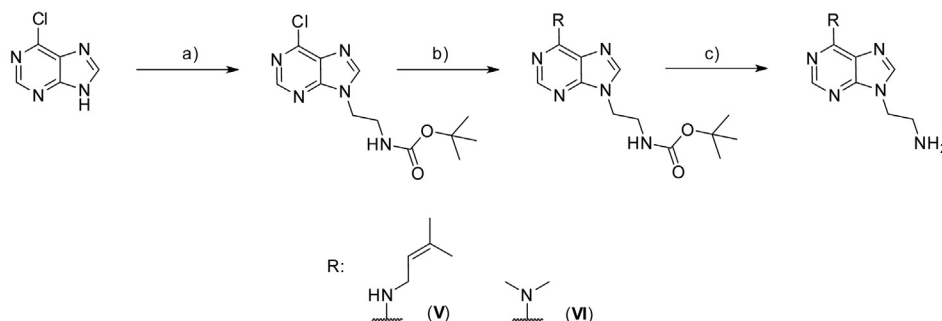
Scheme 2. Reaction scheme for the synthesis of 6,9-disubstituted purine precursors for fluorescent labeling. a) Boc-2-aminoethanol, PPh₃, DIAD, THF, 2 h; b) R-H, Et₃N, n-PrOH, 100 °C, 4 h; c) Dowex 50W X8, DCM, reflux followed by 4 M methanolic ammonia, overnight.

Scheme 3. Preparation of C2-fluorescently labeled purine derivatives. a) NBD-Cl, NaHCO₃, MeOH, 50 °C 1 h followed by RT overnight; b) NHS activated coumarin-3-carboxylic acid, DMSO, MeCN, carbonate buffer pH 8.6, overnight; c) dansyl chloride, Et₃N, MeOH, DCM, overnight; d) NHS activated DEAC-OH, DMSO, MeCN, carbonate buffer pH 8.6, overnight; e) FITC, Et₃N, MeOH, overnight; f) NHS activated rhodamine B, MeCN, carbonate buffer pH 8.6, overnight.
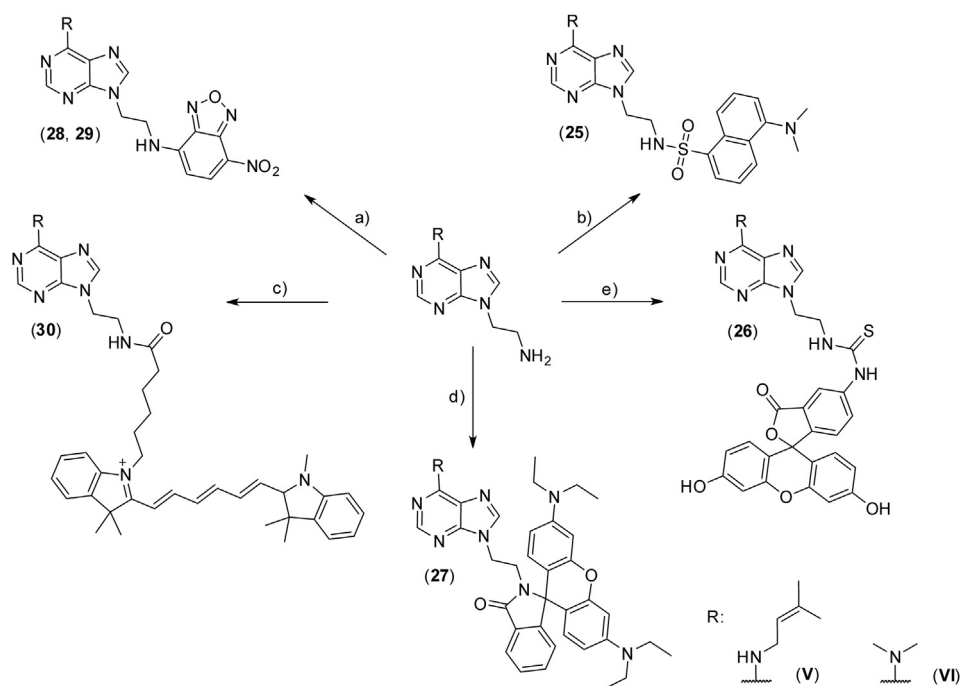
Scheme 4. Fluorescently labeled *N*9-substituted derivatives. a) 4-chloro-7-nitrobenzofurazan, NaHCO₃, MeOH, 50 °C, 1 h; b) dansyl chloride, 2 M Na₂CO₃, acetone, water, RT, overnight; c) cyanine 5 NHS, 0.1 M sodium bicarbonate in water, DMF; d) NHS activated rhodamine B, MeCN, carbonate buffer pH 8.6, overnight; e) FITC, MeOH, NaHCO₃, 50 °C, 1 h. Kation of compound **30** was compensated by [BF₄] anion that was which was omitted to simplify the scheme.
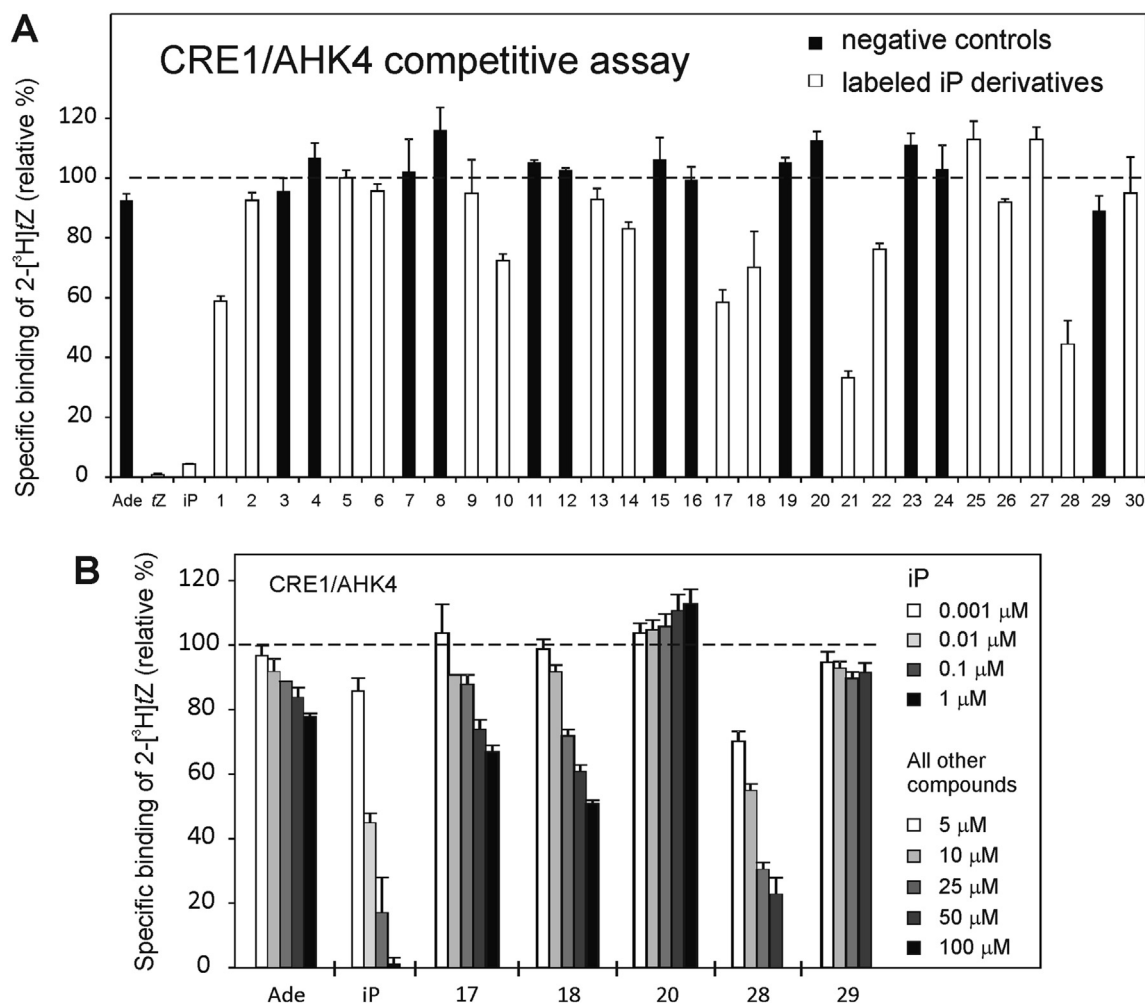
Fig. 1. The ability of the compounds to bind to the cytokinin receptor CRE1/AHK4 in live cell hormone binding assay. (A) Fluorescently labeled DAP and iP derivatives (both 20 μM) competed with 2 nM 2-[³H]tZ. (B) Selected compounds in more detail. Negative control (**19**) for compound **17** is not shown but, exhibited the same affinity pattern as negative control **20**. Adenin (Ade) and DMSO were used as negative controls. The value obtained with DMSO was set as 100% (dashed line). The value obtained with 10 μM iP was set as 0% and was used to discriminate the non-specific binding of 2-[³H]tZ on the bacteria. Error bars show SD values for three replicates.

accessible for linkers bearing spherically advantageous fluorescent labels in molecules **17**, **18** and **28**.

The C2-substituted derivatives were also tested with Arabidopsis cytokinin receptor AHK3, however none showed any affinity toward this receptor (data not shown).

Compounds **17**, **18** and **28** were further tested as to whether they interact with the cytokinin receptor ZmHK1, a maize orthologue of CRE1/AHK4 receptor to extend the potential use of the prepared fluorescent cytokinins to other plant species (Yonekura-Sakakibara et al., 2004). In the assay, we functionally expressed ZmHK1 in *E. coli* strain KMI001 (Podlešáková et al., 2012). Unfortunately, in the bacterial receptor competitive assay, compound **17** showed no affinity to the receptor (data not shown) while compound **18** exhibited an affinity for the ZmHK1 receptor comparable to adenine (Fig. 2A). This result contrasted with the results from CRE1/AHK4 competition assay, where both compounds showed higher affinity than adenine. However, derivative **28** decreased binding of 2-[³H]tZ to the receptor by approximately 70% at 10 μM concentration, while adenine had the same effect at 100 μM concentration. In the higher concentration ranges, **28** was also more effective than adenine, decreasing binding of 2-[³H]tZ to the receptor by approximately 50% at 50 μM concentration (Fig. 2A). The effect of **28** (and its negative control, **29**) at 100 μM concentration was not

evaluated as the compounds were not completely soluble in the tested system at such high concentrations.

In ZmHK1 receptor activation assay, we made several unexpected observations. First, compound **18** was able to activate the receptor (Fig. 2B), even though the ligand-receptor interaction did not seem to be specific; compound **18** was a 100 times weaker activator of ZmHK1 than iP. In contrast, compound **28** was unable to activate this receptor (data not shown), although it exhibited significant affinity for this receptor. Therefore, the compound bound to the cytokinin receptor without triggering its activation in a manner we have described and characterized as anti-cytokinin behavior (Nisler et al., 2010). This may be advantageous for fluorescently labeled cytokinin probes, because it allows for specific interaction with the cytokinin receptor and at the same time limits potential constraints linked to high intracellular cytokinin concentrations.

2.3. Activation of the cytokinin primary response gene ARR5

We employed transgenic Arabidopsis (*Arabidopsis thaliana*) plants harboring the *ARR5:GUS* reporter gene (D'Agostino et al., 2000) to gain more information as to whether compounds **17**, **18** and **28** are able to trigger the cytokinin signaling pathway *in planta*.
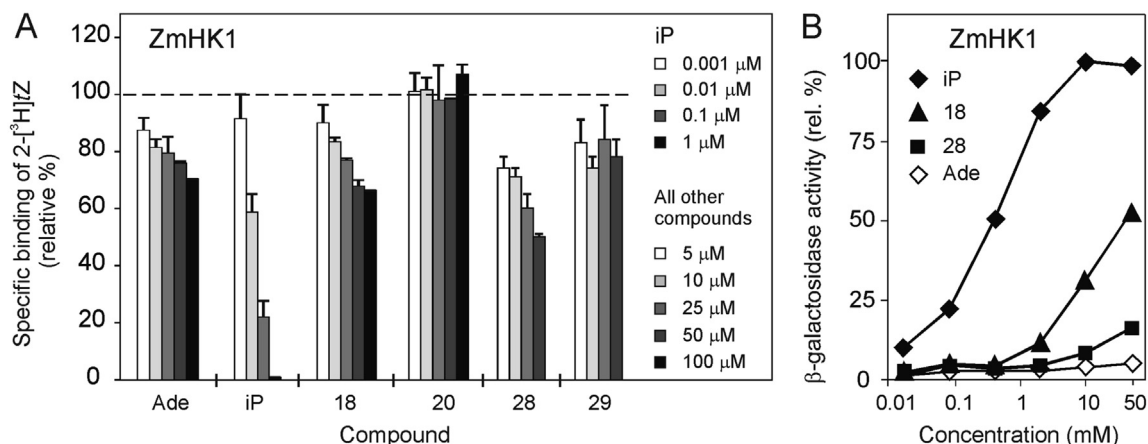
Fig. 2. Interaction of the selected compounds with the cytokinin receptor ZmHK1. Adenine (Ade) and DMSO were used as negative controls. (A) The ability of the compounds to bind to the receptor in live cell hormone binding assay. The value obtained with DMSO was set as 100% (dashed line). The value obtained with 10 μM iP was set as 0% and was used to discriminate the non-specific binding of 2-[^{3}H]tZ on the bacteria. Error bars show SD values for three replicates. (B) The ability of the compounds to activate the receptor. The value obtained with DMSO was set as 0% activation. The value obtained with 10 μM iP was set as 100% activation. Compound 17 activated the receptor similarly to compound 28 and for clarity is not shown. SD values did not exceed 15%.

ARR5 is a primary response gene with a cytokinin-dependent promoter, activation of which integrates the responses of several putative cytokinin signaling pathways.

As shown in Fig. 3, compounds **17**, **18** and **28** were able to activate transcription of the *ARR5:GUS* gene in Arabidopsis in a concentration dependent manner, demonstrating their ability to trigger the cytokinin response in Arabidopsis. Negative controls for the compounds were inactive in this assay. BAP and iP showed maximal activity at 1 μM concentration. None of the tested compounds was able to attain this activity even in 100 μM concentration. However, the selected compounds exhibited activity (20−30%) starting from a concentration of 10 μM. The compounds were approximately 1000 times weaker than iP, which showed activity from 10 nM concentration (Fig. 3) in this assay. Biologically insignificant activity of compound **28** (compared to **17** and **18**) is not surprising, and it is consistent with the negative results of the ZmHK1 receptor activation assay.

2.4. Visualization of cellular structures by fluorescent cytokinin derivatives

We used *Arabidopsis* suspension cell culture that allowed for fast
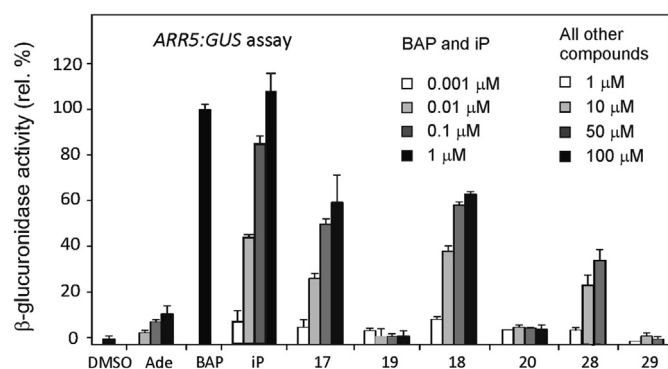
Fig. 3. The ability of the compounds to activate transcription of cytokinin primary response gene *ARR5* in Arabidopsis seedlings three days after germination. The value obtained with DMSO was set as 0% activation. The value obtained with 1 μM BAP was set as 100%. Adenine (Ade) and iP were used as negative and positive controls, respectively. Error bars show SD values for three replicates.

and homogenous staining of individual cells, gave us insight into the distribution of the fluorescent signal at the subcellular level and we adopted a simple staining procedure for visualizing the subcellular structures with selected florescent probes. For staining experiments, we first observed compounds **17** and **18** and their corresponding DAP fluorescent derivatives **19** and **20**, respectively, that were used as negative controls to filter out nonspecific background signals. Arabidopsis cells were treated with 5 μM solution of fluorescent probe or negative control, immediately applied on slides and observed under confocal microscope. The internalization of RhoB-based compounds was relatively fast, reaching apparently constant pattern after approximately 15−20 min of treatment. The fluorescent signal was rather weak in all staining experiments and increased concentration of the fluorescent probe (up to 20 μM) did not significantly change the signal distribution. The signal recorded for the fluorescent probes, compounds **17** and **18,** and their respective negative controls, derivatives **19** and **20**, appeared to be similar in all cases and we observed cytoplasmic distribution of the signal combined with a characteristic patchy-pattern (Fig. 4). We hypothesize that RhoB derivatives may not represent a good candidate for synthesis of cytokinin-based fluorescent probes due to possible nonspecific interactions with cell components that prohibit efficient and specific binding to cytokinin-binding sites.

For this reason, we introduced derivative **28**, an NBD-based green fluorescent cytokinin probe, for *in planta* screening. Based on the results from the cytokinin CRE1/AHK4 competitive bioassay (Fig. 1A) only compound **28** proved to be significantly active in displacing radiolabeled tZ out of all synthesized C2- and N9-based NBD fluorescent probes and concurrently stable. Compound **29**, showed negligible binding to the cytokinin receptor and for this reason, it was used as a negative control. The results from live cell imaging of NBD-based probes are shown in Fig. 4. Similar to RhoB-based probes, staining of Arabidopsis cells with the NBD fluorescent probe was fast, reaching a plateau of the intracellular signal intensity after approximately 10 min of a continuous treatment with 5 μM of compound **28** (Fig. 4). While the negative control showed only weak cytoplasmic fluorescent signal, the NBD-based fluorescent probe at the same concentration showed a clear signal distribution represented by typical mesh-like structures at the cell cortex suggestive of ER structures (Fig. 4 arrows). This is in accordance with the reported localization pattern of the three known cytokinin HK receptors in Arabidopsis (Wulfetange et al.,
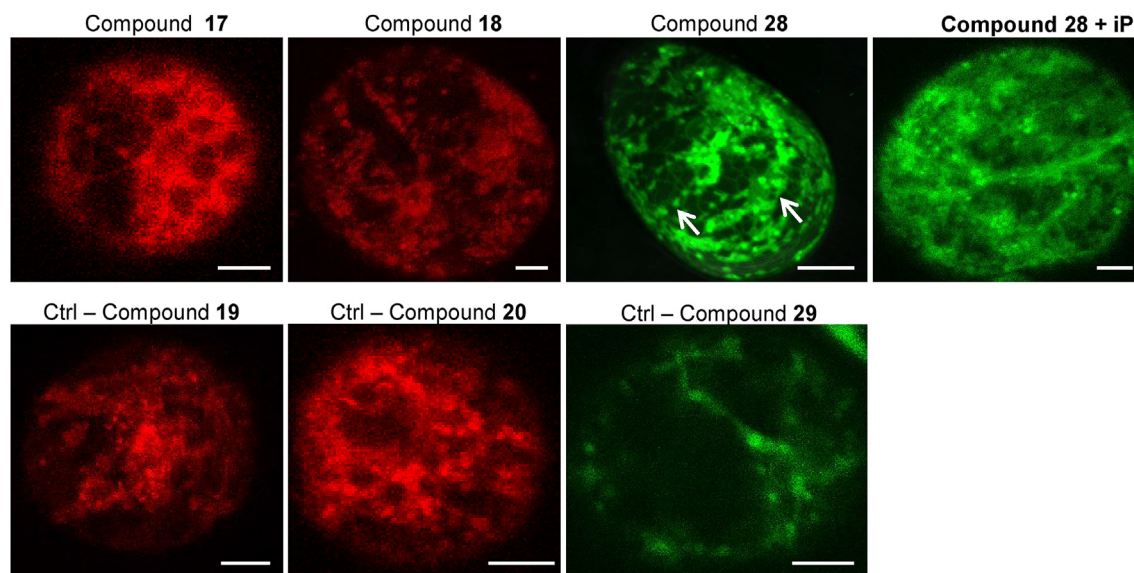
Fig. 4. Confocal fluorescence images of *Arabidopsis* suspension culture cells treated with different fluorescent probes (Compound **17**, **18** and **28**) and their controls (Ctrl - Compound **19**, **20** and **29**), all in 5 μmol concentrations and observed after 15–20 min. Rhodamine B-based compounds are shown in red, 7-nitrobenzofurazan (NBD)-based compounds are shown in green. A mesh-like localization pattern (marked by arrows) characteristic for endoplasmic reticulum was visible in the cell cortex after treatment with compound **28**, but it was lost when compound **28** was co-administered together with equimolar concentration of isopentenyladenine (iP). Scale bars, 5 μm.

2011; Caesar et al., 2011). Further, co-administration of compound **28** together with natural cytokinin iP led to moderate decrease of the fluorescent signal and the signal seemed to be less focused (Fig. 4). This suggests that compound **28** is transported to the cell even in the presence of the endogenous iP, but the competition with intracellular iP leads to the unspecific staining pattern. Therefore, it seems that some NBD-based cytokinin probes can be used for the visualization of the cytokinin HK receptors, but further experiments will be needed to confirm the specificity of the ligand-receptor interaction. N9-based cytokinin fluorescent probes may be particularly suitable for the live cell imaging as the introduction of fluorescent label into N9 position should prevent metabolic conversion of the cytokinin analogue through N-glycosylation that prevents entry into the receptor domain cavity.

3. Conclusion

Thirty new 2,6- and 6,9-disubstituted fluorescently labeled purines bearing fluorescent labels, such as dansyl (DS), fluorescein (FC), 7-nitrobenzofurazan (NBD), rhodamine B (RhoB), coumarin (Cou), and cyanine 5 dye (Cy5) were synthesized. These fluorescent derivatives and their negative controls prepared by labeling of DAP were synthesized with the aim to design probes with ligand affinity to the histidine kinase receptor domain. We prepared several derivatives that were able to bind in the active sites of two different cytokinin receptors - CRE1/AHK4 from *Arabidopsis thaliana* and ZmHK1 from *Zea mays*, and to trigger cytokinin response *in planta*.

Promising derivatives, two 2,6-iP derivatives **17**, **18** and one 6,9-iP derivative **28** underwent more precise binding study in three cytokinin receptors and were found to be active, although at higher concentration ranges than the positive iP control. Overall, our results showed that it is possible to prepare biologically active fluorescent cytokinins by the attachment of a fluorescent label to their purine moiety *via* an appropriate linker without causing extensive structural change. The activity of the prepared probes depended on the position and type of attached label on the adenine moiety. Therefore, the choice of label is also very important for maintaining cytokinin receptor affinity. We used compounds **17**, **18** and **28** and

their controls for *in planta* staining but only compound **28** was an effective competitor as confirmed by radiolabeled tZ receptor binding experiments. Staining of Arabidopsis cells with compound **28** was fast, showed clear intracellular signal distribution represented by typical mesh-like structures at the cell cortex suggestive of ER after approximately 10 min of a continuous treatment with 5 μM fluorescent probe while negative fluorescent control **29** at the same concentration levels showed only weak cytoplasmic fluorescent signal. This is in agreement with reported localization pattern of the three known cytokinin HK receptors in Arabidopsis but further data are needed to confirm the ER localization of receptor-ligand complexes.

4. Experimental procedures

Chemicals and general procedures used in this manuscript are given in Supplementary material.

4.1. Syntheses of purine based intermediates and fluorescent probes

Synthesis of necessary intermediates required for fluorescent marker attachment are given in Supplementary material including their yields, m.p. HPLC purity, ESI+ MS m/z and ^{1}H and ^{13}C NMR data.

4.1.1. C2 fluorescently labeled derivatives

C2-labeled compounds were prepared according to Scheme 3. An appropriate fluorescent label was reacted with amino groups terminating the above mentioned prepared intermediates. Generally, C2-derivatives marked with NBD were prepared as follows: 0.36 mmol of the appropriate intermediate (I, II, III, IV), 1.2 equiv. of NBD-Cl (**1–4**) and 3 equiv. of NaHCO$_3$ were stirred in methanol at 50 °C for one h and then stirred at RT for additional 16 h. Afterwards, the solvent was evaporated under reduced pressure and the residue treated with ice cold water (5 mL). The resulting solid material was filtered, washed with ice cold water (4 x 1 mL) and then dried at 50 °C. The crude material was purified by silica column chromatography using CHCl$_3$/MeOH (4:1) as the mobile phase,

starting from pure chloroform with a methanol gradient.

1 : N^6-(3-methylbut-2-en-1-yl)-N^2-{2-[(7-nitrobenzo[c][1,2,5]oxa-diazol-4-yl)amino]ethyl}-9H-purine-2,6-diamine: Reddish solid; yield 74%.
2 : N^6-(3-methylbut-2-en-1-yl)-N^2-{6-[(7-nitrobenzo[c][1,2,5]oxa-diazol-4-yl)amino]hexyl}-9H-purine-2,6-diamine: Reddish solid; yield 65%.
3 : N^6,N^6-dimethyl-N^2-{2-[(7-nitrobenzo[c][1,2,5]oxadiazol-4-yl)amino]ethyl}-9H-purine-2,6-diamine: Reddish solid; yield 81%.
4 : N^6,N^6-dimethyl-N^2-{6-[(7-nitrobenzo[c][1,2,5]oxadiazol-4-yl)amino]hexyl}-9H-purine-2,6-diamine (**4**): Reddish solid; yield 75%.

C2-derivatives marked with DS-Cl were prepared as follows: 0.36 mmol of I, II, III or IV and Et$_3$N (2 equiv.) were dissolved in dry MeOH (0.4 mL) and dry DCM (3 mL) under an argon atmosphere and added to a mixture of DS-Cl (1.5 equiv.) in DCM (2 mL). The reaction mixture was protected against light and stirred at RT for 16 h. Afterwards, the solvents were removed under reduced pressure, the residue was treated with ice cold water (5 mL) and then kept at 4 °C for 2 h. The resulting solid material was filtered, washed with 5% NaHCO$_3$ (3x 1 mL), ice cold water (5 x 1 mL) and dried in a desiccator over 4 Å molecular sieve. The crude material was purified by silica column chromatography using CHCl$_3$ - MeOH as the mobile phase with methanol gradient.

5 : 5-(dimethylamino)-N-[2-({6-[(3-methylbut-2-en-1-yl)amino]-9H-purin-2-yl}amino)ethyl] naphthalene-1-sulfonamide: Pale yellow solid, yield 64%.
6 : 5-(dimethylamino)-N-[6-({6-[(3-methylbut-2-en-1-yl)amino]-9H-purin-2-yl}amino)hexyl] naphthalene-1-sulfonamide: Pale yellow solid, yield 52%.
7 : 5-(dimethylamino)-N-(2-{[6-(dimethylamino)-9H-purin-2-yl]amino}ethyl)naphthalene-1-sulfonamide: Pale yellow solid.
8: 5-(dimethylamino)-N-(6-{[6-(dimethylamino)-9H-purin-2-yl]amino}hexyl)naphthalene-1-sulfonamide: Pale yellow solid, yield 63%.

C2- derivatives marked with coumarin was prepared as follows: 0.208 mmol)of coumarin-3-carboxylic acid and NHS (1 equiv.) were dissolved under an argon atmosphere in dry MeCN (6 mL) at 45 °C. DCC (1.16 equiv.) was added and the resulting mixture heated at 45 °C for 1 h, then stirred at RT for 20 h. Next, the solid was filtered off and washed carefully with dry MeCN (3 x 5 mL). Coumarin-3-carboxylic acid NHS ester: white solid, yield 90%.^{1}H NMR (300 MHz, DMSO-d_6) δ (ppm): 2.89 (s, 4H), 7.43−7.50 (m, 2H), 7.83 (t, J = 7.2 Hz, 1H), 8.03 (d, J = 7.9 Hz, 1H), 9.13 (s, 1H). A solution of N-hydroxysuccinimidyl coumarin-3-carboxylic acid ester (0.208 mmol) in MeCN (4 mL) was dropwise added to **I, II, III** or **IV** (1 equiv.) dissolved in a mixture of carbonate buffer pH 8.6 (2 mL) and DMSO (2 mL). The reaction mixture was protected against light and stirred under an argon atmosphere at RT for 20 h. After dilution with cold water (5 mL) and storing at 4 °C for 2 h, a solid compound was formed. The crude material was purified by silica column chromatography using CHCl$_3$/MeOH as the mobile phase with methanol gradient.

9 : N-[2-({6-[(3-methylbut-2-en-1-yl)amino]-9H-purin-2-yl}amino)ethyl]-2-oxo-2H-chromene-3-carboxamide: pale yellow solid, yield 92%.
10 : N-[6-({6-[(3-methylbut-2-en-1-yl)amino]-9H-purin-2-yl}amino)hexyl]-2-oxo-2H-chromene-3-carboxamide (10): Pale yellow solid, yield 64%.

11 : N-(2-{[6-(dimethylamino)-9H-purin-2-yl]amino}ethyl)-2-oxo-2H-chromene-3-carboxamide: pale yellow solid, yield 69%.
12: N-(6-{[6-(dimethylamino)-9H-purin-2-yl]amino}hexyl)-2-oxo-2H-chromene-3-carboxamide: pale yellow solid, yield 63%.

C2-derivatives marked with DEAC were prepared as follows: DEAC-OH (0.208 mmol) and NHS (1.04 equiv.) were dissolved under an argon atmosphere in dry MeCN (6 mL) at 45 °C. DCC (1.16 equiv.) was added and the arising mixture was heated at 45 °C for 1 h and then stirred at RT for 20 h. The arising solid was filtered off and the filtrate was evaporated under reduced pressure to give the NHS ester of DEAC-OH: a yellow solid. A solution of N-hydroxysuccinimidyl DEAC-OH ester (1 equiv.) in MeCN (4 mL) was dropwise added to a solution of I, II, III, IV (1 equiv.) dissolved in a mixture of carbonate buffer pH 8.6 (2 mL) and DMSO (2 mL). The reaction mixture was protected against light and stirred under an argon atmosphere at RT for 20 h. After dilution with cold water (5 mL) and storing at 4 °C for 2 h, a solid was formed. The crude material was purified by silica column chromatography using CHCl$_3$/MeOH as the mobile phase with methanol gradient.

13 : 7-(diethylamino)-N-[2-({6-[(3-methylbut-2-en-1-yl)amino]-9H-purin-2-yl}amino)ethyl]-2-oxo-2H-chromene-3-carboxamide: pale yellow solid, yield 61%.
14 : 7-(diethylamino)-N-[6-({6-[(3-methylbut-2-en-1-yl)amino]-9H-purin-2-yl}amino)hexyl]-2-oxo-2H-chromene-3-carboxamide: pale yellow solid, yield 72%.
15 : 7-(diethylamino)-N-(2-{[6-(dimethylamino)-9H-purin-2-yl]amino}ethyl)-2-oxo-2H-chromene-3-carboxamide: pale yellow solid, yield 48%.
16: 7-(diethylamino)-N-(6-{[6-(dimethylamino)-9H-purin-2-yl]amino}hexyl)-2-oxo-2H-chromene-3-carboxamide (**16**): pale yellow solid, yield 52%.

C2-derivatives marked with rhodamine B were prepared as follows: The compound was prepared according to a slightly modified procedure described in the literature (Meng et al., 2007). Briefly, 0.209 mmol of rhodamine B and 0.109 mmol of N-hydroxysuccinimide were dissolved in 3 mL of dry acetonitrile at 45°C1,16 equiv. of DCC in 1 mL of acetonitrile was added and the reaction mixture heated at 45 °C for one h and then stirred at RT for 20 h. The solid was filtered off and the filtrate was evaporated under reduced pressure to give NHS rhodamine B ester: a dark green metallic solid. Afterwards, a solution of NHS rhodamine B ester in MeCN (1 mL) was dropwise added to a solution of 1 equiv. of **I, II, III** or **IV** in 1 mL of carbonate buffer (pH = 8.6). The reaction mixture was stirred at RT for 4 h and then cooled in an ice bath. The obtained solid was filtered off, washed with cold MeCN, cold water and dried at 50 °C.

17 : 3′,6′-bis(diethylamino)-2-{2-[(6-((3-methylbut-2-en-1-yl]amino}-9H-purin-2-yl)amino) ethyl}spiro[isoindoline-1,9′-xanthen]-3-one: pink solid; yield 99%.
18 : 3′,6′-bis(diethylamino)-2-{2-[(6-((3-methylbut-2-en-1-yl]amino}-9H-purin-2-yl)amino hexyl)-spiro[isoindoline-1,9′-xanthen]-3-one: pink solid; yield 99%.
19 : 3′,6′-bis(diethylamino)-2-(2-{[6-(dimethylamino)-9H-purin-2-yl)amino]ethyl}spiro-[isoindoline-1,9′-xanthen]-3-one: pink solid, yield 73%.
20: 3′,6′-bis(diethylamino)-2-(2-{[6-(dimethylamino)-9H-purin-2-yl]amino}hexyl)spiro-[isoindoline-1,9′-xanthen]-3-one: pink solid; yield 86%.

C2-derivatives marked with FITC were prepared as follows: 1 equiv. of FITC was added to a mixture of **I**, **II**, **III** or **IV** (0.136 mmol) and Et₃N (2.76 equiv.) in dry MeOH (2 mL) under an argon atmosphere. The reaction mixture was protected against light and stirred at RT for 20 h. Afterwards, the solvent was evaporated under reduced pressure, the residue was re-suspended in acetate buffer (pH 4.0, 5 mL) and then kept at 4 °C for 1 h. The resulting solid material was filtered, washed with acetate buffer pH 4.0 (5 x 1 mL) followed by water (5 x 2 mL) and dried at 50 °C.

21 :   *2-(6-hydroxy-3-oxo-3H-xanthen-9-yl)-5-{3-[2-({6-[(3-methylbut-2-en-1-yl)amino]-9H-purin-2-yl}amino)ethyl]thioureido}benzoic acid*: orange solid; yield 95%.
22 :   *2-(6-hydroxy-3-oxo-3H-xanthen-9-yl)-5-{3-[6-({6-[(3-methylbut-2-en-1-yl)amino]-9H-purin-2-yl}amino)hexyl]thioureido}benzoic acid*: orange solid; yield 98%.
23 :   *5-[3-(2-{[6-(dimethylamino)-9H-purin-2-yl]amino}ethyl)thioureido]-2-(6-hydroxy-3-oxo-3H-xanthen-9-yl)benzoic acid*: orange solid; yield: 98%.
24: *5-[3-(6-{[6-(dimethylamino)-9H-purin-2-yl]amino}hexyl)thioureido]-2-(6-hydroxy-3-oxo-3H-xanthen-9-yl)benzoic acid*: orange solid, yield: 98%.

4.1.2. N9 fluorescently labeled derivatives

N9 labeled compounds were prepared according to Scheme 4 and given below:

4.1.2.1. 5-(Dimethylamino)-N-{2-[6-((3-methylbut-2-en-1-yl]amino}-9H-purin-9-yl)ethyl)naphthalene-1-sulfonamide (**25**).
Compound **25** was prepared according to a procedure described in the literature (Bartzatt, 2001). Briefly, a solution of DS-Cl (1.2 equiv.) in acetone (2 mL) was added to a solution of V (0.406 mmol) dissolved in a mixture of water (5.5 mL) and 2 M Na₂CO₃ (2 mL). The flask was protected from light and the reaction mixture was stirred at RT overnight. The mixture was then extracted with diethyl ether (3 x 10 mL). The combined organic layers were washed with water (2 x 5 mL) followed by brine (2 x 5 mL), dried over Na₂SO₄ and concentrated *in vacuo*. The product was purified by silica flash column chromatography using CHCl₃/MeOH (9:1) as the mobile phase. Pale yellow solid; yield 65%.

4.1.2.2. 2-(6-Hydroxy-3-oxo-3H-xanthen-9-yl)-4-[3-(2-{6-[(3-methylbut-2-en-1-yl)amino]-9H-purin-9-yl}ethyl)thioureido]benzoic acid (**26**).
Compound **V** (0.406 mmol) was stirred in MeOH (3 mL) with FITC (1.1 equiv.) in the presence of NaHCO₃ (3 equiv.) at a temperature of 50 °C for 1 h. The pH of the reaction mixture was adjusted to pH 4 by adding 1 M HCl. The resulting orange solid was filtered and then washed with MeOH. The pure compound was obtained after flash chromatography using CHCl₃/MeOH (4:1) as the mobile phase. Orange solid: yield 65%.

4.1.2.3. 3′,6′-Bis(diethylamino)-2-(2-(6-((3-methylbut-2-en-1-yl)amino)-9H-purin-9-yl)ethyl)spiro[isoindoline-1,9′-xanthen]-3-one (**27**).
A solution of *NHS* rhodamine B ester (1 equiv.) dissolved in MeCN (1 mL) was dropwise added to a solution of iP (0.105 mmol) dissolved in carbonate buffer pH 8.6 (1 mL). The resulting mixture was stirred at RT for 4 h and then cooled to form pink solid; yield 25%.

4.1.2.4. N⁶-(3-Methylbut-2-en-1-yl)-N⁹-{2-[(7-nitro-2,1,3-benzoxadiazol-4-yl)amino]ethyl}-9H-purin-6-amine hydrochloride (**28**) and N⁶-(dimethylamino)-N⁹-{2-[(7-nitro-2,1,3-benzoxadiazol-4-yl)amino]ethyl}-9H-purin-6-amine (**29**).
Compounds **28** and **29** were prepared according to a protocol described in the literature (Bem et al., 2007). Briefly, **V or VI** (0.39 mmol) was dissolved in MeOH (3 mL) containing 4-chloro-7-nitrobenzofurazan (1.1 equiv.) in the presence of NaHCO₃ (2.5 equiv.) at a temperature of 50 °C for 1 h. The reaction mixture was cooled in an ice bath and 1 M HCl was added dropwise up to the formation of an orange solid. The resulting solid was filtered, washed with ice cold MeOH (3 x 1 mL) followed by ice cold water (4 x 1 mL) and dried at 50 °C. **28**: reddish solid; yield 52%, **29**: a reddish solid; yield 75%.

4.1.2.5. 3,3-Dimethyl-1-{6-[(2-{6-[(3-methylbut-2-en-1-yl)amino]-9H-purin-9-yl}ethyl)amino]-6-oxohexyl}-2-[(1E,3E)-5-((E)-1,3,3-trimethylindolin-2-ylidene)penta-1,3-dien-1-yl]-3H-indole(**30**).
Compound **V** (16.2 μmol) was dissolved in 0.1 M sodium bicarbonate solution (4.5 mL, pH 8.5) to which was added cyanine 5 NHS (1 equiv.) dissolved in amine free DMF (0.5 mL). The reaction mixture was stirred at RT for 4 h and then lyophilized overnight. The resulting residue was dissolved in water (5 mL) and extracted using EtOAc (3 x 5 mL). The product was purified by semi-preparative HPLC. Dark blue solid; yield 50%.

4.2. Live cell hormone binding assays

Receptor direct binding assays were conducted using the *E. coli* strain KMI001 harboring the plasmid pIN-III containing a coding sequence for the cytokinin receptor CRE1/AHK4 (Yonekura-Sakakibara et al., 2004) or ZmHK1 (Podlešáková et al., 2012 or the plasmid pSTV28 containing a coding sequence for AHK3 (Suzuki et al., 2001; Yamada et al., 2001). Bacterial strains were kindly provided by Dr. T. Mizuno (Nagoya, Japan). The assays were performed according to a published procedure (Nisler et al., 2010). The competition reaction of the tested compounds was allowed to proceed with 2 nM 2-[³H]tZ. Labeled *t*Z was provided by the Isotope Laboratory, Academy of Sciences, Czech Republic.

4.3. ZmHK1 receptor activation assay

The assay was performed with *E. coli* strain KMI001 harboring the plasmid pIN-III containing a coding sequence for the cytokinin receptor ZmHK1 according to a previously published protocol (Spíchal et al., 2009; Podlešáková et al., 2012).

4.4. ARR5:GUS reporter gene assay

The assay was performed according to a published protocol (Romanov et al., 2005).

4.5. Confocal laser scanning microscopy

Cell suspension culture of *Arabidopsis thaliana* ecotype Landsberg *erecta* were cultivated under continuous darkness at 23 °C on a rotary shaker with subculture intervals of 3 days in 1 x Murashige and Skoog (MS) medium (Duchefa) containing 3% (w/v) sucrose. Fluorescent probes at concentration of 5 μM were used for *in situ* staining procedure − stained cells in MS medium were immediately mounted onto microscope slides, with a cover slip, and observed with a Zeiss 710 CLSM platform (Carl Zeiss, Jena, Germany) equipped with Plan-Apochromat 40x/1.4 Oil (Carl Zeiss, Germany) objective, using excitation laser 458 nm and 514 nm and emission filters 501−573 nm and 531−703 nm for NBD-based and rhodamine B-based fluoroprobes, respectively. The post-processing of images was done using ZEN 2010 software, Photoshop 6.0/CS, and Microsoft PowerPoint.

Acknowledgements

Appendix A. Supplementary data

Supplementary data related to this article can be found at https://doi.org/10.1016/j.phytochem.2018.02.015.

References

Asami, T., Tao, L., Yamamoto, S., Robertson, M., Min, Y.K., Murofushi, N., Yoshida, S., 1997. Fluorescence-labeled abscisic acid possessing abscisic acid-like activity in barley aleurone protoplasts. Biosci., Biotech. Bioch 61, 1198–1199.

Bartzatt, R., 2001. Dansylation of hydroxyl and carboxylic acid functional groups. J. Pharmacol. Toxicol. 45, 247–253.

Bem, M., Badea, F., Draghici, C., Caprolu, M.T., Vasilescu, M., Voicescu, M., Beteringhe, A., Caragheorgheopol, A., Maganu, M., Constantinescu, T., Balaban, A.T., 2007. Synthesis and fluorescent properties of new derivatives of 4-amino-7-nitrobenzofurazan. Arkivoc 8, 87–104.

Caesar, K., Thamm, A.M., Witthöft, J., Elgass, K., Huppenberger, P., Grefen, C., Horak, J., Harter, K., 2011. Evidence for the localization of the Arabidopsis cytokinin receptors AHK3 and AHK4 in the endoplasmic reticulum. J. Exp. Bot. 62, 5571–5580.

Chattopadhyay, A., 1990. Chemistry and biology of N-(7-nibrobenz-2-oxa-1,3-diazol-4-yl)-labeled lipids: fluorescent probes of biological and model membranes. Physiol. Rev. 90, 1103–1163.

D'Agostino, I.B., Deruère, J., Kieber, J.J., 2000. Characterization of the response of the Arabidopsis response regulator gene family to cytokinin. Plant Physiol. 124, 1706–1717.

Daly, C.J., McGrath, J.C., 2003. Fluorescent ligands, antibodies, and proteins for the study of receptors. Pharmacol. Ther. 100, 101–118.

Davies, P.J., 2007. The nature, occurrence and effects of plant hormones cytokinins (CKs). In: Davies, P.J. (Ed.), Plant Hormones, Biosynthesis, Signal Transduction, Action!, vol. 3. Kluwer Academic Publisher, Dordrecht, pp. 7–8.

Doskočilová, A., Kohoutová, L., Volc, J., Kourová, H., Benada, O., Chumová, J., Plíhal, O., Petrovská, B., Halada, P., Bögre, L., Binarová, P., 2013. NITRILASE1 regulates the exit from proliferation, genome stability and plant development. New Phytol. 198, 685–698.

Du, L., Jiao, F., Chu, J., Jin, G., Chen, M., Wu, P., 2007. The two-component signal system in rice (Oryza sativa L.): a genome-wide study of cytokinin signal perception and transduction. Genomics 89, 697–707.

Gonzalez-Rizzo, S., Crespi, M., Frugier, F., 2006. The Medicago truncatula CRE1 cytokinin receptor regulates lateral root development and early symbiotic interaction with Sinorhizobium meliloti. Plant Cell 18, 2680–2683.

Hamaguchi, N., Iwamura, H., Fujita, T., 1985. Fluorescent anticytokinins as a probe for binding. Eur. J. Biochem. 153, 565–572.

Hayashi, K., Shouichi, N., Shiho, F., Takeshi, N., Jenness, M.K., Murphy, A.S., Motose, H., Nozaki, H., Furutani, M., Aoyama, T., 2014. Auxin transport sites are visualized in planta using fluorescent auxin analogs. Proc. Natl. Acad. Sci. U. S. A. 111, 11557–11562.

Hiratsuka, T., Kato, T., 1987. A fluorescent analog of colcemid, N-(7-nitrobenz-2-oxa-1,3-diazol-4-yl)-colcemid, as a probe for the colcemid binding sites of tubulin and microtubules. J. Biol. Chem. 13, 6318–6322.

Hothorn, M., Dabi, T., Chory, J., 2011. Structural basis for cytokinin recognition by Arabidopsis thaliana histidine kinase 4. Nat. Chem. Biol. 7, 766–768.

Inoue, T., Higuchi, M., Hashimoto, Y., Seki, M., Kobayashi, M., Kato, T., Tabata, S., Shinozaki, K., Kakimoto, T., 2001. Identification of CRE1 as a cytokinin receptor from Arabidopsis. Nature 409, 1060–1063.

Irani, N.G., Di Rubbo, S., Mylle, E., Van den Begin, J., Schneider-Pizoń, J., Hniliková, J., Šíša, M., Buyst, D., Vilarrasa-Blasi, J., Szatmári, A.M., Van Damme, D., Mishev, K., Codreanu, M.C., Kohout, L., Strnad, M., Caño-Delgado, A.I., Friml, J., Madder, A., Russinova, E., 2012. Fluorescent castasterone reveals BRI1 signaling from the plasma membrane. Nat. Chem. Biol. 8, 583–589.

Lace, B., Prandi, K., 2016. Shaping small bioactive molecules to untangle their biological function: a focus on fluorescent plant hormones. Mol. Plant 9, 1099–1118.

Lavis, L.D., Raines, R.T., 2008. Bright ideas for chemical biology. ACS Chem. Biol. 3, 142–155.

Lavis, L.D., Rutkoski, T.J., Raines, R.T., 2007. Tuning the pKa of fluorescein to optimize binding assays. Anal. Chem. 79, 6775–6782.

Leopoldo, M., Lacivita, E., Berardi, F., Perrone, R., 2009. Developments in fluorescent probes for receptor research. Drug Discov. Today 14, 706–712.

Liu, S., Wang, W.H., Dang, Y.L., Fu, Y., Sang, R., 2012. Rational design and efficient synthesis of a fluorescent-labeled jasmonate. Tetrahedron Lett. 53, 4235–4239.

Mason, W.T., 1999. Fluorescent and Luminescent Probes for Biological Activity. A Practical Guide to Technology for Quantitative Real-time Analysis, vol. 2. Academic Press.

McGrath, J.C., Arribas, S., Daly, C.J., 1996. Fluorescent ligands for the study of receptors. Trends Pharmacol. Sci. 17, 393–399.

Meng, Q., Yu, M., Zhang, H., 2007. Synthesis and application of N-hydroxysuccinimidyl rhodamine B ester as an amine-reactive fluorescent probe. Dyes Pigm 73, 254–260.

Murray, J.D., Karas, B.J., Sato, S., Tabata, S., Amyot, L., Szczyglowski, K., 2007. A cytokinin perception mutant colonized by Rhizobium in the absence of nodule organogenesis. Science 315, 101–104.

Nishikawa, S., Kurono, M., Shibayama, K., Okuno, S., Inagaki, M., Kashimura, N., 2000. Synthesis and cytokinin activity of fluorescent 7-phenylethynylimidazo [4,5-d]pyridine and its riboside. J. Agric. Food Chem. 48, 2559–2564.

Nisler, J., Zatloukal, M., Popa, I., Doležal, K., Strnad, M., Spíchal, L., 2010. Cytokinin receptor antagonists derived from 6-benzylaminopurine. Phytochem 71, 1052–1062.

Ovečka, M., Takáč, T., Komis, G., Vadovič, P., Bekešová, S., Doskočilová, A., Šamajová, V., Luptovčiak, I., Šamajová, O., Schweighofer, A., Meskiene, I., Jonak, C., Křenek, P., Lichtscheidl, I., Škultéty, L., Hirt, H., Šamaj, J., 2014. Salt-induced subcellular kinase relocation and seedling susceptibility caused by overexpression of Medicago SIMKK in Arabidopsis. J. Exp. Bot. 65, 2335–2350.

Plíhalová, L., Vylíčilová, H., Doležal, K., Zahajská, L., Zatloukal, M., Strnad, M., 2016. Synthesis of aromatic cytokinins for plant biotechnology. New Biotech. 33 (Part: B), 614–624.

Podlešáková, K., Zalabák, D., Čudejková, M., Plíhal, O., Szücová, L., Doležal, K., Spíchal, L., Strnad, M., Galuszka, P., 2012. Novel cytokinin derivatives do not show negative effects on root growth and proliferation in submicromolar range. PLoS ONE 7, e39293.

Prandi, C., Rosso, H., Lace, B., Occhiato, E.G., Oppedisano, A., Tabasso, S., Alberto, G., Blangetti, M., 2013. Strigolactone analogs as molecular probes in chasing the (SLs) receptor/s: design and synthesis of fluorescent labeled molecules. Mol. Plant 6, 113–127.

Pulici, M., Asami, T., Robertson, M., Seto, H., Youshida, S., 1996. Amylase induction activity of fluorescein labeled gibberellin in barley aleurone protoplasts. Bioorg. Med. Chem. Lett. 6, 2549–2552.

Romanov, G.A., Spíchal, L., Lomin, S.N., Strnad, M., Schmülling, T., 2005. A live cell hormone-binding assay on transgenic bacteria expressing a eukaryotic receptor protein. Anal. Biochem. 347, 129–134.

Šamajová, O., Komis, G., Šamaj, J., 2014. Immunofluorescent localization of MAPKs and colocalization with microtubules in Arabidopsis seedling whole-mount probes. Methods Mol. Biol. 1171, 107–115.

Sjöback, R., Nygren, J., Kubista, M., 1995. Absorption and fluorescence properties of fluorescein. Spectrochim. Acta A 51, 7–21.

Skoog, F., Schmitz, R.Y., Hecht, S.M., Frye, R.B., 1975. Anticytokinin activity of substituted pyrrolo[2,3-d]pyrimidines. Proc. Natl. Acad. Sci. U. S. A. 72, 3508–3512.

Sokolowska, K., Kizinska, J., Szewczuk, Z., Banasiak, A., 2014. Auxin conjugated to fluorescent dyes — a tool for the analysis of auxin. Plant Biol. 16, 866–877.

Specker, M.A., Morrice, A.G., Gruber, B.A., Leonard, N.J., Schmitz, R.Y., Skoog, F., 1976. Fluorescent cytokinins: stretched-out analogues of N^6-benzyladenine and N^6-(Δ^2-isopentenyl)adenine. Phytochemistry 15, 609–613.

Spíchal, L., Werner, T., Popa, I., Riefler, M., Schülling, T., Strnad, M., 2009. The purine derivative PI-55 blocks cytokinin action via receptor inhibition. FEBS J. 276, 244–253.

Suzuki, T., Miwa, K., Ishikawa, K., Yamada, H., Aiba, H., Mizuno, T., 2001. An Arabidopsis histidine-containing phosphotransfer (HPt) factor implicated in phosphorelay signal transduction: overexpression of AHP2 in plants results in hypersensitiveness to cytokinin. Plant Cell Physiol. 42, 107–113.

Tirichine, L., Sandal, N., Madsen, L.H., Radutoiu, S., Albrektsen, A.S., Sato, S., Adamitu, E., Tabata, S., Stougaard, J., 2007. A gain-of-function in a cytokinin receptor triggers spontaneous root nodule organogenesis. Science 315, 104–107.

Tsuda, E., Yang, H., Nishimura, T., Uehara, Y., Sakai, T., Furutani, M., Koshiba, T., Hirose, M., Nozaki, H., Murphy, A.S., Hayashi, K., 2011. Alkoxy-auxins are selective inhibitors of auxin transport mediated by PIN, ABCB and AUX1 transporters. J. Biol. Chem. 286, 2354–2364.

Wulfetange, K., Lomin, S.N., Romanov, G.A., Stolz, A., Heyl, A., Schmülling, T., 2011. The cytokinin receptors of Arabidopsis are located mainly to the endoplasmic reticulum. Plant Physiol. 156, 1808–1818.

Yamada, H., Suzuki, T., Terada, K., Takei, K., Ishikawa, K., Miwa, K., Yamashino, T., Mizuno, T., 2001. The Arabidopsis AHK4 histidine kinase is a cytokinin-binding receptor that transduces cytokinin signals across the membrane. Plant Cell Physiol. 42, 1017–1023.

Yonekura-Sakakibara, K., Kojima, M., Yamaya, T., Sakakibara, H., 2004. Molecular characterization of cytokinin-responsive histidine kinases in maize. Differential ligand preferences and response to cis-zeatin. Plant Physiol. 134, 1654–1661.

Zawadski, P., Slosarek, G., Boryski, J., Wojtaszek, P., 2010. A fluorescence correlation spectroscopy study of ligand interaction with cytokinin-specific binding protein from mung bean. Biol. Chem. 391, 43–53.

Research article

Cytokinin fluoroprobe reveals multiple sites of cytokinin perception at plasma membrane and endoplasmic reticulum.

Kubiasová K., Montesinos J.C., Šamajová O., Nisler J., Mik V., Semerádová H., Plíhalová L., Novák O., Marhavý P., Cavallari N., Zalabák D., Berka K., Doležal K., Galuszka P., Šamaj J., Strnad M., Benková E., Plíhal O., Spíchal L.

ARTICLE

Cytokinin fluoroprobe reveals multiple sites of cytokinin perception at plasma membrane and endoplasmic reticulum

Karolina Kubiasová [1,8], Juan Carlos Montesinos [2,8], Olga Šamajová [3], Jaroslav Nisler [4,5], Václav Mik [4], Hana Semerádová [2], Lucie Plíhalová [4,5], Ondřej Novák [5], Peter Marhavý [2,6], Nicola Cavallari [2], David Zalabák [1], Karel Berka [7], Karel Doležal [4,5], Petr Galuszka [9], Jozef Šamaj [3], Miroslav Strnad [5], Eva Benková [2✉], Ondřej Plíhal [1,4,5✉] & Lukáš Spíchal [4✉]

Plant hormone cytokinins are perceived by a subfamily of sensor histidine kinases (HKs), which via a two-component phosphorelay cascade activate transcriptional responses in the nucleus. Subcellular localization of the receptors proposed the endoplasmic reticulum (ER) membrane as a principal cytokinin perception site, while study of cytokinin transport pointed to the plasma membrane (PM)-mediated cytokinin signalling. Here, by detailed monitoring of subcellular localizations of the fluorescently labelled natural cytokinin probe and the receptor ARABIDOPSIS HISTIDINE KINASE 4 (CRE1/AHK4) fused to GFP reporter, we show that pools of the ER-located cytokinin receptors can enter the secretory pathway and reach the PM in cells of the root apical meristem, and the cell plate of dividing meristematic cells. Brefeldin A (BFA) experiments revealed vesicular recycling of the receptor and its accumulation in BFA compartments. We provide a revised view on cytokinin signalling and the possibility of multiple sites of perception at PM and ER.

[1] Department of Molecular Biology, Centre of the Region Haná for Biotechnological and Agricultural Research, Faculty of Science, Palacký University, Šlechtitelů 27, 783 71 Olomouc, Czech Republic. [2] Institute of Science and Technology (IST), 3400 Klosterneuburg, Austria. [3] Department of Cell Biology, Centre of the Region Haná for Biotechnological and Agricultural Research, Faculty of Science, Palacký University, Šlechtitelů 27, 783 71 Olomouc, Czech Republic. [4] Department of Chemical Biology and Genetics, Centre of the Region Haná for Biotechnological and Agricultural Research, Faculty of Science, Palacký University, Šlechtitelů 27, 783 71 Olomouc, Czech Republic. [5] Laboratory of Growth Regulators, Institute of Experimental Botany of the Czech Academy of Sciences and Faculty of Science of Palacký University, Šlechtitelů 27, 783 71 Olomouc, Czech Republic. [6] Umeå Plant Science Centre, Department of Forest Genetics and Plant Physiology, Swedish University of Agricultural Sciences, 90183 Umeå, Sweden. [7] Department of Physical Chemistry, Regional Centre of Advanced Technologies and Materials, Faculty of Science, Palacký University, 17. listopadu 1192/12, 771 46 Olomouc, Czech Republic. [8] These authors contributed equally: Karolina Kubiasová, Juan Carlos Montesinos. [9] Deceased: Petr Galuszka. ✉email: eva.benkova@ist.ac.at; ondrej.plihal@upol.cz; lukas.spichal@upol.cz

The plant hormone cytokinin regulates various cell and developmental processes, including cell division and differentiation, embryogenesis, activity of shoot and root apical meristems, formation of shoot and root lateral organs and others[1]. Cytokinins are perceived by a subfamily of sensor histidine kinases (HKs), which via a two-component phosphorelay cascade activate transcriptional responses in the nucleus. Based on the subcellular localization of cytokinin receptors in various transient expression systems, such as leaf epidermal cells of tobacco (*Nicotiana benthamiana*), and membrane fractionation experiments of Arabidopsis and maize, the endoplasmic reticulum (ER) membrane has been proposed as a principal hormone perception site[2–4]. Intriguingly, recent study of the cytokinin transporter PURINE PERMEASE 14 (PUP14) has pointed out that the plasma membrane (PM)-mediated signalling might play an important role in the establishment of cytokinin response gradients in various plant organs[5]. However, localization of cytokinin HK receptors to the PM, although initially suggested[6], remains ambiguous. Here, by monitoring subcellular localizations of the fluorescently labelled cytokinin probe iP-NBD[7], derived from the natural bioactive cytokinin iP, and the cytokinin receptor ARABIDOPSIS HISTIDINE KINASE 4 (CRE1/AHK4) fused to GFP reporter, we show that pools of the ER-located cytokinin fluoroprobes and receptors can enter the secretory pathway and reach the PM. We demonstrate that in cells of the root apical meristem, CRE1/AHK4 localizes to the PM and the cell plate of dividing meristematic cells. Brefeldin A (BFA) experiments revealed vesicular recycling of the receptor and its accumulation in BFA compartments. Our results provide a revised view on cytokinin signalling and the possibility of multiple sites of perception at both PM and ER, which may determine specific outputs of cytokinin signalling.

Results and discussion

Cytokinin fluoroprobe iP-NBD shows affinity to receptors. Fluorescently labelled analogues of phytohormones, including auxin, gibberellin, brassinosteroid and strigolactone, have been successfully used to map the intracellular fate of their receptors in planta[8]. To adopt this tool for mapping subcellular localization of cytokinin receptors, using docking experiments and cytokinin activity screening bioassays, we selected a fluorescently labelled bioactive compound that interacts with the binding site of a cytokinin receptor.

Cytokinin groups a collection of N^6-substituted adenine derivatives, including *trans*-zeatin (*t*Z) and isopentenyladenine (iP). They show different localization pattern and distinct partially overlapping functions in planta. *t*Z-type cytokinins play a role of acropetal messengers, whereas iP-type cytokinins operate as systemic or basipetal messengers[9]. The isoprenoid cytokinins (*t*Z- or iP-types) showed similar distribution patterns in different cell type populations within the root apex[10]. While *t*Z-type cytokinins were detected at much lower levels than other isoprenoid cytokinins, when concerns free cytokinin bases, the *t*Z content was found to be the highest among the free bases, followed by free iP that showed relatively enhanced content also in the stele[10]. Hence, iP seems to be a good candidate for a cytokinin fluoroprobe design. Moreover, iP is a natural cytokinin that cannot be transformed through *O*-glycosylation at the cytokinin side chain and thus the possibility of metabolic conversions of the cytokinin fluoroprobe by cytokinin deactivation enzymes in planta is minimized. Furthermore, covalent attachment of 7-nitro-2,1,3-benzoxadiazole (NBD), a small fluorophore, to the *N*9 position of iP eliminates a risk of a metabolic conversion of the final cytokinin fluorescent probe iP-NBD (Fig. 1a) through *N*-glycosylation, or formation of cytokinin

nucleotides. The stable attachment of the *N*9-substituent also prevents modifications at the *N*7 position by making this CK derivative completely inaccessible for *N*-glucosyltransferases[11]. Docking simulations using the CRE1/AHK4-iP crystal structure[12] and corresponding homology models suggested that iP-NBD may be fully embedded into the active sites of all AHK receptors (Fig. 1b) with micromolar range affinity. The affinity of iP-NBD to cytokinin receptors was measured using bacterially expressed recombinant AHK3 and CRE1/AHK4[13]. Both receptors share ligand preference for *t*Z, but AHK3 has about tenfold lower affinity towards iP compared to CRE1/AHK4[13,14]. Competitive binding assays with *E. coli* expressing either AHK3 or CRE1/AHK4[15] showed that iP-NBD competes for receptor binding with radiolabelled natural cytokinins iP and *t*Z in different ranges of ligand concentrations (Fig. 1c; Supplementary Fig. 1a), corresponding with the receptor ligand preferences. As predicted, iP-NBD had lower affinity to AHK3 (with $K_i \sim 37\,\mu M$ and $>100\,\mu M$ against radiolabelled *t*Z and iP, respectively) than to CRE1/AHK4 (with $K_i \sim 1.4\,\mu M$ and $\sim 31\,\mu M$ against radiolabelled *t*Z and iP, respectively), indicating that this fluoroprobe is more specific to CRE1/AHK4 (Fig. 1c; Supplementary Fig. 1a). Docking into the CRE1/AHK4-iP crystal structure[12] showed that iP-NBD binds into the receptor cavity in a similar manner to iP, but the lack of interaction via *N*9 (which links the fluorescent probe) causes the purine ring shift leading to the larger distance and thus weaker interaction between *N*7 and Asp137 (Fig. 1b). Despite iP-NBD being accommodated into the cytokinin-binding pockets of the receptors, it showed limited ability to trigger cytokinin response in *E. coli* (Δ*rcsC, cps::lacZ*) receptor activation assay[13] (Supplementary Fig. 1b). In Arabidopsis seedlings, iP-NBD in a concentration-dependent manner significantly increased the expression of the early cytokinin response gene *ARABIDOPSIS RESPONSE REGULATOR5* (*ARR5*) already 15 min after its application, suggesting that the synthetic cytokinin fluoroprobe can activate cytokinin signalling pathway in planta (Fig. 1d; Supplementary Fig. 1c). In comparison to iP, a natural cytokinin, iP-NBD triggered cytokinin response with significantly lower efficacy and when applied together with iP no additive effect on the *ARR5* expression could be detected (Fig. 1d). In the *pTCSn:: ntdTomato:TNOS* cytokinin reporter assay[16], iP-NBD did not increase expression of the reporter 6 h after treatment, but when applied simultaneously with iP, iP-NBD partially attenuated iP-mediated enhancement of the TCS reporter expression (Supplementary Fig. 1d). Altogether, these analyses suggest partial agonistic mode of action of iP-NBD that binds to a cytokinin receptor and activates it with only minimal efficacy compared to a natural cytokinin ligand. At excess concentrations, iP-NBD is then acting as a competitive antagonist, competing with the full agonist (a natural cytokinin) for receptor occupancy. Altogether, the above experiments show that iP-NBD binds to cytokinin receptors and has potential for specifically tracking their subcellular localization in planta.

Biological characteristics of iP-NBD. To reliably monitor iP-NBD distribution in planta, we first evaluated its biological stability, fluorescence characteristics and saturation kinetics. iP-NBD stability across the different pH conditions that appear in apoplast, cytosol and different cell organelles was tested in vitro in the pH ranging from 4 to 8 by quantitative liquid chromatography-tandem mass spectrometry (LC-MS/MS). No significant changes of iP-NBD concentration were found in the buffered solutions under both 6 and 16 h of incubation pointing to a broad pH stability of iP-NBD (Supplementary Fig. 2a). Taking into account the chemical structure of iP-NBD that prevents *O*- and/or *N*-glycosylation, the presumed in planta catabolic pathway of this
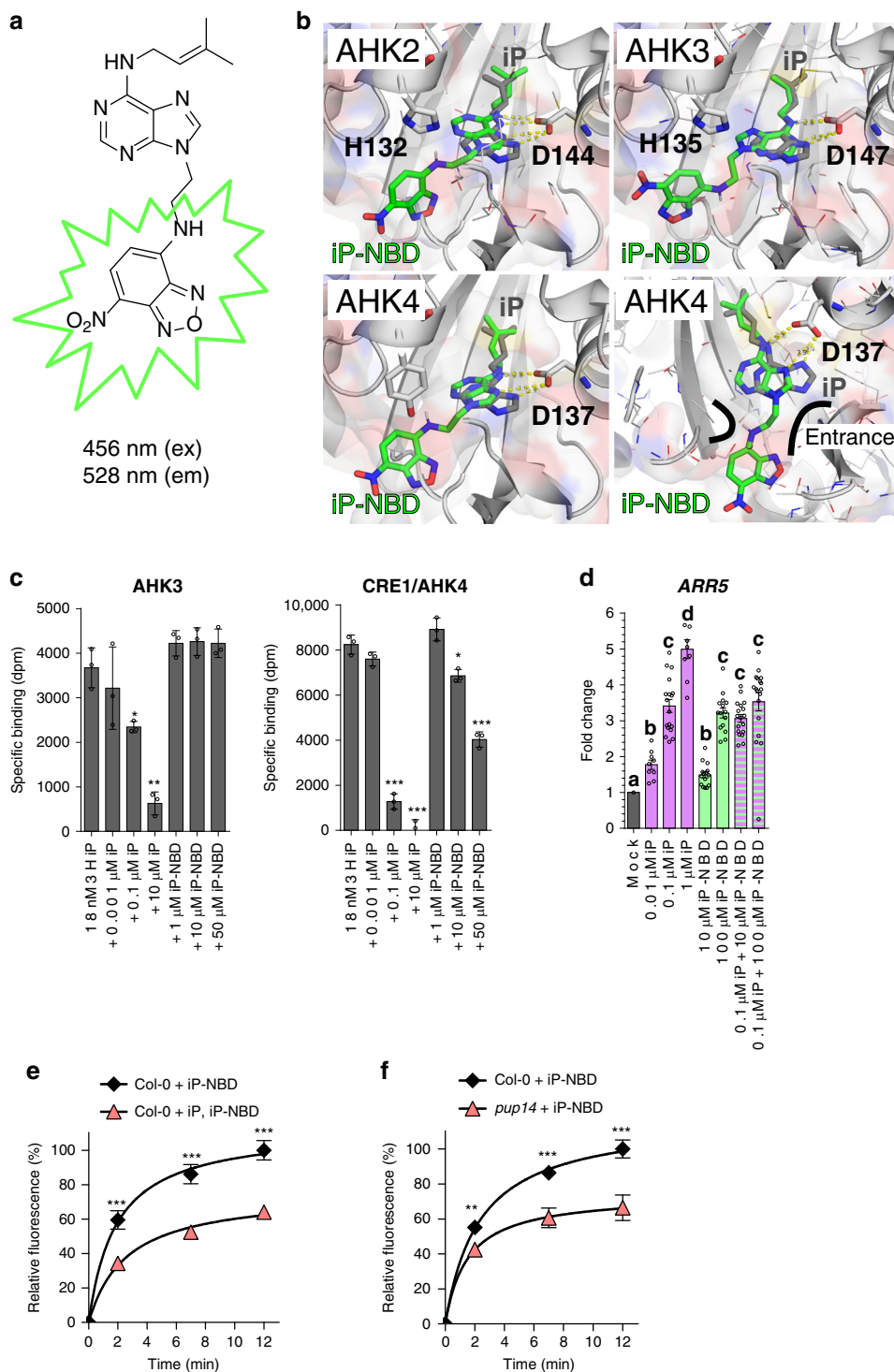
Fig. 1 iP-NBD interacts with cytokinin perception and transport. a Chemical structure of iP-NBD with excitation and emission wavelengths **b** Superposition of docking simulation of iP-NBD (in green) and natural ligand iP (in grey) in AHK2, AHK3 (upper row) and CRE1/AHK4 (left panel of lower row) receptor cavity showing the embedded position of the ligands. CRE1/AHK4 (right panel of lower row) with visualized entrance channel and the fluorophore fitting into an antechamber through the ethylene linker. **c** Competitive binding assay with *Escherichia coli* expressing AHK3 and CRE1/AHK4. Binding of [2-^{3}H]iP (18 and 6 nM in the case of AHK3 and CRE1/AHK4, respectively) was assayed together with increasing concentrations of unlabelled iP and iP-NBD. The bars represent mean ± s.d., ***$p < 0.001$, **$p < 0.01$, *$p < 0.05$; $n = 3$ (Student's t test). **d** Expression of the early cytokinin response gene *ARR5* in 5-day-old seedlings of Col-0 treated with 0.01 μM iP, 0.1 μM iP, 1 μM iP, 10 μM iP-NBD, 100 μM iP-NBD or co-treatments of 0.1 μM iP + 10 μM iP-NBD, 0.1 μM iP + 100 μM iP-NBD or DMSO for 15 min (mean ± s.d., $p < 0.05$ by two-way ANOVA. $n = 9$–18; three technical replicates from three biological replicates per condition). **e** Kinetics of 5 μM iP-NBD uptake in Arabidopsis LRC cells of wild type (Col-0) pre-treated with 5 μM iP. **f** Kinetics of 5 μM iP-NBD uptake in root meristem epidermal cells of wild type (Col-0) and *pup14*. iP-NBD fluorescence was measured in four time points (0, 2, 7 and 12 min). The bars represent mean ± s.d., ***$p < 0.001$, **$p < 0.01$; $n \geq 20$ (Student's t test) (**e**, **f**).

molecule might be N^6 side-chain cleavage by endogenous CYTOKININ OXIDASE/DEHYDROGENASE (CKX) activity. Hence, the in vivo stability of the fluoroprobe was tested. iP-NBD was applied to Arabidopsis cells, and its intracellular processing was followed over a period of 0.5–5 h by LC-MS/MS analysis. Thus, iP-NBD and N9-NBD-labelled adenine (Ade-NBD), the expected product of iP-NBD deprenylation by CKXs, were used as molecular standards. Under these conditions, iP-NBD showed high stability within the first 30 min (≥90% recovery of intact molecule), dropping drastically after 5 h. The concentration of Ade-NBD steadily increased, reaching the maximal concentration after 4 h (Supplementary Fig. 2b). The fact that iP-NBD can be recognized by CKXs as a substrate was confirmed by in vitro enzymatic reaction with AtCKX2, one of the most active CKX isoforms with an apoplastic localization[17]. AtCKX2 converted iP-NBD to the product with approx. six times lower turnover rate k_{cat} compared to the parental iP molecule, but only with 33% lower catalytic efficiency V_{max}/K_m (Supplementary Fig. 2c).

Internalization of iP-NBD follows rapid saturation kinetics. In terms of fluorescent characteristics, the emission maximum of the cytokinin fluoroprobe was in the yellow-green part of the spectrum at 528 nm suitable for co-localization with fluorescent markers emitting at red wavelengths (Supplementary Fig. 2d, f). Quantitative fluorescence microscopy of wild-type plants (Col-0) showed that cellular internalization of iP-NBD followed rapid saturation kinetics, reaching a plateau after approximately 12 min (Fig. 1e). Pre-treatment with non-labelled iP and subsequent application of iP-NBD resulted in a significant reduction of intracellular iP-NBD fluorescence (Fig. 1e). This suggested that transport and/or intracellular binding competition between iP-NBD and the natural cytokinin competitor was taking place, further pointing to the cytokinin-like properties of the iP-NBD molecule. Significantly slower progression of iP-NBD accumulation in cells of a *pup14* mutant (lacking the functional cytokinin transporter PUP14) confirmed that specific cytokinin transport partially accounts for the amount of iP-NBD detected intracellularly (Fig. 1f). Unlike iP-NBD, Ade-NBD, which lacks the cytokinin-specific side chain, has no affinity to the cytokinin receptors (Supplementary Fig. 2e) and exhibited a weak diffused apoplastic and patchy intracellular signal in epidermal cells (Supplementary Fig. 2f).

iP-NBD co-localizes with ER, TGN and early endosomal markers. Affinity of iP-NBD to cytokinin receptors, in particular to CRE1/AHK4, motivated us to monitor subcellular localization of this cytokinin fluoroprobe, aiming to trace potential sites of interaction with the receptor. Two cell types, namely differentiated lateral root cap (LRC) cells and epidermal cells at the root meristematic zone of Arabidopsis root, were selected for in-depth analyses. In a line with reported ER-localization of the AHK cytokinin receptors[2,3], iP-NBD co-localized with p24δ5-RFP, an ER-specific marker, in both cell types (Fig. 2a, b, red arrowheads; Supplementary Table 1). Notably, we also detected strong iP-NBD fluorescence signal in distinct spot-like structures, which did not overlap with the ER reporter (Fig. 2a, b; white arrowheads). Likewise, co-visualization with HDEL-RFP, an ER-specific marker, corroborated dual ER and spot-like localization of iP-NBD in both LRC and epidermal cells (Supplementary Fig. 3a, b).

To further explore the nature of peripheral and spot-like subcellular structures showing affinity to iP-NBD, we performed co-staining with FM4-64, the membrane selective dye labelling PM and endosomal/recycling vesicles in plant cells[18]. In both epidermal and LRC cells, iP-NBD signal was detected intracellularly and

partially co-localized with the FM4-64 stained vesicles corresponding to internalized and recycling endosomes (Fig. 2c, e; Supplementary Fig. 3c). Interestingly, detailed profiles of fluorescence intensity distributions of iP-NBD and FM4-64 revealed their partial co-localization at the PM of epidermal cells, which was not the case for LRC (Fig. 2d compared to Fig. 2f). These observations suggested that apart from ER, iP-NBD might accumulate in subcellular vesicles and at the PM.

To gain further insights into iP-NBD subcellular localization and to test its affinity to endomembrane structures, we analysed the impact of brefeldin A (BFA), a fungal toxin, inhibiting ER-Golgi and post-Golgi trafficking to the PM and to vacuoles, thus causing formation of endosomal clusters, so-called BFA compartments[19]. Strikingly, in root epidermal cells, we observed accumulation of iP-NBD signal in clusters corresponding to BFA compartments stained with FM4-64 (Fig. 2g, blue arrowheads). Co-localization with RabA1e-mCherry, a BFA-sensitive endosome/recycling endosome marker, provided additional supporting evidence that in root epidermal cells iP-NBD exhibits affinity to vesicular endomembrane system where subpopulations of cytokinin receptors may be localized (Supplementary Fig. 3d; Supplementary Table 1). Next, we traced the localization of the cytokinin fluoroprobe using a set of Wave marker lines specific for various subcellular organelles[20]. Notably, in root epidermal cells, we observed a partial co-localization of iP-NBD with a *cis*-Golgi (GA) marker, SYP32-mCherry (Supplementary Fig. 3e; Supplementary Table 1), an integral GA membrane protein, Got1p homologue-mCherry (Supplementary Fig. 3f; Supplementary Table 1), and with TGN/early endosome marker, VTI12-mCherry (Supplementary Fig. 3g; Supplementary Table 1). Interestingly, iP-NBD did not co-localize with a late endosome marker, RabF2b/W2R-mCherry (Supplementary Fig. 3h; Supplementary Table 1) nor with a vacuolar marker, VAMP711-mCherry (Supplementary Fig. 3i; Supplementary Table 1). In cells of LRC, we observed partial co-localization with the GA markers, SYP32-mCherry (Supplementary Fig. 4a; Supplementary Table 1) and Got1p homologue-mCherry (Supplementary Fig. 4b; Supplementary Table 1), an endosome/recycling endosome marker RabA1e-mCherry (Supplementary Fig. 4c; Supplementary Table 1) and with the TGN/early endosomal marker VTI12 (Supplementary Fig. 4d; Supplementary Table 1). However, no co-localization was detected with late endosomal RabF2b-mCherry (Supplementary Fig. 4e; Supplementary Table 1) or vacuolar VAMP711-mCherry markers (Supplementary Fig. 4f; Supplementary Table 1).

Overall, monitoring of iP-NBD in LRC and epidermal cells corroborate the ER as an organelle with affinity to cytokinin. However, co-localization of iP-NBD with TGN and early endosomal markers as well as its accumulation in BFA compartments indicate that proteins with affinity to iP-NBD, such as cytokinin receptors, do not reside exclusively at ER, but may enter the endomembrane trafficking system and possibly localize also to the PM.

Generation and isolation of CRE1/AHK4-GFP transgenic lines. Previously, ER-localization of Arabidopsis cytokinin receptors has been demonstrated using transiently transformed *Nicotiana benthamiana*[2,3] and Arabidopsis[3], and by employing cytokinin-binding assays with fractionated Arabidopsis cells expressing Myc-tagged receptors[2]. However, so far no experimental support has been provided for their possible entry into the subcellular vesicular trafficking and PM localization. Yet, the possibility of cytokinin HKs localization to the PM has been hypothesized within a context of an integrative model for cytokinin perception and signalling[21]. The potential sites of CKs perception had been questioned in relation to the pH dependence of the binding by HKs. It was
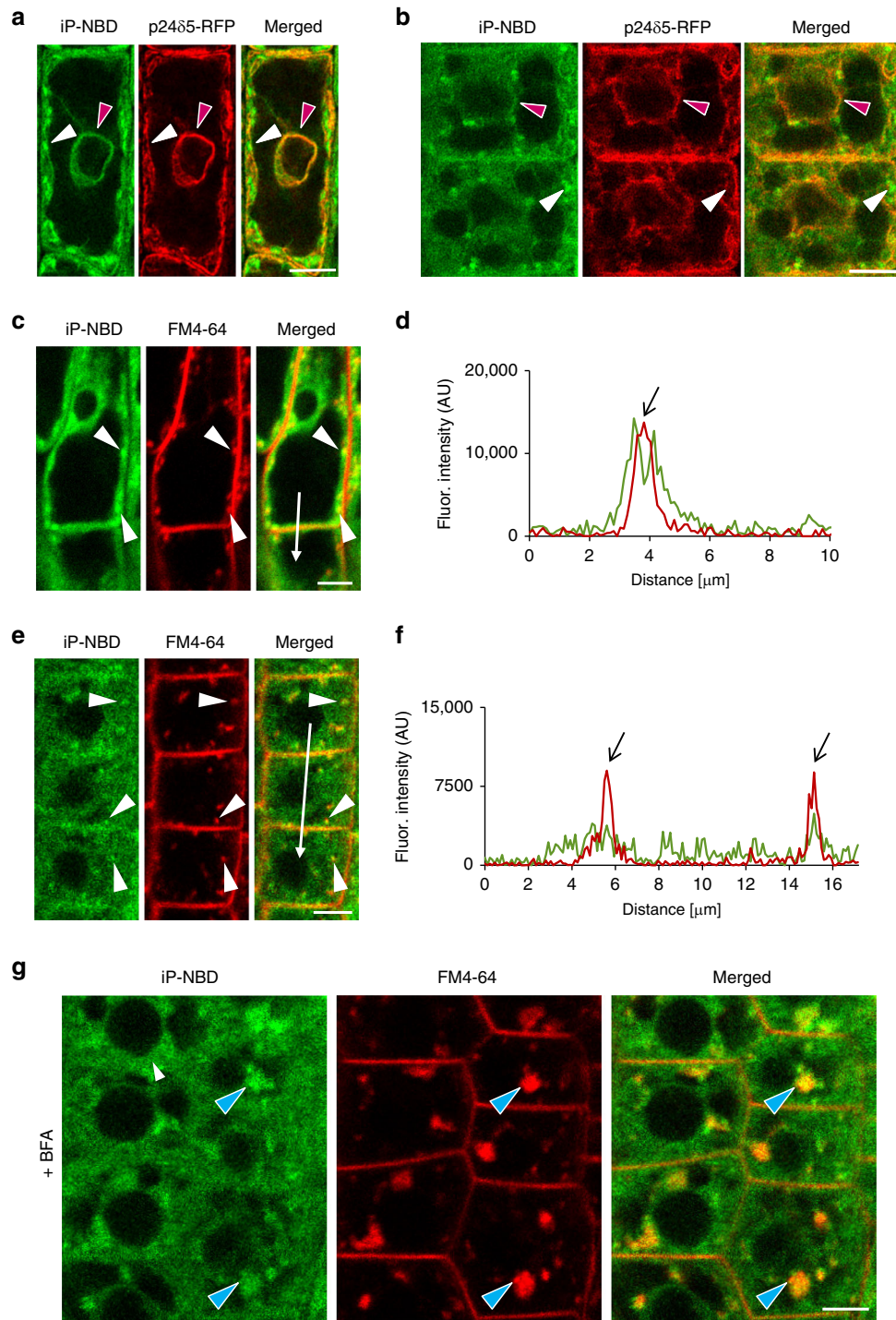
Fig. 2 Monitoring of fluorescently labelled cytokinin iP-NBD in cells of Arabidopsis root. a, b Monitoring of fluorescently labelled cytokinin iP-NBD (green) and ER-marker p24δ5-RFP (red) in LRC cells (**a**) and root meristematic epidermal cells (**b**). iP-NBD detected partially co-localizing with p24δ5-RFP in ER (red arrowheads) and in non-ER cellular structures (white arrowheads). **c–f** Monitoring of iP-NBD (green) and FM4-64 (red, membrane selective dye) in LRC (**c, d**) and root meristematic epidermal cells (**e, f**). White arrowheads (**c, e**) indicate co-localization of iP-NBD and FM4-64 in vesicles. Profiles of fluorescence intensity distribution of both FM4-64 (red line) and iP-NBD (green line) in LRC (**d**) and epidermal (**f**) cells were measured along the white lines (**c, d**) starting from upper end (0 µm) towards the arrowhead. Peaks of FM4-64 fluorescence maxima (black arrows) correlate with the plasma membrane staining. iP-NBD fluorescence maximum does not overlap with FM4-64 fluorescence peak at the plasma membrane in LRC cell (**d**). Peaks of iP-NBD signal partially overlap with FM4-64 maxima and indicate presence of cytokinin fluoroprobe at the plasma membrane of epidermal cells (**f**). **g** Co-localization of iP-NBD and FM4-64 in endosomal compartments (blue arrowheads) formed in root meristematic epidermal cells treated with 50 µM in BFA for 1 h. Scale bars = 5 µm.

shown that CK binding to AHK3 is pH dependent with optimum at basic pH and a dramatic decrease at acidic pH[14]. This finding fits with the ER-localization of CK receptors and has also been used to cast doubt on PM-function of the receptors due to the acidic pH of apoplast acting as a constraint on efficient CK binding. However, in contrary to AHK3, CRE1/AHK4 affinity was shown not to be dramatically altered at acidic pH[14]. Importantly, a recent work by Jaworek et al.[22] shows detailed analysis of pH influence on binding strength of CKs to the receptors from poplar (Populus × canadensis cv. Robusta). They showed that CK binding to PcHK3 (ortholog of AHK3) steadily increases towards higher pH values, whereas binding to PcHK4 (ortholog of CRE1/AHK4) linearly decreased from an optimum for ligand binding at pH 5.5. These findings support the idea that CRE1/AHK4 can effectively sense CKs from the apoplast.

The only cytokinin receptor studied for its localization using stably transformed Arabidopsis plants was AHK3 [3]. Unlike this receptor, subcellular localization of CRE1/AHK4 has not been addressed in much detail. Taking into account a higher affinity of iP-NBD to this receptor, we focused on monitoring its subcellular localization using Arabidopsis stable transgenic lines carrying CRE1/AHK4-GFP construct driven by a constitutive 35S promoter. Two independent lines displaying significantly increased transcription of CRE1/AHK4-GFP when compared to wild type were selected for detailed observations (Supplementary Fig. 5a). Western blot analyses confirmed accumulation of the CRE1/AHK4-GFP product of proper ~150 kDa size in both lines, although lower levels of the fusion protein were detected in the 35S::CRE1/AHK4-GFP line (1) when compared to the line (2) (Supplementary Fig. 5b, c). To test the functionality of the CRE1/AHK4-GFP fusion protein, we performed transient expression assays in Arabidopsis protoplasts. Co-expression of 35S::CRE1/AHK4-GFP with a cytokinin sensitive reporter TCS::LUCIFERASE (TCS::LUC) resulted in 85 ± 6.9-fold upregulation of the reporter activity by cytokinin when compared to protoplasts co-transformed with controls (plasmids carrying either GFP or GUS reporter only resulting in 28 ± 2.4- and 32 ± 1.5-fold increase of LUCIFERASE activity, respectively) (Supplementary Fig. 5d). In planta, functionality of the CRE1/AHK4-GFP was tested by expression analyses of the type-A early cytokinin response genes in the 35S::CRE1/AHK4-GFP transgenic lines. Application of cytokinin resulted in strong upregulation of ARR5 and ARR7 in wild type and both transgenic lines expressing CRE1/AHK4-GFP (Supplementary Fig. 5e). However, a significantly enhanced transcription of ARR5 and ARR7 in response to cytokinin compared to wild type was detected only in 35S::CRE1/AHK4-GFP line (2), which displayed a higher accumulation of CRE1/AHK4-GFP. ARR5 and ARR7 have been reported as being among the most sensitive type-A early cytokinin response genes, reaching expression maxima within 10–15 min following cytokinin application[23]. We argued that a high responsiveness of these genes to cytokinin might hinder detection of more subtle changes in cytokinin sensitivity in line with lower expression of the CRE1/AHK4-GFP. When compared to ARR5 and ARR7, ARR16 showed maximum transcription within 40–60 min following cytokinin application[23]. A significantly higher expression of ARR16 after cytokinin application for 15 min was detected in both CRE1/AHK4-GFP overexpressing lines when compared to wild type. These results suggest that proportionally with levels of CRE1/AHK4-GFP expression, the sensitivity of both lines to cytokinin stimulus is enhanced (Supplementary Fig. 5e), indicating that CRE1/AHK4-GFP maintains its biological activity.

Transgenic Arabidopsis lines expressing CRE1/AHK4-GFP exhibited phenotypes typical of plants with enhanced activity of cytokinin such as a shorter primary root, slower root growth rate and decreased lateral root density (Supplementary Fig. 5f–i). Both transgenic lines expressing CRE1/AHK4-GFP displayed hypersensitive-like responses to exogenous cytokinin treatment on the primary root growth compared to the wild-type control, and in contrast to cytokinin insensitive ahk4/cre1-2 loss-of-function mutant (Supplementary Fig. 5j).

CRE1/AHK4-GFP co-localizes with the ER and the PM markers. As previously reported and in line with iP-NBD subcellular localization, CRE1/AHK4-GFP in LRC and epidermal cells of root apical meristem co-localized with ER marker p24δ5-RFP (Fig. 3a–c, red arrowheads). Intriguingly, in epidermal cells of the root meristematic zone, CRE1/AHK4-GFP signal at the PM area, not co-localizing with ER reporter, could also be detected (Fig. 3d, e). Subsequent analysis revealed strong overlap of CRE1/AHK4-GFP with the PM reporter PIP1;4-mCherry and NPSN12-mCherry (Fig. 4a–d), thus hinting at localization of the cytokinin receptor at the PM. Moreover, in dividing meristematic cells CRE1/AHK4-GFP could also be detected at the expanding cell plate (Fig. 4c–f, asterisks) while it co-localized there with established cell plate vesicular marker FM4-64 (Fig. 4e, f). Importantly, it has been shown that during cytokinesis the cell plate might receive material both from post-Golgi compartments as well as from the PM through sorting and recycling endosomes[24]. Hence, detection of CRE1/AHK4-GFP at the cell plate provides further supporting evidence that the cytokinin receptor might reside outside of ER, namely on cytokinetic vesicles forming cell plate[25]. Further evidence confirming localization of CRE1/AHK4-GFP to the PM resulted from the subcellular study using super-resolution structural illumination microscopy (SIM)[26]. This SIM analysis revealed co-localization of CRE1/AHK4-GFP with FM4-64 labelled PM with average Pearson's coefficient 0.345 ± 0.113 (n = 30; Fig. 4g; Supplementary Fig. 6a). Unlike epidermal cells of the root meristematic zone, in LRC cells the CRE1/AHK4-GFP signal resided in the ER and no co-localization with a PM reporter (NPSN12-mCherry) could be detected (Supplementary Fig. 6b, c). Inhibition of endocytic trafficking and vesicular recycling in meristematic cells by BFA resulted in co-accumulation of CRE1/AHK4-GFP and FM4-64 in the BFA compartments in line with the presence of the receptor in the endomembrane system (Fig. 4h). Wash-out of BFA allowed re-localization of the cytokinin receptor back to the PM indicating that it might cycle between PM and TGN (Supplementary Fig. 6d). Although occasionally in some cells of LRC co-staining with FM4-64 revealed CRE1/AHK4-GFP in BFA compartments, they were relatively rare and randomly scattered in some LRC cells indicating that CRE1/AHK4-GFP trafficking in differentiated cells of LRC might differ from that observed in epidermal cells of root apical meristem (Supplementary Fig. 6e). Importantly, no accumulation of the ER marker p24δ5-RFP in the BFA compartments in either epidermal cells of meristem (Fig. 4i) or LRC cells (Supplementary Fig. 6f) could be detected, suggesting that CRE1/AHK4-GFP signal is specifically enriched in the BFA bodies and not related to structural changes of ER in BFA-treated cells.

Altogether, these results indicate that in LRC cells CRE1/AHK4 may reside preferentially at the ER, whereas in epidermal cells of the root apical meristem the cytokinin receptor can enter the endomembrane system and localizes both at the ER and at the PM.

To further explore whether cytokinin receptor might occupy different subcellular location in cells at distinct stage of differentiation, we monitored CRE1/AHK4-GFP in different cell types. Similarly to epidermis, in provasculature cells in the root meristematic zone, the CRE1/AHK4-GFP seems to localize at the ER, the PM and at the cell plate of dividing stele cells (Supplementary Fig. 6g). To strengthen the conclusion that in meristematically active cells cytokinin receptor might enter the secretory pathway and reach the PM, we performed
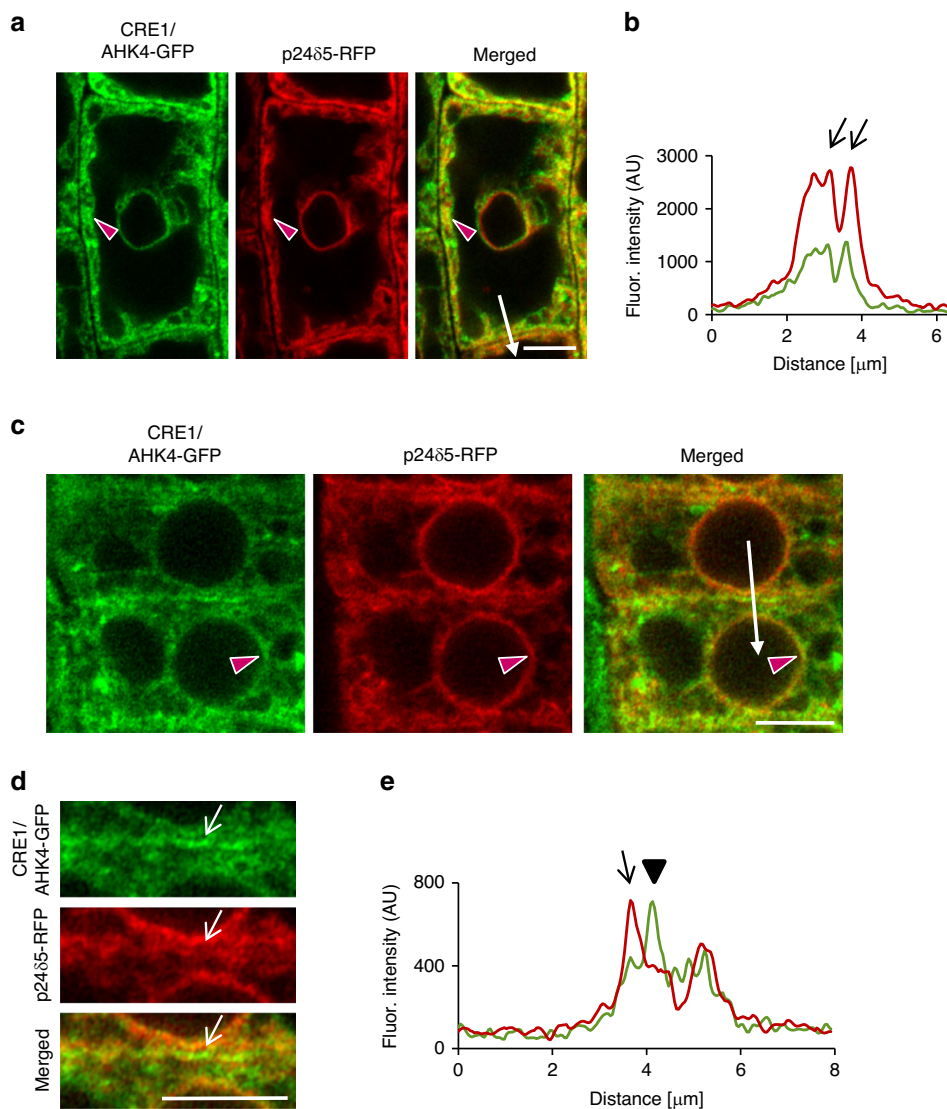
Fig. 3 CRE1/AHK4-GFP subcellular localization in cells of Arabidopsis root. a–e Monitoring of CRE1/AHK4-GFP cytokinin receptor (green) and ER-marker p24δ5-RFP (red) in LRC cells (**a**, **b**) and root meristematic epidermal cells (**c–e**). Red arrowheads mark areas of co-localization. Fluorescence intensity profiles of the ER marker (red line) and CRE1/AHK4-GFP (green line) (**b**, **e**) were measured along the white lines (**a**, **c**) starting from upper end (0 μm) towards the arrowhead. Peaks of p24δ5-RFP fluorescence maxima at the endoplasmic reticulum overlap with CRE1/AHK4-GFP signal maxima in the LRC cells and root meristematic epidermal cells (black arrows; **b**, **e**). Peak of CRE1/AHK4-GFP non-overlapping with peaks of p24δ5-RFP in the root meristematic epidermal cells indicates localization at the plasma membrane (black arrowhead; **e**). Detailed view (**d**; white arrows point to CRE1/AHK4-GFP signal at the area of the PM). Scale bars = 5 μm.

real-time monitoring of the CRE1/AHK4-GFP in developing lateral root primordia (LRP). Although expression of CRE1/AHK4-GFP driven by *35S* promoter in LRP was relatively weak, similarly to cells in the root meristem, the CRE1/AHK4-GFP tends to localize at the ER and the PM (Supplementary Fig. 6h). Furthermore, in actively dividing cells we could detect a weak CRE1/AHK4-GFP signal during cell plate formation (Supplementary Movie 1).

Unlike cells located at the root apical meristem, in the differentiated cells of the LRC the CRE1/AHK4-GFP was detected in the ER, but not at the PM. To support further our conclusion about dominant localization of the cytokinin receptor at the ER in differentiated cells, we performed detailed observations of CRE1/AHK4-GFP in differentiated root epidermal cells above the meristematic zone. In these cells, the CRE1/AHK4-GFP was located at the ER (Supplementary Fig. 6i, j), but no co-localization with the PM reporter NPSN12 could be detected (Supplementary Fig. 6k, l).

Based on these observations we hypothesize that CRE1/AHK4-GFP located either at the ER or at the PM might activate distinct branches of downstream signalling to control specific process in differentiated versus meristematically active cells. Internalization and recycling of the receptor between PM and endosomal compartments in meristematic cells may represent another level in controlling signalling receptor function. Whether similarly to the CRE1/AHK4-GFP, also AHK2 and AHK3 might enter secretory pathway and reach the PM in meristematically active cells remains to be addressed. In previously reported studies localizations of the AHK3-GFP and AHK2-GFP have been observed in above-ground plant parts using transiently trans-formed *Nicotiana benthamiana* epidermal leaf cells[2] and transiently transformed Arabidopsis cotyledon cells[3], all in the differentiated stages. Hence, whether in specific cell types AHK2 and AHK3 might localize to the PM needs to be examined.
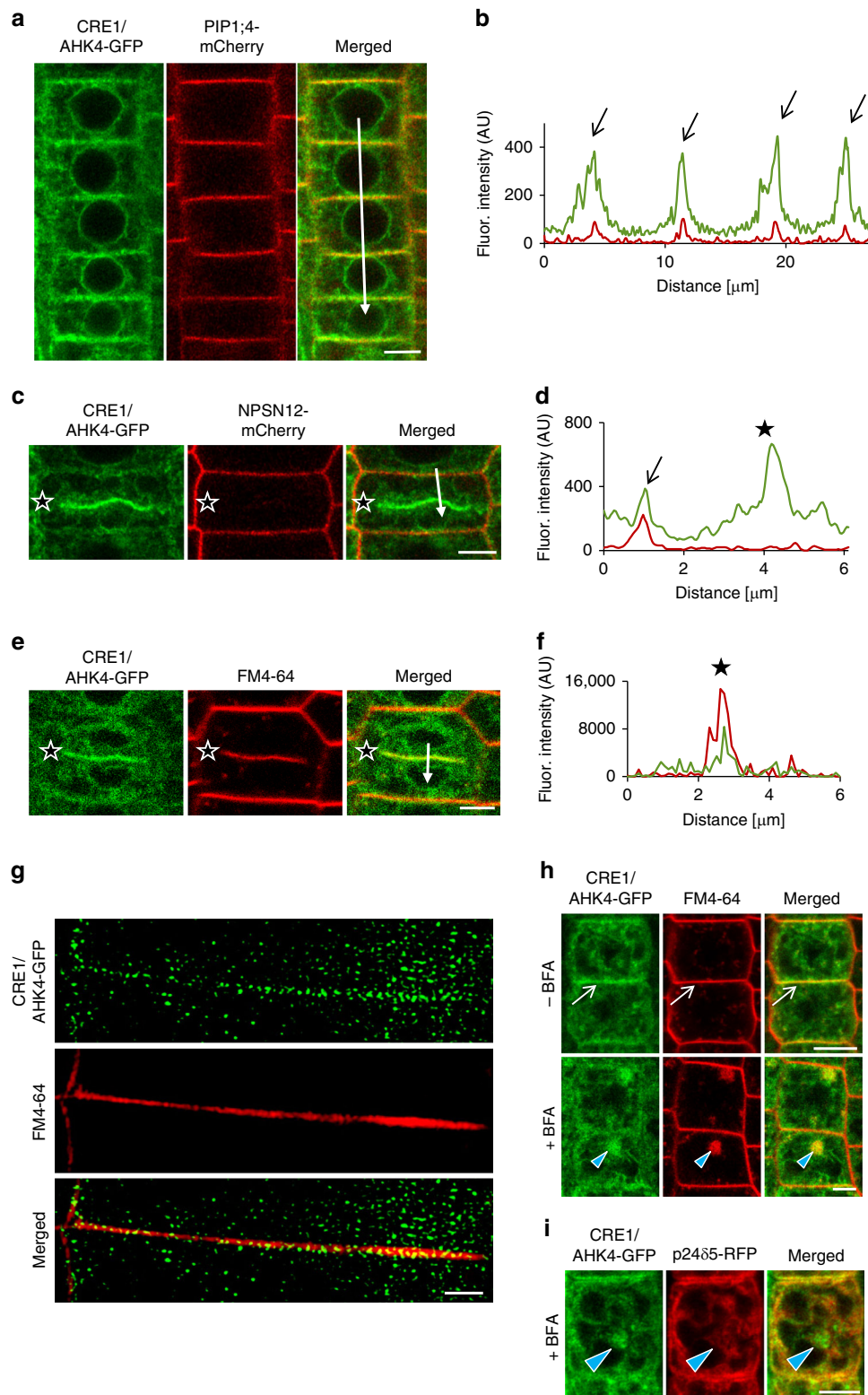
Fig. 4 CRE1/AHK4-GFP co-localization with the plasma membrane markers in Arabidopsis root cells. a–f Co-localization of CRE1/AHK4-GFP with the plasma membrane markers PIP1;4-mCherry (**a**, **b**), NPSN12-mCherry (**c**, **d**) and FM4-64 (**e**, **f**) in the root meristematic epidermal cells. Profiles of fluorescence intensity of PM marker (red line) and CRE1/AHK4-GFP (green line) (**b**, **d**, **f**) were measured along the white lines (**a**, **c**, **e**) starting from the upper end (0 μm) towards the arrowhead. Peaks of PIP1;4-mCherry and NPSN12-mCherry fluorescence maxima correlate with the plasma membrane staining and overlap with CRE1/AHK4-GFP signal maxima (black arrows) (**a–d**). CRE1/AHK4-GFP signal detected at the cell plate of dividing cell (black stars on **c**, **e**) co-localizes with FM4-64 marker (**e**, **f**; black stars) but not with the plasma membrane marker NPSN12-mCherry (**c**, **d**; black stars). **g** Super-resolution imaging (SIM) of CRE1/AHK4-GFP subcellular co-localization with FM4-64 labelled PM. **h**, **i** Co-localization of CRE1/AHK4-GFP and FM4-64 (**h**), but not p24δ5-RFP (**i**) in endosomal compartments (blue arrowheads) formed in root meristematic epidermal cells treated with 50 μM in BFA for 1 h. Note CRE1/AHK4-GFP localization at the plasma membrane (white arrows) prior BFA treatment. Scale bars = 5 μm (**a**, **c**, **e**, **h**, **i**) and 2 μm (**g**).

Taken together, monitoring of intracellular localization of the fluorescent cytokinin probe iP-NBD with higher affinity to CRE1/AHK4 cytokinin receptor, as well as direct visualization of CRE1/AHK4-GFP leads us to the conclusion that besides ER, cytokinin signal might also be perceived at other cellular compartments including the PM. As suggested by different localization of CRE1/AHK4 receptor in differentiated cells of LRC when compared to epidermal cells of root apical meristem, perception of cytokinin at either ER or PM might be cell- and developmental-context dependent. In particular, the strong expression of the cytokinin sensitive reporter *TCS::GFP* detected in columella and LRC cells[27] suggests that the ER-located cytokinin receptors activate cytokinin signalling cascade in these particular cell types. On the other hand, it remains to be resolved whether there is a specific branch of cytokinin signalling activated by receptors located at the PM of meristematic cells.

Methods

Plant material. *Arabidopsis thaliana* (L.) Heynh (Arabidopsis) plants were used. The transgenic lines have been described elsewhere: *cre1-2*[28], *TCSn::ntdT:tNOS-pDR5v2::n3GFP*[16], *pup14*[5], *p24δ5-RFP*[29], HDEL-RFP[30], Wave lines 2R/RabF2b (LE/PVC), 9R/VAMP711 (Vacuole), 13R/VTI12 (TGN/EE), 18R/Got1p (Golgi), 22R/SYP32 (Golgi), 34R/RabA1e (Endosomal/Recycling endosomal), 131R/NPSN12 (PM) and 138R/PIP1;4 (PM)[20], *ARR5::GUS*[23], *35S::GFP* line was kindly provided by Shutang Tan (IST Austria, Austria). *35S::CRE1/AHK4-GFP* plants were generated as described below.

Growth conditions. Surface-sterilized seeds of Arabidopsis ecotype Columbia (Col-0) and the other transgenic lines were plated on half-strength (0.5×) Murashige and Skoog (MS) medium (Duchefa) with 1% (w/v) sucrose and 1% (w/v) agar (pH 5.7). The seeds were stratified for 2–3 days at 4 °C in darkness. Seedlings were grown on vertically oriented plates in growth chambers at 21 °C under long day conditions (16 h light and 8 h darkness) using white light (W), which was provided by blue and red LEDs (70–100 µmol m^{-2} s^{-1} of photosynthetically active radiation), if not stated otherwise.

Pharmacological treatments for bio-imaging. Seedlings 4–5-day-old were transferred onto solid 0.5× MS medium with or without the indicated chemicals. The drugs and hormones used were: N^6-benzyladenine (BA) in different concentrations (0.1, 0.5, 1 and 2 µM), *trans*-zeatin (*t*Z 0.1 and 1 µM), N^6-isopentenyladenine (iP, 5 µM). Mock treatments were performed with equal amounts of solvent (dimethylsulfoxide (DMSO)). Treatments with 5 µM iP-NBD and 5 µM Ade-NBD were performed in liquid 0.5× MS medium and imaging was carried out within 30 min time frame. For co-localization of the cytokinin fluoroprobe with PM marker, seedlings were pre-treated with 2 µM FM4-64 for 5 min and transferred into 5 µM iP-NBD supplemented 0.5× MS medium, followed by imaging within 30 min time frame. To explore affinity of iP-NBD to BFA endosomal compartments, seedlings were incubated in 50 µM BFA for 1 h and afterwards transferred into iP-NBD supplemented medium and imaged. Localization of CRE1/AHK4-GFP in BFA endosomal compartments was examined in 4–5-day-old seedlings incubated in 50 µM BFA for 1 h. For BFA washout experiments, seedlings were placed in a fresh BFA-free 0.5× MS medium, which was replaced every 10 min for at least 1 h.

Recombinant DNA techniques. The coding region of the cytokinin receptor CRE1/AHK4 (*At2g01830*) was amplified without the stop codon by PCR using a gDNA from *Arabidopsis thaliana* Col-0 as a template and cloned into the Gateway vector *pENTR_2B* dual selection (primers: AHK4_Fw_SalI_KOZAK *CGCGTCGACCcaccATGAGAAGAGATTTTGTGTATAATAATAATGC* and AHK4_R_NotI *TTTTCCTTTTGCGGCCGCgaCGACGAAGGTGAGATAGGATTAGG*). To construct C-terminal fusion of CRE1/AHK4 with GFP, CRE1/AHK4 was shuttled into the destination vector *pGWB5*[31] containing *35S* promoter to create *35S::CRE1/AHK4-GFP* construct. For the transient Luciferase assay in Arabidopsis protoplasts, CRE1/AHK4-GFP fusion construct was re-cloned into *p2GW7,0* vector. CRE1/AHK4-GFP region was amplified by PCR using *pGWB5_CRE1/AHK4-GFP* as a template (primers: *35S_FW CCACTATCCTTCGCAAGACCCTTC* and AHK4_5A_NheI_RE *TATTCCAATgctagcTTACTTGTACAGCTCGTCCATGC*) and ligated into the Gateway *pENTR_2B* dual selection entry vector. CRE1/AHK4-GFP was shuttled into the destination vector *p2GW7,0*.

Plant transformation. Transgenic Arabidopsis plants were generated by the floral dip method using *Agrobacterium tumefaciens* strain GV3101[32]. Transformed seedlings were selected on medium supplemented with 30 µg mL^{-1} hygromycin.

Homology modelling and molecular docking. CRE/AHK structures were modelled based on CRE1/AHK4-iP crystal structure (PDBID: 3T4L)[12] using Modeller 9.10[33]. The geometry of iP-NBD was modelled with Marvin (http://www.chemaxon.com), and then the compounds were prepared for docking in the AutoDockTools program suite[34]. The Autodock Vina program[35] was used for docking iP-NBD ligand into the set of AHK structures obtained from homology modelling. A 15 Å box centred at the original ligand binding position was used. The exhaustiveness parameter was set to 20.

Competitive binding assay in *E. coli* strains. Receptor direct binding assays were conducted using the *E. coli* strain KMI001 harbouring either the plasmid *pIN-III-AHK4* or *pSTV28-AHK3*, which express the Arabidopsis histidine kinases CRE1/AHK4 or AHK3[36,37]. Bacterial strains were kindly provided by Dr. T. Mizuno (Nagoya, Japan). The competitive binding assays[15,38] were performed with homogenous bacterial suspension with an OD$_{600}$ of 0.8 and 1.2 for CRE1/AHK4 and AHK3 expressing strains, respectively. The competition reaction was allowed to proceed with 3 nM [2-^{3}H]*t*Z and 6–18 nM [2-^{3}H]iP, and various concentrations of iP and iP-NBD, 0.1% (v/v) DMSO was added as a solvent control. After 30-min incubation at 4 °C, the sample was centrifuged (6000 × *g*, 6 min, 4 °C), the supernatant was carefully removed, and the bacterial pellet was resuspended in 1 ml of scintillation cocktail (Beckman, Ramsey, MN, USA) in an ultrasonic bath. Radioactivity was measured by scintillation counting by a Hidex 300 SL scintillation counter (Hidex, Finland). To discriminate between specific and nonspecific binding, a high excess of unlabelled natural ligand *t*Z, or iP (at least 3000-fold) was used for competition. The functional inhibition curves were used to estimate the IC$_{50}$ values. The K_i values were calculated using the equation $K_i = IC_{50}/(1 + [radio-ligand]/K_D)$ according to Cheng and Prusoff[39]. [2-^{3}H]*t*Z and [2-^{3}H]iP were provided by Dr. Zahajská from the Isotope Laboratory, Institute of Experimental Botany, Czech Academy of Sciences.

Quantitative RT–PCR. RNA was extracted with Monarch® Total RNA Miniprep Kit (NEB) from roots of 5-day-old plants that were sprayed with mock (DMSO) or 0.01 µM iP, 0.1 µM iP, 1 µM iP, 10 µM iP-NBD, 100 µM iP-NBD or co-treatment of 0.1 µM iP + 10 µM iP-NBD, 0.1 µM iP + 100 µM iP-NBD for 15 min (Fig. 1d); Mock (DMSO) or 5 µM iP (Supplementary Fig. 5e); for 15 min. Poly(dT) cDNA was prepared from 1 µg of total RNA with the iScript cDNA Synthesis Kit (Bio-Rad) and analysed on a LightCycler 480 (Roche Diagnostics) with the Luna® Universal qPCR Master Mix (NEB) according to the manufacturer's instructions. The expression of CRE1/AHK4 of the two independent lines was quantified either with a specific primer pair (AHK4-GFP_FW: *TATCTCACCTTCGTCGTCGC* and AHK4-GFP_RE: *CCTTGCTCACCATGGATCCTC*) and their relative expressions were compared to the house-keeping gene PP2A (PP2A_FW: *TAACGTGGC-CAAAATGATGC* and PP2A_RE: *GTTCTCCACAACCGCTTGGT*) or with AHK4_FW: *GAACTGGGCACTCAACAATCA* and AHK4_RE: *ACGAATTCA-GAGCACCACCA* pair of primers and their relative expression refer to the Col-0 mock treatment. All qRT-PCR quantifications were done using PP2A as a reference gene (Fig. 1d; Supplementary Fig. 5a, e). For the *ARR* expressions (ARR5_FW: *TGCCTGGGATGACTGGATATG*, ARR5_RE: *CTCCTTCTTCAAGACATCTATCG*, ARR7_FW: *TACTCAATGCCAGGACTTTCAGG*, ARR7_RE: *TCTTTGAGA-CATTCTTGTATACGAGG*, ARR16_FW: *CGTAAACTCGTTGAGAGGTTGCTC* and ARR16_RE: *GCATTCTCTGCTGTTGTCACTTTG*), the fold change refer to the Col-0 mock treatment. The experiment was performed in three technical and three biological replicates.

Measurements of iP-NBD cell transport kinetics. Seedlings of 4-day-old Arabidopsis Col-0 were pre-treated for 20 min with 5 µM iP or DMSO and transferred into MS media containing 5 µM iP-NBD and 5 µM iP/DMSO and instantly imaged. To examine PUP14-dependent iP-NBD transport kinetics, 4-day-old seedlings of *pup14* and Col-0 were treated with 5 µM iP-NBD and immediately imaged. For both experiments imaging was performed in the same area of the root for 12 min every 2, 7 and 12 min to minimize photobleaching. iP-NBD fluorescence was measured with ImageJ in the LRC cells (iP pre-treatment experiment) and in the root epidermal cells (*pup14* experiment) from 4 to 7 cells originating from 4 to 5 roots.

Imaging. For confocal microscopy imaging, a vertical-stage laser scanning confocal Zeiss 700 (LSM 700) and Zeiss 800 (LSM 800), described in ref.[40], with a ×20/0.8 Plan-Apochromat M27 objective, an LSM 800 inverted confocal scanning microscope Zeiss, with a ×40 Plan-Apochromat water immersion objective and a Zeiss LSM 880 inverted fast Airyscan microscope with a Plan-Apochromat ×63 NA 1.4 oil immersion objective were used. Samples were imaged with excitation lasers 488 nm for GFP (emission spectrum 490–560 nm) and NBD (emission spectrum 529–570 nm), 555/561 nm (inverted/vertical) for RFP (emission spectrum 583–700 nm), FM4-64 (emission spectrum 650–730 nm), mCherry (emission spectrum 570–700 nm) and tdTomato (emission 560–700 nm).

For super-resolution SIM microscopy, an Axioimager Z.1 with Elyra PS.1 system coupled with a PCO.Edge 5.5 sCMOS camera was used. Samples were excited with the 488 nm and 561 nm laser lines. Oil immersion objective (×63/1.40) and standard settings (the grating pattern with five rotations and five standard

phase shifts per angular position) were used for image acquisition. Image reconstruction was done in Zeiss Zen software (black version with structured illumination module) using manual mode with adjusting the noise filter and super-resolution frequency weighting sliders as described in ref. [41]. For image post-processing, profile measurements and co-localization analysis, the Zeiss Zen 2011, ImageJ (National Institute of Health, http://rsb.info.nih.gov/ij), Photoshop 6.0/CS, GraphPad Prism 8 and Microsoft PowerPoint programs were used. For SIM co-localization experiments 30 PM regions originating from root cells of 5 seedling plants were used.

Statistics. The statistical significance was evaluated with the Student's t test and two-way ANOVA.

Data availability

All data in this study are available in the main text or the Supplementary materials. Extra data are available from the corresponding authors upon request. Source data are provided with this paper.

References

1. Kieber, J. J. & Schaller, G. E. Cytokinin signaling in plant development. *Development* **145**, 1–7 (2018).
2. Wulfetange, K. et al. The cytokinin receptors of Arabidopsis are located mainly to the endoplasmic reticulum. *Plant Physiol.* **156**, 1808–1818 (2011).
3. Caesar, K. et al. Evidence for the localization of the Arabidopsis cytokinin receptors AHK3 and AHK4 in the endoplasmic reticulum. *J. Exp. Bot.* **62**, 5571–5580 (2011).
4. Lomin, S. N., Yonekura-Sakakibara, K., Romanov, G. A. & Sakakibara, H. Ligand-binding properties and subcellular localization of maize cytokinin receptors. *J. Exp. Bot.* **62**, 5149–5159 (2011).
5. Zürcher, E., Liu, J., di Donato, M., Geisler, M. & Müller, B. Plant development regulated by cytokinin sinks. *Science* **353**, 1027–1030 (2016).
6. Kim, H. J. et al. Cytokinin-mediated control of leaf longevity by AHK3 through phosphorylation of ARR2 in Arabidopsis. *Proc. Natl Acad. Sci. USA* **103**, 814–819 (2006).
7. Kubiasová, K. et al. Design, synthesis and perception of fluorescently labeled isoprenoid cytokinins. *Phytochemistry* **150**, 1–11 (2018).
8. Lace, B. & Prandi, C. Shaping small bioactive molecules to untangle their biological function: a focus on fluorescent plant hormones. *Mol. Plant* **9**, 1099–1118 (2016).
9. Kudo, T., Kiba, T. & Sakakibara, H. Metabolism and long-distance translocation of cytokinins. *J. Integr. Plant Biol.* **52**, 53–60 (2010).
10. Antoniadi, I. et al. Cell-type-specific cytokinin distribution within the Arabidopsis primary root apex. *Plant Cell* **27**, 1955–1967 (2015).
11. Hou, B., Lim, E.-K., Higgins, G. S. & Bowles, D. J. N-glucosylation of cytokinins by glycosyltransferases of Arabidopsis thaliana. *J. Biol. Chem.* **279**, 47822–47832 (2004).
12. Hothorn, M., Dabi, T. & Chory, J. Structural basis for cytokinin recognition by *Arabidopsis thaliana* histidine kinase 4. *Nat. Chem. Biol.* **7**, 766–768 (2011).
13. Spíchal, L. et al. Two cytokinin receptors of *Arabidopsis thaliana*, CRE1/AHK4 and AHK3, differ in their ligand specificity in a bacterial assay. *Plant Cell Physiol.* **45**, 1299–1305 (2004).
14. Romanov, G. A., Lomin, S. N. & Schmülling, T. Biochemical characteristics and ligand-binding properties of Arabidopsis cytokinin receptor AHK3 compared to CRE1/AHK4 as revealed by a direct binding assay. *J. Exp. Bot.* **57**, 4051–4058 (2006).
15. Romanov, G. A., Spíchal, L., Lomin, S. N., Strnad, M. & Schmülling, T. A live cell hormone-binding assay on transgenic bacteria expressing a eukaryotic receptor protein. *Anal. Biochem.* **347**, 129–134 (2005).
16. Smet, W. et al. DOF2.1 controls cytokinin-dependent vascular cell proliferation downstream of TMO5/LHW. *Curr. Biol.* **29**, 520–529 (2019).
17. Werner, T. et al. Cytokinin-deficient transgenic Arabidopsis plants show multiple developmental alterations indicating opposite functions of cytokinins in the regulation of shoot and root meristem activity. *Plant Cell* **15**, 2532–2550 (2003).
18. Jelínková, A. et al. Probing plant membranes with FM dyes: tracking, dragging or blocking? *Plant J.* **61**, 883–892 (2010).
19. Orci, L. et al. "BFA bodies": a subcompartment of the endoplasmic reticulum. *Proc. Natl Acad. Sci. USA* **90**, 11089–11093 (1993).
20. Geldner, N. et al. Rapid, combinatorial analysis of membrane compartments in intact plants with a multicolor marker set. *Plant J.* **59**, 169–178 (2009).
21. Romanov, G. A., Lomin, S. N. & Schmülling, T. Cytokinin signaling: from the ER or from the PM? That is the question! *N. Phytol.* **218**, 41–53 (2018).
22. Jaworek, P. et al. Characterization of five CHASE-containing histidine kinase receptors from *Populus × canadensis* cv. *Robusta* sensing isoprenoid and aromatic cytokinins. *Planta* **251**, 1 (2020).
23. D'Agostino, I. B., Deruere, J. & Kieber, J. J. Characterization of the response of the Arabidopsis response regulator gene family to cytokinin. *Plant Physiol.* **124**, 1706–1717 (2000).
24. Dhonukshe, P. et al. Endocytosis of cell surface material mediates cell plate formation during plant cytokinesis. *Dev. Cell* **10**, 137–150 (2006).
25. Smertenko, A. et al. Plant cytokinesis: terminology for structures and processes. *Trends Cell Biol.* **27**, 885–894 (2017).
26. Komis, G., Šamajová, O., Ovečka, M. & Šamaj, J. Super-resolution microscopy in plant cell imaging. *Trends Plant Sci.* **20**, 834–843 (2015).
27. Bielach, A. et al. Spatiotemporal regulation of lateral root organogenesis in Arabidopsis by cytokinin. *Plant Cell* **24**, 3967–3981 (2012).
28. Inoue, T. et al. Identification of CRE1 as a cytokinin receptor from Arabidopsis. *Nature* **409**, 1060–1063 (2001).
29. Montesinos, J. C. et al. Coupled transport of Arabidopsis p24 proteins at the ER-Golgi interface. *J. Exp. Bot.* **63**, 4243–4261 (2012).
30. Nelson, B. K., Cai, X. & Nebenführ, A. A multicolored set of in vivo organelle markers for co-localization studies in Arabidopsis and other plants. *Plant J.* **51**, 1126–1136 (2007).
31. Nakagawa, T. et al. Development of series of gateway binary vectors, pGWBs, for realizing efficient construction of fusion genes for plant transformation. *J. Biosci. Bioeng.* **104**, 34–41 (2007).
32. Clough, S. J. & Bent, A. F. Floral dip: a simplified method for *Agrobacterium*-mediated transformation of *Arabidopsis thaliana*. *Plant J.* **16**, 735–743 (1998).
33. Sali, A. & Blundell, T. L. Comparative protein modelling by satisfaction of spatial restraints. *J. Mol. Biol.* **234**, 779–815 (1993).
34. Sanner, M. F. Python: a programming language for software integration and development. *J. Mol. Graph. Model.* **17**, 57–61 (1999).
35. Trott, O. & Olson, A. J. AutoDock Vina: improving the speed and accuracy of docking with a new scoring function, efficient optimization, and multithreading. *J. Comput. Chem.* **31**, 455–461 (2010).
36. Suzuki, T. et al. The Arabidopsis sensor His-kinase, AHK4, can respond to cytokinins. *Plant Cell Physiol.* **42**, 107–113 (2001).
37. Yamada, H. et al. The Arabidopsis AHK4 histidine kinase is a cytokinin-binding receptor that transduces cytokinin signals across the membrane. *Plant Cell Physiol.* **42**, 1017–1023 (2001).
38. Nisler, J. et al. Cytokinin receptor antagonists derived from 6-benzylaminopurine. *Phytochemistry* **71**, 823–830 (2010).
39. Cheng, Y. & Prusoff, W. H. Relationship between the inhibition constant (K_I) and the concentration of inhibitor which causes 50 per cent inhibition (I_{50}) of an enzymatic reaction. *Biochem. Pharmacol.* **22**, 3099–3108 (1973).
40. von Wangenheim, D. et al. Live tracking of moving samples in confocal microscopy for vertically grown roots. *Elife* **6**, e26792 (2017).
41. Komis, G. et al. Superresolution live imaging of plant cells using structured illumination microscopy. *Nat. Protoc.* **10**, 1248–1263 (2015).

Author contributions

L.S., O.P., E.B., P.G. and M.S. conceived the project; K.K. and J.C.M. performed most of the microscopic and biochemical experiments; O.Š. and J.Š. participated in plasma membrane localization studies and helped with evaluation and interpretation of sub-cellular localization data; H.S. contributed to generation and characterization of CRE1/AHK4-GFP transgenic lines; N.C. established the *TCS::LUCIFERASE* assays to test CRE1/AHK4-GFP activity in protoplasts; P.M. contributed to the *TCS* experiment in

planta; L.P., K.D. and V.M. designed and chemically synthesized cytokinin fluorescent probe; J.N. performed cytokinin in vitro assays; O.N. conducted the purification and quantification of cytokinins; K.B. performed in silico docking experiments; D.Z. analysed and interpreted the data; L.S., E.B. and O.P. designed experiments, analysed and interpreted the data; K.K., J.C.M., O.Š. and L.S. made the figures; E.B., O.P. and L.S. wrote the paper.

Competing interests

The authors declare no competing interests.

Additional information

Supplementary information is available for this paper at https://doi.org/10.1038/s41467-020-17949-0.

Correspondence and requests for materials should be addressed to E.B., O.P. or L.S.

Peer review information *Nature Communications* thanks Hitoshi Sakakibara, Bruno Müller, Hao Wang, and the other, anonymous reviewer(s) for their contribution to the peer review of this work. Peer review reports are available.

Reprints and permission information is available at http://www.nature.com/reprints

Publisher's note Springer Nature remains neutral with regard to jurisdictional claims in published maps and institutional affiliations.
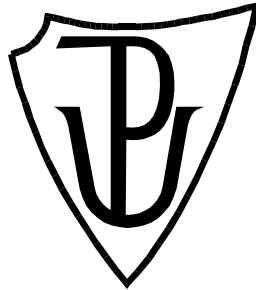
PALACKÝ UNIVERSITY OLOMOUC

Faculty of Science

SUMMARY OF THE DOCTORAL THESIS

Localization studies of the cytokinin receptor CRE1/AHK4 using fluorescently labelled cytokinin

Karolina Kubiasová

P1406 Biochemistry

Olomouc 2020

The experiments included in this Ph.D. thesis have been performed in the laboratories of Department of Molecular Biology, Centre of the Region Haná for Biotechnological and Agricultural Research, Faculty of Science, Palacký University Olomouc and at Institue of Science and Technology (IST) Austria in period 2014-2020.

Ph.D. candidate: Mgr. Karolina Kubiasová
           Department of Molecular Biology, Centre of the Region Haná for
           Biotechnological and Agricultural Research
           Faculty of Science, Palacký University Olomouc
           Šlechtitelů 27, 783 71 Olomouc, Czech Republic

Supervisor: RNDr. Ondřej Plíhal, Ph.D.
           Laboratory of Growth Regulators, Institute of Experimental Botany of
           the Czech Academy of Sciences and Faculty of Science of Palacký
           University, Šlechtitelů 27, 783 71 Olomouc, Czech Republic

Consultants: Prof. Eva Benková
           Juan Carlos Montesinos López, Ph.D.
           Institute of Science and Technology (IST Austria)
           Am Campus 1, 3400 Klosterneuburg, Austria

Reviewers: Krisztina Ötvös, Ph.D.
           Center for Health & Bioresources
           Austrian Institute of Technology GmbH (AIT)
           Konrad-Lorenz-Straße 24, 3430 Tulln an der Donau, Austria

           RNDr. Radomíra Vaňková, CSs.
           Laboratory of Hormonal Regulations in Plants
           Institute of Experimental Botany of the Czech Academy of Sciences
           (UEB)
           Rozvojová 263, 165 02 Prague, Czech Republic

CONTENTS

ABSTRACT

Cytokinins are plant hormones that play an essential role in various aspects of plant growth and development. In *Arabidopsis thaliana* three transmembrane histidine kinases, namely AHK2, AHK3 and CRE1/AHK4, serve as cytokinin receptors. Subcellular localization of the receptors proposed the endoplasmic reticulum (ER) membrane as a principal cytokinin perception site, while the study of cytokinin transport pointed to the plasma membrane (PM)-mediated cytokinin signalling. To gain better insight into the dynamics of cytokinin receptor localization within the cell a series of cytokinin fluorescent probes were developed. The ligand properties of isopentenyladenine (iP)-derived probes were assessed in a bacterial receptor test where the competition of a cytokinin fluoroprobe with radiolabelled *trans*-zeatin was measured. Although the structural changes within the fluorescent probes led mostly to a significant loss of the biological activity, several fluorescent derivatives interacted well. The most promising of them (iP-NBD) was selected as a tool for visualization of the cytokinin receptor pool inside the cell. By detailed monitoring subcellular localizations of the fluorescently labelled natural cytokinin probe and the receptor ARABIDOPSIS HISTIDINE KINASE 4 (CRE1/AHK4) fused to GFP reporter, it is shown that pools of the ER-located cytokinin receptors can enter the secretory pathway and reach the PM in cells of the root apical meristem, and the cell plate of dividing meristematic cells. A revised view on cytokinin signalling and the possibility of multiple sites of perception at PM and ER is provided.

ABSTRACT

Cytokininy jsou rostlinné hormony, které hrají důležitou roli v mnoha růstových a vývojových procesech rostlin. V *Arabidopsis thaliana* se nachází tři transmembránové histidin kinasy, které fungují jako cytokininové receptory, konkrétně AHK2, AHK3 a CRE1/AHK4. Výsledky subcelulární lokalizace receptorů navrhovaly endoplasmatické retikulum (ER) jakožto hlavní místo cytokininové percepce, zatímco studium cytokininového transportu ukazovalo na plasmatickou membránu (PM) jako místo cytokininové signalizace. Pro lepší pochopení dynamiky lokalizace cytokininových receptorů v buňce byla připravena řada fluorescenčních prób. Vlastnosti prób odvozených od isopentenyladeninu (iP) byly stanoveny v bakteriálním receptorovém testu, kde byla sledována kompetice mezi fluorescenčně značeným cytokininem a radioaktivně značeným *trans*-zeatinem. Přestože strukturní změny fluorescenční proby vedly většinou k výrazným ztrátám biologické aktivity, několik fluorescenčních derivátů se vázalo dobře. Jeden z nich (iP-NBD) byl vybrán jako nástroj pro vizualizaci cytokininových receptorů v buňce. Pomocí detailní studie subcelulární lokalizace fluorescenčně značeného cytokininu a ARABIDOPSIS HISTIDINE KINASE 4 (CRE1/AHK4) receptoru sfuzovaného s GFP reporterem bylo ukázáno, že ER-lokalizované cytokininové receptory vstupují do sekreční dráhy až k PM v buňkách kořenového apikálního meristému a k buněčné desce dělících se meristematických buněk. Byl tak poskytnut upravený pohled na signalizaci cytokininů a možnost různých míst percepce na PM a ER.

o   Literature review on the plant hormones cytokinins, with a focus on cytokinin receptors and their localization.

o   Characterization of a series of fluorescent derivatives of the cytokinin iP as a new tool for cytokinin receptor domain mapping.

o   Detailed biochemical and localization study of fluorescently labelled cytokinin iP-NBD.

o   Preparation and characterization of transgenic *Arabidopsis* lines expressing 35S::CRE1/AHK4-GFP construct.

o   Detailed subcellular localization of the cytokinin receptor CRE1/AHK4 using confocal microscopy.

Signal transduction pathways can be regulated by changing subcellular localization of the participating proteins, thus influencing their functioning mode in the cell (Dortay et al., 2008). Plant receptor kinases located on the cell surface mediate plenty of responses according to developmental and environmental inputs. During their lifespan, receptors undergo a complex set of subcellular trafficking events. The endoplasmic reticulum is a place of protein synthesis and maturation, while delivery to the plasma membrane involves passage through the Golgi apparatus. Receptors are eventually inserted into the plasma membrane to perform their function as sensors. Retrieval from the PM comprises of the endocytic pathway and subsequent sorting, either for targeting to late endosomes and eventual degradation in the vacuole or for recycling back to the PM (Geldner and Robatzek, 2008).

Perception of plant hormones occur at different sites of the cell: ethylene receptors are localized in the ER (Chen et al., 2002), brassinosteroid receptors are at the PM (Friedrichsen et al., 2000; Irani et al., 2012) and other hormones like auxins, ABA (abscisic acid) or GAs (gibberellins) possess soluble receptor proteins in the cytosol and/or nucleus (Shan et al., 2012; Larrieu and Vernoux, 2015). The subcellular localization of cytokinin receptors and the initiation of signalling are particularly relevant to understand the cellular architecture of the cytokinin system. However, the sites of cytokinin perception and signal transduction are still under extensive study since the discovery of cytokinin receptors in 2001 (Romanov et al., 2018). The first model of *Arabidopsis* cytokinin signalling presumed the receptor localization at the plasma membrane. This suggestion was based on the prediction of a bioinformatic approach using the PSORT program (Nakai and Horton, 1999). However, the certainty of the prediction for localization in the plasma membrane was 0.6 in all cases, which is far from the maximum of 1 (Ueguchi et al., 2001b). Also, cytokinin receptors were considered to be localized at the PM because of the structural similarity with the sensor His kinase localization in bacteria and yeast (Inoue et al., 2001; Ueguchi et al., 2001a). Moreover, His kinase ethylene receptors were presumed to reside at the PM too (Hirayama and Alonso, 2000). The very first experimental evidence of cytokinin receptor localization came in 2006 when Kim et al. showed transient expression of an AHK3-GFP fusion at the PM in *Arabidopsis* protoplasts (Figure 1A). However, the authors provided only low-resolution supplementary data in a semi-artificial system. Any use of PM/ER markers supporting AHK plasma membrane localization was missing (Kim et al., 2006).
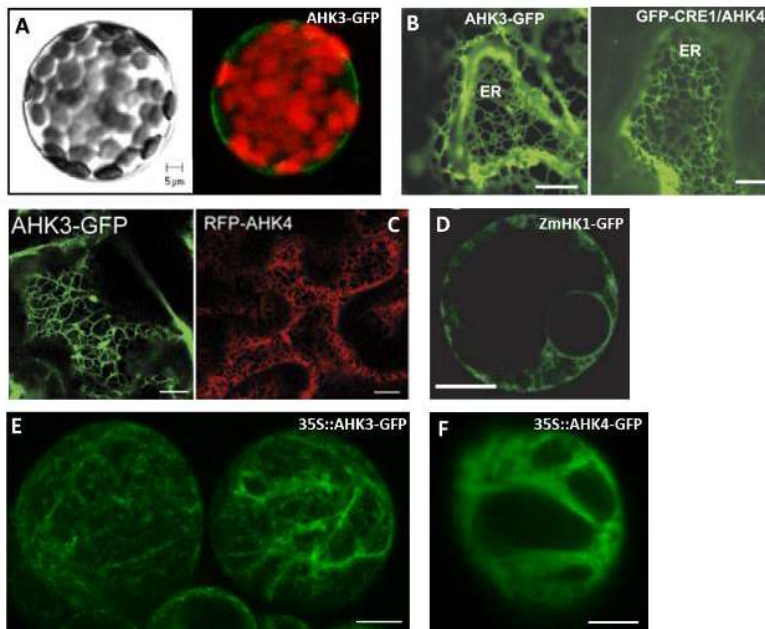

Figure 1: *Localization of cytokinin receptors. A – transient expression of AHK3-GFP in the Arabidopsis protoplasts (Kim et al., 2006); B – transient expression of AHK3-GFP and CRE1/AHK4-GFP in the epidermal cells*

A few years later, three articles focused on subcellular localization of cytokinin receptors were published (Caesar et al, 2011; Lomin et al., 2011; Wulfetange et al., 2011). Fluorescent cytokinin receptor fusion proteins AHK3-GFP and CRE1/AHK4-GFP expressed under the control of 35S constitutive promoter in the epidermal cells of tobacco leaves pointed to the majority of overexpressed cytokinin receptors to be localized inside the cell within the ER membranes (Figure 1B). In the case of AHK2, neither N- nor C-terminal fusion with GFP led to a detectable signal *in planta*. Until now, any attempts to generate transgenic *Arabidopsis* lines stably expressing the receptor-GFP fusion under the control of the 35S promoter have not been successful, most likely due to cellular toxicity of the gene products (Wulfetange et al., 2011).

The localization of *Arabidopsis* receptor-fluorescent protein fusions in the ER was further supported with experiments of transiently transformed tobacco leaf epidermal and *Arabidopsis* cotyledon cells (Figure 1C; Caesar et al., 2011) and of the maize receptor ZmHK1 expressed in the protoplasts derived from maize leaves (Figure 1D; Lomin et al., 2011). Similar results corresponding to the ER network were obtained also with *Arabidopsis* L*er* cell suspension culture stably expressing fluorescently labelled AHK3 (Figure 1E) or transiently expressing CRE1/AHK4 receptor under the control of constitutive promoter (Figure 1F; Kubiasová, 2014).

Also, other biological and biochemical methods were used to investigate the location of cytokinin receptors. Isolated membranes (PM fraction and endomembrane fraction) separated by the two-phase partitioning method showed that [^{3}H]tZ binds with high affinity in the fraction containing endomembranes, both in *Arabidopsis* (Wulfetange et al., 2011) and maize (Lomin et al., 2011). Moreover, fractionation of cell membranes by sucrose gradient centrifugation of AHK-Myc fusion proteins under the control of their own promoters showed, that AHK2-Myc and AHK3-Myc fusion proteins were also detected in the endomembrane fraction. Altogether these data suggest that the endomembrane system is the main compartment for localization of cytokinin receptors (Wulfetange et al., 2011). In addition, AHK3 protein was shown to be susceptible to EndoH treatment (Caesar et al., 2011). Endoglycosidase H cleaves the asparagin-linked high-mannose type and hybrid oligosaccharides that are typical for ER glycoproteins but is not specific for highly processed complex-type oligosaccharides that are associated with the post-Golgi secretory pathway. This observation was used as an argument for ER localization of the AHK3 receptor (Caesar et al., 2011). However, these data have to be carefully considered since other proteins localized on PM (e.g. brassinosteroid receptor BRI1) are also sensitive to endoglycosidase H (Jin et al., 2007; Hong et al., 2008).

As Romanov and colleagues already demonstrated in the bacterial assay, the binding of cytokinin to the receptor is pH-dependent. The maximal hormone-binding activity is close to a neutral or weak alkaline pH, and the ability to bind the cytokinin decreases with decreasing pH. An acidic pH is characteristic for the apoplast whereas neutral or weak alkaline pH is typical for the cytoplasm and the endoplasmic reticulum. These findings lead to a suggestion, that cytokinin receptors may function inside of the cell (Romanov et al., 2006). The authors carried out an analysis of the pH dependence of numerous plant proteins with their known subcellular localization. The analysis showed that the pH optimum of the protein activity strongly corresponds to the compartment where this protein is operating. Therefore, proteins functioning in the ER should have an optimum close to pH 7-8, whereas proteins operating in the apoplast should possess their optimum mainly in the range of pH 4.5-6 (Romanov et al., 2018). This rule helps to predict the localization of active proteins residing in compartments with contrasting pH. The *Arabidopsis* cytokinin receptors AHK2 and AHK3 show a drastic decrease in hormone-binding activity at pH 5. (Romanov et al., 2006; Lomin et al., 2015). Also, after 1h incubation at pH 5, the ligand-binding capacity of AHK3 is not restored upon transfer to the optimal pH conditions. This indicates an irreversible rearrangement in the ligand-binding domain of AHK3 caused by incubation at pH 5. Results from analysis and the cytokinin binding assays performed in various pH corroborate, that cytokinin receptors not only reside but also operate in the ER (Lomin et al., 2015; Romanov et al., 2018). On the other hand, it would be premature to exclude the presence of functioning receptors within the PM since at pH 5 the CRE1/AHK4 receptors, and its maize ortholog ZmHK1, retain a noticeable ligand-binding ability

corresponding to 23.4% and 37.2% of the binding at pH 7, respectively (Lomin et al., 2015). Also, the *ahk2ahk3* mutant plants expressing only CRE1/AHK4 receptor showed higher specific binding in the PM fraction than in the endomembranes fraction (Wulfetange et al., 2011). Moreover, in their recently published work, Jaworek and colleagues (Jaworek et al., 2020) show the influence of pH on the binding strength of cytokinins to the receptors from poplar. Authors showed that binding of cytokinin to PcHK3 (AHK3 ortholog) increases towards alkaline pH values, whereas binding of PcHK4 (CRE1/AHK4 ortholog) displays the strongest ligand binding ability at pH 5.5. These findings support the idea that CRE1/AHK4 can effectively sense cytokinins from the apoplast.

The first step of cytokinin signal transduction includes a transfer of a phosphate group from the activated receptor to a phosphotransfer protein. Lomin et al. (2018b) recently investigated the interaction of a cytokinin receptor with different AHPs in the epidermal tobacco cells. To study the subcellular localization of receptor-AHP interaction, bimolecular fluorescence complementation (BiFC) experiments were performed. Receptor-AHP pairs interacted in every possible combination in a pattern reflecting the ER localization. Moreover, receptor dimers, considered as an active form of the receptors, were also detected in the ER. Based on the BiFC and protease protection assay, the catalytic part of the receptor is exposed to the cytoplasm whereas the hormone-binding module is oriented with its N-terminal portion facing the ER lumen. This topology is favourable for receptor signalling from the ER membrane. Additionally, *in vitro* kinase assay for visualising the phosphorylation of AHPs was tested using the different membrane fractions. The detected cytokinin-dependent phosphotransfer activity was much higher in the ER-enriched fraction. However, the existence of a small pool of active receptors in the PM was not totally excluded (Wulfetange et al., 2011; Lomin et al., 2018b).

One of the features of how cytokinin homeostasis is maintained is by cytokinin-degrading enzymes CKXs. In *Arabidopsis*, the cytokinin breakdown is controlled by seven CKX proteins (encoded by *AtCKX1-AtCKX7*). They differ in the subcellular localization which displays the importance of compartmentalization of cytokinin metabolism for cytokinin action and plant development (Frébort et al., 2011). Moreover, all of the AtCKX isomers have pH optimum in the neutral and weakly basic pH pointing to their intracellular place of activity (Galuszka et al., 2007). The importance of CKX-mediated degradation at different sites of the plant cell and its effect on plant growth was described (Werner et al., 2003; Niemann et al., 2018). Analysis of the subcellular localization of CKX1- and CKX3-GFP fusion proteins pointed to the ER and occasionally vacuole as a place of their activity. When overexpressed, the mutant plants showed retarded shoot development. These results propose ER as a relevant site of cytokinin degradation with an apparent impact on cytokinin signalling (Werner et al., 2003; Niemann et al., 2018). On the other hand, CKX2 resides in the ER and the apoplast. Its overexpression shows milder shoot phenotype compared to CKX1 and CKX3 overexpressors. This result suggests, that the cytokinin pool affected by CKX2 has less impact on the signalling in the shoot. These phenotypic consequences support the ER as a main cellular platform for active cytokinin receptors at least in some tissues (Romanov et al., 2018). However, the localization of individual *Arabidopsis* CKX proteins is still under study (Werner et al., 2003; Frébort et al., 2011; Hoyerová and Hošek, 2020).

The advantages of ER localization as a place of cytokinin perception and transduction are already widely discussed (Wulfetange et al., 2011; Lomin et al., 2018b; Romanov et al., 2018). The velocity and reliability of the cytokinin signalling could be increased due to the better interaction with AHPs. AHPs are distributed withing the whole intracellular space therefore it would shorten the distance for reaching the nucleus to trigger the cytokinin response genes. Moreover, such localization could be from an energetic point of view more efficient and alleviate the disadvantages caused by the long distance export to the PM through the secretory system. Finally, ER-localized receptors would also facilitate intracellular hormonal cross-talk as some other plant receptors are also localized inside the cell (Chen et al., 2002). Nevertheless, the hormone-binding CHASE domain part of the cytokinin receptor would be faced to the lumen of ER but at the moment it stays unclear how cytokinins penetrate the ER lumen and reach the receptor sensor module located inside the ER (Romanov et al., 2018).

Even though most of the results published on the subcellular localization of the cytokinin receptors primarily rely on gene expression studies, using transient systems and constitutive promoters, there is

nevertheless strong experimental evidence that a bulk of cytokinin receptor intracellular pool is present within the ER (Caesar et al, 2011; Lomin et al., 2011; Wulfetange et al., 2011). However, there is also a possibility that some part of the receptors reaches the PM - this should also be considered even though direct evidence of cytokinin receptor localization at the PM has not been demonstrated yet. In that case, cytokinins from apoplast would directly interact with the PM-localized binding domain and trigger the signalling at the surface of the cell (Romanov et al. 2018). As previously published, localization studies of the cytokinin receptors were performed only using protoplasts (transient expression assays); the localization of fusion cytokinin receptors AHK3-GFP and AHK2-GFP were observed in the above-group parts of the plant using transiently transformed *Arabidopsis* cotyledon cells (Caesar et al., 2011) and transiently transformed tobacco epidermal leaf cells (Wulfetange et al., 2011), all in the differentiated stages. Any clear evidence of localization of stable expression of CRE1/AHK4 cytokinin receptor in various cell types is missing (Romanov et al., 2018). The signalling of the receptors starting at the plasma membrane is supported by the observation, that the CRE1/AHK4 receptor interacts in the yeast-two hybrid system with proteins (adaptin, ADL1A, GNOM) involved in vesicular trafficking. The identification of these interactors could show that the cytokinin receptors are not only located at the PM but also in other cellular compartments supporting an intracellular transport of cytokinin receptors between PM and endosomes (Dortay et al., 2008; Wulfetange et al., 2011). A recent publication by Zürcher et al. (2016) shed light on the activity of cytokinin receptors at the PM. As a model, they used *Arabidopsis* heart-stage embryos of synthetic cytokinin reporter TCSn::GFP. Authors reported that a member of the transporter PUP family (PUP14) is involved in the modulation of the cellular cytokinin signalling. Interestingly, a PM-localized PUP14 imports bioactive cytokinins inside the cell in order to suppress the response to cytokinin. Moreover, PUP14 was expressed only in the cells that failed to respond to cytokinins. Also, silencing of *PUP14* produced ectopic cytokinin responses causing morphological defects. In the scenario proposed by Zürcher and colleagues, apoplastic cytokinins are important to initiate the PM-related signalling response, whereas the cytoplasm represents a sink for non-functional bioactive ligands. To test this hypothesis, authors performed experiments comparing the effect of PUP14 uptake with the effects of CKXs differentially targeted (apoplast/cytoplasm) on the cytokinin signalling response. *Arabidopsis* protoplasts transiently transfected with CKX2 (secreted to apoplast) were able to attenuate the cytokinin response triggered by *t*Z but not by the degradation-resistant BA. In contrast, CKX2 lacking the N-terminal signal sequence peptide, thus localized to the cytoplasm, did not affect the cytokinin response. Similar results were obtained with the cytosolic localized CKX7. These results suggest that apoplastic, but not cytoplasmic cytokinins, initiate the signalling (Zürcher et al.; 2016). Nevertheless, the affinity of the PUP transporters and the cytokinin receptors to the ligands would need further investigation to fully support the Zürcher et al. conclusions (Durán-Medina et al., 2017; Kang et al., 2017; Romanov et al., 2018).

Currently, it is clear, that the subcellular localization of cytokinin receptors is only partially resolved. Based on the published results, the AHK receptors are localized predominantly in the membranes of ER (Caesar et al, 2011; Lomin et al., 2011; Wulfetange et al., 2011). However, recent results pointed to the possibility of different subcellular localizations including the PM (Zürcher et al.; 2016). Romanov et al. proposed multiple signalling pathways that may include different localization of the cytokinin receptors, including the PM. Thus, it could be speculated that the different localization of cytokinin receptors and perception of active cytokinin may respond to a different organ or tissue and/or developmental stage, e.g. meristematic activity, differentiation, etc. Also, individual cytokinin receptors might differ in localization within the cell dependent on the cell/tissue type. Therefore, to define the different subcellular origin of cytokinin signalling of all AHK receptors remains elusive and needs to be investigated (Romanov et al., 2018).

Cytokinin fluoroprobe reveals multiple sites of cytokinin perception at plasma membrane and endoplasmic reticulum

Abstract

Plant hormone cytokinins are perceived by a subfamily of sensor histidine kinases, which via a two-component phosphorelay cascade activate transcriptional responses in the nucleus. Subcellular localization of the receptors proposed the ER membrane as a principal cytokinin perception site, while study of cytokinin transport pointed to the PM-mediated cytokinin signalling. Here, by detailed monitoring of the subcellular localizations of the fluorescently labelled natural cytokinin probe and the receptor CRE1/AHK4 fused to GFP reporter, it is shown that pools of the ER-located cytokinin receptors can enter the secretory pathway and reach the PM in cells of the root apical meristem, and the cell plate of dividing meristematic cells. Brefeldin A (BFA) experiments revealed vesicular recycling of the receptor and its accumulation in the BFA compartments. A revised view on cytokinin signalling and the possibility of multiple sites of perception at PM and ER is provided.

Introduction

The plant hormone cytokinin regulates various cell and developmental processes, including cell division and differentiation, embryogenesis, activity of shoot and root apical meristems, formation of the shoot and root lateral organs and others (Kieber and Schaller, 2018). Cytokinins are perceived by a subfamily of sensor histidine kinases, which via a two-component phosphorelay cascade activate transcriptional responses in the nucleus. Based on the subcellular localization of cytokinin receptors in various transient expression systems, such as leaf epidermal cells of tobacco (*Nicotiana benthamiana*), and membrane fractionation experiments of *Arabidopsis* and maize, the ER membrane has been proposed as a principal hormone perception site (Caesar et al., 2011; Lomin et al., 2011; Wulfetange et al., 2011). Intriguingly, a recent study of the cytokinin transporter PUP14 has pointed out that the PM-mediated signalling might play an important role in the establishment of cytokinin response gradients in various plant organs (Zürcher et al., 2016). However, localization of the cytokinin HK receptors to the PM, although initially suggested (Kim et al., 2006), remains ambiguous. Here, by monitoring subcellular localizations of the fluorescently labelled cytokinin probe iP-NBD (Kubiasová et al., 2018), derived from the natural bioactive cytokinin iP, and the cytokinin receptor CRE1/AHK4 fused to GFP reporter, it is shown that pools of the ER-located cytokinin fluoroprobes and receptors can enter the secretory pathway and reach the PM. It is demonstrated that in cells of the root apical meristem, CRE1/AHK4 localizes to the PM and the cell plate of dividing meristematic cells. The BFA experiments revealed vesicular recycling of the receptor and its accumulation in the BFA compartments. Our results provide a revised view on cytokinin signalling and the possibility of multiple sites of perception at both PM and ER, which may determine specific outputs of cytokinin signalling.

Material and Methods

Plant material

Arabidopsis thaliana (L.) Heynh (*Arabidopsis*) plants were used. The transgenic lines have been described elsewhere: *cre1-2* (Inoue et al., 2001), triple mutant *cre1-12, ahk2-2, ahk3-3* (Juan Carlos Montesinos), *TCSn::ntdT:tNOS-pDR5v2::n3GFP* (Smet et al., 2019), *pup14* (Zürcher et al., 2016), p24δ5-RFP (Montesinos et al., 2012), HDEL-RFP (Nelson et al., 2007), Wave lines 2R/RabF2b (LE/PVC), 9R/VAMP711 (Vacuole), 13R/VTI12

(TGN/EE), 18R/Got1p (Golgi), 22R/SYP32 (Golgi), 34R/RabA1e (Endosomal/Recycling endosomal), 131R/NPSN12 (PM) and 138R/PIP1;4 (PM; Geldner et al. 2009), *ARR5::GUS* (D'Agostino et al., 2000), *35S::GFP* line was kindly provided by Shutang Tan (IST Austria, Austria). *35S::CRE1/AHK4-GFP* plants were generated as described below.

Growth conditions

Surface-sterilized seeds of *Arabidopsis* ecotype Columbia (Col-0) and the other transgenic lines were plated on half-strength (0.5x) Murashige and Skoog (MS) medium (Duchefa) with 1% (w/v) sucrose and 1 % (w/v) agar (pH 5.7). The seeds were stratified for 2-3 days at 4 °C in darkness. Seedlings were grown on vertically oriented plates in growth chambers at 21 °C under long day conditions (16 h light and 8 h darkness) using white light (W), which was provided by blue and red LEDs (70-100 µmol m^{-2}s^{-1} of photosynthetically active radiation), if not stated otherwise.

Pharmacological treatments for bio-imaging

Seedlings 4 to 5-day-old were transferred onto solid 0.5x MS medium with or without the indicated chemicals. The drugs and hormones used were: BA in different concentrations (0.1 µM, 0.5 µM, 1 µM and 2 µM), *tZ* (0.1 and 1 µM), iP (5 µM). Mock treatments were performed with equal amounts of solvent (DMSO). Treatments with 5 µM iP-NBD and 5 µM Ade-NBD were performed in liquid 0.5x MS medium and imaging was carried out within 30 min time frame. For co-localization of the cytokinin fluoroprobe with PM marker, seedlings were pre-treated with 2 µM FM4-64 for 5 min and transferred into 5 µM iP-NBD supplemented 0.5x MS medium, followed by imaging within 30 minutes time frame. To explore affinity of iP-NBD to the BFA endosomal compartments, seedlings were incubated in 50 µM BFA for 1 h and afterwards transferred into iP-NBD supplemented medium and imaged. Localization of the CRE1/AHK4-GFP in the BFA endosomal compartments was examined in 4 to 5- day-old seedlings incubated in 50 µM BFA for 1 h. For BFA washout experiments, seedlings were placed in a fresh BFA-free 0.5x MS medium, which was replaced every 10 min for at least 1 h.

Recombinant DNA Techniques

The coding region of the cytokinin receptor CRE1/AHK4 (*At2g01830*) was amplified without the stop codon by PCR using a gDNA from *Arabidopsis thaliana* Col-0 as a template and cloned into the Gateway vector *pENTR_2B* dual selection (primers: AHK4_Fw_SalI_KOZAK *CGCGTCGACCccaccATGAGAAGAGATTTTGTGTATAATAATAATGC* and AHK4_R_NotI *TTTTCCTTTTGCGGCCGCgaCGACGAAGGTGAGATAGGATTAGG*). To construct C-terminal fusion of *CRE1/AHK4* with *GFP*, *CRE1/AHK4* was shuttled into the destination vector *pGWB5* (Nakagawa et al., 2007) containing *35S* promoter to create *35S::CRE1/AHK4-GFP* construct. For the transient Luciferase assay in *Arabidopsis* protoplasts, *CRE1/AHK4-GFP* fusion construct was re-cloned into *p2GW7,0* vector. *CRE1/AHK4-GFP* region was amplified by PCR using *pGWB5_CRE1/AHK4-GFP* as a template (primers: *35S_FW CCACTATCCTTCGCAAGAC*CCTTC and AHK4_5A_NheI_RE *TATTCCAATgctagcTTACTTGTACAGCTCGTCCATGC*) and ligated into the Gateway *pENTR_2B* dual selection entry vector. *CRE1/AHK4-GFP* was shuttled into the destination vector *p2GW7,0*.

Plant transformation

Transgenic *Arabidopsis* plants were generated by the floral dip method using *Agrobacterium tumefaciens* strain GV3101 (Clough et al., 1998). Transformed seedlings were selected on medium supplemented with 30 µg mL^{-1} hygromycin.

Competitive binding assay in E. coli strains

Receptor direct binding assays were conducted using the *E. coli* strain KMI001 harbouring either the plasmid *pIN-III-AHK4* or *pSTV28-AHK3*, which express the *Arabidopsis* histidine kinases CRE1/AHK4 or AHK3 (Suzuki et al., 2001; Yamada et al., 2001). Bacterial strains were kindly provided by Dr. T. Mizuno (Nagoya, Japan). The competitive binding assays (Romanov et al., 2005; Nisler et al., 2010) were performed with homogenous bacterial suspension with an OD_{600} of 0.8 and 1.2 for the CRE1/AHK4 and the AHK3 expressing strains, respectively. The competition reaction was allowed to proceed with 3 nM [2-^{3}H]*t*Z and 6-18 nM [2-^{3}H]iP, and various concentrations of iP and iP-NBD, 0.1% (v/v) DMSO was added as a solvent control. After 30 min incubation at 4 °C, the sample was centrifuged (6000 g, 6 min, 4 °C), the supernatant was carefully removed, and the bacterial pellet was resuspended in 1 mL of a scintillation cocktail (Beckman, Ramsey, MN, USA) in an ultrasonic bath. Radioactivity was measured by scintillation counting by a Hidex 300 SL scintillation counter (Hidex, Finland). To discriminate between specific and nonspecific binding, a high excess of unlabelled natural ligand *t*Z, or iP (at least 3000-fold) was used for competition. The functional inhibition curves were used to estimate the IC_{50} values. The K_i values were calculated using equation $K_i = IC_{50}/(1+ [radioligand]/K_D)$ according to Cheng and Prusoff (Cheng and Prusoff, 1973). [2-^{3}H]*t*Z and [2-^{3}H]iP were provided by Dr. Zahajská from the Isotope Laboratory, Institute of Experimental Botany, Czech Academy of Sciences.

Quantitative RT–PCR

RNA was extracted with Monarch® Total RNA Miniprep Kit (NEB) from roots of 5-day-old plants that were sprayed with mock (DMSO) or 0.01µM iP, 0.1µM iP, 1µM iP, 10µM iP-NBD, 100µM iP-NBD or co-treatment of 0.1µM iP + 10µM iP-NBD, 0.1µM iP + 100µM iP-NBD for 15 min (Figure 4B); mock (DMSO) or 5 µM iP (Figure 14E); for 15 min. Poly(dT) cDNA was prepared from 1 µg of total RNA with the iScript cDNA Synthesis Kit (Biorad) and analyzed on a LightCycler 480 (Roche Diagnostics) with the Luna® Universal qPCR Master Mix (NEB) according to the manufacturer's instructions. The expression of *CRE1/AHK4* of the two independent lines was quantified either with a specific primer pair (AHK4-GFP_FW: *TATCTCACCTTCGTCGTCGC* and *AHK4-GFP*_RE: *CCTTGCTCACCATGGATCCTC*) and their relative expressions were compared to the house-keeping gene *PP2A* (PP2A_FW: *TAACGTGGCCAAAATGATGC* and PP2A_RE: *GTTCTCCACAACCGCTTGGT*) or with AHK4_FW: *GAACTGGGCACTCAACAATCA* and AHK4_RE: *ACGAATTCAGAGCACCACCA* pair of primers and their relative expression refer to the Col-0 mock treatment. All qRT-PCR quantifications were done using PP2A as a reference gene (Figure 4B, Figure 14A, E) For the *ARR* expressions (ARR5_FW: *TGCCTGGGATGACTGGATATG,* ARR5_RE: *CTCCTTCTTCAAGACATCTATCG,* ARR7_FW: TACTCAATGCCAGGACTTTCAGG, ARR7_RE: TCTTTGAGACATTCTTGTATACGAGG, ARR16_FW: *CGTAAACTCGTTGAGAGGTTGCTC* and ARR16_RE: *GCATTCTCTGCTGTTGTCACTTTG*), the fold change refer to the Col-0 mock treatment. The experiment was performed in 3 technical and 3 biological replicates.

Measurements of iP-NBD cell transport kinetics

Seedlings of 4-day-old *Arabidopsis* Col-0 were pre-treated for 20 min with 5 µM iP or DMSO and transferred into MS media containing 5 µM iP-NBD and 5 µM iP/DMSO and instantly imaged. To examine PUP14 dependent iP-NBD transport kinetics, 4-day-old seedlings of *pup14* and Col-0 were treated with 5 µM iP-NBD and immediately imaged. For both experiments imaging was performed in the same area of the root for 12 min every 2, 7 and 12 min to minimize photobleaching. iP-NBD fluorescence was measured with ImageJ in the LRC cells (iP pre-treatment experiment) and in the root epidermal cells (*pup14* experiment) from 4-7 cells originating from 4-5 roots.

Imaging

For confocal microscopy imaging, a vertical-stage laser scanning confocal Zeiss 700 (LSM 700) and Zeiss 800 (LSM 800), described in von Wangenheim et al., 2011, with a 20×/0.8 Plan-Apochromat M27 objective, a LSM 800 inverted confocal scanning microscope Zeiss, with a 40× Plan-Apochromat water immersion objective and a Zeiss LSM 880 inverted fast Airyscan microscope with a Plan-Apochromat 63x NA 1.4 oil immersion objective were used. Samples were imaged with excitation lasers 488 nm for GFP (emission spectrum 490-560 nm) and NBD (emission spectrum 529-570 nm) and 555/561 nm (inverted/vertical) for RFP (emission spectrum 583-700 nm), FM4-64 (emission spectrum 650-730 nm), mCherry (emission spectrum 570-700 nm) and tdTomato (emission 560-700 nm).

For super-resolution SIM microscopy, an Axioimager Z.1 with Elyra PS.1 system coupled with a PCO.Edge 5.5 sCMOS camera was used. Samples were excited with the 488nm and 561nm laser lines. Oil immersion objective (63x/1.40) and standard settings (the grating pattern with 5 rotations and 5 standard phase shifts per angular position) were used for image acquisition. Image reconstruction was done in Zeiss Zen software (black version with structured illumination module) using manual mode with adjusting the noise filter and super-resolution frequency weighting sliders as described in (Komis et al., 2015a). For image post-processing, profile measurements and co-localization analysis, the Zeiss Zen 2011, ImageJ (National Institute of Health, http://rsb.info.nih.gov/ij), Photoshop 6.0/CS, GraphPad Prism 8 and Microsoft PowerPoint programs were used. For the SIM co-localization experiments 30 PM regions originating from the root cells of 5 seedling plants were used.

Receptor activation assay

The receptor activation assays were conducted using the *E. coli* strain KMI001 harbouring either the plasmid *pIN-III-AHK4* or *pSTV28-AHK3*, which express the *Arabidopsis* histidine kinases CRE1/AHK4 or AHK3 (Suzuki et al., 2001; Yamada et al., 2001). Bacterial strains were kindly provided by Dr. T. Mizuno (Nagoya, Japan). The assays were performed in liquid M9 media enriched with 0.1% casamino acids (casein hydrolysate, acid hydrolyzed; Merck, Germany) and antibiotics (ampicilin/carbenicilin, and chloramphenicol for culturing of CRE1/AHK4- and AHK3-expressing bacteria, respectively) using 96-well plate format (Spíchal, 2011). First, the *E. coli* strains were grown overnight in M9 medium (containing 0.1% casamino acids and antibiotics) to OD_{600} ~ 1. These precultures were diluted 1:600 in M9 medium (containing 0.1% casamino acids and antibiotics) and a 96-well plate was filled up with 200 μL of the diluted culture per well. 1 μL stock solution of either the tested compound or solvent control was added to reach desired final concentrations and the cultures were further grown while shaking for 17 h at 25 °C. 50 μL aliquots of the culture were transferred to wells of a 96-well plate containing 2 μL of 25 mM 4-methyl umbelliferyl galactoside (MUG, Sigma)/well. The plate was subsequently incubated for 30 min at 37 °C and the reaction was stopped by adding 100 μL glycine carbonate stop buffer (133 mM glycine, 83 mM Na_2CO_3, pH 10.7). OD_{600} of remaining culture was determined using a spectrophotometer. Fluorescence was measured using Synergy H4 Multi-Mode Microplate Reader (BioTek, USA) at the excitation and emission wavelengths of 365 and 460 nm, respectively. β-galactosidase activity was calculated as nmol 4-methylumbelliferone OD_{600}^{-1} h^{-1}.

ARR5::GUS reporter gene assay

Arabidopsis ARR5::GUS transgenic seeds were surface-sterilized and plated on 0.5x MS medium with 0.1% (w/v) sucrose and 0.05% (w/v) MES–KOH (pH 5.7) in 24-well plates, 20 seeds per well. The plates were stratified for 3 days at 4 °C in darkness and then grown under long-day conditions (16 h light/8 h dark) at 22 °C in a growth chamber. To the wells containing 3-day-old seedlings, BA and/or tested compound or DMSO (solvent control, final concentration 0.1%) was added and the seedlings were grown for an additional 16 h. After that, the seedlings were flash frozen in liquid nitrogen. Quantitative determination of GUS activity in seedlings

extracts was performed using 4-methylumbelliferyl glucuronide as a substrate (Nisler et al., 2010) and the fluorescence was measured using Synergy H4 Multi-Mode Microplate Reader (BioTek, USA) at excitation and emission wavelengths of 365 and 450 nm, respectively. The GUS activity was expressed in relative fluorescence units (RFU) of MU per seedling.

Western blot analysis of AHK4-GFP protein levels

To evaluate levels of the CRE1/AHK4-GFP protein expression, total protein extract was obtained from 5-day-old seedlings extracted with 1x Laemmli buffer (2-Mercaptoethanol, 0.1% Bromophenol blue, 0.0005% Glycerol, 10% SDS (electrophoresis-grade), 2% Tris-HCl, 63 mM pH 6.8). Protein extracts were used for SDS–PAGE using gels acrylamide 10%, and blotted to PVDF transfer membrane (Millipore). Two hours incubation with monoclonal mouse anti-GFP (JL-8, Clontech) 1:5000; or 1 hour incubation with monoclonal mouse anti-Actin (10-B3, Sigma) 1:5000 for protein loading control; as primary antibodies were used. As a secondary antibody, 1 hour incubation sheep anti-mouse IgG Horseradish Peroxidase - Linked F(ab')2 Fragment (NA9310, GE Healthcare) 1:15000 was used. SuperSignal™ West Femto Maximum Sensitivity Substrate Thermo Fisher (4 minutes incubation) was used for detection of the signal.

TCS reporter expression in planta

5-day-old seedlings expressing the cytokinin signalling reporter *TCSn::ntdT:tNOS* (line *TCSn::ntdT:tNOS-pDR5v2::n3GFP*) were transferred on non- or with cytokinin (1 μM iP, 1μM iP-NBD or iP 1 μM + 1 μM iP-NBD) supplemented Murashige and Skoog media for 6 or 15 h. The *TCS:ntdT* expression (red, LUT inferno) in root tip was monitored using a confocal microscope. Fluorescence intensity (arbitrary numbers) of TCS:ntdT signal was measured in cells of provasculature at the root tip meristematic zone (n > 8 roots per treatment).

Luciferase transient expression assay

The Luciferase transient expression assays were performed on the protoplasts isolated from 4-days-old *Arabidopsis* root suspension culture. The protoplasts were isolated in an enzyme solution (1% cellulose; Serva, 0.2% Macerozyme; Yakult in B5-0.34M glucose-mannitol solution; 2.2 g MS with vitamins, 15.25 g glucose, 15.25 g mannitol, H_2O to 500 mL pH to 5.5 with KOH) with slight shaking for 3-4 h and centrifuged at 800 g for 5 min. The pellet was washed with B5-0.34M glucose-mannitol solution and resuspended in B5-0.34M glucose-mannitol solution to a final concentration of $2x10^5$ protoplasts per 50 μl. The protoplasts were co-transfected with 3 μg of a reporter plasmid expressing *Firefly* Luciferase (*f*LUC), 2 μg of a normalization plasmid containing the *Renilla* Luciferase (*r*LUC) and 10 μg of the p2GW7,0 plasmid carrying either the cytokinin receptor (*35S::AHK4-GFP*) or reporter only (*35S::GUS* or *35S::GFP*) constructs. DNAs were gently mixed with 50 μl of protoplast suspension and 60 μl of PEG solution (0.1M Ca(NO$_3$)$_2$, 0.45M mannitol, 25% PEG 6000) and incubated in the dark for 30min. Then 140 μl of 0.275M Ca(NO$_3$)$_2$ solution was added to wash off PEG, wait for sedimentation of the protoplasts and remove 240 μl of the supernatant. The protoplast pellet was resuspended in 200 μl of B5-0.34M glucose-mannitol solution and incubated for 16 h with either 0.5 μM BA or in mock solution in the dark at room temperature. After transfection, the protoplasts were centrifuged at 1200g for 5 min and lyzed; *f*LUC and *r*LUC activities were determined with the Dual-Luciferase reporter assay system (Promega). Variations in transfection efficiency and technical errors were corrected by normalization of *f*LUC by the *r*LUC activities. The mean value was calculated from four measurements and experiment was repeated three times.

Root growth analysis

Root growth and lateral root density were measured on seedlings grown vertically on Murashige and Skoog medium. Images were taken with a vertically positioned scanner, EPSON perfection v800 Photo. The root growth rate was evaluated using 5-day-old seedlings (n ≥ 16). Lateral root density quantification was performed using 9-day-old seedlings (n ≥ 16). Relative root growth inhibition by cytokinin was measured per day (24h) and was calculated as a ratio of 1 μM BA to DMSO treated *Arabidopsis* seedlings in the corresponding days after germination. The statistical significance was evaluated with the Student's t-test and two-way ANOVA.

Results and discussion

Cytokinin fluoroprobe iP-NBD exhibits affinity to the cytokinin receptors

Fluorescently labelled analogues of phytohormones including auxin, gibberellin, brassinosteroid and strigolactone have been successfully used to map the intracellular fate of their receptors *in planta* (Lace and Prandi, 2016). To adopt this tool for mapping subcellular localization of cytokinin receptors, using docking experiments and cytokinin activity screening bioassays, a fluorescently labelled bioactive compound that interacts with the binding site of a cytokinin receptor was selected.

Cytokinin groups a collection of N^6-substituted adenine derivatives, including *t*Z and iP. They show different localization pattern and distinct partially overlapping functions *in planta*. *t*Z-type cytokinins play a role of acropetal messengers, whereas iP-type cytokinins operate as systemic or basipetal messengers (Kudo et al., 2010). The isoprenoid cytokinins (*t*Z- or iP-types) showed similar distribution patterns in different cell type populations within the root apex (Antoniadi et al., 2015). While *t*Z-type cytokinins were detected at much lower levels than other isoprenoid cytokinins, when concerns free cytokinin bases, the *t*Z content was found to be the highest among the free bases, followed by free iP that showed relatively enhanced content also in the stele (Antoniadi et al., 2015). Hence, iP seems to be a good candidate for a cytokinin fluoroprobe design. Moreover, iP is a natural cytokinin that cannot be transformed through *O*-glycosylation at the cytokinin side chain and thus the possibility of metabolic conversions of the cytokinin fluoroprobe by cytokinin deactivation enzymes *in planta* is minimized. Furthermore, a covalent attachment of NBD, a small fluorophore, to the *N*9 position of iP eliminates the risk of metabolic conversion of the final cytokinin fluorescent probe iP-NBD (Figure 2A) through *N*-glycosylation, or formation of cytokinin nucleotides.

The stable attachment of the *N*9-substituent also prevents modifications at the *N*7 position by making this cytokinin derivative completely inaccessible for *N*-glucosyltransferases (Hou et al., 2004). Docking simulations using the CRE1/AHK4-iP crystal structure (Hothorn et al., 2011) and corresponding homology models suggested that iP-NBD may be fully embedded into the active sites of all AHK receptors (Figure 2B) with micromolar range affinity.
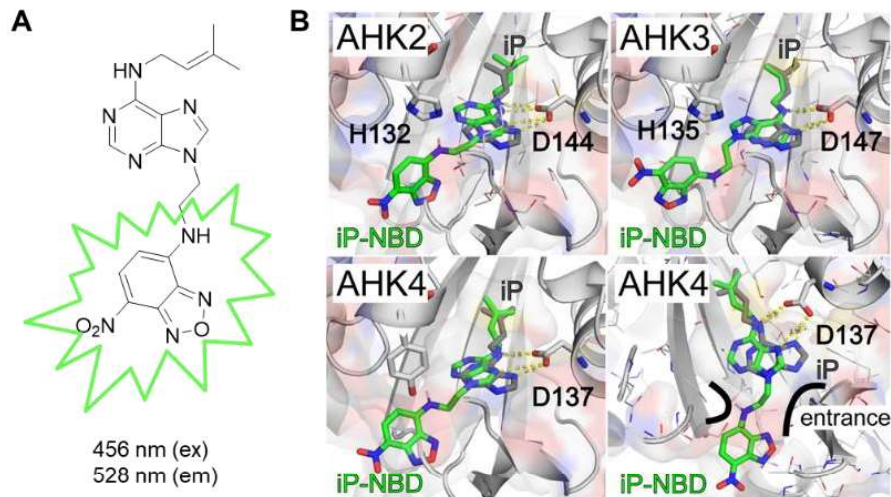
Figure 2: *Structure and docking simulations of iP-NBD. **A** – Chemical structure of iP-NBD with excitation and emission wavelengths. **B** – Superposition of docking simulation of iP-NBD (in green) and natural ligand iP (in grey) in AHK2, AHK3 (upper row) and CRE1/AHK4 (left panel of lower row) receptor cavity showing the embedded position of the ligands. CRE1/AHK4 (right panel of lower row) with visualized entrance channel and the fluorophore fitting into an antechamber through the ethylene linker.*

The affinity of iP-NBD to the cytokinin receptors was measured using bacterially expressed recombinant AHK3 and CRE1/AHK4 (Spíchal et al., 2004). Both receptors share ligand preference for *t*Z, but AHK3 has about 10-fold lower affinity towards iP compared to CRE1/AHK4 (Spíchal et al., 2004; Romanov et al., 2006). Competitive binding assays with *E. coli* expressing either AHK3 or CRE1/AHK4 (Romanov et al., 2005) showed that iP-NBD competes for receptor binding with radiolabelled natural cytokinins iP and *t*Z in different ranges of ligand concentrations (Figure 3A, B), corresponding with the receptor ligand preferences. As predicted, iP-NBD had a lower affinity to the AHK3 (with K_i~ 37 μM and > 100 μM against radiolabelled *t*Z and iP, respectively) than to the CRE1/AHK4 (with K_i ~ 1.4 μM and ~ 31 μM against radiolabelled *t*Z and iP, respectively), indicating that this fluoroprobe is more specific to CRE1/AHK4 (Figure 3A, B).
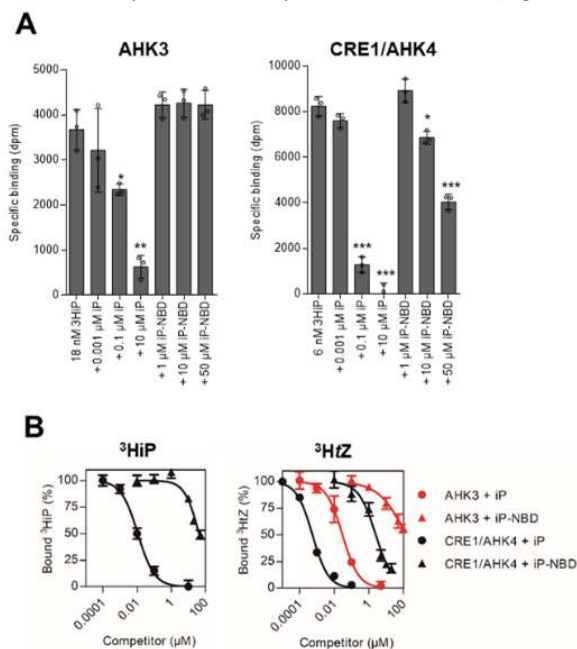
Figure 3: *iP-NBD interacts with cytokinin perception. **A** – Competitive binding assay with E. coli expressing AHK3 and CRE1/AHK4. Binding of [2-³H]iP (18 nM and 6 nM in the case of AHK3 and CRE1/AHK4, respectively) was assayed together with increasing concentrations of unlabelled iP and iP-NBD. The bars represent mean ± s.d., *** = p < 0.001, ** = p < 0.01, * = p < 0.05; n = 3 (Student's t-test). **B** – Competitive binding assay with E. coli expressing AHK3 and CRE1/AHK4. Binding of 6 nM [2-³H]iP and 3 nM [2-³H]tZ was assayed together with increasing concentrations of of iP-NBD (triangles) and unlabelled iP (circles). The functional inhibition curves for AHK3 and CRE1/AHK4 are presented in red and black, respectively.*

Docking into the CRE1/AHK4-iP crystal structure (Hothorn et al., 2011) showed that iP-NBD binds into the receptor cavity in a similar manner to iP, but the lack of interaction via *N*9 (which links the fluorescent probe) causes the purine ring shift leading to the larger distance and thus weaker interaction between *N*7 and Asp137 (Figure 2B). Despite iP-NBD being accommodated into the cytokinin-binding pockets of the receptors, it showed limited ability to trigger cytokinin response in *E. coli* (*ΔrcsC, cps::lacZ*) receptor activation assay (Spíchal et al., 2004; Figure 4A). In *Arabidopsis* seedlings, iP-NBD in a concentration dependent manner significantly increased expression of the early cytokinin response gene *ARABIDOPSIS RESPONSE REGULATOR5* (*ARR5*) already 15 minutes after its application, suggesting that the synthetic cytokinin fluoroprobe can activate cytokinin signalling pathway *in planta* (Figure 4B, C).
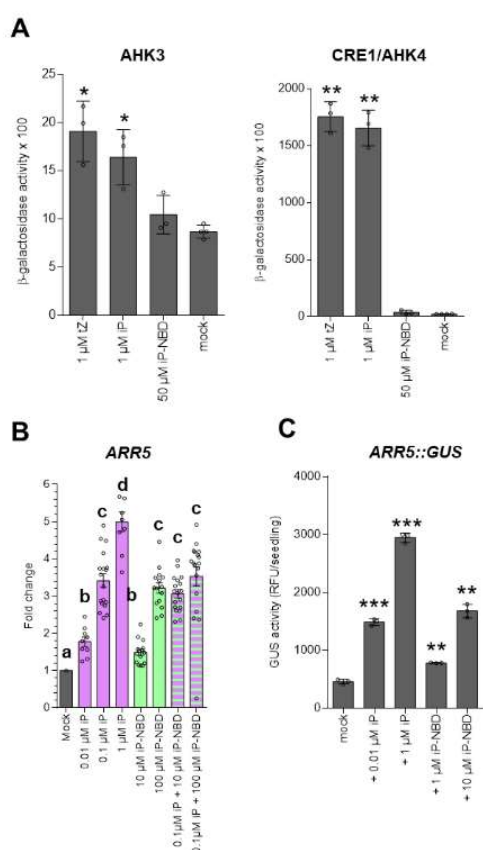

Figure 4: *A* *– Comparison of the cytokinin response in E. coli (ΔrcsC, cps::lacZ) receptor activation assay with recombinant AHK3 and CRE1/AHK4 receptors, triggered by 1 μM tZ and 1 μM iP (positive controls) and 50 μM iP-NBD. Mock treatment represents solvent control DMSO (0.1%). The bars represent mean ± s.d., ** = p < 0.01, * = p < 0.05; by Student's t-test, n = 3. **B** –Expression of the early cytokinin response gene ARR5 in 5-day-old seedlings of Col-0 treated with 0.01 μM iP, 0.1 μM iP, 1 μM iP, 10 μM iP-NBD, 100 μM iP-NBD or co-treatments of 0.1 μM iP + 10 μM iP-NBD, 0.1 μM iP + 100 μM iP-NBD or DMSO for 15 min. (mean ± s.d., p < 0.05 by two-way ANOVA. n = 9-18; 3 technical replicates from 3 biological replicates per condition). **C** - Quantitative evaluation of β-glucuronidase activity in Col-0 seedlings harbouring ARR5::GUS after incubation with 0.01 μM and 1 μM cytokinin iP, and 1 μM and 10 μM fluoroprobe iP-NBD. Mock treatment represents solvent control DMSO (0.1%). The bars represent mean ± s.d., *** = p < 0.001, ** = p < 0.01; n = 3 (Student's t-test).*

In comparison to iP, a natural cytokinin, iP-NBD triggered cytokinin response with significantly lower efficacy and when applied together with iP no additive effect on the *ARR5* expression could be detected (Figure 4B). In the *pTCSn::ntdTomato:TNOS* cytokinin reporter assay (Smet et al., 2019), iP-NBD did not increase expression of the reporter 6 hours after treatment, but when applied simultaneously with iP, iP-NBD partially attenuated iP-mediated enhancement of the TCS reporter expression (Figure 5).
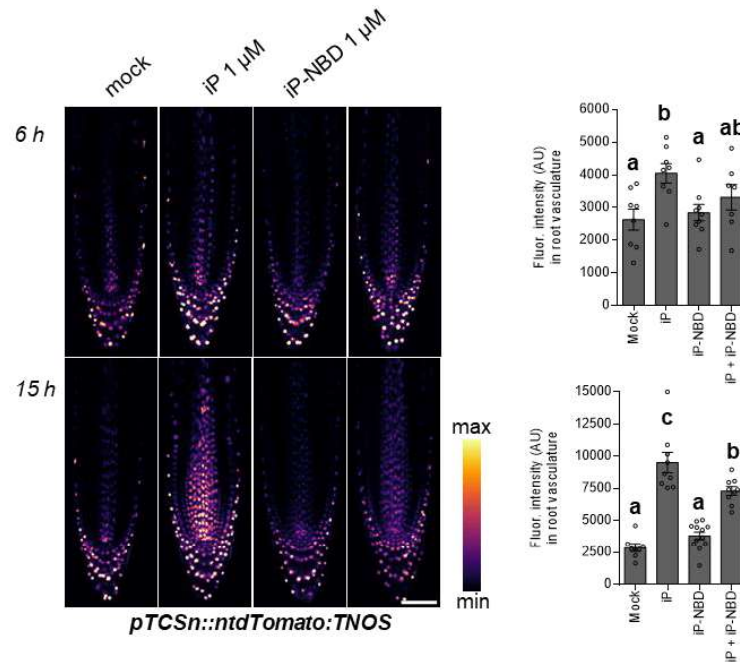

Figure 5: *Expression of the cytokinin sensitive reporter pTCSn::ntdTomato:TNOS in Arabidopsis roots treated with 1 µM iP (positive control) and 1 µM iP-NBD for 6 and 15 h. Fluorescence intensity measured in the root vasculature (mean ± s.d., p < 0.05 by two-way ANOVA, n > 8 root tips per condition). Scale bar = 50 µm.*

Altogether, these analyses suggest a partial agonistic mode of action of iP-NBD that binds to a cytokinin receptor and activates it with only minimal efficacy compared to a natural cytokinin ligand. At excess concentrations, iP-NBD is then acting as a competitive antagonist, competing with the full agonist (a natural cytokinin) for receptor occupancy. Altogether, the above experiments show that iP-NBD binds to cytokinin receptors and has potential for specifically tracking their subcellular localization *in planta*.

Biological characteristics of iP-NBD

To reliably monitor iP-NBD distribution *in planta*, its biological stability, fluorescence characteristics and saturation kinetics was evaluated as first. iP-NBD stability across the different pH conditions that appear in apoplast, cytosol and different cell organelles, was tested *in vitro* in the pH ranging from 4 to 8 by quantitative liquid chromatography-tandem mass spectrometry (LC-MS/MS). No significant changes of iP-NBD concentration were found in the buffered solutions under both 6 and 16 hours of incubation pointing to a broad pH stability of iP-NBD (Figure 6A).
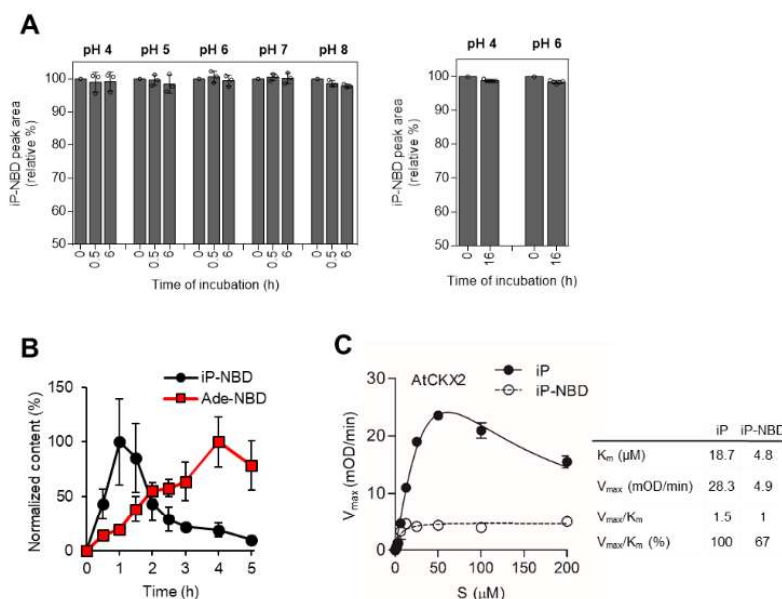
Figure 6: *Evaluation of iP-NBD biological stability.* ***A*** *– In vitro pH stability of iP-NBD. Stability of iP-NBD was followed by LC-MS/MS analysis in water solution after 0.5 h and 6 h of incubation in the McIlvaine buffer (pH range 4-8; left panel) and after 16 hours of incubation in the McIlvaine buffer (pH 4 and pH 6; right panel). Bars represent relative peak areas of iP-NBD, which was incubated for given time periods in the respective buffer solution as compared to the iP-NBD control (0 h) at the same concentration (mean ± s.d., n≥3).* ***B*** *– In vivo iP-NBD stability. iP-NBD was applied to Arabidopsis (Ler) cells suspension and in the timeframe of 0.5-5 h its intracellular processing was followed by quantitative LC-MS/MS analysis using iP-NBD and Ade-NBD (the expected product of side-chain cleavage by endogenous CKXs) as molecular standards. The values presented in the graph are normalized to the respective highest content of both compounds analysed. The highest contents of intracellular iP-NBD and Ade-NBD were 7920 ± 3150 pmol/g and 19633 ± 4903 pmol/g, respectively (fresh weight, mean ± s.d., n = 4).* ***C*** *– Kinetics and kinetic parameters of in vitro AtCKX2 enzymatic activity estimated using iP and iP-NBD as substrates, respectively, in the concentration range of 1.6 - 200 µM.*

Taking into account the chemical structure of iP-NBD that prevents *O*- and/or *N*-glycosylation, the presumed *in planta* catabolic pathway of this molecule might be N^6 side-chain cleavage by endogenous CKX activity. Hence, the *in vivo* stability of the fluoroprobe was tested. iP-NBD was applied to *Arabidopsis* cells, and its intracellular processing was followed over a period of 0.5 - 5 h by LC-MS/MS analysis. Thus, iP-NBD and *N*9-NBD-labelled adenine (Ade-NBD), the expected product of iP-NBD deprenylation by CKXs, were used as molecular standards. Under these conditions, iP-NBD showed high stability within the first 30 minutes (> 90% recovery of intact molecule), dropping drastically after 5 hours. The concentration of Ade-NBD steadily increased, reaching the maximal concentration after 4 hours (Figure 6B). The fact that iP-NBD can be recognized by CKXs as a substrate was confirmed by *in vitro* enzymatic reaction with AtCKX2, one of the most active CKX isoforms with an apoplastic localization (Werner et al., 2003). AtCKX2 converted iP-NBD to the product with approx. 6-times lower turnover rate k_{cat} compared to the parental iP molecule, but only with 33% lower catalytic efficiency V_{max}/K_m (Figure 6C).

Cellular internalization of iP-NBD follows rapid saturation kinetics

In terms of fluorescent characteristics, the emission maximum of the cytokinin fluoroprobe was in the yellow-green part of the spectrum at 528 nm suitable for co-localization with fluorescent markers emitting at red wavelengths (Figure 7A, B).
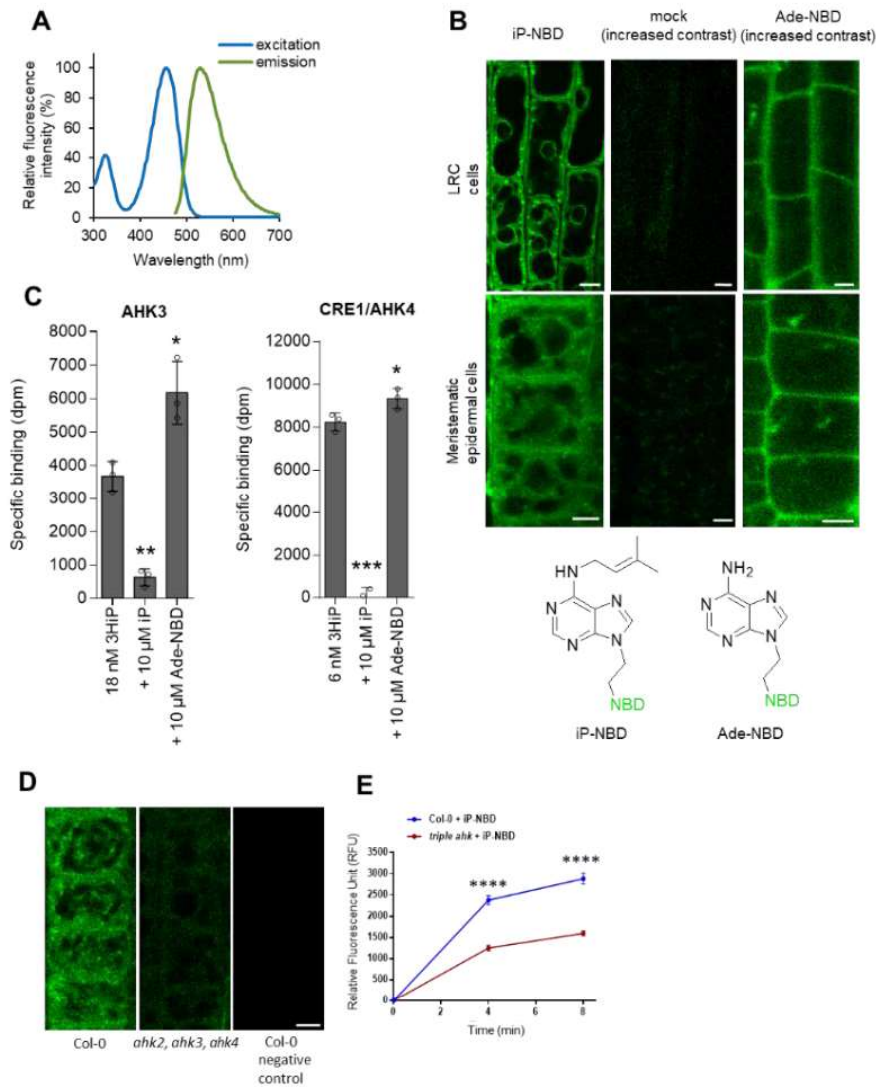
19

Figure 7: *Evaluation of iP-NBD fluorescence characteristics. **A** – Fluoroprobe absorption-emission spectral diagram measured with 100 µM iP-NBD dissolved in 100% ethanol. Absorption (excitation) and emission spectra are reaching their maximal fluorescence intensities in 456 nm (ex) and 528 nm (em). **B** – Chemical structures and differential localization of iP-NBD and Ade-NBD in Arabidopsis LRC and epidermal cells. Roots were treated for 10 min with iP-NBD or Ade-NBD (5 µM). Roots without any treatment (mock) were used as a control. **C** – Competitive binding assay with E. coli expressing AHK3 and CRE1/AHK4 with Ade-NBD. Binding of [2-^{3}H]iP (18 nM and 6 nM in the case of AHK3 and CRE1/AHK4, respectively) was assayed together with high excess concentration of Ade-NBD (10 µM), and unlabelled iP (10 µM) as a positive control (mean ± s.d., **** = p < 0.0001, *** = p < 0.001, ** = p < 0.01, * = p < 0.05; by Student's t-test, n = 3). **D, E** – Localization of iP-NBD (5 µM) in the Arabidopsis epidermal cells stained for 8 min in wild type (Col-0) and triple ahk mutant. All pictures were taken with the same settings. Col-0 without any treatment was used as a control (**D**). Graph shows kinetics of 5 uM iP-NBD uptake in the root epidermal cells of wild type and triple ahk mutant. Fluorescence was measured in 3 time points (0, 4, 8 min). The bars represent average ± s.e., **** = p < 0.0001; n ≥ 30 (Student's t-test). Scale bar = 5 µm.*

The quantitative fluorescence microscopy of the wild type plants (Col-0) showed that the cellular internalization of iP-NBD followed rapid saturation kinetics, reaching a plateau after approximately 12 min (Figure 8A). Pre-treatment with non-labelled iP and subsequent application of iP-NBD resulted in a significant reduction of intracellular iP-NBD fluorescence (Figure 8A). This suggested that transport and/or intracellular binding competition between iP-NBD and the natural cytokinin competitor was taking place, further pointing

to the cytokinin-like properties of the iP-NBD molecule. Significantly slower progression of iP-NBD accumulation in cells of a *pup14* mutant (lacking the functional cytokinin transporter PUP14) confirmed that specific cytokinin transport partially accounts for the amount of iP-NBD detected intracellularly (Figure 8B).
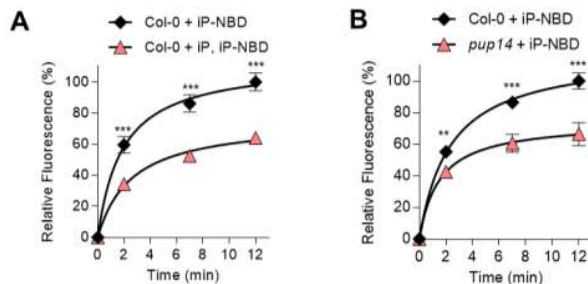

Figure 8: *iP-NBD interacts with cytokinin transport. **A** – Kinetics of 5 µM iP-NBD uptake in Arabidopsis LRC cells of wild type (Col-0) pre-treated with 5 µM iP. **B** – Kinetics of 5 µM iP-NBD uptake in root meristem epidermal cells of wild type (Col-0) and pup14. iP-NBD fluorescence was measured in four time points (0, 2, 7 and 12 min). The bars represent mean ± s.d., *** = p < 0.001, ** = p < 0.01; n ≥ 20 (Student's t-test; **A, B**).*

Unlike iP-NBD, Ade-NBD, which lacks the cytokinin-specific side chain, has no affinity to the cytokinin receptors (Figure 7C) and exhibited a weak diffused apoplastic and patchy intracellular signal in the epidermal cells (Figure 7B). The results from analyses of the *ahk2*, *ahk3*, *ahk4* triple mutant show a reduced accumulation of iP-NBD in the root epidermal cells when compared to the WT (Figure 7D, E). However, the mutant lacking all three receptors exhibits severe developmental defects, seedlings are small with short roots. Thus, the reduced iP-NBD signal in cells might be a result of less efficient transport or overall affected fitness of these seedlings.

iP-NBD co-localizes with ER, TGN and early endosomal markers

The affinity of iP-NBD to the cytokinin receptors, in particular to the CRE1/AHK4, motivated us to monitor subcellular localization of this cytokinin fluoroprobe, aiming to trace potential sites of interaction with the receptor. Two cell types, namely differentiated lateral root cap (LRC) cells and epidermal cells at the root meristematic zone of *Arabidopsis* root, were selected for in depth analyses. In a line with reported ER-localization of the AHK cytokinin receptors (Caesar et al., 2011; Wulfetange et al., 2011), iP-NBD co-localized with p24δ5-RFP, an ER-specific marker, in both cell types (Figure 9A, B; red arrowheads; Table 1).
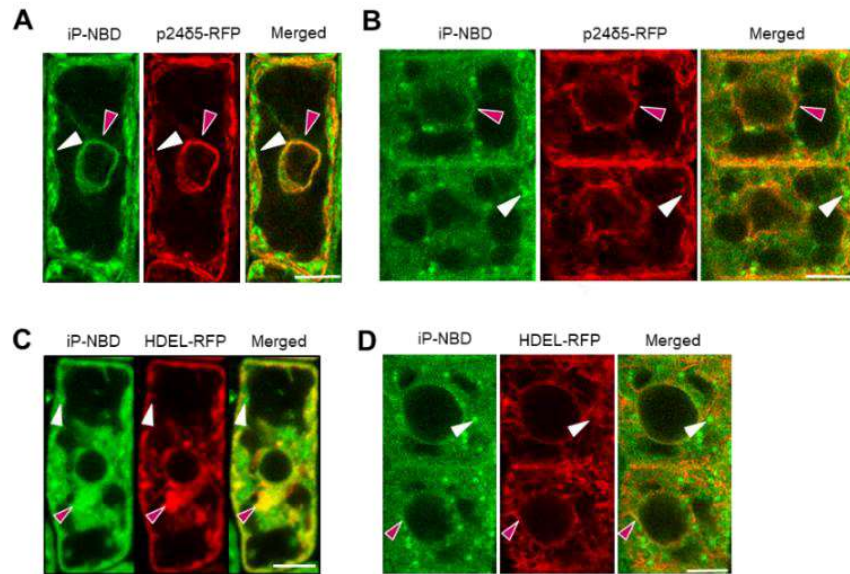
Figure 9: *Monitoring of the fluorescently labelled cytokinin iP-NBD in cells of Arabidopsis root. **A, B** – Monitoring of the fluorescently labelled cytokinin iP-NBD (green) and ER marker p24δ5-RFP (red) in LRC cells (**A**) and root meristematic epidermal cells (**B**). iP-NBD detected partially co-localizing with p24δ5-RFP in the ER (red arrowheads) and in non-ER cellular structures (white arrowheads). **C, D** – Monitoring of iP-NBD (green) and ER marker HDEL-RFP (red) in LRC cells (**C**) and epidermal cells (**D**). iP-NBD detected partially co-localizing with HDEL-RFP in ER (red arrowheads) and in non-ER cellular structures (white arrowheads). Scale bars = 5 μm.*

Notably, also a strong iP-NBD fluorescence signal was detected in distinct spot-like structures, which did not overlap with the ER reporter (Figure 9A, B; white arrowheads). Likewise, co-visualization with HDEL-RFP, an ER-specific marker, corroborated dual ER and spot-like localization of iP-NBD in both LRC and epidermal cells (Figure 9C, D).

Table 1: *Pearson's correlation coefficients of iP-NBD co-localization with marker lines. Quantification of co-localization of iP-NBD staining with various markers for different subcellular compartments (ER – endoplasmic reticulum, GA – Golgi apparatus, RE – recycling endosomes, TGN/EE – trans-Golgi network, early endosomes, LE/PVC – late endosomes/pre-vacuolar compartments). Average ± s.e., n = 8-25.*

iP-NBD colocalization with marker lines			Pearson's correlation coefficient	
line	compartment	fusion protein	LRC cells	Meristematic epidermal cells
p24δ5-RFP	ER	p24δ5-RFP	0.61 ± 0.02	0.50 ± 0.02
W18	GA	Got1p-mCherry	0.67 ± 0.02	0.56 ± 0.03
W22	GA	SYP32-mCherry	0.69 ± 0.02	0.53 ± 0.03
W34	endosomes, RE	RabA1e-mCherry	0.39 ± 0.06	0.43 ± 0.04
W13	TGNIEE	VTI12-mCherry	0.28 ± 0.04	0.32 ± 0.04
W2	LE/PVC	RabF2b-mCherry	-0.15 ± 0.03	-0.18 ± 0.05
W9	vacuoles	VAMP711-mCherry	-0.12 ± 0.04	0.00 ± 0.00

To further explore the nature of the peripheral and spot-like subcellular structures showing affinity to the iP-NBD, co-staining with FM4-64, the membrane selective dye labelling PM and endosomal/recycling vesicles in plant cells was performed (Jelínková et al., 2010). In both epidermal and LRC cells, iP-NBD signal was detected intracellularly and partially co-localized with the FM4-64 stained vesicles corresponding to the internalized and recycling endosomes (Figure 10A, C and Figure 11A). Interestingly, detailed profiles of fluorescence intensity distributions of iP-NBD and FM4-64 revealed their partial co-localization at the PM of

the epidermal cells, which was not the case for LRC (Figure 10B compared to 10D). These observations suggested that apart from ER, iP-NBD might accumulate in subcellular vesicles and at the PM.
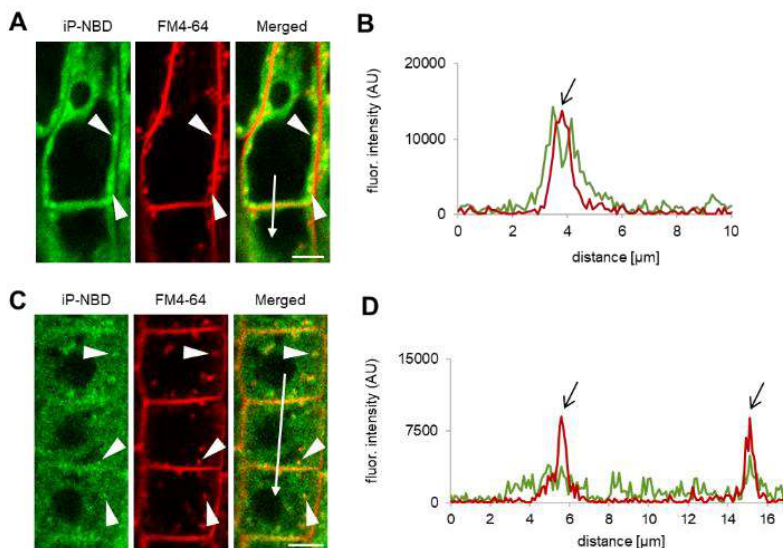

Figure 10: *Monitoring of iP-NBD (green) and FM4-64 (red, membrane selective dye) in LRC (**A, B**) and root meristematic epidermal cells (**C, D**). White arrowheads (**A, C**) indicate co-localization of iP-NBD and FM4-64 in vesicles. Profiles of the fluorescence intensity distribution of both FM4-64 (red line) and iP-NBD (green line) in LRC (**B**) and epidermal (**D**) cells were measured along the white lines (**A, B**) starting from the upper end (0 µm) towards the arrowhead. Peaks of FM4-64 fluorescence maxima (black arrows) correlate with the PM staining. iP-NBD fluorescence maximum does not overlap with FM4-64 fluorescence peak at the PM in LRC cell (**B**). Peaks of iP-NBD signal partially overlap with FM4-64 maxima and indicate the presence of cytokinin fluoroprobe at the PM of epidermal cells (**D**). Scale bars = 5 µm.*

To gain further insights into the iP-NBD subcellular localization and to test its affinity to endomembrane structures the impact of brefeldin A (BFA) was analysed. BFA is a fungal toxin, inhibiting ER-Golgi and post-Golgi trafficking to the PM and to vacuoles, thus causing the formation of endosomal clusters, so-called BFA compartments (Orci et al., 1993). Strikingly, in the root epidermal cells accumulation of iP-NBD signal in clusters corresponding to the BFA compartments stained with FM4-64 was observed (Figure 11B, blue arrowheads).
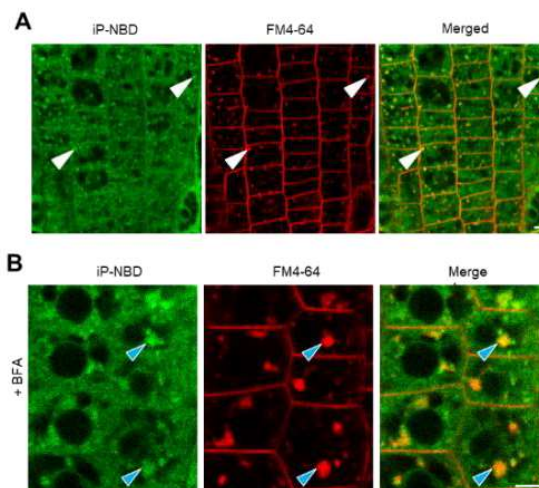

Figure 11: *Monitoring of iP-NBD subcellular localization in Arabidopsis root cells. **A** – Co-staining of root epidermal cells with iP-NBD (green) and FM4-64 (red) monitored 15 minutes after co-treatment. White arrowheads indicate co-localization of iP-NBD and FM4-64 in vesicles. **B** – Co-localization of iP-NBD and FM4-*

64 in endosomal compartments (blue arrowheads) formed in root meristematic epidermal cells treated with 50 µM in BFA for 1 h. Scale bars = 5 µm.

Co-localization with RabA1e-mCherry, a BFA-sensitive endosome/recycling endosome marker, provided additional supporting evidence that in the root epidermal cells iP-NBD exhibits affinity to the vesicular endomembrane system where subpopulations of cytokinin receptors may be localized (Figure 12A; Table 1). Next, the localization of the cytokinin fluoroprobe using a set of Wave marker lines specific for various subcellular organelles was traced (Geldner et al., 2009). Notably, in the root epidermal cells, a partial co-localization of iP-NBD with a *cis*-Golgi (GA) marker, SYP32-mCherry (Figure 12B; Table 1), an integral GA membrane protein, Got1p homolog-mCherry (Figure 12C; Table 1), and with TGN/early endosome marker, VTI12-mCherry (Figure 12D; Table 1) was observed. Interestingly, iP-NBD did not co-localize with a late endosome marker, RabF2b/W2R-mCherry (Figure 12E; Table 1) nor with a vacuolar marker, VAMP711-mCherry (Figure 12F; Table 1).
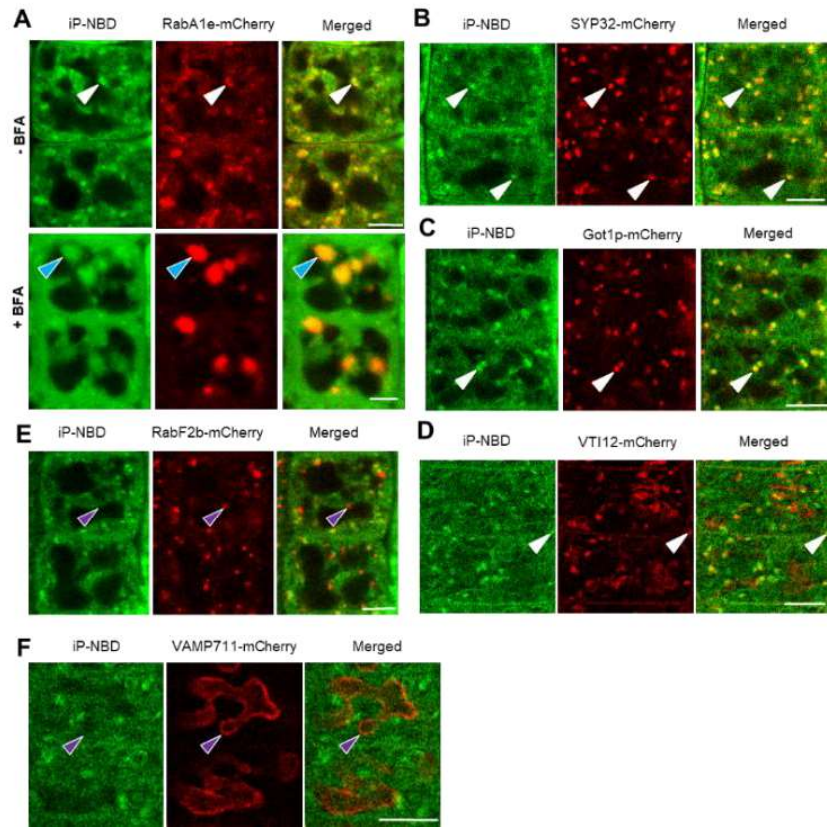

Figure 12: *Monitoring of iP-NBD subcellular localization in Arabidopsis root epidermal cells. A – Co-localization of iP-NBD (green) and RabA1e-mCherry (red) endosome/recycling endosome marker. Upper panel: co-localization of iP-NBD with RabA1e in vesicles (white arrowheads) before BFA treatment. Lower panel: accumulation of iP-NBD and RabA1e in endosomal compartments (blue arrowheads) formed in root epidermal cells treated with 50 µM BFA for 1 h. B – Partial co-localization of iP-NBD (green) with a cis-GA marker SYP32-mCherry in root epidermal cells. White arrowheads indicate overlapping signals. C, D – Partial co-localization of iP-NBD (green) with an integral GA membrane protein Got1p-mCherry (C) and TGN/early endosome marker VTI12-mCherry (D) in root epidermal cells. White arrowheads indicate overlapping signals. E, F – Non-overlapping signals of iP-NBD (green) and late endosome marker RabF2b-mCherry (red, E) or vacuolar marker VAMP711-mCherry (red, F) in root epidermal cells. Purple arrowheads indicate RabF2-mCherry stained endosomes (E) and VAMP711-mCherry vacuolar compartments (F). Scale bars = 5 µm.*

In cells of LRC, a partial co-localization with the GA markers, SYP32-mCherry (Figure 13A; Table 1) and Got1p homolog-mCherry (Figure 13B; Table 1), an endosome/recycling endosome marker RabA1e-mCherry (Figure 13C; Table 1) and with the TGN/early endosomal marker VTI12 (Figure 13D; Table 1) was observed. However, no co-localization was detected with late endosomal RabF2b-mCherry (Figure 13E; Table 1) or vacuolar VAMP711-mCherry markers (Figure 13F; Table 1).
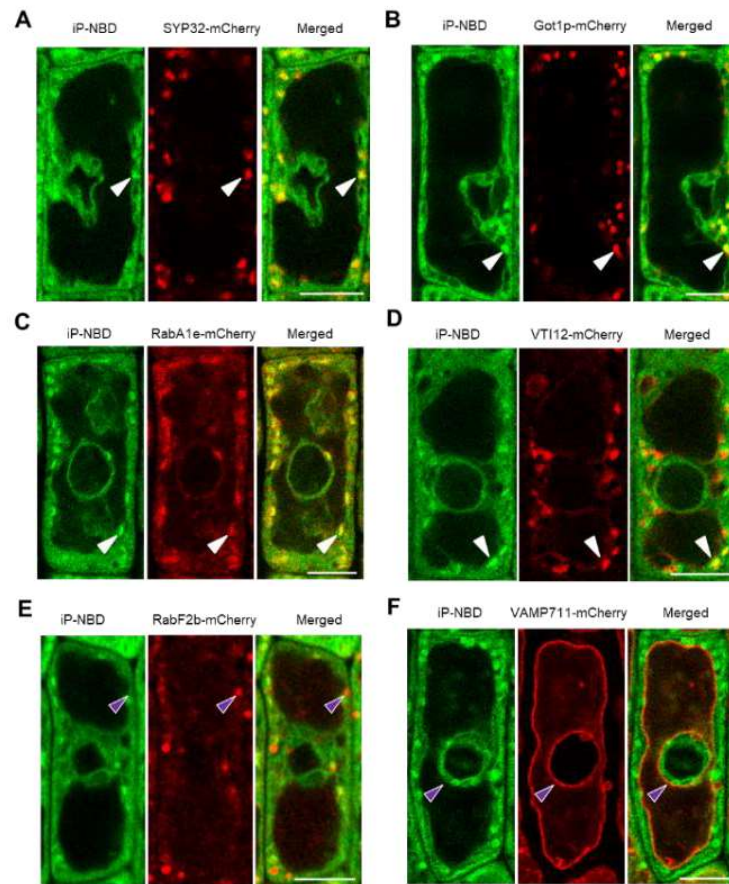

Figure 13: *Monitoring of iP-NBD subcellular localization in Arabidopsis lateral root cap cells. **A-D** – Co-localization of iP-NBD (green) with a cis-GA marker SYP32-mCherry (red, **A**), an integral GA membrane protein Got1p-mCherry (red, **B**), endosome/recycling endosome marker RabA1e-mCherry (red, **C**) and TGN/early endosome marker VTI12-mCherry (**D**) in the LRC cells. White arrowheads indicate overlapping signals. **E, F** – Non-overlapping signals of iP-NBD (green) and late endosome marker RabF2b-mCherry (**E**) or vacuolar marker VAMP711-mCherry (**F**, red) in the LRC cells. Purple arrowheads indicate subcellular compartments visualised by specific markers. Scale bars = 5 μm.*

Overall, monitoring of iP-NBD in the LRC and epidermal cells corroborate the ER as an organelle with affinity to cytokinin. However, co-localization of iP-NBD with TGN and early endosomal markers as well as its accumulation in the BFA compartments indicate that proteins with the affinity to iP-NBD, such as cytokinin receptors, do not reside exclusively at ER, but may enter the endomembrane trafficking system and possibly localize also to the PM.

Generation and isolation of the CRE1/AHK4-GFP transgenic lines

Previously, ER-localization of *Arabidopsis* cytokinin receptors has been demonstrated using transiently transformed *Nicotiana benthamiana* (Caesar et al., 2011; Wulfetange et al., 2011) and *Arabidopsis* (Caesar et

al., 2011), and by employing cytokinin-binding assays with fractionated *Arabidopsis* cells expressing Myc-tagged receptors (Wulfetange et al., 2011). However, so far no experimental support has been provided for their possible entry into the subcellular vesicular trafficking and PM localization. Yet, the possibility of cytokinin HKs localization to the PM has been hypothesised within the context of an integrative model for cytokinin perception and signalling (Romanov et al., 2018). The potential sites of CKs perception had been questioned in relation to the pH dependence of the binding by HKs. It was shown that the cytokinin binding to AHK3 is pH dependent with an optimum at basic pH and a dramatic decrease at acidic pH (Romanov et al., 2006). This finding fits with the ER-localization of cytokinin receptors and has also been used to cast doubt on PM-function of the receptors due to the acidic pH of apoplast acting as a constraint on efficient cytokinin binding. However, in contrary to the AHK3, CRE1/AHK4 affinity was shown not to be dramatically altered at acidic pH (Romanov et al., 2006). Importantly, a recent work by Jaworek et al. (Jaworek et al., 2020) shows a detailed analysis of pH influence on binding strength of CKs to the receptors from poplar (*Populus × canadensis* cv. *Robusta*). They showed that cytokinin binding to PcHK3 (ortholog of AHK3) steadily increases towards higher pH values, whereas binding to PcHK4 (ortholog of CRE1/AHK4) linearly decreased from an optimum for ligand binding at pH 5.5. These findings support the idea that CRE1/AHK4 can effectively sense CKs from the apoplast.

The only cytokinin receptor studied for its localization using stably-transformed *Arabidopsis* plants was AHK3 (Caesar et al., 2011). Unlike this receptor, subcellular localization of CRE1/AHK4 has not been addressed in much detail. Taking into account a higher affinity of iP-NBD to this receptor, this study focused on monitoring its subcellular localization using *Arabidopsis* stable transgenic lines carrying *CRE1/AHK4-GFP* construct driven by a constitutive *35S* promoter. Two independent lines displaying significantly increased transcription of *CRE1/AHK4-GFP* when compared to the wild type were selected for detailed observations (Figure 14A). Western blot analyses confirmed the accumulation of the CRE1/AHK4-GFP product of proper ~150 kDa size in both lines, although lower levels of the fusion protein were detected in the *35S::CRE1/AHK4-GFP* line (1) when compared to the line (2) (Figure 14B, C). To test the functionality of the CRE1/AHK4-GFP fusion protein, transient expression assays in the *Arabidopsis* protoplasts were performed. Co-expression of *35S::CRE1/AHK4-GFP* with a cytokinin sensitive reporter *TCS::LUCIFERASE* (*TCS::LUC*) resulted in 85 $\pm$ 6.9 fold upregulation of the reporter activity by cytokinin when compared to protoplasts co-transformed with controls (plasmids carrying either *GFP* or *GUS* reporter only resulting in 28 $\pm$ 2.4 and 32 $\pm$ 1.5 fold increase of Luciferase activity, respectively; Figure 14D). *In planta,* the functionality of the CRE1/AHK4-GFP was tested by expression analyses of the type-A early cytokinin response genes in the *35S::CRE1/AHK4-GFP* transgenic lines. Application of cytokinin resulted in a strong upregulation of *ARR5* and *ARR7* in a wild type and both transgenic lines expressing CRE1/AHK4-GFP (Figure 14E). However, a significantly enhanced transcription of *ARR5* and *ARR7* in response to cytokinin compared to wild type was detected only in the *35S::CRE1/AHK4-GFP* line (2)*,* which displayed a higher accumulation of CRE1/AHK4-GFP. *ARR5* and *ARR7* have been reported as being among the most sensitive type-A early cytokinin response genes, reaching expression maxima within 10-15 minutes following cytokinin application (D'Agostino et al., 2000). It can be argued that high responsiveness of these genes to cytokinin might hinder the detection of more subtle changes in cytokinin sensitivity in the line with lower expression of the CRE1/AHK4-GFP.
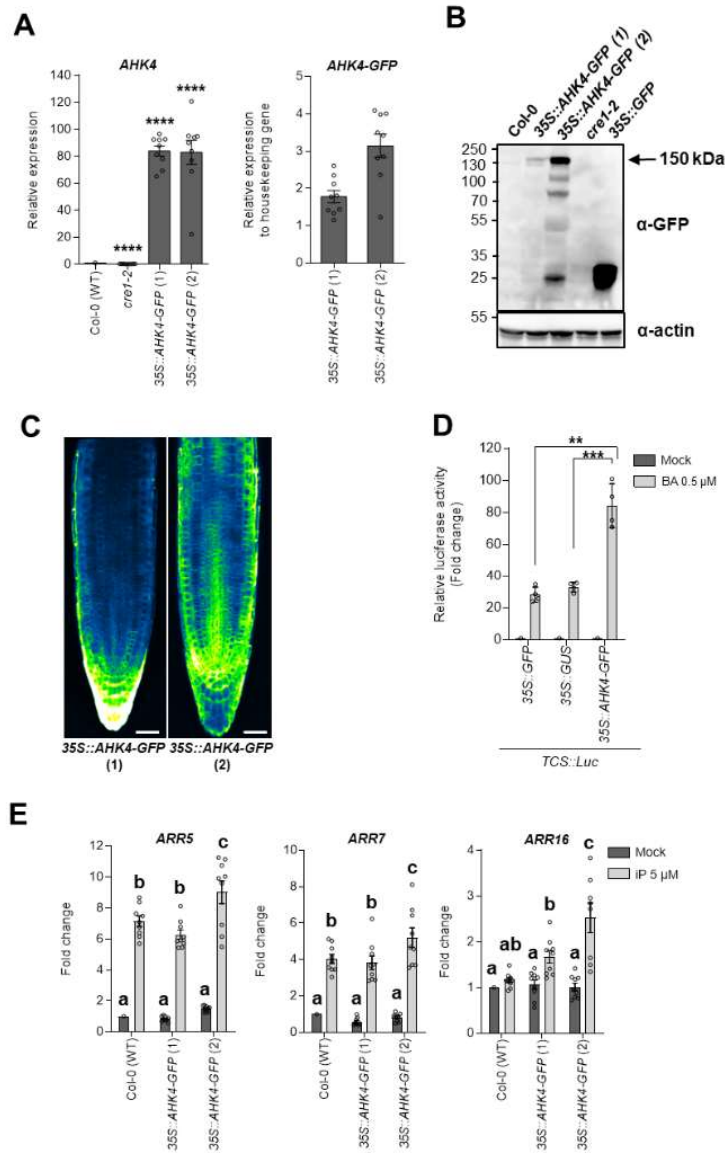
Figure 14: *Analysis of CRE1/AHK4-GFP functionality in vivo.* **A** *– Expression analysis of AHK4 and AHK4-GFP in 5-day-old seedlings using quantitative RT-PCR. Relative expression of cytokinin reporter in two 35S::AHK4-GFP independent lines was evaluated when compared to Col-0 (WT; left panel), or housekeeping gene (right panel). Mean ± s.d., p < 0.05 by two-way ANOVA. n = 9 (3 technical replicates from 3 biological replicates) per condition. Specific primer pairs for CRE1/AHK4 (left graph) and CRE1/AHK4-GFP (right graph) were used.* **B** *– Western blot analysis of AHK4-GFP in total protein extracts from the two independent 35S::AHK4-GFP lines. Col-0, cre1-2, 35S::GFP used as controls. Membranes were incubated with anti-GFP and anti-actin antibodies. The arrow marks the expected molecular weight of AHK4-GFP (150 kDa).* **C** *– Monitoring of CRE1/AHK4-GFP signal in the meristematic zone of the Arabidopsis root in two independent 35S::AHK4-GFP lines.* **D** *– TCS::LUCIFERASE cytokinin reporter activity in Arabidopsis protoplasts co-transformed with the CRE1/AHK4-GFP reporter is significantly upregulated in response to cytokinin (0.5 µM BA) when compared to protoplasts co-transformed with either GFP or GUS reporter only (mean ± s.d; *** p < 0.001 Student's t-test indicates significant difference when compared to protoplasts transformed with 35S::GUS, n = 4).* **E** *– Expression of early cytokinin response genes ARR5, ARR7 and ARR16 in 5-day-old seedlings of Col-0 and the two independent 35S::AHK4-GFP lines treated with 5µM iP or DMSO for 15 min. (mean ± s.d., p < 0.05 by two-way ANOVA. n = 9; 3 technical replicates from 3 biological replicates per condition). Scale bar = 10 µm (**C**).*

When compared to *ARR5* and *ARR7*, *ARR16* showed maximum transcription within 40-60 min following cytokinin application (D'Agostino et al., 2000). A significantly higher expression of *ARR16* after cytokinin application for 15 minutes was detected in both CRE1/AHK4-GFP overexpressing lines when compared to the wild type. These results suggest that proportionally with levels of CRE1/AHK4-GFP expression, the sensitivity of both lines to cytokinin stimulus is enhanced (Figure 14E), indicating that CRE1/AHK4-GFP maintains its biological activity.

The transgenic *Arabidopsis* lines expressing CRE1/AHK4-GFP exhibited phenotypes typical of plants with enhanced activity of cytokinin such as a shorter primary root, slower root growth rate and decreased lateral root density (Figure 15A-D). Both transgenic lines expressing CRE1/AHK4-GFP displayed hypersensitive-like responses to exogenous cytokinin treatment on the primary root growth compared to the wild type control, and in contrast to the cytokinin insensitive *ahk4/cre1-2* loss of function mutant (Figure 15E).
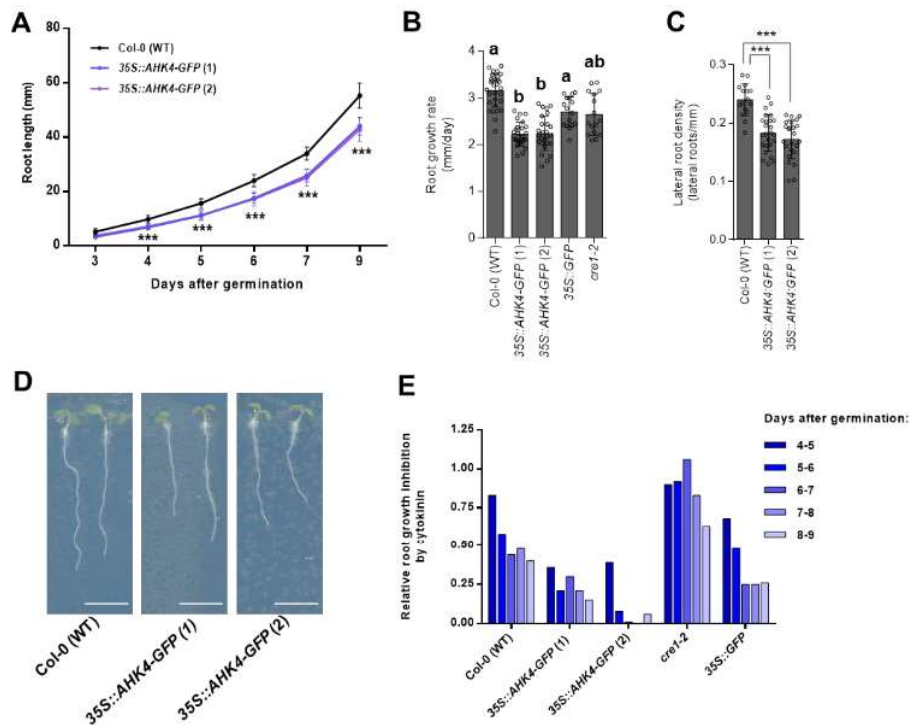

Figure 15: *Analysis of CRE1/AHK4-GFP functionality in vivo.* ***A*** *– Root length of 3- to 9-day-old seedlings of control Col-0 (black) and two independent 35S::AHK4-GFP lines (mean ± s.d., *** = p < 0.001 by Student's t-test, n ≥15).* ***B*** *– Average root growth rate (mm/day) of control Col-0, two independent 35S::AHK4-GFP lines, 35S::GFP and cre1-2 seedlings during 5 days (mean ± s.d.; p < 0.01 by ANOVA test, n ≥ 15).* ***C*** *– Lateral root density (number of lateral roots/root length) was evaluated in 9-day-old seedlings of control Col-0 and two independent 35S::AHK4-GFP lines (mean ± s.d.; *** = p < 0.001 by Student's t-test, n ≥15).* ***D*** *– Representative images of 5-day-old seedlings of control Col-0 and two independent 35S::AHK4-GFP lines.* ***E*** *– Relative inhibition of root growth by cytokinin in control Col-0, two independent 35S::AHK4-GFP lines, 35S::GFP and cre1-2 seedlings. Root growth on medium with and without cytokinin (BA 1 µM) monitored during 5 days (day 4 to 9 after germination) and relative root growth inhibition per day calculated (n = 10-15 roots). Scale bar = 5 mm* (***D***).

CRE1/AHK4-GFP co-localizes with the ER and the PM markers

As previously reported and in line with iP-NBD subcellular localization, CRE1/AHK4-GFP in the LRC and epidermal cells of root apical meristem co-localized with the ER marker p24δ5-RFP (Figure 16A-C; red arrowheads). Intriguingly, in the epidermal cells of root meristematic zone, CRE1/AHK4-GFP signal at the PM area, not co-localizing with the ER reporter, could also be detected (Figure 16D, E).
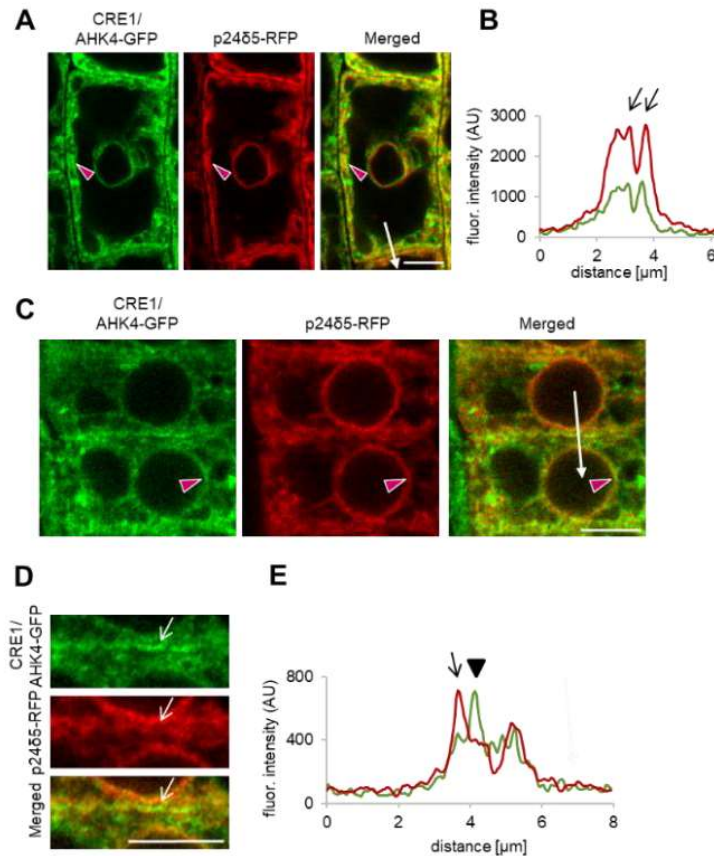
28

Figure 16: *CRE1/AHK4-GFP subcellular localization in cells of Arabidopsis root. **A-E** – Monitoring of the CRE1/AHK4-GFP cytokinin receptor (green) and ER marker p24δ5-RFP (red) in LRC cells (**A, B**) and root meristematic epidermal cells (**C-E**). Red arrowheads mark areas of co-localization. Fluorescence intensity profiles of the ER marker (red line) and CRE1/AHK4-GFP (green line; **B, E**) were measured along the white lines (**A, C**) starting from the upper end (0 μm) towards the arrowhead. Peaks of p24δ5-RFP fluorescence maxima at the ER overlap with CRE1/AHK4-GFP signal maxima in LRC cells and root meristematic epidermal cells (black arrows; **B, E**). Peak of CRE1/AHK4-GFP non-overlapping with peaks of p24δ5-RFP in root meristematic epidermal cells indicates localization at the PM (black arrowhead; **E**). Detailed view (**D**; white arrows point to CRE1/AHK4-GFP signal at the area of the PM). Scale bars = 5 μm.*

The subsequent analysis revealed a strong overlap of the CRE1/AHK4-GFP with the PM reporter PIP1;4-mCherry and NPSN12-mCherry (Figure 17A-D), thus hinting at localization of the cytokinin receptor at the PM. Moreover, in the dividing meristematic cells CRE1/AHK4-GFP could also be detected at the expanding cell plate (Figure 17C-F; asterisks) while it co-localized there with the established cell plate vesicular marker FM4-64 (Figure 17E, F).
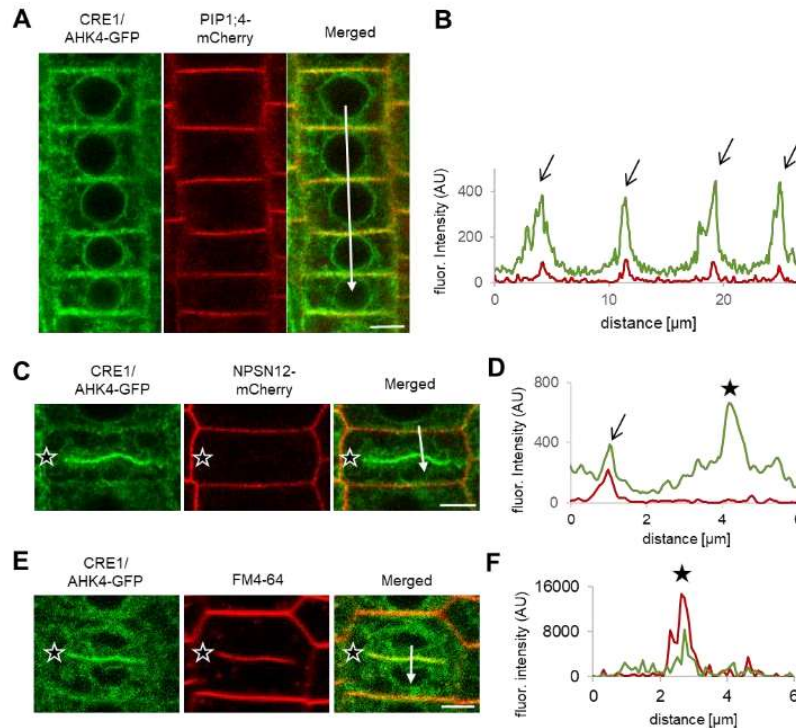
Figure 17: *CRE1/AHK4-GFP co-localization with the PM markers in Arabidopsis root cells. **A-F** – Co-localization of CRE1/AHK4-GFP with the PM markers PIP1;4-mCherry (**A, B**), NPSN12-mCherry (**C, D**) and FM4-64 (**E, F**) in root meristematic epidermal cells. Profiles of fluorescence intensity of the PM marker (red line) and CRE1/AHK4-GFP (green line; **B, D, F**) were measured along the white lines (**A, C, E**) starting from the upper end (0 µm) towards the arrowhead. Peaks of PIP1;4-mCherry and NPSN12-mCherry fluorescence maxima correlate with the PM staining and overlap with CRE1/AHK4-GFP signal maxima (black arrows; **A**-**D**). CRE1/AHK4-GFP signal detected at the cell plate of dividing cell (black stars on **C, E**) co-localizes with the FM4-64 marker (**E, F**; black stars) but not with the PM marker NPSN12-mCherry (**C, D**; black stars). Scale bars = 5 µm (**A, C, E**).*

Importantly, it has been shown that during cytokinesis the cell plate might receive material both from post-Golgi compartments as well as from the PM through sorting and recycling endosomes (Dhonukshe et al., 2006). Hence, detection of CRE1/AHK4-GFP at the cell plate provides further supporting evidence that the cytokinin receptor might reside outside of ER, namely on cytokinetic vesicles forming a cell plate (Smertenko et al., 2017).

Further evidence confirming localization of the CRE1/AHK4-GFP to the PM resulted from the subcellular study using super-resolution structural illumination microscopy (SIM; Komis et al., 2015b). This SIM analysis revealed co-localization of the CRE1/AHK4-GFP with FM4-64 labelled PM with average Pearson's coefficient 0.345 ± 0.113 (n = 30; Figure 18A). Unlike epidermal cells of the root meristematic zone, in LRC cells, the CRE1/AHK4-GFP signal resided in the ER and no co-localization with a PM reporter (NPSN12-mCherry) could be detected (Figure 18B, C). Inhibition of endocytic trafficking and vesicular recycling in meristematic cells by BFA resulted in co-accumulation of the CRE1/AHK4-GFP and FM4-64 in the BFA compartments in line with the presence of the receptor in the endomembrane system (Figure 18D). Wash-out of BFA allowed re-localization of the cytokinin receptor back to the PM indicating that it might cycle between PM and TGN (Figure 18F). Although occasionally in some cells of LRC co-staining with FM4-64 revealed CRE1/AHK4-GFP in the BFA compartments, they were relatively rare and randomly scattered in some LRC cells indicating that CRE1/AHK4-GFP trafficking in differentiated cells of LRC might differ from that observed in the epidermal cells of root apical meristem (Figure 18G). Importantly, no accumulation of the ER marker p24δ5-RFP in the BFA compartments in either epidermal cells of the meristem (Figure 18E) or the LRC cells (Figure 18H) could be detected,

suggesting that the CRE1/AHK4-GFP signal is specifically enriched in the BFA bodies and not related to structural changes of ER in the BFA-treated cells.

Altogether, these results indicate that in the LRC cells CRE1/AHK4 may reside preferentially at the ER, whereas in the epidermal cells of root apical meristem the cytokinin receptor can enter the endomembrane system and localizes both at the ER and the PM.
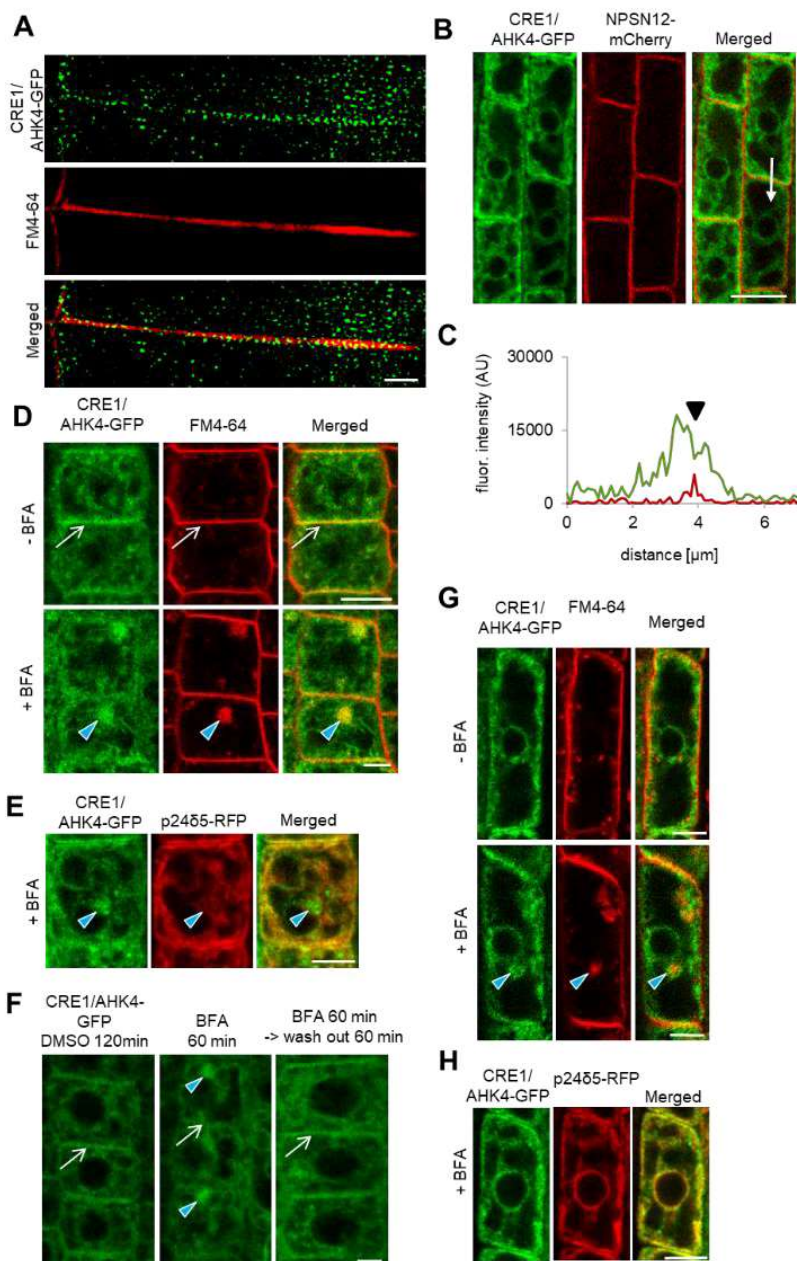

Figure 18: *CRE1/AHK4-GFP localization in Arabidopsis root cells. A – Super-resolution imaging (SIM) of CRE1/AHK4-GFP subcellular co-localization with the FM4-64 labelled PM. B, C – Monitoring of the CRE1/AHK4-GFP cytokinin receptor (green) and the NPSN12-mCherry PM reporter (red) in the LRC cells (B). Profiles of fluorescence intensity of the PM marker (red line) and CRE1/AHK4-GFP (green line) were measured along the white line (B) starting from the upper end (0 µm) towards the arrowhead. Peak of NPSN12-mCherry fluorescence maxima at the PM does not overlap with CRE1/AHK4-GFP fluorescence maximum (black arrowhead, C). D, E – Co-localization of CRE1/AHK4-GFP and FM4-64 (D), but not p24δ5-RFP (E) in the endosomal compartments (blue arrowheads) formed in the root meristematic epidermal cells treated with 50 µM in BFA for 1 h. Note CRE1/AHK4-GFP localization at the PM (white arrows) prior BFA treatment. F – Re-*

*location of the CRE1/AHK4-GFP cytokinin receptor from the endosomal compartments to the PM after BFA wash-out in the root epidermal cells. Blue arrowheads indicate CRE1/AHK4 in the BFA-bodies. Note the attenuated AHK4-GFP signal at the PM and its re-localization back after 60 min wash-out of BFA (white arrows). **G, H** – Monitoring of the CRE1/AHK4-GFP (green), FM4-64 (red; **G**) and p24δ5-RFP (red; **H**) in the LRC cells treated for 1 h with 50 μM BFA. FM4-64, but not p24δ5-RFP detected in the BFA endosomal compartments (blue arrowheads). In some cells of LRC, CRE1/AHK4-GFP signal scattered around BFA bodies detected (**G**). Scale bars = 5 μm (**B**, **D**, **E**, **F**, **G**, **H**) and 2 μm (**A**).*

To further explore whether the cytokinin receptor might occupy a different subcellular location in cells at a distinct stage of differentiation, CRE1/AHK4-GFP in different cell types was monitored. Similarly to the epidermis, in the provasculature cells in the root meristematic zone, the CRE1/AHK4-GFP seems to localize at the ER, the PM and at the cell plate of dividing stele cells (Figure 19A). To strengthen the conclusion that in the meristematically active cells cytokinin receptor might enter the secretory pathway and reach the PM, real time monitoring of the CRE1/AHK4-GFP in the developing lateral root primordia (LRP) was performed. Although expression of CRE1/AHK4-GFP driven by *35S* promoter in the LRP was relatively weak, similarly to cells in the root meristem, the CRE1/AHK4-GFP tends to localize at the ER and the PM (Figure 19B). Furthermore, in actively dividing cells a weak CRE1/AHK4-GFP signal could be detected during the cell plate formation.

Unlike cells located at the root apical meristem, in the differentiated cells of the LRC the CRE1/AHK4-GFP was detected in the ER, but not at the PM. To support further our conclusion about dominant localization of the cytokinin receptor at the ER in differentiated cells, detailed observations of the CRE1/AHK4-GFP in the differentiated root epidermal cells above the meristematic zone were performed. In these cells, the CRE1/AHK4-GFP was located at the ER (Figure 19C, D), but no co-localization with the PM reporter NPSN12 could be detected (Figure 19E, F).
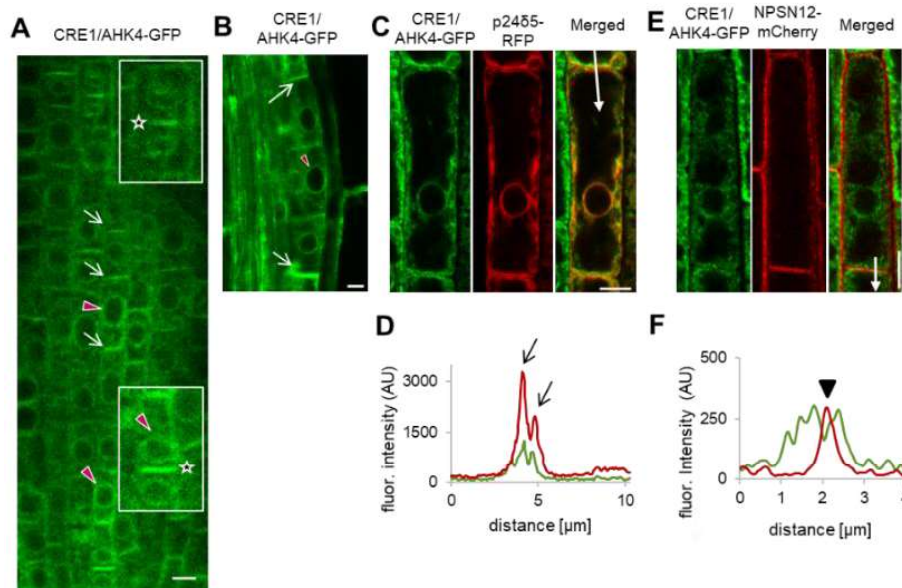

Figure 19: *CRE1/AHK4-GFP localization in Arabidopsis root cells. **A, B** – Monitoring of the CRE1/AHK4-GFP signal in the cells of provasculature at the root meristematic zone (**A**) and the developing lateral root primordia (**B**). Black stars mark AHK4-GFP signal at the cell plate of diving cells, white arrows and red arrowheads point to the PM and ER structures, respectively. **C-F** – Monitoring of the CRE1/AHK4-GFP cytokinin receptor (green), ER marker p24δ5-RFP (red; **C, D**) and the PM marker NPSN12-mCherry (red; **E, F**) in the differentiated epidermal cells at the root elongation zone. Profile of fluorescence intensity of p24δ5-RFP ER marker (red line) and CRE1/AHK4-GFP (green line; **D**) was measured along the white line (**C**) starting from the upper end (0 μm) towards the arrowhead. Peaks of p24δ5-RFP fluorescence maxima correlate with ER signal and overlap with CRE1/AHK4-GFP signal maxima (black arrows; **D**). Profile of fluorescence intensity of the NPSN12-mCherry PM marker (red line) and CRE1/AHK4-GFP (green line; **F**) was measured along the white line (**E**) starting from the upper end (0 μm) towards the arrowhead. Peak of NPSN12-mCherry fluorescence maxima at the PM signal*

32

*does not overlap with CRE1/AHK4-GFP signal maxima in epidermal cells (black arrowhead; **F**). Scale bars = 5 µm (**A-C, E**).*

Based on these observations it can be hypothesised that the CRE1/AHK4-GFP located either at the ER or at the PM might activate distinct branches of downstream signalling to control specific process in the differentiated versus meristematically active cells. Internalization and re-cycling of the receptor between PM and endosomal compartments in the meristematic cells may represent another level in controlling signalling receptor function. Whether similarly to the CRE1/AHK4-GFP, also AHK2 and AHK3 might enter secretory pathway and reach the PM in the meristematically active cells remains to be addressed. In previously reported studies localizations of the AHK3-GFP and AHK2-GFP have been observed in above-ground plant parts using transiently transformed *Nicotiana benthamiana* epidermal leaf cells (Wulfetange et al., 2011) and transiently transformed *Arabidopsis* cotyledon cells (Caesar et al., 2011), all in the differentiated stages. Hence, whether in specific cell types AHK2 and AHK3 might localize to the PM needs to be examined.

It is necessary to mention, that presented findings of PM localization of the cytokinin receptor CRE1/AHK4 are supported by a recently published article by Antoniadi et al. (2020). Both independent back-to-back articles (Kubiasova et al., 2020 and Antoniadi et al., 2020) were accepted in Nature Communications and the research groups were separately studying cellular sites of cytokinin signalling, especially the localization of receptors on different plant membranes. Each paper has used almost completely non-overlapping approaches and yet both came to the same conclusion (that cytokinin receptors not only exist at the ER but also on the PM).

Both works are set in the context of the long-standing debate on the localization of cytokinin receptors, with substantial evidence in recent years supporting predominant location on the ER. The presence of PM receptors was also proposed by Zürcher et al., 2016 as the logical implication of their cytokinin transporter and metabolism data. Moreover, three recent reviews have highlighted the ER versus PM debate and have pointed to the lack of convincing direct data (Kieber and Schaller, 2018; Romanov et al., 2018; Durán-Medina et al., 2017). Therefore multiple strands of evidence that individually and collectively support the hypothesis that some of the cytokinin perception occurs at the cell surface rather than intracellularly were provided.

Antoniadi and colleagues provided functional evidence that extracellular cytokinin ligands acting through the cell surface receptors are effective at initiating cytokinin signalling. Authors used cytokinins covalently linked to Sepharose beads that could not enter the cell and yet are able to increase the expression of both *TCSn::GFP* and *CRFs*. Lastly, super-resolution microscopy of GFP-labelled receptors and diminished *TCSn::GFP* response to immobilised cytokinins in cytokinin receptor mutants, further indicate that receptors can function at the cell surface. Dual location of receptors may potentially provide plants with additional flexibility in cytokinin responses. It remains to be discovered whether different biological functions are associated with each location (Antoniadi et al., 2020).

Conclusion

Taken together, monitoring of intracellular localization of the fluorescent cytokinin probe iP-NBD with higher affinity to the CRE1/AHK4 cytokinin receptor, as well as direct visualization of the CRE1/AHK4-GFP leads to the conclusion that besides ER, cytokinin signal might also be perceived at other cellular compartments including the PM. As suggested by different localization of the CRE1/AHK4 receptor in the differentiated cells of LRC when compared to the epidermal cells of root apical meristem, perception of cytokinin at either ER or PM might be cell- and developmental- context dependent. In particular, the strong expression of the cytokinin sensitive reporter TCS::GFP detected in the columella and LRC cells (Bielach et al., 2012) suggests that the ER-located cytokinin receptors activate cytokinin signalling cascade in these particular cell types. On the other hand, it remains to be resolved whether there is a specific branch of cytokinin signalling activated by receptors located at the PM of meristematic cells.

Antoniadi I., Plačková L., Simonovik B., Doležal K., Turnbull C., Ljung K., Novák O. (2015): Cell-type-specific cytokinin distribution within the *Arabidopsis* primary root apex. *Plant Cell* **27**, 1955–1967.

Antoniadi I., Novák O., Gelová Z., Johnson A., Plíhal O., Simerský R., Mik V., Vain T., Mateo-Bonmatí E., Karady M., Pernisová M., Plačková L., Opassathian K., Hejátko J., Robert S., Friml J., Doležal K., Ljung K., Turnbull C. (2020): Cell-surface receptors enable perception of extracellular cytokinins. *Nat Commun.* **11**, 4284.

Bielach A., Podlešáková K., Marhavý P, Duclercq J., Cuesta C., Müller B., Grunewald W., Tarkowski P., Benková E. (2012): Spatiotemporal regulation of lateral root organogenesis in *Arabidopsis* by cytokinin. *Plant Cell* **24**, 3967–3981.

Caesar K., Thamm A. M. K., Witthöft J., Elgass K., Huppenberger P., Grefen C., et al. (2011): Evidence for the localization of the *Arabidopsis* cytokinin receptors AHK3 and AHK4 in the endoplasmic reticulum. *J. Exp. Bot.* **62**, 5571–5580.

Chen Y.F., Randlett M.D., Findell J.L., Schaller G.E. (2002): Localization of the ethylene receptor ETR1 to the endoplasmic reticulum of *Arabidopsis*. *J Biol Chem.* **277**, 19861–19866.

Cheng Y., Prusoff W. H. (1973): Relationship between the inhibition constant (KI) and the concentration of inhibitor which causes 50 per cent inhibition (I50) of an enzymatic reaction. *Biochem. Pharmacol.* **22**, 3099–3108.

Clough S. J., Bent A. F. (1998): Floral dip: a simplified method for Agrobacterium-mediated transformation of *Arabidopsis thaliana. Plant J.* **16**, 735–743.

D'Agostino I. B., Deruere J., Kieber J. J. (2000): Characterization of the response of the *Arabidopsis* response regulator gene family to cytokinin. *Plant Physiol.* **124**, 1706–532.

Dhonukshe P., Baluška F., Schlicht M., Hlavacka A., Šamaj J., Friml J., T. W. J. Gadella Jr. (2006): Endocytosis of cell surface material mediates cell plate formation during plant cytokinesis. *Dev. Cell* **10**, 137–150.

Dortay H., Gruhn N. , Pfeifer A., Schwerdtner M., Schmülling T., Heyl A. (2008): Toward an Interaction Map of the Two-Component Signaling Pathway of *Arabidopsis thaliana*. *J. Proteome Res* **7**, 3649–3660.

Durán-Medina Y., Díaz-Ramírez D., Masch-Martíınez N. (2017): Cytokinins on the move. *Front. Plant Sci.* **8**, 146.

Frébort I., Kowalska M., Hluska T., Frébortová J., Galuszka P. (2011): Evolution of cytokinin biosynthesis and degradation. *J. Exp. Bot.* **62**, 2431–52.

Friedrichsen D.M., Joazeiro C.A., Li J., Hunter T., Chory J. (2000): Brassinosteroid-insensitive-1 is a ubiquitously expressed leucine-rich repeat receptor serine/threonine kinase. *Plant Physiol.* **123**, 1247–1256.

Galuszka, P., Popelková, H., Werner, T., Frébortová J., Pospíšilová H., Mik V., Schwarz I., Schmülling T., Frébort I. (2007): Biochemical Characterization of Cytokinin Oxidases/Dehydrogenases from *Arabidopsis thaliana* Expressed in *Nicotiana tabacum L*.. J. Plant Growth Regul. **26**, 255–267.

Geldner N., Robatzek S. (2008): Plant Receptors Go Endosomal: A Moving View on Signal Transduction. *Plant Phys.* **147**, 1565–1574.

Geldner N., Dénervaud-Tendon V., Hyman D. L., Mayer U., Stierhof Y.-D., Chory J. (2009): Rapid, combinatorial analysis of membrane compartments in intact plants with a multicolor marker set. *Plant J.* **59**, 169–178.

Hong Z., Jin H., Tzfira,T., Li J. (2008): Multiple mechanism-mediated retention of a defective brassinosteroid receptor in the endoplasmic reticulum of *Arabidopsis*. *Plant Cell* **20**, 3418–3429.

Hothorn M., Dabi T., Chory J. (2011): Structural basis for cytokinin recognition by *Arabidopsis thaliana* histidine kinase 4. *Nat. Chem. Biol.* **7,** 766–768.

Hou B., Lim E.-K., Higgins G. S., Bowles D. J. (2004): N-glucosylation of cytokinins by glycosyltransferases of *Arabidopsis thaliana*. *J. Biol. Chem.* **279**, 47822–47832.

Hoyerová K., Hošek P. (2020): New Insights Into the Metabolism and Role of Cytokinin N-Glucosides in Plants. *Front. Plant Sci.* **11,** 741.

Hirayama T., Alonso J. M. (2000): Ethylene captures a metal! Metal ions are involved in ethylene perception and signal transduction. *Plant Cell Physiol.* **41**, 548–555.

Inoue T., Higuchi M., Hashimoto Y., Seki M., Kobayashi M., Kato T., Tabata S., Shinozaki K., Kakimoto T. (2001): Identifcation of CRE1 as a cytokinin receptor from *Arabidopsis*. *Nature* **409**, 1060–1063.

Irani N. G., Di Rubbo S., Myllel E., Van den Begin J., Schneider-Pizoń J., Hnilíková J., Šíša M., Buyst D., Vilarrasa-Blasi J., Szatmári A.-M., Van Damme D., Mishev K., Codreanu M.-C., Kohout L., Strnad M., Caño-Delgado A. I, Friml J., Medder A., Russinova E. (2012): Fluorescent castasterone reveals BRI1 signalling from the plasma membrane. *Nat. Chem. Biol.* **8**, 583–589.

Jaworek P., Tarkowski P., Hluska T., Kouřil Š., Vrobel O., Nisler J., Kopečný D. (2020): Characterization of five CHASE-containing histidine kinase receptors from *Populus × canadensis cv. Robusta* sensing isoprenoid and aromatic cytokinins. *Planta* **251**.

Jelínková A., Malínská K., Simon S., Kleine-Vehn J., Parezová M., Pejchar P, Kubes M., Martinec J., Friml J., Zazímalová E., Petrásek J. (2010): Probing plant membranes with FM dyes: tracking, dragging or blocking? *Plant J.* **61**, 883–892.

Jin H., Yan Z., Nam K.H., Li J. (2007): Allele-specific suppression of a defective brassinosteroid receptor reveals a physiological role of UGGT in ER quality control. *Mol. Cell* **26**, 821–830.

Kang J., Lee Y., Sakakibara H., Martinoia E. (2017): Cytokinin transporters: GO and STOP in signaling. *Trends Plant Sci.* **6**, 455–461.

Kieber J. J., Schaller G. E. (2018): Cytokinin signaling in plant development. *Development* **145**, 1–7.

Kim H. J., Ryu H., Hong S. H., Woo H. R., Lim P. O., Lee I. Ch., Sheen J., Nam H. G., Hwan I. (2006): Cytokinin-mediated control of leaf longevity by AHK3 through phosphorylation of ARR2 in *Arabidopsis*. *Proc. Natl. Acad. Sci. U.S.A* **103**, 814–819.

Komis G., Mistrik M., Šamajová O., Ovečka M., Bartek J., Šamaj J. (2015a): Superresolution live imaging of plant cells using structured illumination microscopy. *Nat. Protoc.* **10**, 1248–1263.

Komis G., Šamajová O., Ovečka M., Šamaj, J. (2015b): Super-resolution microscopy in plant cell imaging. *Trends Plant Sci.* **20**, 834–843.

Kubiasová K. (2014): Localization of cytokinin receptors in *Arabidopsis thaliana* using fluorescent labeling. Diploma thesis. Palacký University Olomouc, Czech Republic.

Kubiasová K., Mik V., Nisler J., Honig M., Husičková A., Spíchal L., Pěkná Z., Šamajová O., Doležal K., Plíhal O., Benková E., Strnad M., Plíhalová L. (2018): Design, synthesis and perception of fluorescently labeled isoprenoid cytokinins. *Phytochemistry* **150**, 1–11.

Kudo, T., Kiba T., Sakakibara H. (2010): Metabolism and long-distance translocation of cytokinins. *J. Integr. Plant Biol.* **52**, 53–60.

Lace B., Prandi K. (2016): Shaping small bioactive molecules to untangle their biological function: a focus on fluorescent plant hormones. *Mol. Plant* **9**, 1099–1118.

Larrieu A., Vernoux T. (2015): Comparison of plant hormone signalling systems. *Essays Biochem.* **58**, 165–181.

Lomin S. N., Yonekura-Sakakibara K., Romanov G. A., Sakakibara H. (2011): Ligand-binding properties and subcellular localization of maize cytokinin receptors. *J. Exp. Bot.* **62**, 5149–5159.

Lomin S. N., Krivosheev D. M., Steklov M. Y., Arkhipov D. V., Osolodkin D. I., Schmülling T., Romanov G.A. (2015): Plant membrane assays with cytokinin receptors underpin the unique role of free cytokinin bases as biologically active ligands. *J. Exp. Bot.* **66**, 1851–1863.

Lomin, S. N., Myakushina, Y. A., Kolachevskaya, O. O., Getman, I. A., Arkhipov, D. V., Savelieva, E. M., Osolodkin D.I., Romanov G.A. (2018a): Cytokinin perception in potato: new features of canonical players. *J. Exp. Bot.* **69**, 3839–3853.

Lomin S., Myakushina Y., Arkhipov D., Leonova O., Popenko V., Schmülling T., Romanov G (2018b): Studies of cytokinin receptor-phosphotransmitter interaction provide evidences for the initiation of cytokinin signalling in the endoplasmic reticulum. *Funct. Plant Biol.* **45**, 192–202.

Nakagawa T., Kurose T., Hino T., Tanaka K., Kawamukai M., Niwa Y., Toyooka K., Matsuoka K., Jinbo T., Kimura T. (2007): Development of series of gateway binary vectors, pGWBs, for realizing efficient construction of fusion genes for plant transformation. *J. Biosci. Bioeng.* **104**, 34–41.

Nakai K., Horton P. (1999): PSORT: a program for detecting sorting signals in proteins and predicting their subcellular localization. *Trends Biochem Sci* **24**, 34–36.

Nelson B. K., Cai X., Nebenführ A. (2007): A multicolored set of *in vivo* organelle markers for co-localization studies in *Arabidopsis* and other plants. *Plant J.* **51**, 1126–1136.

Niemann M., Weber H., Hluska T., Leonte G., Anderson S., Novak O., Senes A., Werner T. (2018): The cytokinin oxidase/dehydrogenase CKX1 is a membrane-bound protein requiring homooligomerization in the endoplasmic reticulum for its cellular activity. *Plant Physiol.* **176**, 2024–2039.

Nisler J., Zatloukal M., Popa I., Dolezal K., Strnad M., Spíchal L. (2010): Cytokinin receptor antagonists derived from 6-benzylaminopurine. *Phytochemistry* **71**, 1052–1062.

Orci L., Perrelet A., Ravazzola M., Wieland F. T., Schekman R., Rothman J. E. (1993): "BFA bodies": a subcompartment of the endoplasmic reticulum. *Proc. Natl Acad. Sci. U.S.A* **90**, 11089–11093.

Romanov G. A., Spíchal L., Lomin S. N., Strnad M., Schmülling T. (2005): A live cell hormone-binding assay on transgenic bacteria expressing a eukaryotic receptor protein. *Anal. Biochem*. **347**, 129–134.

Romanov GA, Lomin SN, Schmülling T. (2006): Biochemical characteristics and ligand-binding properties of *Arabidopsis* cytokinin receptor AHK3 compared to CRE1/AHK4 as revealed by a direct binding assay. *J. Exp. Bot.* **57,** 4051–4058.

Romanov G. A., Lomin S. N., Schmülling T. (2018): Cytokinin signaling: from the ER or from the PM? That is the question! *New Phytol.* **218**, 41–53.

Shan X., Yan J., Xie D. (2012): Comparison of phytohormone signalling mechanisms. *Curr. Opin. Plant Biol.* **15**, 84–91.

Smertenko A., Assaad F., Baluška F., Bezanilla M., Buschmann H., Drakakaki G., Hauser M.-T., Janson M., Mineyuki Y., Moore I., Müller S., Murata T., Otegi M. S., Panteris E., Rasmussen C., Schmit A.-C., Šamaj J., Samuels L., Staehelin L. A., Van Damme D., Wasteneys G., Žárský V. (2017): Plant cytokinesis: terminology for structures and processes. *Trends Cell Biol.* **27**, 885–894.

Smet W., Sevilem I., de Luis Balaguer M. A., Wybouw B., Mor E., Miyashima S., Blob B., Roszak P., Jacobs T. B., Boekschoten M., Hooiveld G., Sozzani R., Helariutta Y., De Rybel B. (2019): DOF2.1 controls cytokinin-dependent vascular cell proliferation downstream of TMO5/LHW. *Curr. Biol.* **29**, 520–529.

Spíchal L., Rakova N. Y., Riefler M., Mizuno T., Romanov G. A., Strnad M., Schmülling T. (2004): Two cytokinin receptors of *Arabidopsis thaliana*, CRE1/AHK4 and AHK3, differ in their ligand specificity in a bacterial assay. *Plant Cell Physiol.* **45**, 1299–1305.

Spíchal L. (2011): Bacterial assay to study plant sensor histidine kinases. *Methods Mol. Biol*. **779**, 139–147.

Suzuki T., Miwa K., Ishikawa K., Yamada H., Aiba H., Mizuno T. (2001): The *Arabidopsis* sensor His-kinase, AHK4, can respond to cytokinins. *Plant Cell Physiol.* **42**, 107–113.

Ueguchi C., Sato S., Kato T., Tabata S. (2001a): The AHK4 gene involved in the cytokinin-signalling pathway as a direct receptor molecule in *Arabidopsis thaliana*. *Plant Cell Physiol* **42**, 751–755.

Ueguchi C., Koizumi H., Suzuki T., Mizuno T. (2001b): Novel Family of Sensor Histidine Kinase Genes in *Arabidopsis thaliana*. *Plant Cell Physiol.* **42**, 231–235.

von Wangenheim D., Hauschild R., Fendrych M., Barone V., Benkova E., Friml J. (2017): Live tracking of moving samples in confocal microscopy for vertically grown roots. *Elife* **6**, e26792.

Werner T., Motyka V., Laucou V., Smets R., van Onckelen H. (2003): Cytokinin-deficient transgenic *Arabidopsis* plants show multiple developmental alterations indicating opposite functions of cytokinins in the regulation of shoot and root meristem activity. *Plant Cell* **15**, 1–20.

Wulfetange K., Lomin S. N., Romanov G. A., Stolz A., Heyl A., Schmülling T. (2011): The cytokinin receptors of *Arabidopsis* are located mainly to the Endoplasmic reticulum. *Plant Physiol.* **156**, 1808–1818.

Yamada H., Suzuki T., Terada K., Takei K., Ishikawa K., Miwa K., Yamashino T., Mizuno T. (2001): The *Arabidopsis* AHK4 histidine kinase is a cytokinin-binding receptor that transduces cytokinin signals across the membrane. Plant Cell Physiol **42**, 1017–1023.

Zürcher E., Liu J., di Donato M., Geisler M., Müller B. (2016): Plant development regulated by cytokinin sinks. *Science* **353**, 1027–1030.

Karolina Kubiasová

ORCID iD	0000-0001-5630-9419
Nationality:	Czech
Contact:	KubiasovaK@seznam.cz

Education:

2014-present	PhD programme, Biochemistry, Faculty of Science, Palacký University in Olomouc, Czech Republic (topic: Localization studies of the cytokinin receptor CRE1/AHK4 using fluorescently labelled cytokinin)
2014	Master's degree in Biochemistry, Faculty of Science Palacký University in Olomouc, Czech Republic (topic: Localization of cytokinin receptors in *Arabidopsis thaliana* using fluorescent labelling)
2012	Bachelor's degree in Biochemistry, Faculty of Science, Palacký University in Olomouc, Czech Republic (topic: Synthesis and characterization of fluorescently labelled cytokinin derivatives)

Work Experience:

2020-present	Laboratory manager for Benkova and Friml groups, Institute of Science and Technology Austria (IST Austria)
2014-2019	Research assistant, Department of Molecular Biology, Centre of the Region Hana for Biotechnological and Agricultural Research, Palacký University in Olomouc, Czech Republic

Research Internships:

2016 – 2019	Institute of Science and Technology (IST Austria), Klosterneuburg, Austria Benkova group, 16 months divided into 7 stays
October 2015 (1 month)	The Interfaculty Institute for Microbiology and Infection Medicine, Eberhard Karls University of Tübingen, Germany Maldener lab

Courses:

April 2015 (1 week)	Institute of Molecular Biology (IMG), Prague, Czech Republic Course "Processing and analysis of microscopical data in Biomedicine"
November 2013 (1 week)	Center of Medical Biotechnology, University of Duisburg-Essen, Germany COST training school: Chemical probes in chemical proteomics and biosynthesis studies

Grants and projects:

2018-2020   GAČR (18-23972Y): Is *Arabidopsis* AHK4/CRE1 decoy receptor? (a member of the research team)

2019   GAČR (17-23702S): Distinct transcription factor families controlling meristem activity and organogenesis in *Arabidopsis* (a member of the research team)

2016-2018   GAČR (16-04184S): Study of the intracellular distribution of cytokinins and their transport to vacuoles (a member of the research team)

2017   Erasmus+
Detailed study of localization of cytokinin receptors in *Arabidopsis thaliana*

2017   Internal Grant Agency (IGA) of Palacký University
Studium prostorové a časové lokalizace cytokininových receptorů a jejich funkční charakterizace v *Arabidopsis thaliana*

2016   Endowment Fund of Palacký University
Zkoumání distribuce klíčových komponent cytokininového metabolismu v buňce

2014-2016   GAČR (GAP501/12/0161): Cyanobacterium *Nostoc* as a genetic and functional model for the plant cytokinin hormone metabolism (a member of the research team)

Teaching Experience:

2014-2018   Basic Course in Laboratory Work (KBC/LABT)

2017   Supervising a bachelor student

Conferences:

2015   Kubiasová K., Plíhal O., Mik V., Šamajová O., Galuszka P., Spíchal L.
Green for good (G4G), Olomouc, Czech Republic
Localization of cytokinin receptors in *Arabidopsis thaliana* using fluorescent labelling; poster presentation

2014   Kubiasová K., Plíhal O., Mik V., Šamajová O., Galuszka P., Spíchal L.
KEBR 2014 - 12th PhD Student Conference of Plant Experimental Biology, Olomouc, Czech Republic
Localization of cytokinin receptors in *Arabidopsis thaliana* using fluorescent labelling; poster presentation

Publications:

Kubiasová K., Montesinos J.C., Šamajová O., Nisler J., Mik V., Semerádová H., Plíhalová L., Novák O., Marhavý P., Cavallari N., Zalabák D., Berka K., Doležal K., Galuszka P., Šamaj J., Strnad M., Benková E., Plíhal O., Spíchal L. (2020): Cytokinin fluoroprobe reveals multiple sites of cytokinin perception at plasma membrane and endoplasmic reticulum. *Nat. Commun*. **11**, 4285.
doi: 10.1038/s41467-020-17949-0

Kubiasová K., Mik V., Nisler J., Hönig M., Husičková A., Spíchal L., Pěkná Z., Šamajová O., Doležal K., Plíhal O., Benková E., Strnad M., Plíhalová L. (2018): Design, synthesis and perception of fluorescently labeled isoprenoid cytokinins. *Phytochemistry* **150**, 1-11.
doi:10.1016/j.phytochem.2018.02.015

Frébortová J., Plíhal O., Florová V., Kokáš F., Kubiasová K., Greplová M., Šimura J., Novák O., Frébort I. (2017): Light influences cytokinin biosynthesis and sensing in *Nostoc* (cyanobacteria). *J Phycol.* **53(3)**, 703-714.
doi:10.1111/jpy.12538

de Montaigu A., Oeljeklaus J., Krahn J.H., Suliman M.N.S, Halder V., de Ansorena E., Nickel S., Schlicht M., Plíhal O., Kubiasová K., Radová L, Kracher B., Tóth R., Kaschani F., Coupland G., Kombrink E., Kaiser M. (2017): The Root Growth-Regulating Brevicompanine Natural Products Modulate the Plant Circadian Clock. *ACS Chem Biol.* **12(6)**, 1466-1471.
doi:10.1021/acschembio.6b00978.